The climate effects of increasing ocean albedo: An idealized representation of solar geoengineering

Ben Kravitz[1], Philip J. Rasch[1], Hailong Wang[1], Alan Robock[2], Corey Gabriel[3], Olivier Boucher[4], Jason N. S. Cole[5], Jim Haywood[6,7], Duoying Ji[8], Andy Jones[6], Andrew Lenton[9], John C. Moore[8], Helene Muri[10,11], Ulrike Niemeier[12], Steven Phipps[13,14], Hauke Schmidt[12], Shingo Watanabe[15], Shuting Yang[16], and Jin-Ho Yoon[17]

[1]Atmospheric Sciences and Global Change Division, Pacific Northwest National Laboratory, Richland, WA, USA
[2]Department of Environmental Sciences, Rutgers University, New Brunswick, NJ, USA
[3]Scripps Institution of Oceanography, La Jolla, CA, USA
[4]Laboratoire de Météorologie Dynamique, CNRS / Sorbonne Université, Paris, France
[5]Environment and Climate Change Canada, Toronto, Canada
[6]Met Office Hadley Centre, Exeter, UK
[7]College of Engineering, Mathematics, and Physical Sciences, University of Exeter, Exeter, UK
[8]State Key Laboratory of Earth Surface Processes and Resource Ecology, College of Global Change and Earth System Science, Beijing Normal University, Beijing, China
[9]CSIRO Oceans and Atmosphere, Hobart, Tasmania, Australia
[10]Department of Geosciences, University of Oslo, Oslo, Norway
[11]Department of Energy and Process Engineering, Norwegian University of Science and Technology, Trondheim, Norway
[12]Max Planck Institute for Meteorology, Hamburg, Germany
[13]Climate Change Research Centre, University of New South Wales, Sydney, Australia
[14]Institute for Marine and Antarctic Studies, University of Tasmania, Hobart, Tasmania, Australia
[15]Japan Agency for Marine-Earth Science and Technology, Yokohama, Japan
[16]Danish Meteorological Institute, Copenhagen, Denmark
[17] School of Earth Sciences and Environmental Engineering, Gwangju Institute of Science and Technology, Gwangju, South Korea

Correspondence: Ben Kravitz, P.O. Box 999, MSIN K9-30, Richland, WA 99352, USA. (ben.kravitz@pnnl.gov)

Abstract. ~~Marine cloud brightening has been proposed as a means of geoengineering/climate intervention , or~~ Geoengineering or climate intervention describe methods of deliberately altering the climate system to offset anthropogenic climate change. As an idealized representation of ~~marine cloud brightening~~near-surface solar geoengineering over the ocean, this paper discusses experiment G1ocean-albedo of the Geoengineering Model Intercomparison Project (GeoMIP), involving an abrupt quadrupling of the CO_2 concentration and an instantaneous increase in ocean albedo to maintain approximate net top-of-atmosphere radiative flux balance. Eleven Earth System Models are relatively consistent in their temperature, radiative flux, and hydrological cycle responses to this experiment. Due to the imposed forcing, air over the land surface warms by a model average of 1.14 K, while air over most of the ocean cools. Some parts of the near-surface air temperature over ocean warm due to heat transport from land to ocean. These changes generally resolve within a few years, indicating that changes in ocean heat content play at most a small role in the warming over the oceans. The hydrological cycle response is a general slowing down, with high heterogeneity in the response, particularly in the tropics. While idealized, these results have important implications

for marine cloud brightening, or other methods of geoengineering involving spatially heterogeneous forcing, or other general forcings with a strong land/ocean contrast. It also reinforces previous findings that keeping top-of-atmosphere net radiative flux constant is not sufficient for preventing changes in global mean temperature.

1 Introduction

Geoengineering (also called "climate intervention") describes a set of technological approaches to reduce the effects of climate change by deliberately intervening in the climate system (e.g., Shepherd et al., 2009). There are two broad categories of geoengineering that are commonly discussed: solar geoengineering (modifying the amount of shortwave radiation incident at the surface; NAS, 2015b) and carbon dioxide removal (NAS, 2015a). There are also proposals, such as cirrus cloud thinning (Mitchell and Finnegan, 2009) that do not fit neatly into either of these two categories. In all subsequent discussions in this manuscript, we only discuss solar geoengineering methods.

Two of the most commonly proposed methods of global geoengineering are stratospheric sulfate aerosol geoengineering and marine cloud brightening (MCB). Comparison of the different climate effects of these two methods (e.g., Niemeier et al., 2013; Crook et al., 2015) reveals that, among other things, the spatial distribution of the applied forcing strongly affects the climate effects. Many of the effects of sulfate geoengineering can be reasonably well approximated by a uniform reduction in shortwave radiative flux reaching the surface (Kalidindi et al., 2014). Conversely, MCB targets low clouds over oceans (Latham, 1990), which are not ubiquitous. In addition, there are higher-order effects due to the altitude at which the shortwave scattering occurs, including multiple scattering effects, infrared absorption of shortwave and longwave radiative flux by sulfate aerosols or cloud particles, and absorption of shortwave radiative flux by atmospheric CO_2 and water vapor (e.g., Kravitz et al., 2013b).

Idealized simulations of solar geoengineering are useful in the context of multi-model intercomparisons, in that they capture many of the effects of more complicated methods of representing geoengineering, yet can be performed by a wide variety of models. In simulations conducted under the Geoengineering Model Intercomparison Project (GeoMIP; Kravitz et al., 2011), an idealized method of representing stratospheric sulfate aerosol geoengineering is via reductions in total solar irradiance. As an example of this representation, experiment G1 involved offsetting the global radiative flux imbalance from a quadrupling of the CO_2 concentration via solar reduction. Thus far, 15 models have participated in this simulation, providing information about model commonalities and differences in the global climate response, including effects on temperature, the hydrological cycle, cryosphere, terrestrial biosphere, and extreme events (Schmidt et al., 2012; Kravitz et al., 2013a, b; Tilmes et al., 2013; Moore et al., 2014; Glienke et al., 2015; Curry et al., 2014, among numerous other studies). The GeoMIP website (http://climate.envsci.rutgers.edu/GeoMIP/) provides an up-to-date list of publications using GeoMIP model output.

While total solar irradiance reductions are straightforward to simulate in all models, this idealization is not a good approximation of MCB, nor of near-surface solar geoengineering approaches over the ocean in general. The dominant effect of MCB would be an increase in albedo of marine low clouds through aerosol effects. ~~Changes~~ More generally, changes in the albedo near the ~~surface~~ marine surface (such as in the G4Foam experiment; Gabriel et al., 2017) can produce different signatures from reductions in energy input at the top of the atmosphere, particularly in terms of spatial distribution. While some forms of albedo modification like stratospheric sulfate aerosol geoengineering operate over broad areas (on a hemispheric or larger scale), albedo changes produced by ~~MCB~~ near-surface marine geoengineering would operate on smaller spatial scales and be concentrated over particular oceanic regions. ~~Previous studies suggest that the clouds that are most susceptible to albedo modification are located on the eastern side of ocean basins in the subtropics, in regions dominated by stratocumulus clouds (Oreopoulos and Platnick, 2008). So, rather than considering a reduction of solar input operating uniformly over both land and ocean, an idealized representation of MCB that better approximates the effects is to increase the albedo only over ocean surfaces, as described by Kravitz et al. (2013c). This method can also be used to assess some effects of geoengineering by creating microbubbles at the ocean surface to increase reflectivity (e.g., Seitz, 2011; Robock, 2011; Gabriel et al., 2017).~~

In this study, we investigate the climate effects of using ocean albedo increases to offset CO_2 warming and compare those effects with those of total solar irradiance reduction (experiments are described in more detail in the following section). All simulations were conducted under the auspices of GeoMIP, allowing us to characterize a range of model responses to these different idealized methods of representing solar geoengineering.

2 Methodology and Description

Our analyses focus on four simulations: (1) a preindustrial control simulation (piControl), (2) a simulation in which the CO_2 concentration is abruptly quadrupled from its preindustrial value (abrupt4xCO2), (3) a simulation in which the net radiative flux imbalance in abrupt4xCO2 is offset by a reduction in total solar irradiance (G1), and (4) a simulation in which the net top-of-atmosphere radiative flux imbalance in abrupt4xCO2 is offset by an increase in ocean albedo everywhere by a uniform factor (G1ocean-albedo). piControl and abrupt4xCO2 are standard experiments in the Coupled Model Intercomparison Project Phase 5 (CMIP5; Taylor et al., 2012). G1 is described further by Kravitz et al. (2011), and many of the gross features of the results are described by Kravitz et al. (2013a). All models participating in experiment G1 needed to reduce model total solar irradiance by 3.5-5.0% to offset the radiative forcing from a quadrupling of the CO_2 concentration. In G1ocean-albedo, the ocean surface albedo was increased abruptly at the start of the simulation such that net top-of-atmosphere radiative flux perturbation was within ± 0.1 W m^{-2} of the piControl value in an average over years 21-30 of simulation. Based on preliminary simulations described by Kravitz et al. (2013c), it took approximately 20 years for the climate to reach steady state after an abrupt simultaneous change in the CO_2 concentration and the ocean albedo. As will be shown in subsequent sections, once the appropriate value of ocean albedo increase is found and imposed, the climate system adjusts rapidly, requiring at most a few years to reach steady state (as was the case in experiment G1). Table 1 lists the models participating in this study, including relevant references and the required change in albedo to meet the objectives of experiment G1ocean-albedo. A similar table

for experiment G1 is given by Kravitz et al. (2013a). One of the advantages of G1ocean-albedo is that, like G1, all models can conduct this simulation fairly easily. Supplemental Table S1 quantifies how well each model achieved radiative balance in the G1 and G1ocean-albedo experiments.

Kravitz et al. (2013c) found that in test simulations, one could only determine whether the objectives of G1ocean-albedo were met after several decades of simulation. However, as our analysis will show, once the proper value of ocean albedo increase is ascertained, the climate response reaches steady state in a few years, as in experiment G1 (Kravitz et al., 2013a). Supplemental Table S2 quantifies temperature trends in each participating model over years 11-50 of simulation. The mean model trend over this period is approximately zero K decade^{-1} (to four decimal places), and with little exception, the trends in G1 and G1ocean-albedo are an order of magnitude smaller than the trends in the abrupt4xCO2 simulation. As such, for the purpose of analysis, we assume that "slow responses," i.e., responses operating on time scales longer than a few years (e.g., Andrews and Forster, 2010; Sherwood et al., 2015) are negligible in the G1 and G1ocean-albedo simulations. We do not separate results into rapid adjustment and slow response timescales, and with the exception of time series plots, all figures show averages over the years 11-50 of simulation, which we take as a sufficient indication of the dominant climate response after the transient response has resolved.

Except where indicated, all plots show the mean model response. All values in the text are reported as mean (min to max), where mean indicates the all-model mean for that particular quantity, min is the lower bound of the range of model responses, and max is the upper bound of the range of model responses. In all maps, stippling indicates where fewer than 75% of the models agree on the sign of the response. All models in Table 1 were able to provide output for all variables except for cloud radiative forcing. The models included in cloud forcing analyses are BNU-ESM, CanESM2, CESM-CAM5.1-FV, HadGEM2-ES, IPSL-CM5A-LR, and MPI-ESM-LR. Supplemental Tables S1-S15 provide more quantitative information for all of the analyses presented in this study.

3 Results

3.1 Albedo and Temperature

Figure 1 shows the change in albedo at the top-of-atmosphere and at the surface for the abrupt4xCO2, G1, and G1ocean-albedo simulations, where albedo is defined as the ratio of upwelling to downwelling all-sky shortwave radiative flux. Quantitative values are given in Supplemental Tables S3 and S4. Results for abrupt4xCO2 and G1 are consistent with known responses of an increase in absorbed shortwave by increased CO_2, reduced cloud cover, and reduced snow and sea ice cover (e.g., Schmidt et al., 2012; Kravitz et al., 2013b). These result in a broad decrease in albedo at the top of atmosphere and a decrease in surface albedo in many regions with substantial snow and ice cover. G1ocean-albedo retains many of these local high latitude features, but with large albedo increases over ocean, consistent with the experimental design and imposed forcing.

Figures 2 and 3 expand upon this picture by showing changes in shortwave and longwave cloud forcing and clear sky flux in G1 and G1ocean-albedo. In Figure 2, cloud forcing is defined as all-sky minus clear-sky radiative flux measured at the top of the atmosphere. Positive shortwave values and negative longwave values in Figure 2 are indicative of less cloud cover. In

Figure 3, values indicate changes in top-of-atmosphere net clear sky flux, where net is defined as downward minus upward. Positive values indicate less upward flux in the perturbed experiment (G1 or G1ocean-albedo), and negative values indicate more upward flux.

Kravitz et al. (2013b) showed that cloud cover in G1 tends to be reduced, which is consistent with what is depicted in Figure 2 over broad swaths of the globe. For G1ocean-albedo, cloud cover is reduced over most ocean regions and large portions of land. Exceptions include negative shortwave and positive longwave values over the Arctic, much of Africa, South Asia, Australia, and the leeward side of the Andes. The results of Figure 3 are consistent with an increase in the CO_2 concentration, with more absorption of shortwave and more outgoing longwave radiative flux. Exceptions are many of the same regions as in Figure 2, which show negative (or less positive) shortwave values and less negative longwave values. Thus, over most regions of the globe, the results are consistent with a combination of increased CO_2 and less cloud cover. Over the other regions (named previously), Figure 2 would indicate that cloud cover increases, which would result in less shortwave absorption and less outgoing longwave radiative flux, consistent with the results in Figure 3. These changes in cloudiness have implications for the hydrologic cycle, which we revisit in Section 3.5.

Figures 2 and 3 admittedly only report the first-order explanations of the radiative flux changes in G1 and G1ocean-albedo. Second-order effects could include additional shortwave absorption by clouds or feedbacks on water vapor flux due to reduced evaporation. Additional work is needed to better understand the role of individual flux changes and processes on clouds and circulation patterns.

Figure 4 shows changes in global mean, land mean, and ocean mean surface air temperature for the G1 and G1ocean-albedo multi-model ensembles. Quantitative values are provided in Supplemental Table S5. Whereas the G1 simulation largely offsets global temperature changes due to increased CO_2 concentration, G1ocean-albedo is approximately 0.36 K (-0.12 to 1.20) warmer than the control simulation. This is predominantly due to warming over land by 1.14 K (0.41 to 1.83). The temperature results in Figure 4 indicate that the temperature change happens within the first few years, and while some models show a slight trend in temperature over the 50-year G1ocean-albedo simulation (Supplemental Table S2), in general, any such trends are small, especially as compared to the warming in the abrupt4xCO2 simulation. This lack of substantial transient behavior after an initial fast response indicates that G1ocean-albedo has entered a new approximate steady state.

Figure 5 shows spatial patterns of change in temperature and top-of-atmosphere net radiative flux. (Also see Supplemental Tables S5 and S6.) The temperature changes are broadly consistent with the net radiative flux changes in the respective experiments. As was discussed by Kravitz et al. (2013a), G1 results in an "overcooling" of the tropics and an "undercooling" of the poles, consistent with offsetting the ubiquitous longwave forcing from CO_2 with a latitudinally dependent reduction in shortwave. G1ocean-albedo shows warming at high latitudes, over land regions, and in some ocean regions near or downwind of large continents, with the remaining ocean regions generally showing cooling.

While the warming over land is easily explainable from first principles, the temperature response over the ocean is heterogeneous (likely due to clouds – see above), and it is perhaps somewhat counterintuitive that on average temperatures over the global oceans do not decrease. Because net top-of-atmosphere radiative flux is approximately zero in G1ocean-albedo, the global warming cannot be the result of energy being added to or subtracted from the climate system, and instead must be the

result of energy redistribution. Three hypotheses for why these temperature change patterns look the way they do (which will be tested in subsequent sections) include

1. Based on energy balance arguments, G1ocean-albedo should experience global average warming.
2. Most warming over oceanic regions is due to transport of heat from land to ocean.
3. Any contributions to temperature or radiative flux changes from changes in ocean heat content are small on the timescales being evaluated here.

3.2 Hypothesis 1: Energy Balance

The Earth system can be considered as a simple surface-atmosphere energy budget model

$$\frac{S(1-A)}{4} = (1-\epsilon/2)\sigma T_s^4 \tag{1}$$

where S is total solar irradiance at the top of the atmosphere (i.e., the solar "constant"), A is albedo of Earth, ϵ is the longwave emissivity of the atmosphere, and T_s is surface temperature. In this model, $T_s = 2^{1/4}T_a$, where T_a is atmospheric temperature.

Taking the total differential yields

$$\frac{dS(1-A)}{4} - \frac{SdA}{4} = \left(1-\frac{\epsilon}{2}\right)4\sigma T_s^3 dT_s - \frac{d\epsilon}{2}\sigma T_s^4 \tag{2}$$

Isolating dT_s yields

$$dT_s = \left[\frac{dS(1-A)}{4} - \frac{SdA}{4} + \frac{d\epsilon}{2}\sigma T_s^4\right] / \left[\left(1-\frac{\epsilon}{2}\right)4\sigma T_s^3\right] \tag{3}$$

Simplifying,

$$dT_s = \frac{dS(1-A)}{16\sigma T_s^3(1-\epsilon/2)} - \frac{SdA}{16\sigma T_s^3(1-\epsilon/2)} + \frac{d\epsilon/2}{1-\epsilon/2}\frac{T_s}{4} \tag{4}$$

From Equation 1 and using $T_s = 286.491$ K (the average piControl value from the Earth System Models), $S = 1366$ W m^{-2}, and $A = 0.3$, it follows that $\epsilon = 0.748$.

~~Under conditions corresponding to G1, Equation 2 can be solved to yield changes in emissivity for an abrupt quadrupling of the CO_2 concentration:~~

~~$$\frac{d\epsilon/2}{1-\epsilon/2} = \frac{-dS(1-A)}{4(1-\epsilon/2)\sigma T_s^4}$$~~

~~by assuming $dA = dT_s = 0$. (See below for a discussion of the impacts of this assumption.) Substituting the values above and $dS/S = -0.042$ (Kravitz et al., 2013a), the left side of this equation is equal to 0.042.~~

~~In Equation 4 , the first term is for solar changes, the second term is for planetary albedo changes, and the third term is for emissivity (greenhouse gas) changes. The emissivity term yields a temperature change of approximately 3.01 K. The albedo~~

~~change term (for G1ocean-albedo only) with $dA = 0.0145$ (Supplemental Table S3) yields a temperature change of −1.48 K. The solar reduction term (for G1 only) yields a temperature change of −3.01 K. As such, the net temperature change for G1 is by construction approximately 0, and the net temperature change for G1ocean-albedo would be $dT_s = 1.53$. As such, under the assumptions of basic global energy balance (Equation 1) and incorporating some values from the more complicated Earth System Models, global mean surface air temperature in G1ocean-albedo is found to be positive and higher than in experiment G1.~~

~~Equation 4~~ Equation 4 can be augmented to consider changes in land and ocean components separately. F_ℓ and F_o are the land and ocean fractions, 0.3 and 0.7 respectively, such that $F_\ell + F_o = 1$. The land and ocean albedos are A_ℓ and A_o, respectively. Greenhouse gases are assumed to be well mixed (i.e., ~~ϵ~~ $d\epsilon$ is the same over land and ocean). Then ~~for G1 ($dA = 0$), this equation becomes~~ after solving for change in ocean temperature $dT_{s,o}$, Equation 4 becomes

$$dT_{s,o} = \frac{1}{F_o}\left[\frac{dS(1-A)}{16\sigma T_s^3(1-\epsilon/2)}\frac{(F_\ell dS_\ell + F_o dS_o)(1-A)}{16\sigma T_s^3(1-\epsilon/2)} - \frac{S(F_\ell dA_\ell + F_o dA_o)}{16\sigma T_s^3(1-\epsilon/2)} + \frac{d\epsilon/2}{1-\epsilon/2}\frac{T_s}{4} - F_\ell dT_{s,\ell}\right] \quad (5)$$

~~Substituting the values above and $dT_{s,\ell} = 0.24$ K (Supplemental Table S5)yields $dT_{s,o} = -0.10$ K, which is consistent with the value of −0.07 K reported in Supplemental Table S5.~~

~~For~~ Nearly all of the variables on the right sides of Equations 4 and 5 can be solved from values provided in the supplemental material, values provided above, and $dS/S = -0.042$ (Kravitz et al., 2013b). The only variable that is difficult to solve for in this idealized context is $d\epsilon$, representing changes in emissivity. Such changes can occur due to changes in the CO_2 concentration (or other greenhouse gases), changes in water vapor, or changes in cloud cover. Estimating this quantity using the abrupt4xCO2 scenario would correctly capture changes in emissivity due to CO_2 changes under the G1ocean-albedo ~~(assuming $dS = dA_\ell = 0$), this equation becomes~~

$$dT_{s,o} = \frac{1}{F_o}\left[-\frac{SF_o dA_o}{16\sigma T_s^3(1-\epsilon/2)} + \frac{d\epsilon/2}{1-\epsilon/2}\frac{T_s}{4} - F_\ell dT_{s,\ell}\right]$$

~~Taking the Earth System Model results of $dA_o = 0.023$ (Supplemental Table S3) and $dT_{s,\ell} = 1.14$ K~~simulation, but it would likely overestimate contributions due to water vapor because of tropospheric warming. As such, estimates of $d\epsilon$ under G1ocean-albedo will be calculated using G1, which will capture changes in emissivity from the CO_2 changes but without large changes in atmospheric water vapor. Admittedly, water vapor and cloud cover will likely differ between G1 and G1ocean-albedo, rendering this estimate imperfect. However, this process is far more likely to yield an appropriate result than using abrupt4xCO2.

Using Equation 4 and substituting $dT_s = 0$ K, $dS = 1366 \cdot (-0.042)$ W m^{-2}, $A = 0.3$, $T_s = 286.491$ K, $\epsilon = 0.748$, and $dA = -0.007$ (Supplemental Table ~~S5) yields $dT_{s,o} = 1.43$ K.~~ S3) yields $d\epsilon = 0.0401$. For G1, each of the three terms on the right side of Equation 4 are then -3.01, 0.72, and 2.29 K, respectively. The first of these terms corresponds to solar changes, the second term is for planetary albedo changes, and the third term is for emissivity (greenhouse gas) changes.

~~Admittedly, according to the results in Supplemental Table S3, $dA = -0.007$~~ From the Supplemental Tables, for ~~G1, which is a non-negligible change, particularly in comparison to $dA = 0.015$ for G1ocean albedo. Without the assumption of $dA = dT_s = 0$, obtaining the a closed form for Equation ?? would be difficult. However, by Equation 2, this means that~~

~~the change in emissivity is overestimated, indicating that $dT_{s,o}$ is also overestimated. Under the (incorrect) assumption that Equation ?? holds, if $dA = 0$, then $dc = 0.0526$, whereas if $dA = -0.0067$, then $dc = 0.0406$. Substituting this new dc value~~ Gl ocean-albedo, $dA_o = 0.023$, $dA_\ell = -0.004$, $dS_\ell = dS_o = 0$, and $dT_{s,\ell} = 1.14$ K. Then substituting into Equation 5 yields ~~$dT_{s,o} = 0.45$ K for Gl ocean-albedo~~ $dT_{s,o} = 0.61$ K, which is ~~much more in line with the~~ higher than the Earth System Model ensemble average of 0.03 K. For comparison with the values from G1, the term corresponding to changes in solar input is 0 K, the term corresponding to changes in albedo is -1.52 K, and the term for changes in emissivity is 2.29 K. By Equation 4, these values yield a global mean temperature change of 0.77 K, which is higher than the Earth System Model ensemble average of 0.36 K~~(Supplemental Table S5)~~.

This simple energy balance formulation clearly cannot incorporate all of the feedbacks and complex behaviors of the Earth System Models. Nevertheless, based on energy balance constraints, Glocean-albedo results in both land and ocean warming. ~~While energy balance can explain the temperature changes in Gl~~However, the values recovered by the energy balance model are not entirely consistent with the results of the Earth System Models for Glocean-albedo. To account for these differences, we turn to circulation changes, which are described in the following section.

3.3 Hypothesis 2: The role of Land-Ocean Energy Transport (LOET)

Although the air over the ocean warms somewhat in Glocean-albedo, it does not warm uniformly. Figure 5 shows that much of the warming over the ocean is in areas near land, indicating the potential for some of the heating energy over land to be transported to ocean regions. Indeed, the oceans far from land experience cooling, which is consistent with expectations for a large increase in albedo (Table 1).

Transport of heating energy from land to ocean can be quantified via calculating what Geoffroy et al. (2015) call horizontal energy transport, and which we call land-ocean energy transport (LOET), as it represents an aggregate transport of energy from the atmosphere over the land (averaged over all land regions) to the atmosphere over the ocean (averaged over all ocean regions). Geoffroy et al. (2015) provide a more detailed description, calculation, and validation of this concept using a three-box energy balance model that can be fitted to changes in land/ocean temperature and TOA energy imbalance such that the model captures the relevant energy transport dynamics; we repeat here only the calculations germane to our discussions.

Gregory et al. (2004) describe a method of estimating adjusted radiative forcing and the aggregate strength of global feedbacks via linear regression of the net global, annual mean TOA radiative flux imbalance (ΔR) against the global, annual mean temperature change (ΔT) in response to a forcing. The y-intercept of the regression line gives an estimate of adjusted radiative forcing ($\mathcal{F}$), and the negative of the slope of the regression line gives the feedback parameter (λ). Similarly, one can perform regression just over land-averaged quantities (denoted with the subscript ℓ) or just over ocean quantities (subscript o). Feedback parameter values are provided in Table 2.

In addition, as is derived in detail by Geoffroy et al. (2015), one can regress ΔT_ℓ against ΔT_o to obtain the equation

$$\Delta T_\ell = \frac{\alpha_o / F_\ell}{\lambda_\ell + \alpha_\ell / F_\ell} \delta T_o + \frac{\mathcal{F}}{\lambda_\ell + \alpha_\ell / F_\ell} \tag{6}$$

where α_ℓ is the land heat transport parameter (units of W m^{-2} K^{-1}) and F_ℓ is the land fraction (approximately 0.3). If one solves this equation for α_ℓ and α_o, then one can define

$$\Delta AQ = \alpha_\ell \Delta T_\ell - \alpha_o \Delta T_o \tag{7}$$

The quantity ~~ΔA~~ ΔQ is the time-dependent LOET (units of W m^{-2}).

Figure 6 provides calculations of LOET for the simulations presented here. See Supplemental Table S7 for more details on individual model values. In the abrupt4xCO2 simulation, changes in LOET are positive (indicating an increase in heat transport from the land to the ocean) and decrease in magnitude steadily over the course of the simulation; these results are discussed in more detail by Geoffroy et al. (2015).

In ~~Experiment~~ experiment G1, LOET increases by a model-dependent constant value and remains relatively unchanged over the course of the simulation. Although the air temperature over land in G1 increases slightly, and the air temperature over ocean decreases slightly (Kravitz et al., 2013a), the temperature changes in G1 are more latitude-dependent than representative of a clear land-ocean contrast (Figure 5), so it is perhaps not unexpected that LOET would be small.

Experiment G1ocean-albedo exhibits a strong land-ocean contrast in temperature (Figure 5), and the response is in steady state after a few years. As such, consistent with the behavior of other fluxes, LOET in G1ocean-albedo does not show transient behavior. LOET in G1ocean-albedo is approximately 2.20 (1.35 to 3.21) W m^{-2}, which is larger than in the other experiments examined here.

~~Converting LOET into temperature change is not necessarily straightforward, but an approximate change in temperature can be calculated by combining values of ΔA (Supplemental Table S7) with feedback parameter calculations (Table 2). More specifically, the temperature "added" to the air over the oceans by LOET can be calculated as $\Delta A/\lambda_o$, and the temperature "subtracted" from the air over land by LOET can be calculated as $\Delta A/\lambda_\ell$. Performing these calculations, LOET in the G1ocean-albedo experiment contributes 1.87 K (0.57 to 3.06) to ocean temperature and "subtracts" 2.03 K (0.68 to 3.06) from land temperature. We caution that this naive calculation is somewhat circular, and it inherently includes in the ocean calculations both regions unaffected by LOET (e.g., tropical oceans) and regions strongly affected by LOET (e.g., Northeast Atlantic and Pacific Oceans).~~

Based on the calculations in the present section, it seems unlikely that LOET can on average transport enough energy from the land to the ocean to offset the radiative deficit over the ocean due to an ocean albedo increase. However, locally, LOET appears to be able not only to offset these radiative changes, but also result in net warming.

3.4 Hypothesis 3: Atmospheric Column Energetics and Net Energy Flux into the Oceans

An additional potential source of energy to the atmosphere is a reduction in net ocean heat uptake. Calculating changes in ocean heat uptake are challenging and not particularly revealing in this study for three reasons:

1. It is possible that the models used in simulating G1ocean-albedo were not entirely spun up to steady state. As such, any remaining imbalances could manifest as changes in ocean heat content. In principle, one could subtract off the

preindustrial control value, which likely has a similar trend in ocean heat content arising from spinup. However, this would not remove the influence of nonlinearities (state dependence), so there is no way to guarantee that the signal is entirely due to the G1ocean-albedo forcing.

2. As is seen in Supplemental Table S1, not all models were able to achieve top-of-atmosphere net radiative flux balance over the course of the simulation. These small changes can lead to large changes in ocean heat content over the course of a 50-year simulation, consistent with CMIP5 models (Hobbs et al., 2016). For example, a 0.1 W m^{-2} imbalance over a 50-year period can lead to an additional 5.5×10^{22} J of energy incident at the ocean surface. As such, we are unable to properly assess the degree to which ocean heat content changes may be due to small imbalances.

3. Ocean heat content can be (and is often) calculated up to a certain depth, meaning calculations of it can be sensitive to redistribution of heat to/from lower depths, obscuring the signal of the forcing.

As an alternative, we calculate net energy exchange across the surface in terms of changes in radiative and turbulent fluxes. Kravitz et al. (2013b) calculated energetics changes in the entire atmospheric column. However, because we are only interested in net surface fluxes, we calculate

$$\Delta SB = \Delta R_{\text{surf}} + \Delta SH + \Delta LH \tag{8}$$

where ΔR_{surf} is the change in net surface radiative flux (shortwave and longwave), ΔSH is change in sensible heat flux from the atmosphere to the surface, and ΔLH is change in latent heat flux from the atmosphere to the surface. By convention, all fluxes are positive downward unless specifically noted. Calculations of individual terms in this budget, as well as of ~~ΔS~~ΔB, are provided in Supplemental Tables S8-S12. Because these calculations are performed at the surface, no advection term (e.g., LOET) is needed, and ~~ΔS~~ ΔB is well defined as a land or ocean average.

Figure 7 shows the all-model mean for all of the terms in Equation 8. Several clear conclusions emerge. The first is that ~~ΔS~~ ΔB is approximately zero globally, over land, and over ocean for nearly the entire 50-year period, after an initial rapid adjustment that resolves within a few years. With the exception of latent heat over land, ~~this is true of~~ all fluxes for G1ocean-albedo ~~in~~ reach a steady state after a few years (Figure 7), and even latent heat flux over land reaches an approximate steady state within ten years. If ~~ΔS~~ ΔB indeed serves as a useful proxy for global net energy flux into or out of the ocean, then these results indicate that there is no sizable contribution to atmospheric energetics by changes in global mean ocean heat content. Moreover, even if ~~ΔS~~ ΔB were not zero over ocean, global mean ocean heat content changes would still be an insufficient explanation for global mean temperature changes due to incongruent timescales. The oceanic mixed layer operates on an approximately decadal timescale, but all transient behavior in these simulations is resolved well before ten years. The transient response is much more consistent with a land surface time scale, which is on the order of 1-3 years. As such, it seems plausible that the temperature changes over ocean in G1ocean-albedo are due to land processes and land surface feedbacks rather than ocean heat content changes. This is not to say that the ocean plays no role in the observed temperature changes. Rather, given the discussions in this section and the two previous sections, the role of ~~the~~ global mean ocean heat content in causing temperature changes over the ocean in G1ocean-albedo (over the timescales being analyzed here) is likely small.

Because forcings and feedbacks are likely to be realized heterogeneously, there may be roles for local changes or for patterns of circulation (e.g., the Atlantic meridional overturning circulation) in altering oceanic heat content. However, such analyses are beyond the scope of the present work.

The remainder of the results in Figure 7 are consistent with the applied forcing. There is a large sensible heat flux increase from the land to the atmosphere of 2.87 (-0.99 to 6.00) W m^{-2}, with a comparatively smaller sensible heat flux decrease from the ocean to the atmosphere of 1.47 (0.34 to 2.20) W m^{-2}. Over the ocean, latent heat flux from the surface to the atmosphere is 6.71 (4.95 to 7.89) W m^{-2} lower in G1ocean-albedo than in the preindustrial control simulation. These results indicate a greater shift of energy away from evaporating water and toward increasing land temperature. Large differences in flux magnitude between G1 and G1ocean-albedo can be found over land for net shortwave flux and latent heat flux, and differences in sign can be found over land for total radiative flux. These features are consistent with the applied forcing being different over land and ocean.

3.5 Hydrological cycle changes

Introducing a strong land-ocean energy and temperature gradient, as in G1ocean-albedo, will undoubtedly impact the hydrological cycle. Although the G1ocean-albedo simulation is idealized, more realistic representations of MCB have shown important hydrological cycle impacts, including secondary circulation patterns that shift precipitation onto land in the tropics and extratropics (Bala et al., 2010; Alterskjær et al., 2013) and changes in the Walker circulation (Niemeier et al., 2013). Here we evaluate the large-scale hydrological cycle changes in G1ocean-albedo, with possible applicability to other realizations of MCB.

Figure 8 shows global, land, and ocean averaged precipitation, evaporation, and precipitation minus evaporation (P-E) for all of the simulations considered in this manuscript; quantitative descriptions are given in Tables S13-15. The abrupt4xCO2 simulation is the only one with a distinct rapid adjustment and slow response. Over both land and ocean, G1 shows decreases in precipitation and evaporation of approximately equal magnitude, resulting in net changes in P-E of 0.02 (-0.05 to 0.11) mm day^{-1} over land and -0.01 (-0.04 to 0.01) mm day^{-1} over ocean. In G1ocean-albedo, global precipitation and evaporation both decrease by approximately 0.19 (0.11 to 0.26) mm day^{-1} to yield little net change in P-E. However, this net small change is due to differential effects over land and ocean. Over land, precipitation remains relatively unchanged, but evaporation decreases, resulting in a net change in P-E by 0.09 (-0.18 to 0.18) mm day^{-1}. Over the ocean, both precipitation and evaporation decrease, with a net negative P-E of -0.06 (-0.19 to -0.01) mm day^{-1}.

Annual mean land/ocean contrasts in precipitation and evaporation changes tend to be more uniform in sign in experiment G1 (Figure 9), resulting in few large regions of change in P-E with the exception of the tropics (mostly driven by a southward shift in the intertropical convergence zone; Kravitz et al., 2013a). In G1ocean-albedo, precipitation and evaporation over the oceans are reduced in most regions, consistent with the applied forcing. Over land, the signs of precipitation and evaporation changes are regionally heterogeneous, yet the precipitation and evaporation changes are concordant, e.g., land regions with increased precipitation also generally show increased evaporation. The net P-E map is highly heterogeneous, but in general, tropical land areas are projected to have more available moisture (as measured by P-E) under G1ocean-albedo, and midlatitude land

areas are projected to have less. There is a general drying (reduced P-E) in the midlatitudes, as well as some reductions in the intertropical convergence zone, with important implications for tropospheric circulation (to be evaluated in future work).The implications of these changes for people and ecosystems are ~~important to research~~also important to investigate further.

4 Discussion and Conclusions

In Section 3.1, three hypotheses were posed as to why G1ocean-albedo experienced warming over both land and ocean. Based on the analysis presented here, we confirmed that G1ocean-albedo should experience global average warming, based on energy balance arguments. However, energy balance arguments alone cannot explain the magnitude of oceanic warming. Explaining that warming requires a model that can represent horizontal transport of heat from the land to the ocean. Because these processes reach steady state within a decade or less, it is unlikely that long-term oceanic processes, including changes in global mean ocean heat content, are responsible for the majority of the changes seen in G1ocean-albedo.

The results presented here indicate that even though experiments G1 and G1ocean-albedo both achieve approximate net top-of-atmosphere radiative flux balance, the climate system responses differ dramatically between the two experiments. The idea that global energy balance can still result in local changes is perhaps not surprising, as feedbacks operate locally (Armour et al., 2013). These different climate responses for the same magnitude in global forcing are effectively an illustration of different efficacies (Hansen et al., 2005). Even in the absence of slow responses, forcings with different efficacies can cause different climate system changes (Kravitz et al., 2015). G1ocean-albedo serves as an excellent reminder not to conflate small net top-of-atmosphere radiative flux imbalance with small temperature change; a clear relationship between those two quantities is not guaranteed.

Relatedly, the results obtained for G1ocean-albedo were to some extent by design. The objective of G1ocean-albedo was to achieve net top-of-atmosphere radiative flux balance, which resulted in warming. Conceivably, one could define an objective of no global temperature change, implying a net negative radiative flux at the top-of-atmosphere, or no global land temperature change, requiring adjustments over the oceans to make up the imbalance. It is unclear whether, unlike G1ocean-albedo, such alternate approaches would result in transient behavior that lasts longer than a few years. Such an experiment could be accomplished using feedback methods that have been introduced to geoengineering research in recent years (e.g., MacMartin et al., 2014b; Kravitz et al., 2016).

Related to this discussion, Supplemental Figures S1-S3 show monthly differences (from piControl) of net top-of-atmosphere radiative flux change and temperature change for the abrupt4xCO2, G1, and G1ocean-albedo simulations. These were calculated by naively subtracting each monthly value of the three perturbed experiments from the monthly values of the corresponding piControl simulation, so all differences are subject to noise introduced by chaos. G1 shows an indication of slight transient behavior, starting out with positive temperature anomaly that relaxes to near-zero within a few years. G1ocean-albedo does not show any discernible anomaly, in that it starts out slightly warmer (globally) than piControl and stays slightly warm. The Gregory plot for G1ocean-albedo similarly shows no discernible trend, unlike the abrupt4xCO2 simulation. There are several possibilities of explanations for this behavior. One is that the adjustments are happening on a short enough timescale in

Glocean-albedo that any transient response is difficult to detect with only monthly averages (Cao et al., 2012). Another possibility is that the noise introduced by chaos on the timescales of interest (months to a few years) obscures our ability to detect any transient behavior. An ensemble of shorter simulations (e.g., Wan et al., 2014) might be well equipped to reveal transience in the response on these timescales. A third option is model artifact related to how the climate models treat energy conservation, indicating that experiments like Glocean-albedo could be useful in testing models beyond their originally conceived application space. While it is beyond the scope of the present manuscript to fully assess all of these possibilities, it becomes clear that Glocean-albedo and simulations of geoengineering in general are useful for improving understanding about climate modeling and climate science.

The results presented here have several features that were not necessarily expected from the outset. (Kravitz et al., 2013c) found that determining whether the climate system was in balance took up to 30 years of simulation. However, once that balance is achieved, the climate does not change appreciably after the initial rapid adjustment. Potential future work could investigate these results, shedding light on timescales of climate response and potential thresholds, e.g., how large does the energy imbalance need to be to trigger slower adjustments?

Related to this issue of different timescales of adjustment is the traditional separation of climate response into rapid adjustment and slow response components (e.g., Andrews and Forster, 2010; Sherwood et al., 2015). The rapid adjustment is often defined as the climate response unassociated with global mean temperature change, and the slow response describes a transient response due to temperature change, largely as a result of climate system feedbacks. The results from Glocean-albedo, like those of Gl (Kravitz et al., 2013b), show an initial rapid change and no appreciable slower change. However, in Glocean-albedo, there is a sustained temperature increase without appreciable transient behavior. Thus, Glocean-albedo represents an experiment that does not cleanly delineate into the traditional definitions of rapid adjustment and slow response. Additionally, this sustained temperature increase is to some extent decoupled from net energy imbalances in the climate system, as ΔR_{TOA} and ΔS (Equation 8) are both approximately zero. Reconciling all of these features suggests a potentially rich research topic focused on understanding the relationships between radiative flux changes, temperature changes, and the circumstances under which climate feedbacks are excited, particularly for forcings with strong land/ocean contrast (e.g., anthropogenic aerosols).

The results presented here are broadly relevant to more sophisticated representations of MCB, such as increasing cloud droplet number concentration or directly injecting sea salt aerosols into the marine boundary layer (Kravitz et al., 2013c). Stjern et al. (2018) analyzed a multi-model ensemble of simulations of G4cdnc (Kravitz et al., 2013c), involving a 50% increase in cloud droplet number concentration in all marine low clouds, wherever the model forms those clouds. Although smaller in magnitude, they found similar patterns of top-of-atmosphere radiative flux change as in Glocean-albedo. Also similar between the two experiments was an increase in land precipitation and a decrease in ocean precipitation. Perhaps an even more realistic representation is G4sea-salt (Ahlm et al., 2017), involving direct injection of sea salt into the marine boundary layer between 30°S and 30°N to achieve an effective radiative forcing of -2.0 W m^{-2}. In the injection area (the tropics), this experiment also showed similar patterns of net top-of-atmosphere radiative flux perturbation and hydrologic cycle response. As such, while Glocean-albedo is highly idealized and exerts a perhaps unrealistically large forcing, it has relevance for other global representations of MCB or sea spray geoengineering. However, there are important differences in boundary layer stability

changes from surface albedo increases versus marine stratocumulus cloud top brightening. Also, it appears impossible for marine cloud brightening to be conducted over all ocean regions and with a sufficient magnitude to offset the radiative forcing from a quadrupling of the CO_2 concentration. The purpose of this manuscript is to describe the broad features of change under a uniform ocean albedo increase, and some of these changes are likely to be present with more realistic scenarios of marine cloud brightening. We anticipate that future research can more deeply explore the applicability of this simulation to marine cloud brightening.

Glocean-albedo may be more apposite to the impact of geoengineering via "ocean microbubbles," whereby surfactants are added to the ocean surface, promoting the formation of microscopic, highly reflective bubbles ~~(Seitz, 2011; Robock, 2011)~~ (Robock, 2011). An area of investigation we did not undertake, yet one that repeatedly emerges in discussions of microbubbles, is the resulting effects of surface albedo increase on the ocean mixed layer. By reflecting more solar radiation, microbubbles have the potential to inhibit vertical mixing and available light in the euphotic zone, which could have profound effects on marine biota. This implies that another useful future area of investigation for the Glocean-albedo simulation is an analysis of the marine carbon cycle.

There are numerous potential areas of research prompted by this study. The stark land/ocean contrast in warming has potential implications for ocean dynamics, including the meridional overturning circulation, Western boundary ocean currents, and mixed layer depths, with consequent implications for marine ecosystems and the ocean carbon cycle. This contrast also has implications for the terrestrial biosphere, including ecosystem services and the land and ocean carbon cycles. Although we did not evaluate seasonal changes in this manuscript, such investigations could prove fruitful for more detailed assessments of variability, such as monsoon precipitation, extreme events, and sea ice extent. In addition, the changes in precipitation described earlier indicate important potential changes in large-scale circulation, atmospheric dynamics, and the hydrological cycle, all of which warrant further study.

~~Despite being informative for MCB, there are limits as to the applicability of this idealized approach. There are important differences in boundary layer stability changes from surface albedo increases versus marine stratocumulus cloud top brightening. Also, it appears impossible for marine cloud brightening to be conducted over all ocean regions and with a sufficient magnitude to offset the radiative forcing from a quadrupling of the CO_2 concentration. The purpose of this manuscript is to describe the broad features of change under a uniform ocean albedo increase, and some of these changes are likely to be present with more realistic scenarios of marine cloud brightening. We anticipate that future research can more deeply explore the applicability of this simulation to marine cloud brightening.~~

Data availability. All output involved in the Geoengineering Model Intercomparison Project is publicly available, and much of it is accessible through the Earth System Grid Federation. Please see the GeoMIP website (http://climate.envsci.rutgers.edu/GeoMIP/) or contact the corresponding author for details.

Competing interests. None.

Acknowledgements. We thank Jón Egill Kristjánsson, who tragically passed away, for invaluable comments on an earlier version of this manuscript. We acknowledge the World Climate Research Programme's Working Group on Coupled Modelling, which is responsible for CMIP, and we thank the climate modeling groups for producing and making available their model output. For CMIP the U.S. Department of Energy's Program for Climate Model Diagnosis and Intercomparison provides coordinating support and led development of software infrastructure in partnership with the Global Organization for Earth System Science Portals. We thank all participants of the Geoengineering Model Intercomparison Project and their model development teams, CLIVAR/WCRP Working Group on Coupled Modeling for endorsing GeoMIP, and the scientists managing the Earth System Grid data nodes who have assisted with making GeoMIP output available. The Pacific Northwest National Laboratory is operated for the U.S. Department of Energy by Battelle Memorial Institute under contract DE-AC05-76RL01830. Simulations performed by Ben Kravitz were supported by the NASA High-End Computing (HEC) Program through the NASA Center for Climate Simulation (NCCS) at Goddard Space Flight Center. Alan Robock is supported by NSF grant AGS-1617844. Olivier Boucher acknowledges HPC resources from CCRT under the allocation 2015-t2012012201 made by GENCI (Grand Equipement National de Calcul Intensif). This work is a contribution to the German DFG-funded Priority Program 'Climate Engineering: Risks, Challenges, Opportunities?' (SPP 1689). Helene Muri was supported by the Research Council of Norway (229760/E10), and acknowledges Sigma2 NOTUR resources nn9182k, NS9033K and nn9448k. U. Niemeier and H. Schmidt are supported by the SPP 1689 within the projects CEIBRAL and CELARIT. This research was supported under the Australian Research Council's Special Research Initiative for the Antarctic Gateway Partnership (project SR140300001). Shingo Watanabe was supported by the Integrated Research Program for Advancing Climate Models, MEXT, Japan. The Earth Simulator was used in his simulations. Jin-Ho Yoon was supported by the National Strategic Project – Find particle of the National Research of Korea (NRF) funded by the Ministry of Science and ICT (MSIT), the Ministry of Environment (ME), and the Ministry of Health and Welfare (MOHW) NRF-2017M3D8A1092022.

References

Ahlm, L., Jones, A., Stjern, C. W., Muri, H., Kravitz, B., and Kristjánsson, J. E.: Marine cloud brightening – as effective without clouds, Atmospheric Chemistry and Physics, 17, 13 071–13 087, https://doi.org/10.5194/acp-17-13071-2017, 2017.

Alterskjær, K., Kristjánsson, J. E., Boucher, O., Muri, H., Niemeier, U., Schmidt, H., Schulz, M., and Timmreck, C.: Sea-salt injections into the low-latitude marine boundary layer: The transient response in three Earth system models, J. Geophys. Res., 118, 12 195–12 206, https://doi.org/10.1002/2013JD020432, 2013.

Andrews, T. and Forster, P. M.: The transient response of global-mean precipitation to increasing carbon dioxide levels, Environ. Res. Lett., 5, 025 212, https://doi.org/10.1088/1748-9326/5/2/025212, 2010.

Armour, K. C., Bitz, C. M., and Roe, G. H.: Time-varying climate sensitivity from regional feedbacks, J. Climate, 26, 4518–4534, https://doi.org/10.1175/JCLI-D-12-00544.1, 2013.

Arora, V. K., Scinocca, J. F., Boer, G. J., Christian, J. R., Denman, K. L., Flato, G. M., Kharin, V. V., Lee, W. G., and Merryfield, W. J.: Carbon emission limits required to satisfy future representative concentration pathways of greenhouse gases, Geophys. Res. Lett., 38, L05 805, https://doi.org/10.1029/2010GL046270, 2011.

Bala, G., Caldeira, K., and Nemani, R.: Fast versus slow response in climate change: Implications for the global hydrological cycle, Clim. Dyn., 35, 423–434, https://doi.org/10.1007/s00382-009-0583-y, 2010.

Bentsen, M., Bethke, I., Debernard, J. B., Iversen, T., Kirkevåg, A., Seland, Ø., Drange, H., Roelandt, C., Seierstad, I. A., Hoose, C., , and Kristjaánsson, J. E.: The Norwegian Earth System Model, NorESM1-M – Part 1: Description and basic evaluation of the physical climate, Geoscientific Model Development, 6, 687–720, 2013.

Cao, L., Bala, G., and Caldeira, K.: Climate response to changes in atmospheric carbon dioxide and solar irradiance on the time scale of days to weeks, Environ. Res. Lett., 7, 034 015, https://doi.org/10.1088/1748-9326/7/3/034015, 2012.

Collins, W. J., Bellouin, N., Doutriaux-Boucher, M., Gedney, N., Halloran, P., Hinton, T., Hughes, J., Jones, C. D., Joshi, M., Liddicoat, S., Martin, G., O'Connor, F., Rae, J., Senior, C., Sitch, S., Totterdell, I., Wiltshire, A., and Woodward, S.: Development and evaluation of an Earth-System model—HadGEM2, Geosci. Model Dev., 4, 1051–1075, https://doi.org/10.5194/gmd-4-1051-2011, 2011.

Crook, J. A., Jackson, L. S., Osprey, S. M., and Forster, P. M.: A comparison of temperature and precipitation responses to different Earth radiation management geoengineering schemes, J. Geophys. Res., 120, 9352–9373, https://doi.org/10.1002/2015JD023269, 2015.

Curry, C. L., Sillmann, J., Bronaugh, D., Alterskjær, K., Cole, J. N. S., Kravitz., B., Kristjánsson, J. E., Muri, H., Niemeier, U., Robock, A., and Tilmes, S.: A multi-model examination of climate extremes in an idealized geoengineering experiment, J. Geophys. Res., 119, 3900–3923, https://doi.org/10.1002/2013JD020648, 2014.

Dufresne, J.-L., Foujols, M.-A., Denvil, S., Caubel, A., Marti, O., Aumont, O., Balkanski, Y., Bekki, S., Bellenger, H., Benshila, R., Bony, S., Bopp, L., Braconnot, P., Brockmann, P., Cadule, P., Cheruy, F., Codron, F., Cozic, A., Cugnet, D., de Noblet, N., Duvel, J.-P., Ethé, C., Fairhead, L., Fichefet, T., Flavoni, S., Friedlingstein, P., Grandpeix, J.-Y., Guez, L., Guilyardi, E., Hauglustaine, D., Hourdin, F., Idelkadi, A., Ghattas, J., Joussaume, S., Kageyama, M., Krinner, G., Labetoulle, S., Lahellec, A., Lefebvre, M.-P., Lefevre, F., Levy, C., Li, Z. X., Lloyd, J., Lott, F., Madec, G., Mancip, M., Marchand, M., Masson, S., Meurdesoif, Y., Mignot, J., Musat, I., Parouty, S., Polcher, J., Rio, C., Schulz, M., Swingedouw, D., Szopa, S., Talandier, C., Terray, P., Viovy, N., and Vuichard, N.: Climate change projections using the IPSL-CM5 Earth System Model: From CMIP3 to CMIP5, Clim. Dynam., 40, 2123–2165, https://doi.org/10.1007/s00382-012-1636-1, 2013.

Gabriel, C. J., Robock, A., Xia, L., Zambri, B., and Kravitz, B.: The G4Foam Experiment: Global climate impacts of regional ocean albedo modification, Atmospheric Chemistry and Physics, 17, 595–613, https://doi.org/10.5194/acp-17-595-2017, 2017.

Geoffroy, O., Saint-Martin, D., and Voldoire, A.: Land-sea warming contrast: the role of the horizontal energy transport, Clim. Dynam., 45, 3493–3511, https://doi.org/10.1007/s00382-015-2552-y, 2015.

Giorgetta, M. A., Jungclaus, J., Reick, C. H., Legutke, S., Bader, J., Böttinger, M., Brovkin, V., Crueger, T., Esch, M., Fieg, K., Glushak, K., Gayler, V., Haak, H., Hollweg, H.-D., Ilyina, T., Kinne, S., Kornblueh, L., Matei, D., Mauritsen, T., Mikolajewicz, U., Mueller, W., Notz, D., Pithan, F., Raddatz, T., Rast, S., Redler, R., Roeckner, E., Schmidt, H., Schnur, R., Segschneider, J., Six, K. D., Stockhause, M., Timmreck, C., Wegner, J., Widmann, H., Wieners, K.-H., Claussen, M., Marotzke, J., and Stevens, B.: Climate and carbon cycle changes from 1850 to 2100 in MPI-ESM simulations for the Coupled Model Intercomparison Project Phase 5, J. Adv. Model. Earth Syst., 5, 572–597, https://doi.org/10.1002/jame.20038, 2013.

Glienke, S., Irvine, P. J., and Lawrence, M. G.: The impact of geoengineering on vegetation in experiment G1 of the GeoMIP, J. Geophys. Res., 120, 10 196–10 213, https://doi.org/10.1002/2015JD024202, 2015.

Gregory, J. M., Ingram, W. J., Palmer, M. A., Jones, G. S., Stott, P. A., Thorpe, R. B., Lowe, J. A., Johns, T. C., and Williams, K. D.: A new method for diagnosing radiative forcing and climate sensitivity, Geophys. Res. Lett., 31, L03 205, https://doi.org/10.1029/2003GL018747, 2004.

Hansen, J., Sato, M., Ruedy, R., Nazarenko, L., Lacis, A., Schmidt, G. A., Russell, G., Aleinov, I., Bauer, M., Bauer, S., Bell, N., Cairns, B., Canuto, V., Chandler, M., Cheng, Y., Del Genio, A., Faluvegi, G., Fleming, E., Friend, A., Hall, T., Jackman, C., Kelley, M., Kiang, N., Koch, D., Lean, J., Lerner, J., Lo, K., Menon, S., Miller, R., Minnis, P., Novakov, T., Oinas, V., Perlwitz, J., Perlwitz, J., Rind, D., Romanou, A., Shindell, D., Stone, P., Sun, S., Tausnev, N., Thresher, D., Wielicki, B., Wong, T., Yaho, M., and Zhang, S.: Efficacy of Climate Forcings, J. Geophys. Res., 110, D18 104, https://doi.org/10.1029/2005JD005776, 2005.

Hazeleger, W., Wang, X., Severijns, C., Ştefănescu, S., Bintanja, R., Sterl, A., Wyser, K., Semmler, T., Yang, S., van den Hurk, B., van Noije, T., van der Linden, E., and van der Wiel, K.: EC-Earth V2.2: Description and validation of a new seamless Earth system prediction model, Clim. Dynam., 39, 2611–2629, https://doi.org/10.1007/s00382-011-1228-5, 2011.

Hobbs, W., Palmer, M. D., and Monselesan, D.: An Energy Conservation Analysis of Ocean Drift in the CMIP5 Global Coupled Models, J. Climate, 29, 1639–1653, https://doi.org/10.1175/JCLI-D-15-0477.1, 2016.

Hurrell, J. W., Holland, M. M., Gent, P. R., Ghan, S., Kay, J. E., Kushner, P. J., Lamarque, J.-F., Large, W. G., Lawrence, D., Lindsay, K., Lipscomb, W. H., Long, M. C., Mahowald, N., Marsh, D. R., Neale, R. B., Rasch, P., Vavrus, S., Vertenstein, M., Bader, D., Collins, W. D., Hack, J. J., Kiehl, J., , and Marshall, S.: The Community Earth System Model: A Framework for Collaborative Research, Bull. Amer. Meteor. Soc., 94, 1339–1360, https://doi.org/10.1175/BAMS-D-12-00121.1, 2013.

Ji, D., Wang, L., Feng, J., Wu, Q., Cheng, H., Zhang, Q., Yang, J., Dong, W., Dai, Y., Gong, D., Zhang, R.-H., Wang, X., Liu, J., Moore, J. C., Chen, D., and Zhou, M.: Description and basic evaluation of Beijing Normal University Earth System Model (BNU-ESM) version 1, Geosci. Model. Dev., 7, 2039–2064, https://doi.org/10.5194/gmd-7-2039-2014, 2014.

Kalidindi, S., Bala, G., Modak, A., and Caldeira, K.: Modeling of solar radiation management: A comparison of simulations using reduced solar constant and stratospheric sulfate aerosols, Clim. Dynam., 44, 2909–2925, https://doi.org/10.1007/s00382-014-2240-3, 2014.

Kravitz, B., Robock, A., Boucher, O., Schmidt, H., Taylor, K. E., Stenchikov, G., and Schulz, M.: The Geoengineering Model Intercomparison Project (GeoMIP), Atmos. Sci. Lett., 12, 162–167, https://doi.org/10.1002/asl.316, 2011.

Kravitz, B., Caldeira, K., Boucher, O., Robock, A., Rasch, P. J., Alterskjær, K., Karam, D. B., Cole, J. N. S., Curry, C. L., Haywood, J. M., Irvine, P. J., Ji, D., Jones, A., Kristjánsson, J. E., Lunt, D. J., Moore, J., Niemeier, U., Schmidt, H., Schulz, M., Singh, B., Tilmes, S.,

Watanabe, S., Yang, S., , and Yoon, J.-H.: Climate model response from the Geoengineering Model Intercomparison Project (GeoMIP), J. Geophys. Res., 118, 8320–8332, https://doi.org/10.1002/jgrd.50646, 2013a.

Kravitz, B., Rasch, P. J., Forster, P. M., Andrews, T., Cole, J. N. S., Irvine, P. J., Ji, D., Kristjánsson, J. E., Moore, J. C., Muri, H., Niemeier, U., Robock, A., Singh, B., Tilmes, S., Watanabe, S., , and Yoon, J.-H.: An energetic perspective on hydrological cycle changes in the Geoengineering Model Intercomparison Project (GeoMIP), J. Geophys. Res., 118, 13 087–13 102, https://doi.org/10.1002/2013JD020502, 2013b.

Kravitz, B., Forster, P. M., Jones, A., Robock, A., Alterskjær, K., Boucher, O., Jenkins, A. K. L., Korhonen, H., Kristjánsson, J. E., Muri, H., Niemeier, U., Partanen, A.-I., Rasch, P. J., Wang, H., , and Watanabe, S.: Sea spray geoengineering experiments in the Geoengineering Model Intercomparison Project (GeoMIP): Experimental design and preliminary results, J. Geophys. Res., 118, 11 175–11 186, https://doi.org/10.1002/jgrd.50856, 2013c.

Kravitz, B., MacMartin, D. G., Rasch, P. J., and Jarvis, A. J.: A new method of comparing forcing agents in climate models, J. Climate, 28, 8203–8218, https://doi.org/10.1175/JCLI-D-14-00663.1, 2015.

Kravitz, B., MacMartin, D. G., Wang, H., and Rasch, P. J.: Geoengineering as a design problem, Earth System Dynamics, 7, 469–497, https://doi.org/10.5194/esd-469-2016, 2016.

Latham, J.: Control of global warming?, Nature, 347, 339–340, 1990.

MacMartin, D. G., Kravitz, B., Keith, D. W., and Jarvis, A.: Dynamics of the coupled human-climate system resulting from closed-loop control of solar geoengineering, Clim. Dynam., 43, 243–258, https://doi.org/10.1007/s00382-013-1822-9, 2014b.

Mitchell, D. L. and Finnegan, W.: Modification of cirrus clouds to reduce global warming, Environ. Res. Lett., 4, 045 102, https://doi.org/10.1088/1748-9326/4/4/045102, 2009.

Moore, J. C., Rinke, A., Yu, X., Ji, D., Cui, X., Li, Y., Alterskjær, K., Kristjánsson, J. E., Boucher, O., Huneeus, N., Kravitz, B., Robock, A., Niemeier, U., Schmidt, H., Schulz, M., Tilmes, S., and Watanabe, S.: Arctic sea ice and atmospheric circulation under the GeoMIP G1 scenario, J. Geophys. Res., 119, 567–583, https://doi.org/10.1002/2013JD021060, 2014.

NAS: Climate Intervention: Carbon Dioxide Removal and Reliable Sequestration, Tech. rep., National Research Council, https://www.nap.edu/catalog/18805/climate-intervention-carbon-dioxide-removal-and-reliable-sequestration, (last access: 7 May 2015), 2015a.

NAS: Climate Intervention: Reflecting Sunlight to Cool Earth, Tech. rep., National Research Council, http://www.nap.edu/catalog/18988/climate-intervention-reflecting-sunlight-to-cool-earth, (last access: 7 May 2015), 2015b.

Niemeier, U., Schmidt, H., Alterskjær, K., and Kristjánsson, J. E.: Solar irradiance reduction via climate engineering: Impact of different techniques on the energy balance and the hydrological cycle, J. Geophys. Res., 118, 11 905–11 917, https://doi.org/10.1002/2013JD020445, 2013.

Oreopoulos, L. and Platnick, S.: Radiative susceptibility of cloudy atmospheres to droplet number perturbations: 2. Global analysis from MODIS, J. Geophys. Res., 113, D14S21, https://doi.org/10.1029/2007JD009655, 2008.

Phipps, S. J., Rotstayn, L. D., Gordon, H. B., Roberts, J. L., Hirst, A. C., , and Budd, W. F.: The CSIRO Mk3L climate system model version 1.0 – Part 1: Description and evaluation, Geosci. Model Dev., 4, 483–509, https://doi.org/10.5194/gmd-4-483-2011, 2011.

Robock, A.: Bubble, bubble, toil and trouble. An editorial comment., Climatic Change, 105, 383–385, https://doi.org/10.1007/s10584-010-0017-1, 2011.

Schmidt, G. A., Kelley, M., Nazarenko, L., Ruedy, R., Russell, G. L., Aleinov, I., Bauer, M., Bauer, S. E., Bhat, M. K., Bleck, R., Canuto, V., Chen, Y.-H., Cheng, Y., Clune, T. L., Genio, A. D., de Fainchtein, R., Faluvegi, G., Hansen, J. E., Healy, R. J., Kiang, N. Y., Koch, D., Lacis, A. A., LeGrande, A. N., Lerner, J., Lo, K. K., Matthews, E. E., Menon, S., Miller, R. L., Oinas, V., Oloso, A. O., Perlwitz, J. P.,

Puma, M. J., Putman, W. M., Rind, D., Romanou, A., Sato, M., Shindell, D. T., Sun, S., Syed, R. A., Tausnev, N., Tsigaridis, K., Under, N., Volugarakis, A., Yao, M.-S., and Zhang, J.: Configuration and assessment of the GISS ModelE2 contributions to the CMIP5 archive, J. Adv. Modell. Earth Syst., 6, 141–184, https://doi.org/10.1002/2013MS000265, 2014.

Schmidt, H., Alterskjær, K., Karam, D. B., Boucher, O., Jones, A., Kristjánsson, J. E., Niemeier, U., Schulz, M., Aaheim, A., Benduhn, F., Lawrence, M., and Timmreck, C.: Solar irradiance reduction to counteract radiative forcing from a quadrupling of CO_2: Climate responses simulated by four Earth system models, Earth System Dynamics, 3, 63–78, https://doi.org/10.5194/esd-3-63-2012, 2012.

Seitz, R.: Bright water: hydrosols, water conservation and climate change, Climatic Change, 105, 365–381, https://doi.org/10.1007/s10584-010-9965-8, 2011.

Shepherd, J., Caldeira, K., Cox, P., Haigh, J., Keith, K., Launder, B., Mace, G., MacKerron, G., Pyle, J., Rayner, S., Redgwell, C., and Watson, A.: Geoengineering the climate: Science, governance, and uncertainty, Tech. rep., royal Society Policy document 10/09, 82 pp., 2009.

Sherwood, S. C., Bony, S., Boucher, O., Bretherton, C., Forster, P. M., Gregory, J. M., and Stevens, B.: Adjustments in the forcing-feedback framework for understanding climate change, Bull. Amer. Meteor. Soc., 96, 217–228, https://doi.org/10.1175/BAMS-D-13-00167.1, 2015.

Stjern, C. W., Muri, H., Ahlm, L., Boucher, O., Cole, J. N. S., Ji, D., Jones, A., Haywood, J., Kravitz, B., Lenton, A., Moore, J. C., Niemeier, U., Phipps, S. J., Schmidt, H., Watanabe, S., and Kristjánsson, J. E.: Response to marine cloud brightening in a multi-model ensemble, Atmospheric Chemistry and Physics, 18, 621–634, https://doi.org/10.5194/acp-18-621-2018, 2018.

Taylor, K. E., Stouffer, R. J., and Meehl, G. A.: An overview of CMIP5 and the experiment design, Bull. Amer. Meteor. Soc., 93, 485–498, https://doi.org/10.1175/BAMS-D-11-00094.1, 2012.

Tilmes, S., Fasullo, J., Lamarque, J.-F., Marsh, D. R., Mills, M., Alterskjær, K., Muri, H., Kristjánsson, J. E., Boucher, O., Schulz, M., Cole, J. N. S., Curry, C. L., Jones, A., Haywood, J., Irvine, P. J., Ji, D., Moore, J. C., Karam, D. B., Kravitz, B., Rasch, P. J., Singh, B., Yoon, J.-H., Niemeier, U., Schmidt, H., Robock, A., Yang, S., and Watanabe, S.: The hydrological impact of geoengineering in the Geoengineering Model Intercomparison Project (GeoMIP), J. Geophys. Res., 118, 11 036–11 058, https://doi.org/10.1002/jgrd.50868, 2013.

Wan, H., Rasch, P. J., Zhang, K., Qian, Y., Yan, H., , and Zhao, C.: Short ensembles: an efficient method for discerning climate-relevant sensitivities in atmospheric general circulation models, Geosci. Model. Dev., 7, 1961–1977, https://doi.org/10.5194/gmd-7-1961-2014, 2014.

Watanabe, S., Hajima, T., Sudo, K., Nagashima, T., Takemura, T., Okajima, H., Nozawa, T., Kawase, H., Abe, M., Yokohata, T., Ise, T., Sato, H., Kato, E., Takata, K., Emori, S., and Kawamiya, M.: MIROC-ESM 2010: Model description and basic results of CMIP5-20c3m experiments, Geosci. Mod. Dev., 4, 845–872, https://doi.org/10.5194/gmd-4-845-2011, 2011.

Table 1. Description of the 11 models participating in this study. Column 1 gives the standard model name. Columns 2 and 3 give the default and perturbed surface ocean albedo, defined as upward shortwave divided by downward shortwave radiative flux at the surface, both averaged over ocean regions and over years 11-50 of simulation. Column 4 is the ratio of column 3 to column 2 (calculated prior to rounding the values in Columns 2 and 3). Column 5 gives the factor (δ) by which the model default ocean albedo was multiplied to achieve negligible top-of-atmosphere radiative flux changes under an abrupt4xCO2 simulation (described in greater detail by Kravitz et al., 2015). The differences between Ratio and δ are caused in part by cloud responses. Column 6 gives a relevant reference for each model. All values are rounded to two decimal places.

Model name	piControl ocean albedo	G1ocean-albedo ocean albedo	Ratio	δ	Reference
BNU-ESM	0.12	0.17	1.48	2.50	Ji et al. (2014)
CanESM2	0.11	0.19	1.73	2.45	Arora et al. (2011)
CESM-CAM5.1-FV	0.10	0.18	1.79	2.70	Hurrell et al. (2013)
CSIRO-Mk3L-1.2	0.12	0.19	1.61	2.04	Phipps et al. (2011)
EC-Earth	0.10	0.19	1.97	3.17	Hazeleger et al. (2011)
GISS-E2-R	0.08	0.16	1.95	2.53	Schmidt et al. (2014)
HadGEM2-ES	0.10	0.17	1.83	2.44	Collins et al. (2011)
IPSL-CM5A-LR	0.10	0.17	1.78	2.33	Dufresne et al. (2013)
MIROC-ESM	0.10	0.20	2.00	3.10	Watanabe et al. (2011)
MPI-ESM-LR	0.09	0.23	2.40	5.42	Giorgetta et al. (2013)
NorESM1-M	0.09	0.18	1.95	2.77	Bentsen et al. (2013)

Table 2. Feedback parameters (Section 3.3; units W m^{-2} K^{-1}) for global, land, and ocean averages, calculated via the "Gregory method" (Gregory et al., 2004), where annual mean top-of-atmosphere net radiative flux is regressed against annual mean temperature.

	Global feedback parameter (λ_g)	Land feedback parameter λ_ℓ	Ocean feedback parameter λ_o
BNU-ESM	0.9019	0.7181	0.9838
CanESM2	1.1539	1.1898	1.1260
CESM-CAM5.1-FV	1.1435	1.0357	1.1591
CSIRO-Mk3L-1.2	1.0192	0.9300	0.8034
EC-Earth	1.2124	1.1937	1.3155
GISS-E2-R	2.2440	1.9751	2.3560
HadGEM2-ES	0.8411	0.8363	0.8351
IPSL-CM5A-LR	0.8367	1.2891	0.5894
MIROC-ESM	1.0378	0.8736	1.0383
MPI-ESM-LR	1.3701	1.0573	1.3986
NorESM1-M	1.4285	1.8828	1.6063

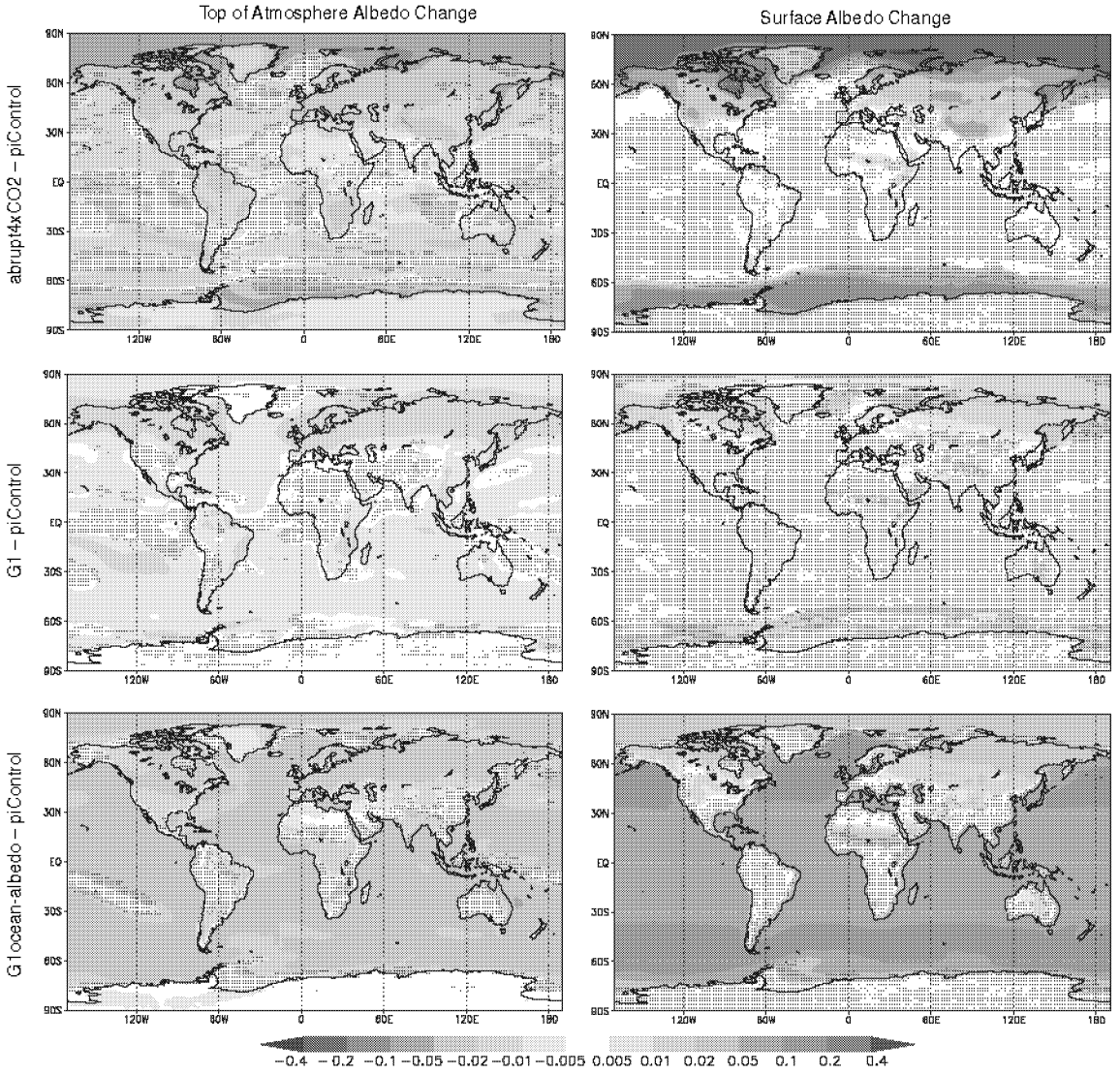

Figure 1. Top-of-atmosphere (TOA) and surface albedo differences (relative to piControl) for the abrupt4xCO2, G1, and G1ocean-albedo experiments. Albedo here is calculated as the ratio of upwelling to downwelling all-sky shortwave radiative flux, either at TOA or at the surface. Values are averages over years 11-50 of simulation. Stippling indicates where fewer than 8 out of 11 models agree on the sign of the response.

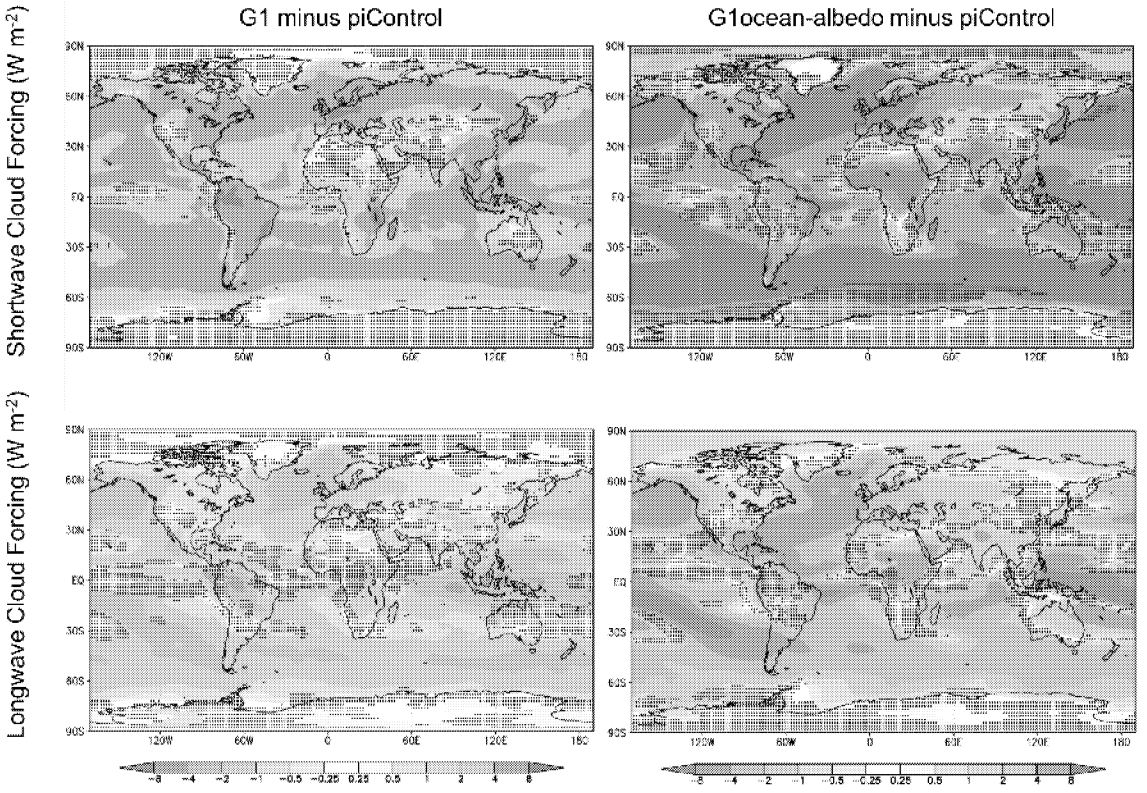

Figure 2. Shortwave (top) and longwave (bottom) cloud forcing changes due to the G1 (left) and G1ocean-albedo perturbations. Cloud forcing is defined as all-sky minus clear-sky radiative flux at the top of the atmosphere, with positive values indicating more net downward flux.

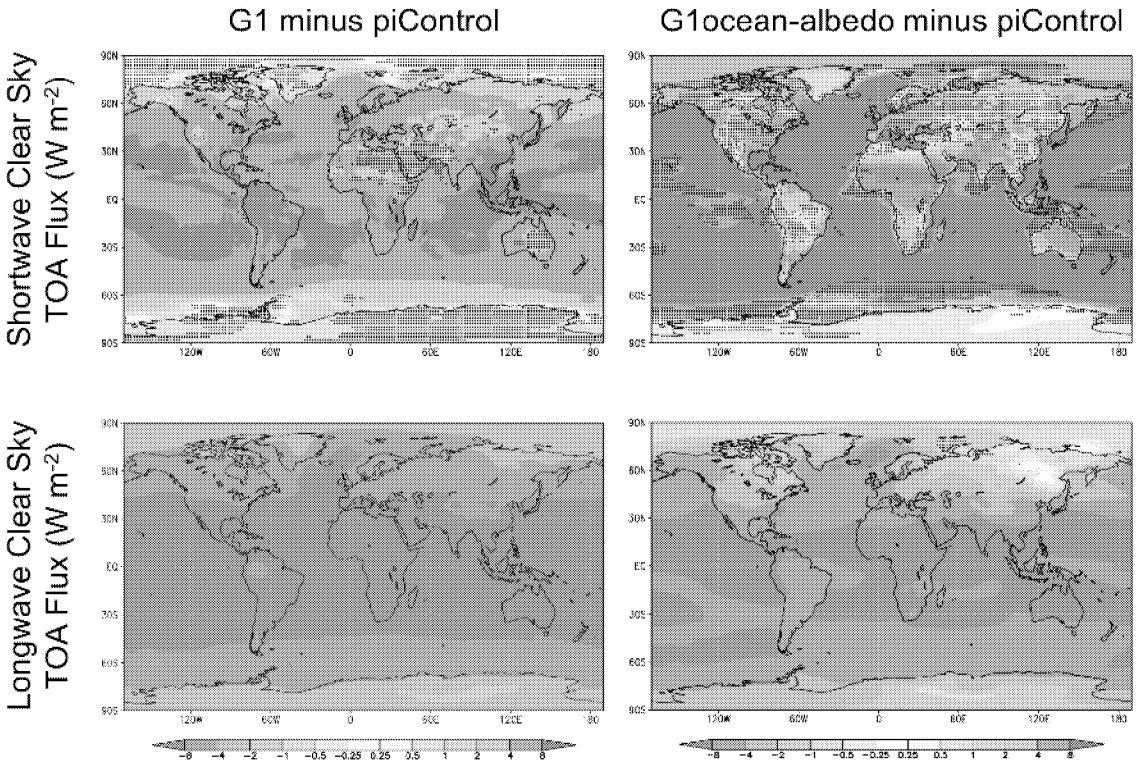

Figure 3. Shortwave (top) and longwave (bottom) net (downward minus upward) clear sky radiative flux changes at the top-of-atmosphere due to the G1 (left) and G1ocean-albedo perturbations, with positive values indicating more net downward flux. Positive values indicate that upward clear sky flux decreased in the perturbed (G1 or G1ocean-albedo) experiments, and negative values indicate that upward clear sky flux increased in the perturbed experiments.

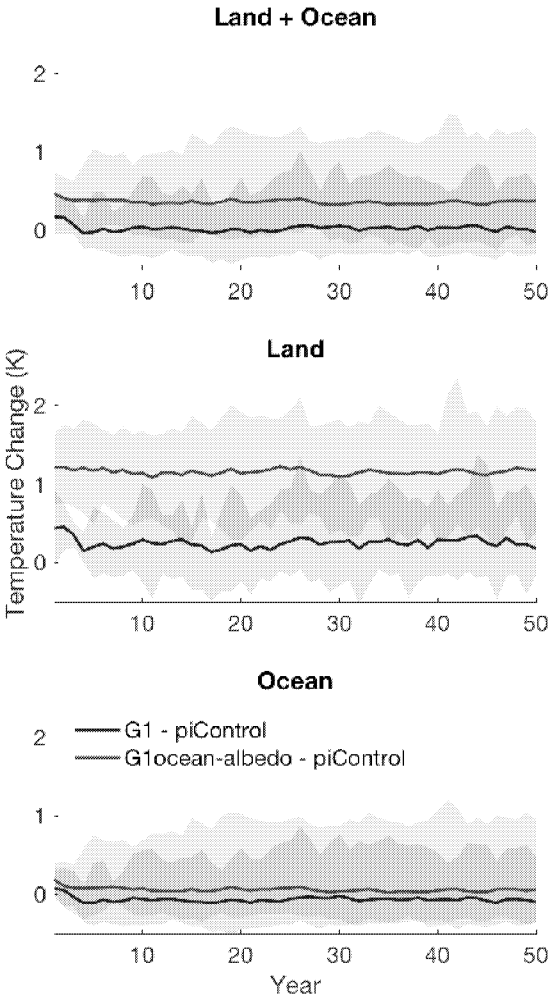

Figure 4. Global (top), land (middle), and ocean (bottom) average temperature change for the G1 (blue) and G1ocean-albedo (red) simulations. Lines show the all-model ensemble mean, and shading shows model spread (smallest to largest values).

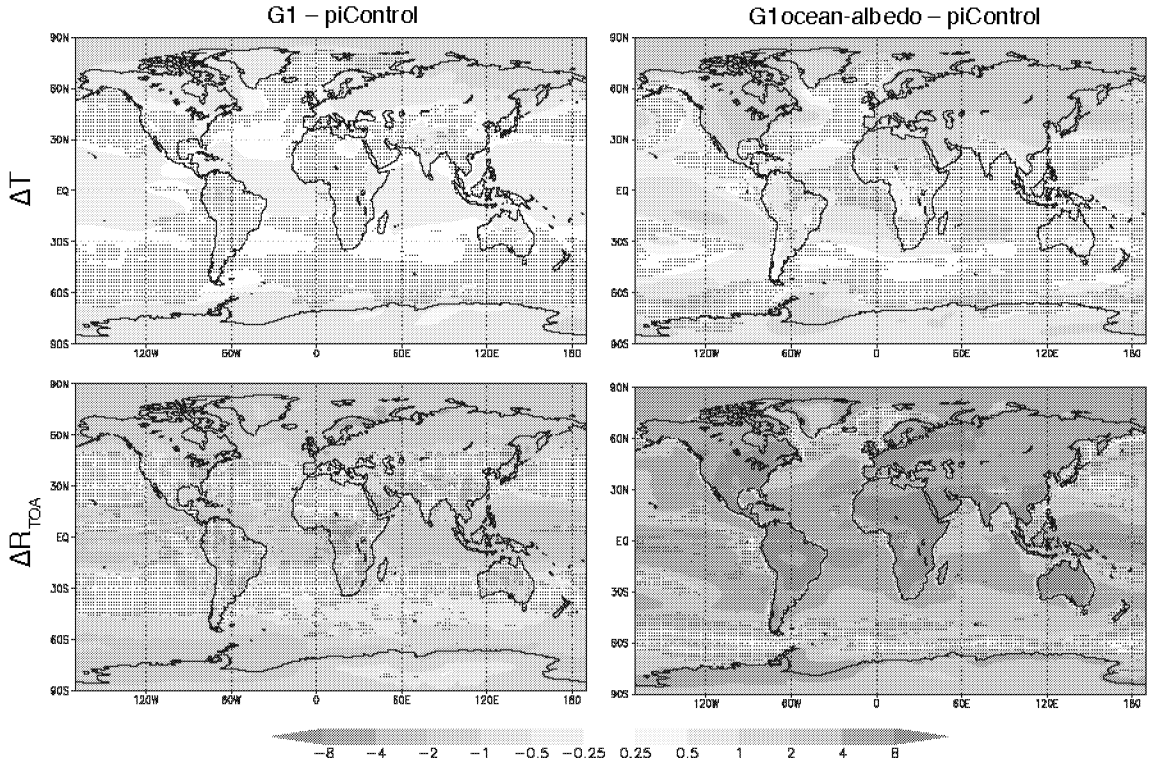

Figure 5. Surface air temperature (top row; K) and TOA net radiative flux (bottom row; W m^{-2}) changes for experiments G1 (left) and G1ocean-albedo (right). Values are averages over years 11-50 of simulation. Stippling indicates where fewer than 8 out of 11 models agree on the sign of the response.

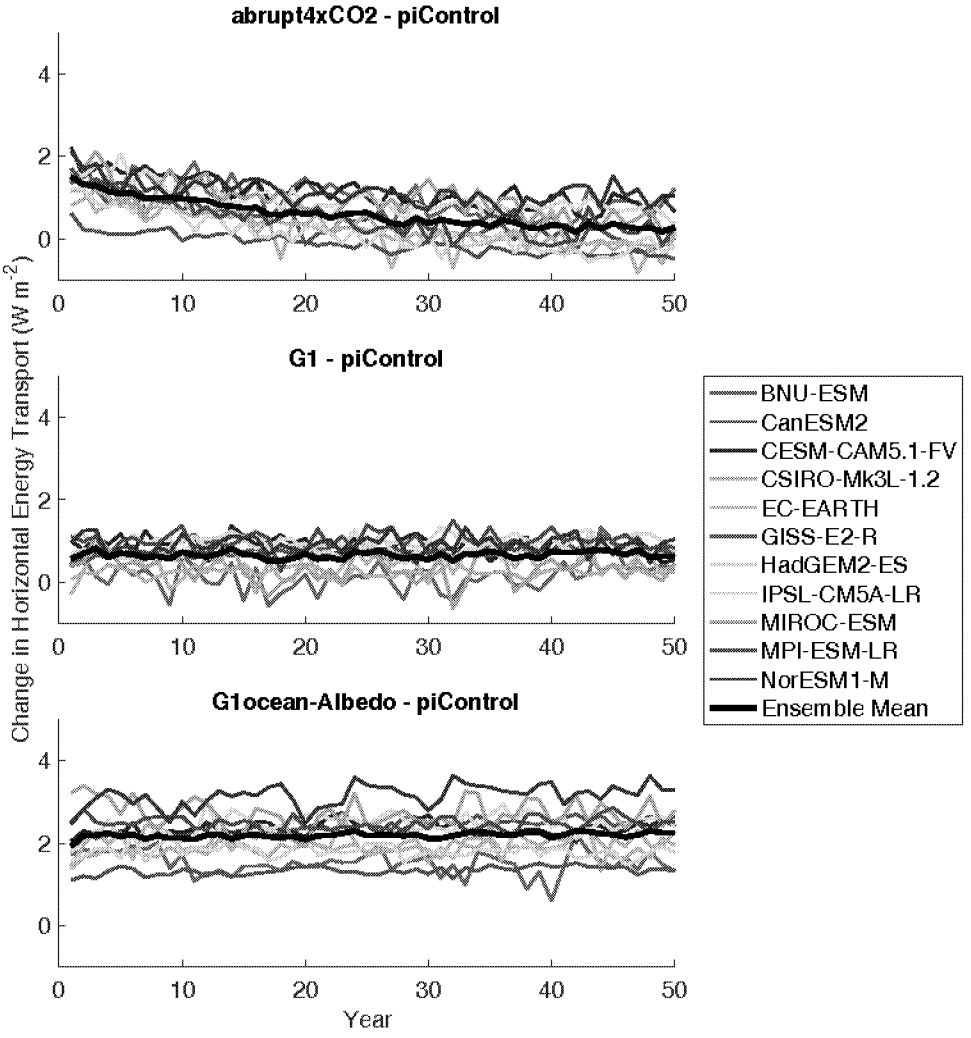

Figure 6. Annual mean change in land-ocean energy transport (Section 3.3; W m^{-2}) from piControl. See Equation 7 for a formal definition.

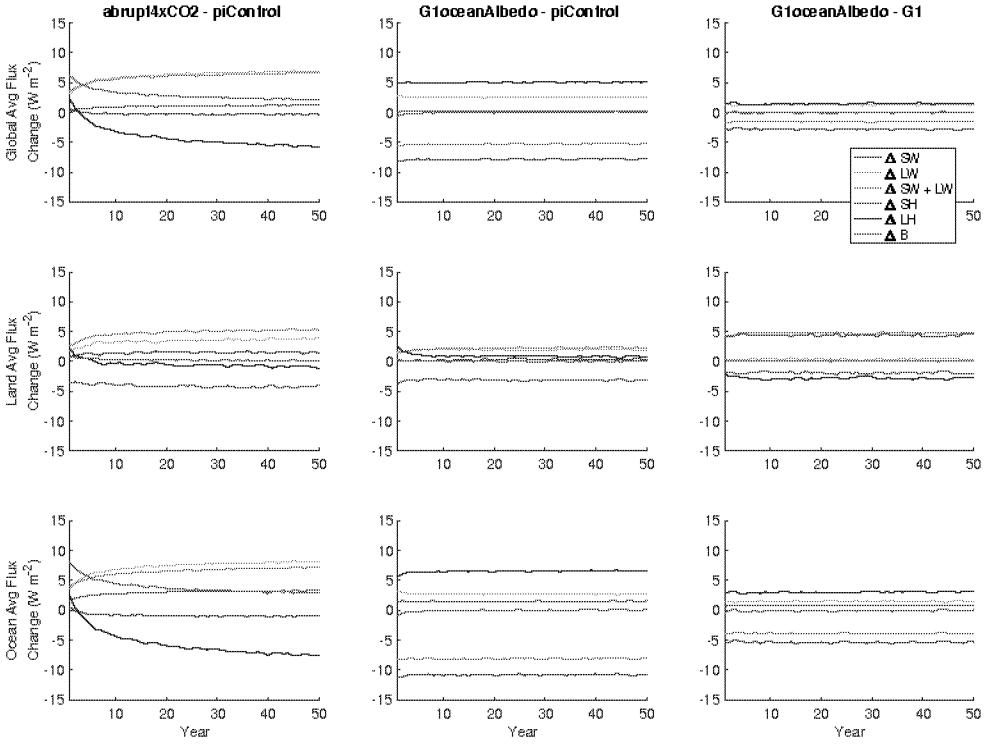

Figure 7. Annual mean time series of all-model mean surface fluxes (terms in Equation 3.8) for global averages (top), land averages (middle), and ocean averages (bottom). All fluxes are positive in the downward direction.

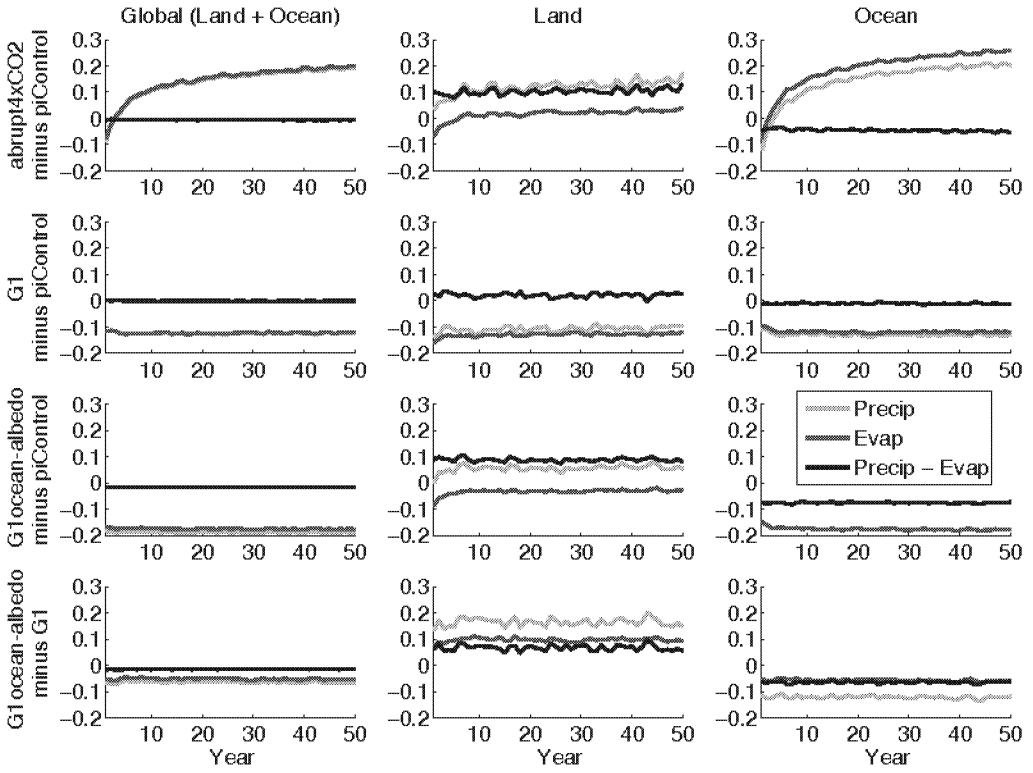

Figure 8. Annual mean time series of hydrological cycle changes (all in mm day^{-1}). Green lines show precipitation changes, red lines show evaporation changes, and black lines show precipitation minus evaporation. In the first column, green lines are difficult to see because they are largely overlaid by red lines. In the third row, third column, the green line has values below -0.2 for all years.

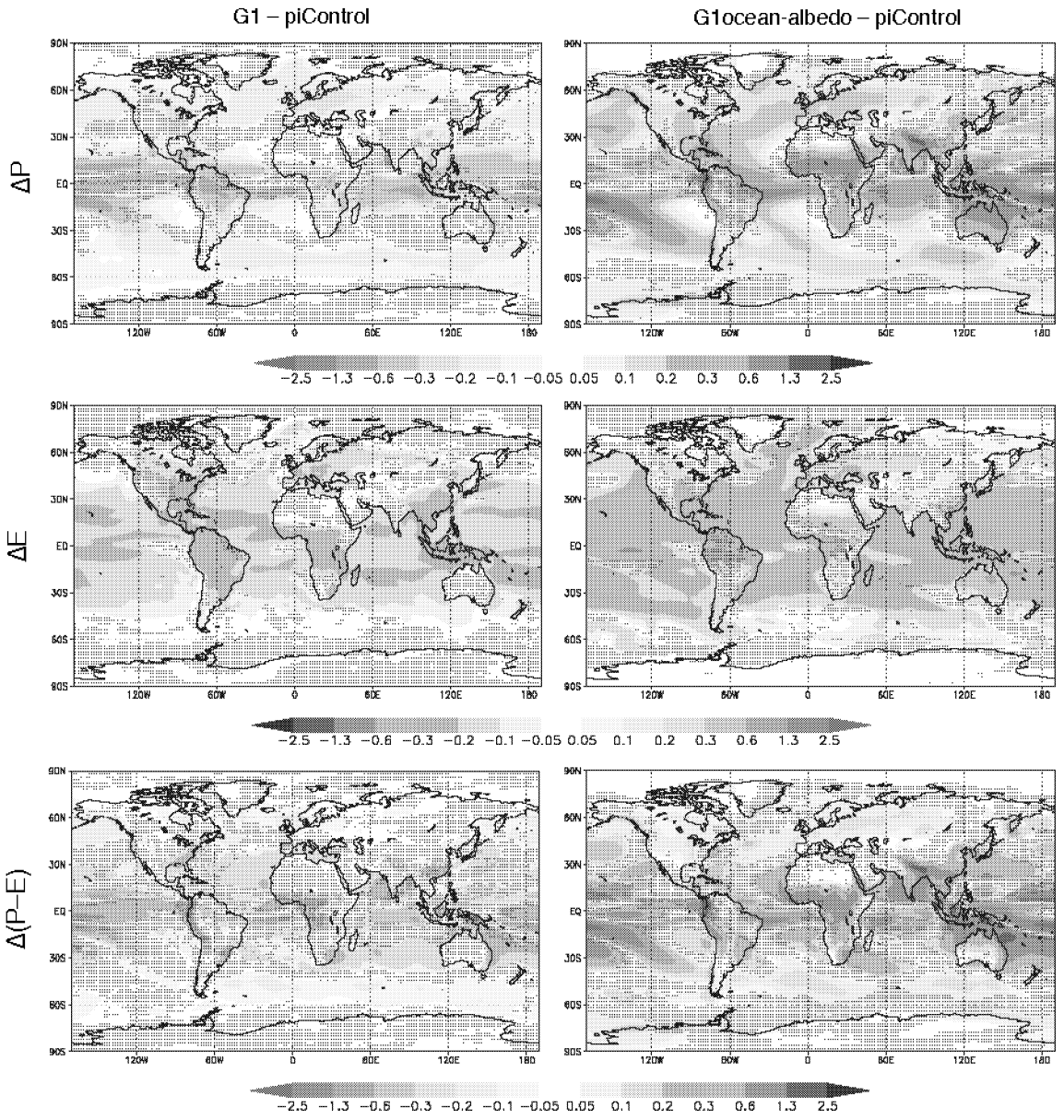

Figure 9. Precipitation (top row), evaporation (middle row), and precipitation minus evaporation (bottom row) changes (all panels have units mm day^{-1}) for experiments G1 and G1ocean-albedo. Values are averages over years 11-50 of simulation. Stippling indicates where fewer than 8 out of 11 models agree on the sign of the response.

The climate effects of increasing ocean albedo: An idealized representation of solar geoengineering
(Supplemental Online Material)

Ben Kravitz,[1*] Philip J. Rasch,[1] Hailong Wang,[1] Alan Robock,[2] Corey Gabriel,[3] Olivier Boucher,[4] Jason N. S. Cole,[5] Jim Haywood,[6,7] Duoying Ji,[8] Andy Jones,[6] Andrew Lenton,[9] John C. Moore,[8] Helene Muri,[10] Ulrike Niemeier,[11] Steven Phipps,[12,13] Hauke Schmidt,[11] Shingo Watanabe,[14] Shuting Yang,[15] and Jin-Ho Yoon[16]

[1]Atmospheric Sciences and Global Change Division, Pacific Northwest National Laboratory, Richland, WA, USA
[2]Department of Environmental Sciences, Rutgers University, New Brunswick, NJ, USA
[3]Scripps Institution of Oceanography, La Jolla, CA, USA
[4]Laboratoire de Météorologie Dynamique, Institut Pierre-Simon Laplace, CNRS / Université P. et M. Curie, Paris, France
[5]Environment and Climate Change Canada, Toronto, Canada
[6]Met Office Hadley Centre, Exeter, UK
[7]College of Engineering, Mathematics, and Physical Sciences, University of Exeter, Exeter, UK
[8]State Key Laboratory of Earth Surface Processes and Resource Ecology, College of Global Change and Earth System Science, Beijing Normal University, Beijing, China
[9]CSIRO Oceans and Atmosphere, Hobart, Tasmania, Australia
[10]Department of Geosciences, University of Oslo, Oslo, Norway
[11]Max Planck Institute for Meteorology, Hamburg, Germany
[12]Climate Change Research Centre, University of New South Wales, Sydney, Australia
[13]Institute for Marine and Antarctic Studies, University of Tasmania, Hobart, Tasmania, Australia
[14]Japan Agency for Marine-Earth Science and Technology, Yokohama, Japan
[15]Danish Meteorological Institute, Copenhagen, Denmark
[16]Gwangju Institute of Science and Technology, Gwangju, South Korea

Submission to *Atmospheric Chemistry and Physics*
Special Issue: The Geoengineering Model Intercomparison Project

[*]To whom correspondence should be addressed: P.O. Box 999, MSIN K9-30, Richland, WA 99352, USA. E-mail: ben.kravitz@pnnl.gov.

Table S1. Change in top-of-atmosphere net radiative flux (calculated as a difference from piControl), averaged over years 11-50. Units are in W m^{-2}. In each box, the top value is the global mean, the middle value is the land mean, and the bottom value is the ocean mean.

	abrupt4xCO2	G1	G1ocean-Albedo
BNU-ESM	2.7034 3.0115 2.5737	0.0225 1.1062 -0.4334	0.3902 8.6776 -3.0965
CanESM2	2.6143 0.9064 3.3572	0.0157 0.2731 -0.0964	-0.2090 7.8560 -3.7167
CESM-CAM5.1-FV	2.6255 3.4981 2.2672	-0.1285 2.0866 -1.0379	-1.4300 7.6058 -5.1396
CSIRO-Mk3L-1.2	2.6297 0.4771 3.5258	0.1231 0.6013 -0.0758	0.0185 6.4003 -2.6378
EC-Earth	2.2190 0.3640 2.1971	-0.2027 0.0434 -0.2245	-0.1969 5.7491 -2.5721
GISS-E2-R	2.4457 -0.7055 3.7458	-0.1763 -1.1029 0.2059	-0.0461 5.0568 -2.1515
HadGEM2-ES	2.4941 2.9576 2.3075	0.1978 2.5157 -0.7363	-0.0694 10.1434 -4.1839
IPSL-CM5A-LR	2.8225 -0.0944 4.0603	0.0842 0.1188 0.0695	-0.0730 6.6513 -2.9265
MIROC-ESM	3.6240 2.7807 3.6263	0.2318 -0.4711 0.2337	0.1329 9.4762 0.1060
MPI-ESM-LR	2.7332 1.2825 3.3211	0.1576 1.8587 -0.5319	0.0220 8.9188 -3.5837
NorESM1-M	2.4198 3.6437 1.9218	-0.0120 1.4902 -0.6234	-0.0986 8.2321 -3.4879
Model mean	2.6665 1.6474 2.9913	0.0285 0.7745 -0.2955	-0.1417 7.7061 -3.0355

Table S2. Temperature trend for each model over years 11-50, as calculated by ordinary linear regression. Units are in K per decade. In each box, the top value is the global mean, the middle value is the land mean, and the bottom value is the ocean mean.

	abrupt4xCO2	G1	G1ocean-Albedo
BNU-ESM	0.2702 0.2830 0.2649	0.0450 0.0877 0.0270	0.0441 0.0630 0.0361
CanESM2	0.2881 0.3193 0.2745	-0.0359 -0.0353 -0.0362	-0.0124 0.0086 -0.0215
CESM-CAM5.1-FV	0.2230 0.2195 0.2244	-0.0221 -0.0431 -0.0135	-0.0088 -0.0169 -0.0056
CSIRO-Mk3L-1.2	0.2395 0.2631 0.2297	0.0152 0.0185 0.0138	-0.0169 -0.0184 -0.0162
EC-Earth	0.2600 0.2890 0.2484	-0.0383 -0.0400 -0.0376	0.0369 0.0457 0.0334
GISS-E2-R	0.1029 0.0922 0.1073	0.0091 0.0097 0.0088	-0.0373 -0.0408 -0.0359
HadGEM2-ES	0.2976 0.3593 0.2727	0.0397 0.0551 0.0335	0.1075 0.1384 0.0950
IPSL-CM5A-LR	0.3782 0.4404 0.3518	0.0238 0.0278 0.0220	-0.0486 -0.0792 -0.0355
MIROC-ESM	0.3391 0.4033 0.3390	0.0161 0.0253 0.0161	-0.0251 -0.0216 -0.0251
MPI-ESM-LR	0.2214 0.2698 0.2019	0.0300 0.0497 0.0220	0.0196 0.0385 0.0119
NorESM1-M	0.1852 0.2180 0.1718	-0.0243 -0.0352 -0.0199	-0.0592 -0.0546 -0.0611
Model mean	0.2550 0.2870 0.2442	0.0053 0.0109 0.0033	-0.0000 0.0057 -0.0022

Table S3. Change (from piControl) in albedo as measured at the top of the atmosphere, averaged over years 11-50 of simulation. Calculations are differences in ratios of upward to downward shortwave radiative flux at TOA. Values in each box are (in order) ensemble minimum, ensemble mean, and ensemble maximum. All values are rounded to four decimal places.

	Global	Land	Ocean
abrupt4xCO2	-0.0243 -0.0130 0.0017	-0.0293 -0.0192 0.0031	-0.0239 -0.0104 0.0011
G1	-0.0096 -0.0067 -0.0036	-0.0130 -0.0074 0.0003	-0.0110 -0.0065 -0.0036
G1ocean-Albedo	-0.0036 0.0145 0.0232	-0.0271 -0.0068 0.0033	0.0061 0.0233 0.0334

Table S4. Change (from piControl) in surface albedo, averaged over years 11-50 of simulation. Calculations are differences in ratios of upward to downward shortwave radiative flux at the surface. Values in each box are (in order) ensemble minimum, ensemble mean, and ensemble maximum. All values are rounded to four decimal places.

	Global	Land	Ocean
abrupt4xCO2	-0.0358 -0.0193 -0.0063	-0.0414 -0.0216 -0.0112	-0.0336 -0.0184 -0.0043
G1	-0.0104 -0.0020 0.0006	-0.0154 -0.0034 0.0006	-0.0083 -0.0015 0.0010
G1ocean-Albedo	0.0340 0.0599 0.0927	-0.0214 -0.0020 0.0041	0.0568 0.0854 0.1317

Table S5. Change in surface air temperature (K) from piControl, averaged over years 11-50 of simulation. Values in each box are (in order) ensemble minimum, ensemble mean, and ensemble maximum. All values are rounded to four decimal places.

	Global	Land	Ocean
abrupt4xCO2	2.7921 4.4207 5.2867	4.0407 5.9323 7.3039	2.2780 3.7983 4.6467
G1	-0.3121 0.0219 0.6433	-0.2428 0.2405 0.8094	-0.3835 -0.0681 0.5749
G1ocean-Albedo	-0.1150 0.3595 1.2025	0.4061 1.1366 1.8263	-0.3296 0.0395 0.9456

Table S6. Change in TOA net radiative flux (W m^{-2}) from piControl, averaged over years 11-50 of simulation. Values in each box are (in order) ensemble minimum, ensemble mean, and ensemble maximum. All values are rounded to four decimal places.

	Global	Land	Ocean
abrupt4xCO2	2.2171 2.6543 3.6238	-0.6630 1.7063 3.6351	1.9168 3.0447 4.0082
G1	-0.2030 0.0296 0.2328	-1.0747 0.7384 2.4538	-1.0347 -0.2623 0.5433
G1ocean-Albedo	-1.4455 -0.1444 0.3850	4.8524 7.2214 9.7284	-5.1055 -3.1774 -2.0628

77 **Table S7.** Change in Horizontal Energy Transport (Section 3.4; W m^{-2}) from
78 piControl, averaged over years 11-50 of simulation.
79

	abrupt4xCO2	G1	G1ocean-Albedo
BNU-ESM	0.8841	0.1272	1.4590
CanESM2	0.2692	0.7860	2.4572
CESM-CAM5.1-FV	1.0178	0.8764	2.3648
CSIRO-Mk3L-1.2	0.1369	0.2559	1.8933
EC-Earth	0.0922	0.4281	2.0179
GISS-E2-R	-0.2096	0.7228	1.3489
HadGEM2-ES	0.8401	1.0271	2.5350
IPSL-CM5A-LR	-0.0402	0.8239	1.8023
MIROC-ESM	0.8100	0.2917	2.6708
MPI-ESM-LR	0.3462	0.9928	2.4516
NorESM1-M	1.0670	0.9204	3.2067
Model mean	0.4740	0.6593	2.2007

80

Table S8. Change in net shortwave radiative flux at the surface (W m^{-2}) from piControl, averaged over years 11-50 of simulation. Values in each box are (in order) ensemble minimum, ensemble mean, and ensemble maximum. All values are rounded to four decimal places.

	Global	Land	Ocean
abrupt4xCO2	-2.1671 -0.2830 1.8646	-3.5186 1.5559 4.1210	-3.0579 -1.0401 2.0111
G1	-6.4131 -5.0029 -4.0065	-6.5193 -4.0800 -1.6973	-6.6912 -5.3829 -3.6521
G1ocean-Albedo	-9.8711 -7.8274 -6.0680	-3.5994 -0.2060 2.7900	-13.0138 -10.9657 -8.5389

Table S9. Change in net longwave radiative flux at the surface (W m^{-2}) from piControl, averaged over years 11-50 of simulation. Values in each box are (in order) ensemble minimum, ensemble mean, and ensemble maximum. All values are rounded to four decimal places.

	Global	Land	Ocean
abrupt4xCO2	4.2188 6.6073 8.6313	1.8003 3.7548 6.3119	4.5272 7.7818 9.8035
G1	0.7702 1.2745 2.5119	0.3031 1.5366 3.6859	0.4394 1.1666 2.2724
G1ocean-Albedo	1.0227 2.5708 6.2470	-0.1474 2.0528 4.7390	0.9634 2.7840 7.2199

Table S10. Change in sensible heat flux from the surface to the atmosphere (positive upward; W m^{-2}) from piControl, averaged over years 11-50 of simulation. Values in each box are (in order) ensemble minimum, ensemble mean, and ensemble maximum. All values are rounded to four decimal places.

	Global	Land	Ocean
abrupt4xCO2	-2.3625 -1.1389 0.1424	0.7265 3.8471 6.6390	-4.4561 -3.1920 -2.2544
G1	-1.1581 -0.2061 0.8142	-1.7343 1.1302 3.8898	-1.0483 -0.7563 -0.2803
G1ocean-Albedo	-1.8505 -0.2028 1.0485	-0.9924 2.8650 6.0004	-2.2039 -1.4660 -0.3389

Table S11. Change in latent heat flux from the surface to the atmosphere (positive upward; W m^{-2}) from piControl, averaged over years 11-50 of simulation. Values in each box are (in order) ensemble minimum, ensemble mean, and ensemble maximum. All values are rounded to four decimal places.

	Global	Land	Ocean
abrupt4xCO2	1.3994 4.9044 7.2406	-4.7517 1.0980 6.5022	3.9322 6.4717 8.3796
G1	-5.9854 -3.5747 -1.2305	-8.6432 -3.6358 1.1154	-4.8910 -3.5496 -2.1965
G1ocean-Albedo	-7.2742 -5.0481 -2.1549	-6.4748 -1.0120 4.6424	-7.8862 -6.7101 -4.9538

105 **Table S12.** Change in ΔS (Equation 4; W m^{-2}) from piControl, averaged over years
106 11-50 of simulation. Values in each box are (in order) ensemble minimum,
107 ensemble mean, and ensemble maximum. All values are rounded to four decimal
108 places.
109

	Global	Land	Ocean
abrupt4xCO2	2.1704 2.5683 3.2566	-0.1485 0.2046 0.4413	2.9713 3.4356 3.9824
G1	-0.2053 0.0512 0.2856	-0.1232 -0.0380 0.0354	-0.2756 0.0834 0.3908
G1ocean-Albedo	-0.2915 0.0147 0.5674	-0.1350 -0.0084 0.1352	-0.3695 0.0229 0.7491

110

111 **Table S13.** Change in precipitation (mm day^{-1}) from piControl, averaged over years
112 11-50 of simulation. Values in each box are (in order) ensemble minimum,
113 ensemble mean, and ensemble maximum. All values are rounded to four decimal
114 places.
115

	Global	Land	Ocean
abrupt4xCO2	0.0483 0.1705 0.2769	-0.0833 0.1333 0.2393	0.0850 0.1858 0.3303
G1	-0.2069 -0.1245 -0.0563	-0.2757 -0.1052 -0.0137	-0.1907 -0.1325 -0.0739
G1ocean-Albedo	-0.2621 -0.1917 -0.1112	-0.1415 0.0515 0.1963	-0.3603 -0.2919 -0.2178

116

Table S14. Change in evaporation (mm day^{-1}) from piControl, averaged over years 11-50 of simulation. Values in each box are (in order) ensemble minimum, ensemble mean, and ensemble maximum. All values are rounded to four decimal places.

	Global	Land	Ocean
abrupt4xCO2	0.0484 0.1765 0.2770	-0.1642 0.0403 0.2261	0.1359 0.2326 0.3860
G1	-0.2069 -0.1234 -0.0424	-0.2987 -0.1256 0.0387	-0.1690 -0.1225 -0.0758
G1ocean-Albedo	-0.2514 -0.1752 -0.0744	-0.2238 -0.0356 0.1602	-0.2714 -0.2326 -0.1710

Table S15. Change in precipitation minus evaporation (mm day^{-1}) from piControl, averaged over years 11-50 of simulation. Values in each box are (in order) ensemble minimum, ensemble mean, and ensemble maximum. All values are rounded to four decimal places.

	Global	Land	Ocean
abrupt4xCO2	-0.0634 -0.0061 0.0016	-0.0076 0.0930 0.1994	-0.0863 -0.0468 -0.0081
G1	-0.0140 -0.0011 0.0012	-0.0524 0.0204 0.1059	-0.0435 -0.0100 0.0099
G1ocean-Albedo	-0.1877 -0.0166 0.0021	-0.1837 0.0871 0.1801	-0.1893 -0.0593 -0.0069

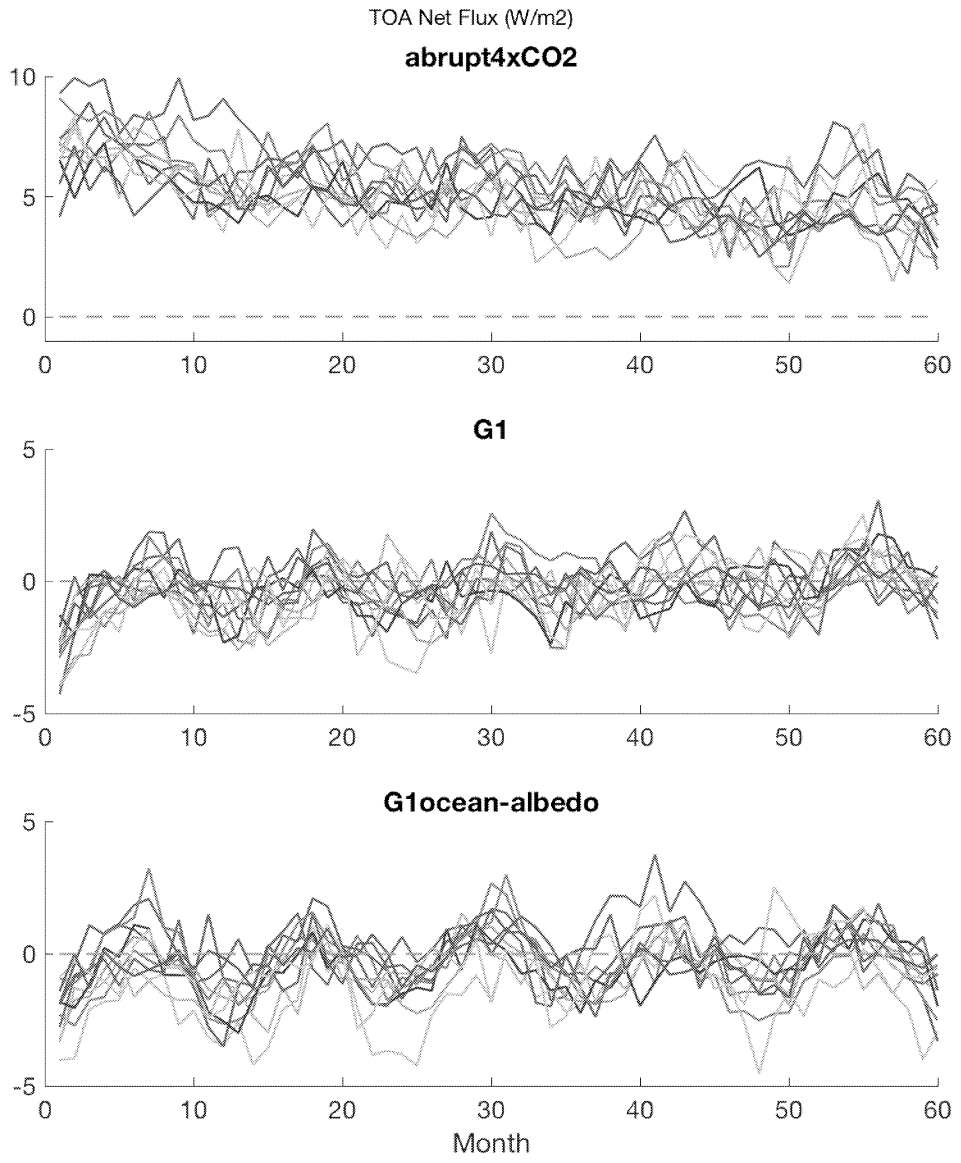

Figure S1. Top-of-atmosphere net radiative flux change (W m^{-2}) in the abrupt4xCO2 (top), G1 (middle), and G1ocean-albedo (bottom) experiments. Each color represents a different model. All values are subtracted month-by-month from the corresponding months of the preindustrial control simulation for the first 60 months (5 years) of simulation.

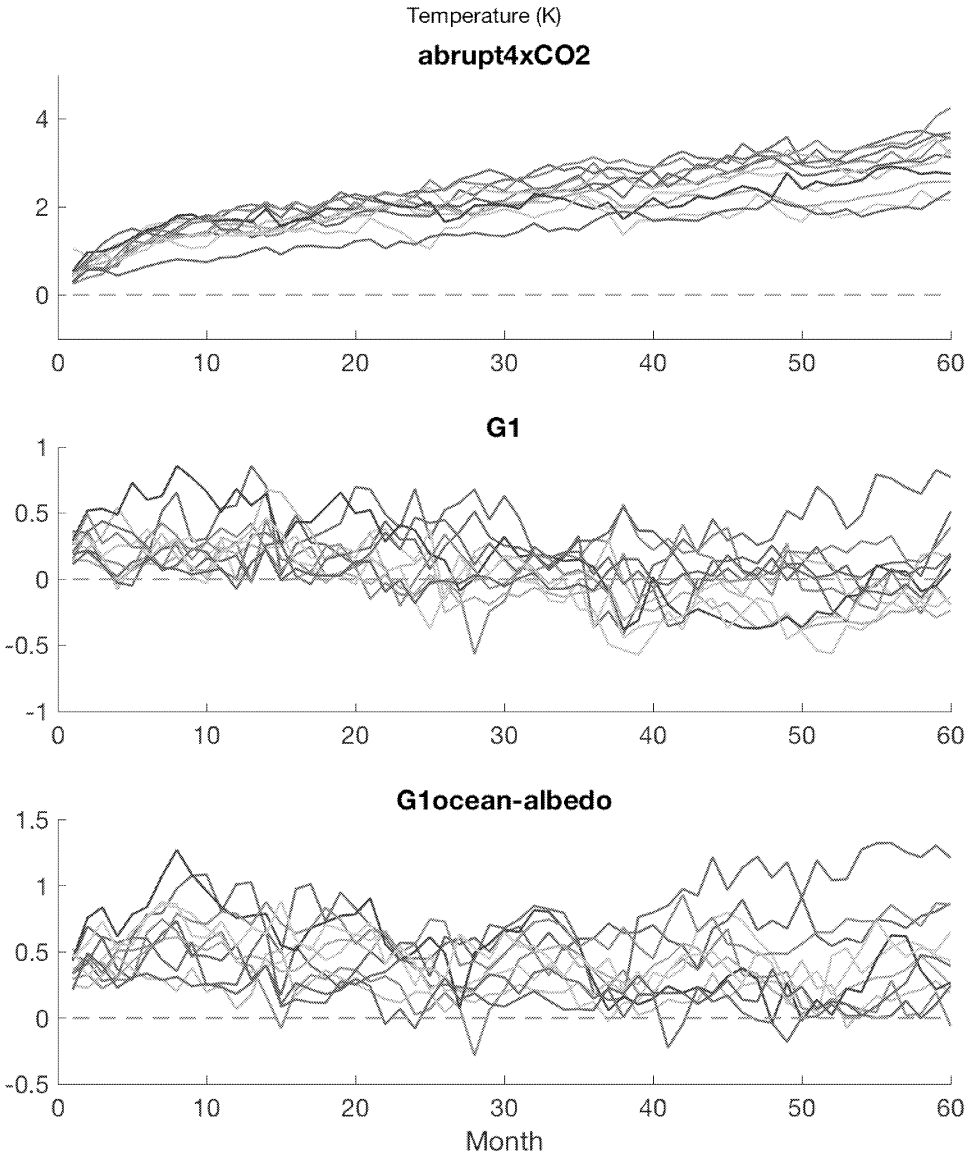

Figure S2. As in Figure S1 but for global mean temperature change (K).

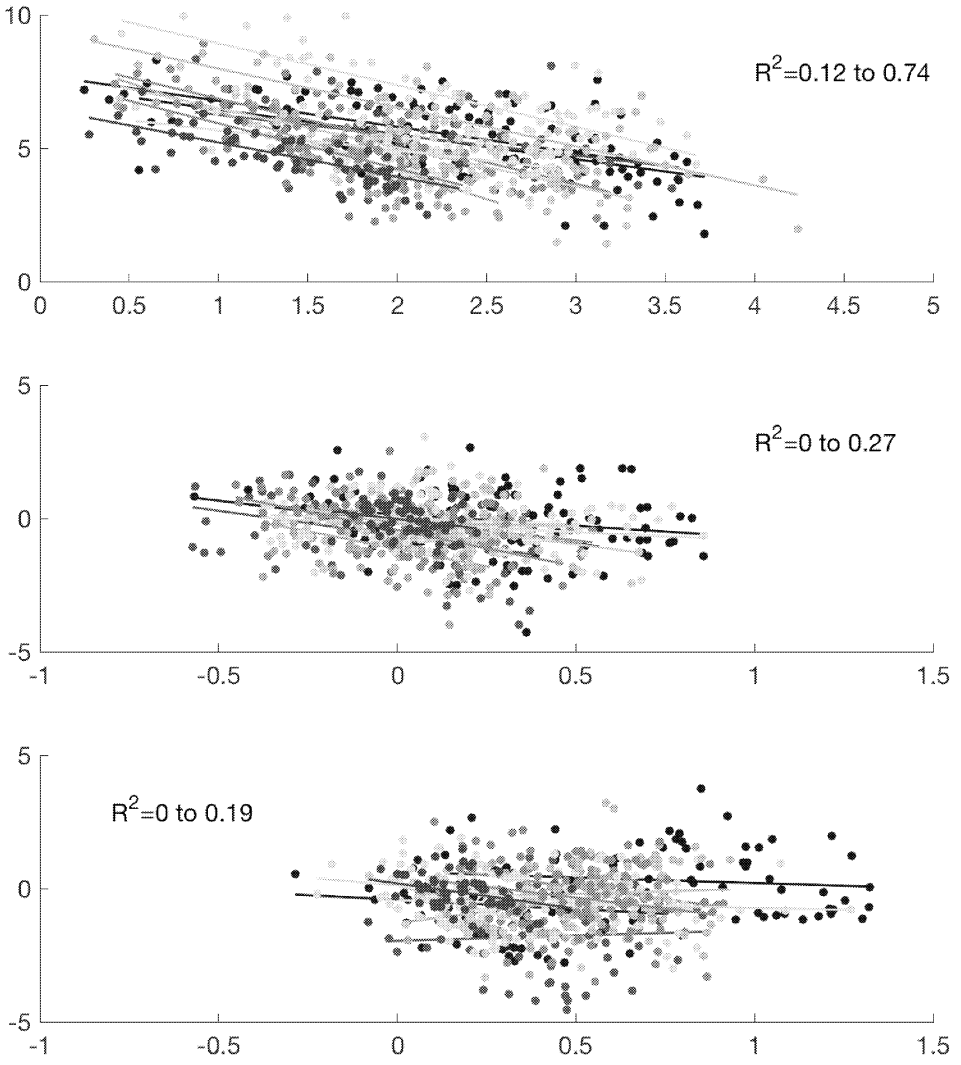

Figure S3. Gregory plots (Gregory et al., 2004), as described in Section 3.2 of the main text. All values are monthly averages over the first five years of simulation, essentially scatter plots of the values in Figures S1 and S2. Each color represents a different model. Lines are obtained through ordinary least squares regression through the points of the same color. R^2 ranges indicate the minimum and maximum R^2 value among the model ensemble in each panel.

The climate effects of increasing ocean albedo: An idealized representation of solar geoengineering
(Supplemental Online Material)

Ben Kravitz,[1*] Philip J. Rasch,[1] Hailong Wang,[1] Alan Robock,[2] Corey Gabriel,[3] Olivier Boucher,[4] Jason N. S. Cole,[5] Jim Haywood,[6,7] Duoying Ji,[8] Andy Jones,[6] Andrew Lenton,[9] John C. Moore,[8] Helene Muri,[10] Ulrike Niemeier,[11] Steven Phipps,[12,13] Hauke Schmidt,[11] Shingo Watanabe,[14] Shuting Yang,[15] and Jin-Ho Yoon[16]

[1]Atmospheric Sciences and Global Change Division, Pacific Northwest National Laboratory, Richland, WA, USA
[2]Department of Environmental Sciences, Rutgers University, New Brunswick, NJ, USA
[3]Scripps Institution of Oceanography, La Jolla, CA, USA
[4]Laboratoire de Météorologie Dynamique, Institut Pierre-Simon Laplace, CNRS / Université P. et M. Curie, Paris, France
[5]Environment and Climate Change Canada, Toronto, Canada
[6]Met Office Hadley Centre, Exeter, UK
[7]College of Engineering, Mathematics, and Physical Sciences, University of Exeter, Exeter, UK
[8]State Key Laboratory of Earth Surface Processes and Resource Ecology, College of Global Change and Earth System Science, Beijing Normal University, Beijing, China
[9]CSIRO Oceans and Atmosphere, Hobart, Tasmania, Australia
[10]Department of Geosciences, University of Oslo, Oslo, Norway
[11]Max Planck Institute for Meteorology, Hamburg, Germany
[12]Climate Change Research Centre, University of New South Wales, Sydney, Australia
[13]Institute for Marine and Antarctic Studies, University of Tasmania, Hobart, Tasmania, Australia
[14]Japan Agency for Marine-Earth Science and Technology, Yokohama, Japan
[15]Danish Meteorological Institute, Copenhagen, Denmark
[16]Gwangju Institute of Science and Technology, Gwangju, South Korea

Submission to *Atmospheric Chemistry and Physics*
Special Issue: The Geoengineering Model Intercomparison Project

[*]To whom correspondence should be addressed: P.O. Box 999, MSIN K9-30, Richland, WA 99352, USA. E-mail: ben.kravitz@pnnl.gov.

Table S1. Change in top-of-atmosphere net radiative flux (calculated as a difference from piControl), averaged over years 11-50. Units are in W m^{-2}. In each box, the top value is the global mean, the middle value is the land mean, and the bottom value is the ocean mean.

	abrupt4xCO2	G1	G1ocean-Albedo
BNU-ESM	2.7034 3.0115 2.5737	0.0225 1.1062 -0.4334	0.3902 8.6776 -3.0965
CanESM2	2.6143 0.9064 3.3572	0.0157 0.2731 -0.0964	-0.2090 7.8560 -3.7167
CESM-CAM5.1-FV	2.6255 3.4981 2.2672	-0.1285 2.0866 -1.0379	-1.4300 7.6058 -5.1396
CSIRO-Mk3L-1.2	2.6297 0.4771 3.5258	0.1231 0.6013 -0.0758	0.0185 6.4003 -2.6378
EC-Earth	2.2190 0.3640 2.1971	-0.2027 0.0434 -0.2245	-0.1969 5.7491 -2.5721
GISS-E2-R	2.4457 -0.7055 3.7458	-0.1763 -1.1029 0.2059	-0.0461 5.0568 -2.1515
HadGEM2-ES	2.4941 2.9576 2.3075	0.1978 2.5157 -0.7363	-0.0694 10.1434 -4.1839
IPSL-CM5A-LR	2.8225 -0.0944 4.0603	0.0842 0.1188 0.0695	-0.0730 6.6513 -2.9265
MIROC-ESM	3.6240 2.7807 3.6263	0.2318 -0.4711 0.2337	0.1329 9.4762 0.1060
MPI-ESM-LR	2.7332 1.2825 3.3211	0.1576 1.8587 -0.5319	0.0220 8.9188 -3.5837
NorESM1-M	2.4198 3.6437 1.9218	-0.0120 1.4902 -0.6234	-0.0986 8.2321 -3.4879
Model mean	2.6665 1.6474 2.9913	0.0285 0.7745 -0.2955	-0.1417 7.7061 -3.0355

Table S2. Temperature trend for each model over years 11-50, as calculated by ordinary linear regression. Units are in K per decade. In each box, the top value is the global mean, the middle value is the land mean, and the bottom value is the ocean mean.

	abrupt4xCO2	G1	G1ocean-Albedo
BNU-ESM	0.2702 0.2830 0.2649	0.0450 0.0877 0.0270	0.0441 0.0630 0.0361
CanESM2	0.2881 0.3193 0.2745	-0.0359 -0.0353 -0.0362	-0.0124 0.0086 -0.0215
CESM-CAM5.1-FV	0.2230 0.2195 0.2244	-0.0221 -0.0431 -0.0135	-0.0088 -0.0169 -0.0056
CSIRO-Mk3L-1.2	0.2395 0.2631 0.2297	0.0152 0.0185 0.0138	-0.0169 -0.0184 -0.0162
EC-Earth	0.2600 0.2890 0.2484	-0.0383 -0.0400 -0.0376	0.0369 0.0457 0.0334
GISS-E2-R	0.1029 0.0922 0.1073	0.0091 0.0097 0.0088	-0.0373 -0.0408 -0.0359
HadGEM2-ES	0.2976 0.3593 0.2727	0.0397 0.0551 0.0335	0.1075 0.1384 0.0950
IPSL-CM5A-LR	0.3782 0.4404 0.3518	0.0238 0.0278 0.0220	-0.0486 -0.0792 -0.0355
MIROC-ESM	0.3391 0.4033 0.3390	0.0161 0.0253 0.0161	-0.0251 -0.0216 -0.0251
MPI-ESM-LR	0.2214 0.2698 0.2019	0.0300 0.0497 0.0220	0.0196 0.0385 0.0119
NorESM1-M	0.1852 0.2180 0.1718	-0.0243 -0.0352 -0.0199	-0.0592 -0.0546 -0.0611
Model mean	0.2550 0.2870 0.2442	0.0053 0.0109 0.0033	-0.0000 0.0057 -0.0022

Table S3. Change (from piControl) in albedo as measured at the top of the atmosphere, averaged over years 11-50 of simulation. Calculations are differences in ratios of upward to downward shortwave radiative flux at TOA. Values in each box are (in order) ensemble minimum, ensemble mean, and ensemble maximum. All values are rounded to four decimal places.

	Global	Land	Ocean
abrupt4xCO2	-0.0243 -0.0130 0.0017	-0.0293 -0.0192 0.0031	-0.0239 -0.0104 0.0011
G1	-0.0096 -0.0067 -0.0036	-0.0130 -0.0074 0.0003	-0.0110 -0.0065 -0.0036
G1ocean-Albedo	-0.0036 0.0145 0.0232	-0.0271 -0.0068 0.0033	0.0061 0.0233 0.0334

Table S4. Change (from piControl) in surface albedo, averaged over years 11-50 of simulation. Calculations are differences in ratios of upward to downward shortwave radiative flux at the surface. Values in each box are (in order) ensemble minimum, ensemble mean, and ensemble maximum. All values are rounded to four decimal places.

	Global	Land	Ocean
abrupt4xCO2	-0.0358 -0.0193 -0.0063	-0.0414 -0.0216 -0.0112	-0.0336 -0.0184 -0.0043
G1	-0.0104 -0.0020 0.0006	-0.0154 -0.0034 0.0006	-0.0083 -0.0015 0.0010
G1ocean-Albedo	0.0340 0.0599 0.0927	-0.0214 -0.0020 0.0041	0.0568 0.0854 0.1317

Table S5. Change in surface air temperature (K) from piControl, averaged over years 11-50 of simulation. Values in each box are (in order) ensemble minimum, ensemble mean, and ensemble maximum. All values are rounded to four decimal places.

	Global	Land	Ocean
abrupt4xCO2	2.7921 4.4207 5.2867	4.0407 5.9323 7.3039	2.2780 3.7983 4.6467
G1	-0.3121 0.0219 0.6433	-0.2428 0.2405 0.8094	-0.3835 -0.0681 0.5749
G1ocean-Albedo	-0.1150 0.3595 1.2025	0.4061 1.1366 1.8263	-0.3296 0.0395 0.9456

Table S6. Change in TOA net radiative flux (W m^{-2}) from piControl, averaged over years 11-50 of simulation. Values in each box are (in order) ensemble minimum, ensemble mean, and ensemble maximum. All values are rounded to four decimal places.

	Global	Land	Ocean
abrupt4xCO2	2.2171 2.6543 3.6238	-0.6630 1.7063 3.6351	1.9168 3.0447 4.0082
G1	-0.2030 0.0296 0.2328	-1.0747 0.7384 2.4538	-1.0347 -0.2623 0.5433
G1ocean-Albedo	-1.4455 -0.1444 0.3850	4.8524 7.2214 9.7284	-5.1055 -3.1774 -2.0628

77 **Table S7.** Change in Horizontal Energy Transport (Section 3.3; W m^{-2}) from
78 piControl, averaged over years 11-50 of simulation.
79

	abrupt4xCO2	G1	G1ocean-Albedo
BNU-ESM	0.8841	0.1272	1.4590
CanESM2	0.2692	0.7860	2.4572
CESM-CAM5.1-FV	1.0178	0.8764	2.3648
CSIRO-Mk3L-1.2	0.1369	0.2559	1.8933
EC-Earth	0.0922	0.4281	2.0179
GISS-E2-R	-0.2096	0.7228	1.3489
HadGEM2-ES	0.8401	1.0271	2.5350
IPSL-CM5A-LR	-0.0402	0.8239	1.8023
MIROC-ESM	0.8100	0.2917	2.6708
MPI-ESM-LR	0.3462	0.9928	2.4516
NorESM1-M	1.0670	0.9204	3.2067
Model mean	0.4740	0.6593	2.2007

80

Table S8. Change in net shortwave radiative flux at the surface (W m^{-2}) from piControl, averaged over years 11-50 of simulation. Values in each box are (in order) ensemble minimum, ensemble mean, and ensemble maximum. All values are rounded to four decimal places.

	Global	Land	Ocean
abrupt4xCO2	-2.1671 -0.2830 1.8646	-3.5186 1.5559 4.1210	-3.0579 -1.0401 2.0111
G1	-6.4131 -5.0029 -4.0065	-6.5193 -4.0800 -1.6973	-6.6912 -5.3829 -3.6521
G1ocean-Albedo	-9.8711 -7.8274 -6.0680	-3.5994 -0.2060 2.7900	-13.0138 -10.9657 -8.5389

Table S9. Change in net longwave radiative flux at the surface (W m^{-2}) from piControl, averaged over years 11-50 of simulation. Values in each box are (in order) ensemble minimum, ensemble mean, and ensemble maximum. All values are rounded to four decimal places.

	Global	Land	Ocean
abrupt4xCO2	4.2188 6.6073 8.6313	1.8003 3.7548 6.3119	4.5272 7.7818 9.8035
G1	0.7702 1.2745 2.5119	0.3031 1.5366 3.6859	0.4394 1.1666 2.2724
G1ocean-Albedo	1.0227 2.5708 6.2470	-0.1474 2.0528 4.7390	0.9634 2.7840 7.2199

Table S10. Change in sensible heat flux from the surface to the atmosphere (positive upward; W m^{-2}) from piControl, averaged over years 11-50 of simulation. Values in each box are (in order) ensemble minimum, ensemble mean, and ensemble maximum. All values are rounded to four decimal places.

	Global	Land	Ocean
abrupt4xCO2	-2.3625 -1.1389 0.1424	0.7265 3.8471 6.6390	-4.4561 -3.1920 -2.2544
G1	-1.1581 -0.2061 0.8142	-1.7343 1.1302 3.8898	-1.0483 -0.7563 -0.2803
G1ocean-Albedo	-1.8505 -0.2028 1.0485	-0.9924 2.8650 6.0004	-2.2039 -1.4660 -0.3389

Table S11. Change in latent heat flux from the surface to the atmosphere (positive upward; W m^{-2}) from piControl, averaged over years 11-50 of simulation. Values in each box are (in order) ensemble minimum, ensemble mean, and ensemble maximum. All values are rounded to four decimal places.

	Global	Land	Ocean
abrupt4xCO2	1.3994 4.9044 7.2406	-4.7517 1.0980 6.5022	3.9322 6.4717 8.3796
G1	-5.9854 -3.5747 -1.2305	-8.6432 -3.6358 1.1154	-4.8910 -3.5496 -2.1965
G1ocean-Albedo	-7.2742 -5.0481 -2.1549	-6.4748 -1.0120 4.6424	-7.8862 -6.7101 -4.9538

105 **Table S12.** Change in ΔB (Equation 8; W m^{-2}) from piControl, averaged over years
106 11-50 of simulation. Values in each box are (in order) ensemble minimum,
107 ensemble mean, and ensemble maximum. All values are rounded to four decimal
108 places.
109

	Global	Land	Ocean
abrupt4xCO2	2.1704 2.5683 3.2566	-0.1485 0.2046 0.4413	2.9713 3.4356 3.9824
G1	-0.2053 0.0512 0.2856	-0.1232 -0.0380 0.0354	-0.2756 0.0834 0.3908
G1ocean-Albedo	-0.2915 0.0147 0.5674	-0.1350 -0.0084 0.1352	-0.3695 0.0229 0.7491

110

111 **Table S13.** Change in precipitation (mm day^{-1}) from piControl, averaged over years
112 11-50 of simulation. Values in each box are (in order) ensemble minimum,
113 ensemble mean, and ensemble maximum. All values are rounded to four decimal
114 places.
115

	Global	Land	Ocean
abrupt4xCO2	0.0483 0.1705 0.2769	-0.0833 0.1333 0.2393	0.0850 0.1858 0.3303
G1	-0.2069 -0.1245 -0.0563	-0.2757 -0.1052 -0.0137	-0.1907 -0.1325 -0.0739
G1ocean-Albedo	-0.2621 -0.1917 -0.1112	-0.1415 0.0515 0.1963	-0.3603 -0.2919 -0.2178

116

Table S14. Change in evaporation (mm day^{-1}) from piControl, averaged over years 11-50 of simulation. Values in each box are (in order) ensemble minimum, ensemble mean, and ensemble maximum. All values are rounded to four decimal places.

	Global	Land	Ocean
abrupt4xCO2	0.0484 0.1765 0.2770	-0.1642 0.0403 0.2261	0.1359 0.2326 0.3860
G1	-0.2069 -0.1234 -0.0424	-0.2987 -0.1256 0.0387	-0.1690 -0.1225 -0.0758
G1ocean-Albedo	-0.2514 -0.1752 -0.0744	-0.2238 -0.0356 0.1602	-0.2714 -0.2326 -0.1710

123 **Table S15.** Change in precipitation minus evaporation (mm day^{-1}) from piControl,
124 averaged over years 11-50 of simulation. Values in each box are (in order)
125 ensemble minimum, ensemble mean, and ensemble maximum. All values are
126 rounded to four decimal places.
127

	Global	Land	Ocean
abrupt4xCO2	-0.0634 -0.0061 0.0016	-0.0076 0.0930 0.1994	-0.0863 -0.0468 -0.0081
G1	-0.0140 -0.0011 0.0012	-0.0524 0.0204 0.1059	-0.0435 -0.0100 0.0099
G1ocean-Albedo	-0.1877 -0.0166 0.0021	-0.1837 0.0871 0.1801	-0.1893 -0.0593 -0.0069

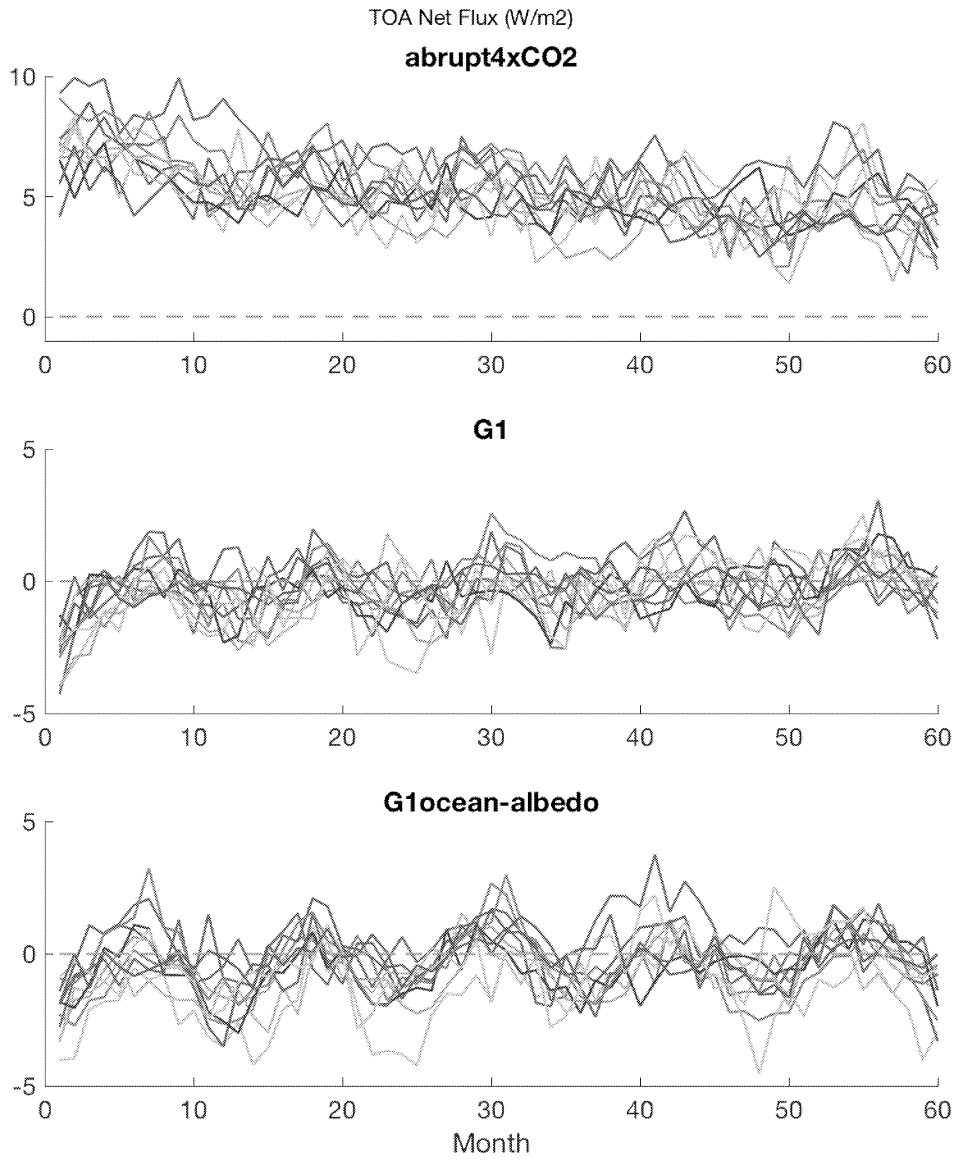

Figure S1. Top-of-atmosphere net radiative flux change (W m^{-2}) in the abrupt4xCO2 (top), G1 (middle), and G1ocean-albedo (bottom) experiments. Each color represents a different model. All values are subtracted month-by-month from the corresponding months of the preindustrial control simulation for the first 60 months (5 years) of simulation.

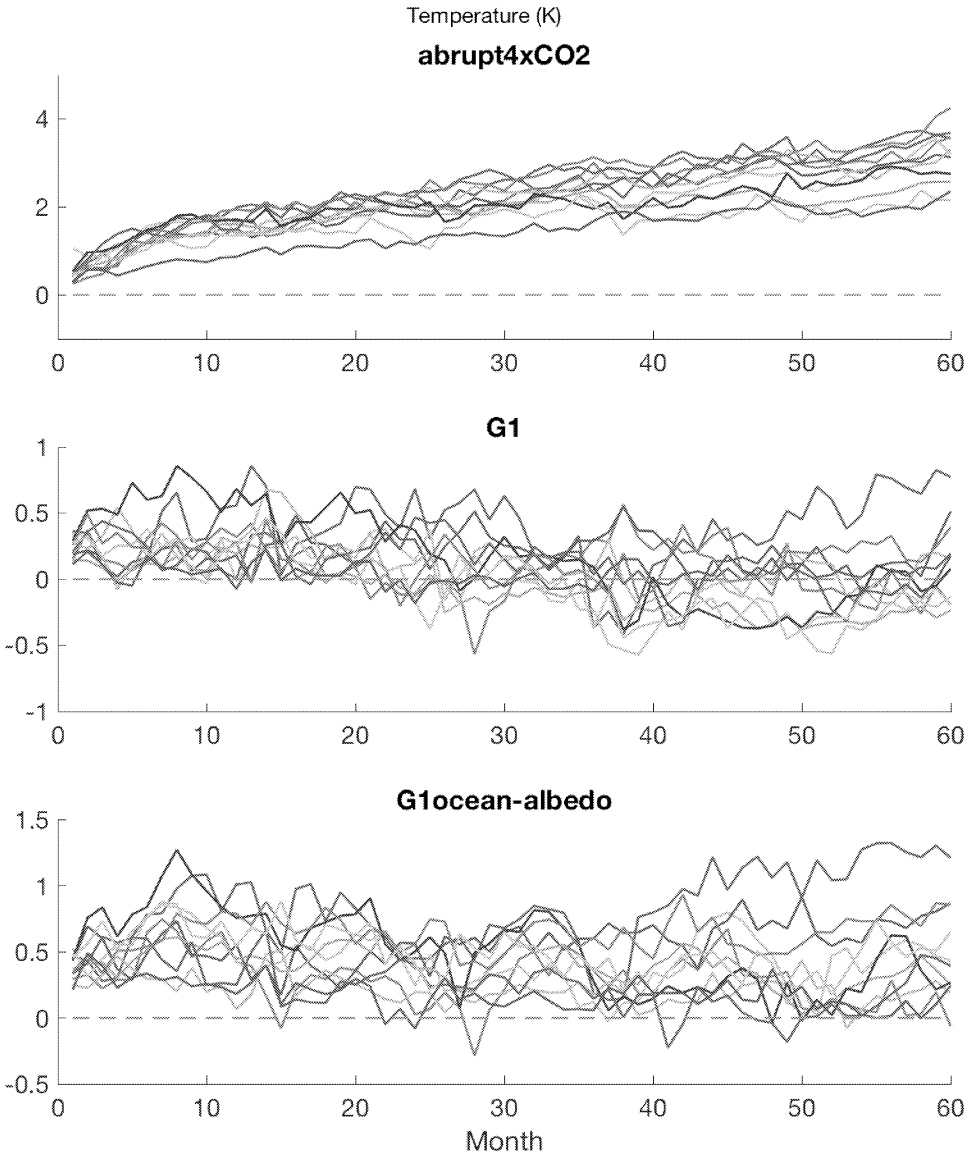

Figure S2. As in Figure S1 but for global mean temperature change (K).

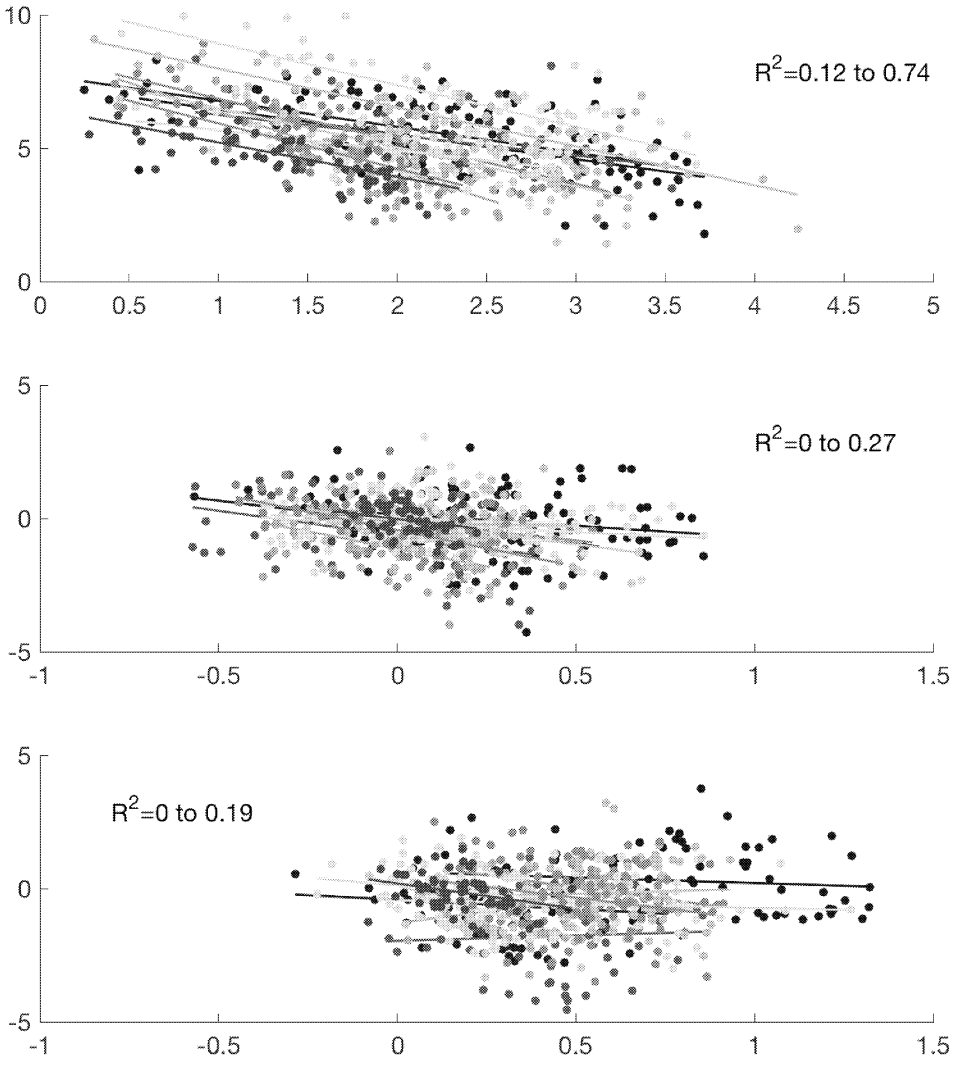

Figure S3. Gregory plots (Gregory et al., 2004), as described in Section 3.2 of the main text. Top panel corresponds to abrupt4xCO2, middle panel corresponds to G1, and bottom panel corresponds to G1ocean-albedo. All values are monthly averages over the first five years of simulation, essentially scatter plots of the values in Figures S1 (net TOA radiative flux change; y-axis in this figure) and S2 (global mean temperature change; x-axis in this figure). Each color represents a different model. Lines are obtained through ordinary least squares regression through the points of the same color. R^2 ranges indicate the minimum and maximum R^2 value among the model ensemble in each panel.

The climate effects of increasing ocean albedo: An idealized representation of solar geoengineering

Ben Kravitz,[1*] Philip J. Rasch,[1] Hailong Wang,[1] Alan Robock,[2] Corey Gabriel,[3] Olivier Boucher,[4] Jason N. S. Cole,[5] Jim Haywood,[6,7] Duoying Ji,[8] Andy Jones,[6] Andrew Lenton,[9] John C. Moore,[8] Helene Muri,[10] Ulrike Niemeier,[11] Steven Phipps,[12,13] Hauke Schmidt,[11] Shingo Watanabe,[14] Shuting Yang,[15] and Jin-Ho Yoon[16]

[1]Atmospheric Sciences and Global Change Division, Pacific Northwest National Laboratory, Richland, WA, USA
[2]Department of Environmental Sciences, Rutgers University, New Brunswick, NJ, USA
[3]Scripps Institution of Oceanography, La Jolla, CA, USA
[4]Laboratoire de Météorologie Dynamique, Institut Pierre-Simon Laplace, CNRS / Université P. et M. Curie, Paris, France
[5]Environment and Climate Change Canada, Toronto, Canada
[6]Met Office Hadley Centre, Exeter, UK
[7]College of Engineering, Mathematics, and Physical Sciences, University of Exeter, Exeter, UK
[8]State Key Laboratory of Earth Surface Processes and Resource Ecology, College of Global Change and Earth System Science, Beijing Normal University, Beijing, China
[9]CSIRO Oceans and Atmosphere, Hobart, Tasmania, Australia
[10]Department of Geosciences, University of Oslo, Oslo, Norway
[11]Max Planck Institute for Meteorology, Hamburg, Germany
[12]Climate Change Research Centre, University of New South Wales, Sydney, Australia
[13]Institute for Marine and Antarctic Studies, University of Tasmania, Hobart, Tasmania, Australia
[14]Japan Agency for Marine-Earth Science and Technology, Yokohama, Japan
[15]Danish Meteorological Institute, Copenhagen, Denmark
[16]Gwangju Institute of Science and Technology, Gwangju, South Korea

Submission to *Atmospheric Chemistry and Physics*
Special Issue: The Geoengineering Model Intercomparison Project

[*]To whom correspondence should be addressed: P.O. Box 999, MSIN K9-30, Richland, WA 99352, USA. E-mail: ben.kravitz@pnnl.gov.

Abstract. Marine cloud brightening has been proposed as a means of geoengineering, or deliberately altering the climate system to offset climate change. As an idealized representation of marine cloud brightening, this paper discusses experiment G1ocean-albedo of the Geoengineering Model Intercomparison Project (GeoMIP), involving an abrupt quadrupling of the CO_2 concentration and an instantaneous increase in ocean albedo to maintain approximate net top-of-atmosphere radiative flux balance. Eleven Earth System Models are relatively consistent in their temperature, radiative flux, and hydrological cycle responses to this experiment. Due to the imposed forcing, the land surface warms by 1.14°C, while most of the ocean cools. Some parts of the near-surface air temperature over ocean warm due to heat transport from land to ocean. These changes generally resolve within a few years, indicating that changes in ocean heat content play at most a small role in the warming over the oceans. The hydrological cycle response is a general slowing down, with little net change in large-scale precipitation minus evaporation, but also with substantial heterogeneity. While idealized, these results have important implications for marine cloud brightening or any other method of geoengineering involving spatially heterogeneous forcing, particularly if that forcing has a strong land/ocean contrast.

Main points:

1) Under an increase in the CO_2 concentration and ocean albedo, the climate transitions to a new, warmer steady state.
2) The land surface warms substantially, and oceans near the land warm due to heat transport
3) The hydrological cycle slows down, with regional heterogeneity in the response

Suggested reviewers:

Tim Andrews
Olivier Geoffroy
Govindasamy Bala

1. Introduction

Geoengineering (also called "climate intervention") describes a set of technological approaches to reduce the effects of climate change by deliberately intervening in the climate system (e.g., Shepherd et al., 2009). There are two broad categories of geoengineering that are commonly discussed: solar geoengineering (modifying the amount of shortwave radiation incident at the surface; NAS, 2015a) and carbon dioxide removal (NAS, 2015b). There are also proposals, such as cirrus cloud thinning (Mitchell and Finnegan, 2009) that do not fit neatly into either of these two categories. In all subsequent discussions in this manuscript, we only discuss solar geoengineering methods.

Two of the most commonly proposed methods of global geoengineering are stratospheric sulfate aerosol injection (SAI) and marine cloud brightening (MCB). Comparison of the different climate effects of these two methods (e.g., Niemeier et al., 2013; Crook et al., 2015) reveals that, among other things, the spatial distributions of the applied forcings strongly affect the climate effects. Many of the effects of SAI can be reasonably well approximated by a uniform reduction in shortwave radiative flux reaching the surface (Kalidindi et al., 2015). Conversely, MCB targets low clouds over oceans (Latham, 1990), which are not ubiquitous. In addition, there are higher order effects due to the altitude at which the shortwave scattering occurs, including multiple scattering effects, infrared absorption of shortwave and longwave radiative flux by sulfate aerosols or cloud particles, and absorption of shortwave radiative flux by atmospheric CO_2 and water vapor (e.g., Kravitz et al., 2013b).

Idealized simulations of solar geoengineering are useful in the context of multi-model intercomparisons, in that they capture many of the effects of more complicated methods of representing geoengineering, yet can be performed by a wide variety of models. In simulations conducted under the Geoengineering Model Intercomparison Project (GeoMIP; Kravitz et al., 2011), an idealized method of representing SAI is via reductions in total solar irradiance; experiment G1 involved offsetting the global radiative flux imbalance from a quadrupling of the CO_2 concentration via solar reduction. Thus far, 15 models have participated in this simulation, providing information about model commonalities and differences in the global climate response, including effects on temperature, the hydrological cycle, cryosphere, terrestrial biosphere, and extreme events (Schmidt et al., 2012; Kravitz et al., 2013a, 2013b; Tilmes et al. 2013; Moore et al., 2014; Glienke et al., 2015; Curry et al., 2014; among numerous other studies). The GeoMIP website (http://climate.envsci.rutgers.edu/GeoMIP/) provides an up-to-date list of publications using GeoMIP model output.

While total solar irradiance reductions are straightforward to simulate in all models, this idealization is not a good approximation of MCB. The dominant effect of MCB is an increase in albedo in and near marine low clouds through "direct" and "indirect" effects. Changes in the albedo near the surface can produce different signatures

from reductions in energy input at the top of the atmosphere. There are also likely to be differences in the spatial distribution of the energy reduction. While some forms of albedo modification like SAI operate over broad areas (on a hemispheric or larger scale), albedo changes produced are likely to operate on smaller spatial scales and be concentrated over particular oceanic regions. Previous studies suggest that the clouds that are most susceptible to albedo modification are located on the western side of ocean basins in the subtropics, in regions dominated by stratocumulus clouds (Oreopoulos and Platnick, 2008). So, rather than considering a reduction of solar input operating uniformly over both land and ocean, an idealized representation of MCB that better approximates the effects is to increase the albedo only over ocean surfaces, as described by Kravitz et al. (2013c). This method can also be used to assess some effects of geoengineering by creating microbubbles at the ocean surface to increase reflectivity (e.g., Seitz, 2011).

In this study, we investigate the climate effects of using ocean albedo increases to offset CO_2 warming and compare those effects with those of total solar irradiance reduction (experiments are described in more detail in the following section). All simulations were conducted under the auspices of GeoMIP, allowing us to characterize a range of model responses to these different idealized methods of representing solar geoengineering.

2. Methodology and Description

Our analyses focus on four simulations: (1) a preindustrial control simulation (piControl), (2) a simulation in which the CO_2 concentration is abruptly quadrupled from its preindustrial value (abrupt4xCO2), (3) a simulation in which the net radiative flux imbalance in abrupt4xCO2 is offset by a reduction in total solar irradiance (G1), and (4) a simulation in which the net radiative flux imbalance in abrupt4xCO2 is offset by an increase in ocean albedo everywhere by a uniform factor (G1ocean-albedo). piControl and abrupt4xCO2 are standard experiments in the Coupled Model Intercomparison Project Phase 5 (CMIP5; Taylor et al., 2012). G1 is described further by Kravitz et al. (2011). The protocol for G1ocean-albedo is described in more detail by Kravitz et al. (2013c). Table 1 lists the models participating in this study, including relevant references and the required change in albedo to meet the objectives of experiment G1ocean-albedo. A similar table for experiment G1 is given by Kravitz et al. (2013a). One of the advantages of G1ocean-albedo is that, like G1, all models can conduct this simulation fairly easily. Supplemental Table S1 quantifies how well each model achieved radiative balance in the G1 and G1ocean-albedo experiments.

Kravitz et al. (2013c) found that in test simulations, one could only determine whether the objectives of G1ocean-albedo were met after several decades of simulation. However, as our analysis will show, once the proper value of ocean albedo increase is ascertained, the climate response reaches steady state in a few years, as in experiment G1 (Kravitz et al., 2013a). Supplemental Table S2 quantifies temperature trends in each participating model over years 11-50 of simulation. The

mean model trend over this period is approximately zero (to four decimal places), and with little exception, the trends in G1 and G1ocean-albedo are an order of magnitude smaller than the trends in the abrupt4xCO2 simulation. As such, for the purpose of analysis, we assume that "slow responses," i.e., responses operating on time scales longer than a few years (e.g., Andrews and Forster, 2010; Sherwood et al., 2015) are negligible in the G1 and G1ocean-albedo simulations. We do not separate results into rapid adjustment and slow response timescales, and with the exception of time series plots, all figures show averages over the years 11-50 of simulation, which we take as a sufficient indication of the dominant climate response after the transient response has resolved.

Except where indicated, all plots show the mean model response. All values in the text are reported as mean (min to max), where mean indicates the all-model mean for that particular quantity, min is the lower bound of the range of model responses, and max is the upper bound of the range of model responses. In all maps, stippling indicates where fewer than 75% of the models agree on the sign of the response. All models in Table 1 were able to provide output for all variables except for cloud radiative forcing. The models included in cloud forcing analyses are BNU-ESM, CanESM2, CESM-CAM5.1-FV, HadGEM2-ES, IPSL-CM5A-LR, and MPI-ESM-LR. Supplemental Tables S1-S15 provide more quantitative information for all of the analyses presented in this study.

3. Results

3.1. Albedo and Temperature

Figure 1 shows the change in albedo at the top-of-atmosphere and at the surface for the abrupt4xCO2, G1, and G1ocean-albedo simulations, where albedo is defined as the ratio of upwelling to downwelling all-sky shortwave radiative flux. Quantitative values are given in Supplemental Tables S3 and S4. Results for abrupt4xCO2 and G1 are consistent with known responses of an increase in absorbed shortwave by carbon dioxide, reduced cloud cover, and reduced snow and sea ice cover (e.g., Schmidt et al., 2012; Kravitz et al., 2013b). These result in a broad decrease in albedo at the top of atmosphere and a decrease in surface albedo in many regions with substantial snow and ice cover. G1ocean-albedo retains many of these local high latitude features, but with large albedo increases over ocean, consistent with the experimental design and imposed forcing.

Figure 2 expands upon this picture by showing changes in shortwave and longwave cloud forcing in G1 and G1ocean-albedo, where cloud forcing is defined as all-sky minus clear-sky radiative flux measured at the top of the atmosphere. Positive shortwave values and negative longwave values in Figure 2 generally indicate less cloud cover. As was shown by Kravitz et al. (2013b), cloud cover in G1 tends to be reduced, which is consistent with what is depicted in Figure 2. For G1ocean-albedo, cloud cover is reduced over most ocean regions and large portions of land. Exceptions include an increase in cloudiness over the Arctic, much of Africa, South

Asia, Australia, and the leeward side of the Andes. These changes in cloudiness have implications for the hydrologic cycle, which we revisit in Section 3.5.

Figure 3 shows changes in global mean, land mean, and ocean mean surface air temperature for the G1 and G1ocean-albedo multi-model ensembles. Quantitative values are provided in Supplemental Table S5. Whereas the G1 simulation largely offsets temperature changes due to increased CO_2 concentration, G1ocean-albedo is approximately 0.36°C (-0.12 to 1.20) warmer than the control simulation. This is predominantly due to warming over land by 1.14°C (0.41 to 1.83). The temperature results in Figure 3 indicate that the temperature change happens within the first few years, and while some models show a slight trend in temperature over the 50-year G1ocean-albedo simulation (Supplemental Table S2), in general, any such trends are small, especially as compared to the warming in the abrupt4xCO2 simulation. This lack of substantial transient behavior after an initial fast response indicates that G1ocean-albedo has entered a new approximate steady state.

Figure 4 shows spatial patterns of change in temperature and top-of-atmosphere net radiative flux. (Also see Supplemental Tables S5 and S6.) The temperature changes are broadly consistent with the net radiative flux changes in the respective experiments. As was discussed by Kravitz et al. (2013a), G1 results in an "overcooling" of the tropics and an "undercooling" of the poles, consistent with offsetting the ubiquitous longwave forcing from CO_2 with a latitudinally dependent reduction in shortwave. G1ocean-albedo shows warming at high latitudes, over land regions, and in some ocean regions near or downwind of large continents, with the remaining ocean regions generally showing cooling. Because net top-of-atmosphere radiative flux is approximately zero in G1ocean-albedo, these temperature changes cannot be the result of energy being added to or subtracted from the climate system, and instead must be the result of energy redistribution. Hypotheses for why these temperature change patterns look the way they do (which will be tested in subsequent sections) include

1) The global average warming experienced in G1ocean-albedo is primarily due to increased heating over land.

2) Most warming over oceanic regions is due to transport of heat from land to ocean.

3) Any contributions to temperature or radiative flux changes from changes in ocean heat content are small on the timescales being evaluated here.

3.2. Hypothesis 1: Increased heating over land drives global average warming in G1ocean-albedo

The first hypothesis is fairly straightforward to argue based on first principles. To do so, we employ a one-dimensional radiative equilibrium model with 15 vertical layers extending from the surface to the nominal top-of-atmosphere. In the model,

each layer behaves as a gray body with a specified emissivity, and the model computes radiative transfer between each layer via Planck radiation (the Stefan-Boltzmann equation). Although this model represents a gross oversimplification of the vertical profile of temperature response to idealized forcing, it is useful here for understanding differences between land and ocean temperature changes in response to the forcing imposed in G1ocean-albedo.

Figure 5 shows temperature profiles calculated using this model for four experiments: a control simulation, an abrupt4xCO2-like simulation (modeled as an increase in the emissivity of each model layer), a simulation with increased surface albedo, and G1ocean-albedo-like simulation involving an increase in emissivity and an increase in surface albedo. These simulations were conducted separately for global average and ocean-only regions.

Values of emissivity in the control simulation were prescribed to be 0.80 at all layers, consistent with a gray body (Pandey et al., 1995). The emissivity in the abrupt4xCO2 simulation was calculated to be the value such that global mean temperature change in the first model layer is approximately 4.42 K (Supplemental Table S5), yielding an emissivity value of 0.8265. In the control simulations, the surface albedos for the global and ocean-only simulations are 0.3 and 0.1, respectively, consistent with estimates provided by Stephens et al. (2015) and the values given in Table 1. In the global average simulation, the albedo increase in the G1-ocean albedo simulation was calculated to be the value such that global mean temperature change in the first model layer is approximately 0.36 K (Supplemental Table S5). In the ocean average simulation, the albedo increase is the all-model average of the required albedo increase in Table 1, which is a multiplication factor of 1.8627.

The results in Figure 5 show that under reasonable assumptions around atmospheric emissivity and surface albedo, oceanic cooling is expected in the G1ocean-albedo simulation. Based on these results, any increase in global average temperature must be due to warming over land. The oceanic temperature change in this simple model's simulation of G1ocean-albedo is -2.77 K, which is far too large in magnitude as compared to the results from the Earth System Models. Figure 2 indicates that changes in cloud cover in G1ocean-albedo are more likely to increase the magnitude of this temperature change than decrease it. In subsequent sections, we discuss some additional mediating factors that could act to reduce the magnitude of this change, such as land-ocean energy transport or reduced net ocean heat uptake. Nevertheless, the dominant radiative effects in G1ocean-albedo are to cause cooling over the oceans, as is seen in Figure 4.

3.3. Hypothesis 2: The role of Land-Ocean Energy Transport (LOET)

Although the air over the ocean warms somewhat in G1ocean-albedo, it does not warm uniformly. Figure 4 shows that much of the warming over the ocean is in areas near land, indicating the potential for some of the heating energy over land to

be transported to ocean regions. This can be quantified via calculating what Geoffroy et al. (2015) call horizontal energy transport, and which we call land-ocean energy transport (LOET), as it represents an aggregate transport of energy from the atmosphere over the land (averaged over all land regions) to the atmosphere over the ocean (averaged over all ocean regions). They provide a more detailed description, calculation, and validation of this concept using a three-box energy balance model that can be fitted to changes in land/ocean temperature and TOA energy imbalance such that the model captures the relevant energy transport dynamics; we repeat here only the calculations germane to our discussions.

Gregory et al. (2004) describe a method of estimating adjusted radiative forcing and the aggregate strength of global feedbacks via linear regression of the net global, annual mean TOA radiative flux imbalance (ΔR) against the global, annual mean temperature change (ΔT) in response to a forcing. The *y*-intercept of the regression line gives an estimate of adjusted radiative forcing ($\boldsymbol{\mathcal{F}}$), and the negative of the slope of the regression line gives the feedback parameter (λ). Similarly, one can perform regression just over land-averaged quantities (denoted with the subscript ℓ) or just over ocean quantities (subscript o). Feedback parameter values are provided in Table 3.

In addition, one can regress ΔT_ℓ against ΔT_o to obtain a *y*-intercept of

$$\boldsymbol{\mathcal{F}}_\ell/(\lambda_\ell+\alpha_\ell/f_\ell) \quad (1)$$

where α_ℓ is the land heat transport parameter and f_ℓ is the land fraction (approximately 0.3). The slope is

$$(\alpha_o/f_\ell)/(\lambda_\ell+\alpha_\ell/f_\ell) \quad (2)$$

If one solves these two equations for α_ℓ and α_o, then one can define

$$\Delta A= \alpha_\ell \Delta T_\ell - \alpha_o \Delta T_o \quad (3)$$

The quantity ΔA is the time-dependent LOET (units of W m^{-2}).

Figure 7 provides calculations of LOET for the simulations presented here. See Supplemental Table S7 for more details on individual model values. In the abrupt4xCO2 simulation, changes in LOET are positive (indicating an increase in heat transport from the land to the ocean) and decrease in magnitude steadily over the course of the simulation; these results are discussed in more detail by Geoffroy et al. (2015).

In Experiment G1, LOET increases by a model-dependent constant value and remains relatively unchanged over the course of the simulation. Although the air temperature over land in G1 increases slightly, and the air temperature over ocean decreases slightly (Kravitz et al., 2013a), the temperature changes in G1 are more

latitude-dependent than representative of a clear land-ocean contrast (Figure 4), so it is perhaps not unexpected that LOET would be small.

Experiment G1ocean-albedo exhibits a strong land-ocean contrast in temperature (Figure 4), and the response is in steady state after a few years. As such, consistent with the behavior of other fluxes, LOET in G1ocean-albedo does not show transient behavior. LOET in G1ocean-albedo is approximately 2.20 (1.35 to 3.21) W m^{-2}, which is larger than in the other experiments examined here.

Converting LOET into temperature change is not necessarily straightforward, but an approximate change in temperature can be calculated by combining values of ΔA (Supplemental Table S7) with feedback parameter calculations (Table 3). More specifically, the temperature "added" to the air over the oceans by LOET can be calculated as $\Delta A/\lambda_o$, and the temperature "subtracted" from the air over land by LOET can be calculated as $\Delta A/\lambda_l$. Performing these calculations, LOET in the G1ocean-albedo experiment contributes 1.87°C (0.57 to 3.06) to ocean temperature and "subtracts" 2.03°C (0.68 to 3.06) from land temperature. We caution that this naïve calculation is somewhat circular, and it inherently includes in the ocean calculations both regions unaffected by LOET (e.g., tropical oceans) and regions strongly affected by LOET (e.g., Northeast Atlantic and Pacific Oceans).

Based on the calculations in Section 3.2 and the present section, it seems unlikely that LOET can on average transport enough energy from the land to the ocean to offset the radiative deficit due to an ocean albedo increase. However, locally, LOET appears to be able not only to offset these radiative changes, but also result in net warming.

3.4. Hypothesis 3: Atmospheric Column Energetics and Net Energy Flux into the Oceans

An additional potential source of energy to the atmosphere is a reduction in net ocean heat uptake. Calculating changes in ocean heat uptake are challenging and not particularly revealing in this case for three reasons:

1) It is possible that the models used in simulating G1ocean-albedo were not entirely spun up to steady state. As such, any remaining imbalances could manifest as changes in ocean heat content. In principle, one could subtract off the preindustrial control value, which likely has a similar trend in ocean heat content arising from spinup. However, this would not remove the influence of nonlinearities (state dependence), so there is no way to guarantee that the signal is entirely due to the G1ocean-albedo forcing.
2) As is seen in Supplemental Table S1, not all models were able to achieve top-of-atmosphere net radiative flux balance over the course of the simulation. These small changes can lead to large changes in ocean heat content over the course of a 50-year simulation. For example, a 0.1 W m^{-2} imbalance over a 50-year period can lead to an additional 5.5$\times$$10^{22}$ J of energy incident

at the ocean surface. As such, we are unable to properly assess the degree to which ocean heat content changes may be due to small imbalances.

3) Ocean heat content requires a depth threshold for calculation, meaning calculations of it are sensitive to redistribution of heat to/from lower depths, obscuring the signal of the forcing.

As an alternative, we calculate net energy exchange across the surface in terms of changes in radiative and turbulent fluxes. Kravitz et al. (2013b) calculated energetics changes in the entire atmospheric column. However, because we are only interested in net surface fluxes, we calculate

$$\Delta S = \Delta R_{surf} + \Delta SH + \Delta LH \quad (1)$$

where ΔR_{surf} is the change in net surface radiative flux (shortwave and longwave), ΔSH is change in sensible heat flux from the atmosphere to the surface, and ΔLH is change in latent heat flux from the atmosphere to the surface. By convention, all fluxes are positive downward unless specifically noted. Calculations of individual terms in this budget, as well as of ΔS, are provided in Supplemental Tables S8-S12. Because these calculations are performed at the surface, no advection term (e.g., LOET) is needed, and ΔS is well defined as a land or ocean average.

Figure 7 shows the all-model mean for all of the terms in Equation 4. Several clear conclusions emerge. The first is that ΔS is approximately zero globally, over land, and over ocean for nearly the entire 50-year period, after an initial rapid adjustment that resolves within a few years. With the exception of latent heat over land, this is true of all fluxes for G1ocean-albedo in Figure 7, and even latent heat flux over land reaches an approximate steady state within ten years. If ΔS indeed serves as a useful proxy for net energy flux into or out of the ocean, then these results indicate that there is no sizable contribution to atmospheric energetics by changes in ocean heat content. Moreover, even if ΔS were not zero over ocean, ocean heat content changes would still be an insufficient explanation for temperature changes due to incongruent timescales. The oceanic mixed layer operates on an approximately decadal timescale, but all transient behavior in these simulations is resolved well before ten years. The transient response is much more consistent with a land surface time scale, which is on the order of 1-3 years. As such, it seems plausible that the temperature changes over ocean in G1ocean-albedo are due to land processes rather than ocean heat content changes. This is not to say that the ocean plays no role in the observed temperature changes. Rather, given the discussions in this section and the two previous sections, the role of the ocean heat content in causing temperature changes over the ocean in G1ocean-albedo is likely small.

The remainder of the results in Figure 7 are consistent with the applied forcing. There is a large sensible heat flux increase from the land to the atmosphere of 2.87 (-0.99 to 6.00) W m^{-2}, with a comparatively smaller sensible heat flux decrease from the ocean to the atmosphere of 1.47 (0.34 to 2.20) W m^{-2}. Over the ocean, latent heat flux from the surface to the atmosphere is 6.71 (4.95 to 7.89) W m^{-2} lower in

G1ocean-albedo than in the preindustrial control simulation. These results indicate a greater shift of energy away from evaporating water and toward increasing land temperature. Large differences in flux magnitude between G1 and G1ocean-albedo can be found over land for net shortwave flux and latent heat flux, and differences in sign can be found over land for total radiative flux. These features are consistent with the applied forcing being different over land and ocean.

3.5. Hydrological cycle changes

Introducing a strong land-ocean energy and temperature gradient, as in G1ocean-albedo, will undoubtedly impact the hydrological cycle. Although the simulation is idealized, more realistic representations of MCB have shown important hydrological cycle impacts, including secondary circulation patterns that shift precipitation onto land in the tropics and extratropics (Bala et al., 2010), changes in the monsoon (Alterskjær et al., 2013), and changes in the Walker circulation (Niemeier et al., 2013). Here we evaluate the large-scale hydrological cycle changes in G1ocean-albedo, with possible applicability to other realizations of MCB.

Figure 8 shows global, land, and ocean averaged precipitation, evaporation, and precipitation minus evaporation (P–E) for all of the simulations considered in this manuscript; quantitative descriptions are given in Tables S13–15. The abrupt4xCO2 simulation is the only one with a distinct rapid adjustment and slow response. Over both land and ocean, G1 shows decreases in precipitation and evaporation of approximately equal magnitude, resulting in net changes in P–E of 0.02 (-0.05 to 0.11) mm day^{-1} over land and -0.01 (-0.04 to 0.01) mm day^{-1} over ocean. In G1ocean-albedo, global precipitation and evaporation both decrease by approximately 0.19 (0.11 to 0.26) mm day^{-1} to yield little net change in P–E. However, this net small change is due to differential effects over land and ocean. Over land, precipitation remains relatively unchanged, but evaporation decreases, resulting in a net change in P–E by 0.09 (-0.18 to 0.18) mm day^{-1}. Over the ocean, both precipitation and evaporation decrease, with a net negative P–E of -0.06 (-0.19 to -0.01) mm day^{-1}.

Annual mean land/ocean contrasts in precipitation and evaporation changes tend to be more uniform in sign in experiment G1 (Figure 9), resulting in few large regions of change in P–E with the exception of the tropics (mostly driven by a southward shift in the intertropical convergence zone; Kravitz et al., 2013a). In G1ocean-albedo, precipitation and evaporation over the oceans are reduced in most regions, consistent with the applied forcing. Over land, the signs of precipitation and evaporation changes are regionally heterogeneous, yet the precipitation and evaporation changes are concordant, e.g., land regions with increased precipitation also generally show increased evaporation. The net P–E map is highly heterogeneous, but in general, tropical land areas are projected to have more available moisture (as measured by P–E) under G1ocean-albedo, and midlatitude land areas are projected to have less. The implications of these changes for people and ecosystems is an important area of future research.

4. Discussion and Conclusions

The results presented here indicate that even though experiments G1 and G1ocean-albedo both achieve approximate net top-of-atmosphere radiative flux balance, the climate system responses differ dramatically between the two experiments. The idea that global energy balance can still result in local changes is perhaps not surprising, as feedback operate locally (Armour et al., 2013). These different climate responses for the same forcing are effectively an illustration of different efficacies (Hansen et al., 2005). Even in the absence of slow responses, forcings with different efficacies can cause different climate system changes (Kravitz et al., 2015). G1ocean-albedo serves as an excellent reminder not to conflate small net top-of-atmosphere radiative flux imbalance with small temperature change; a clear relationship between those two quantities is not guaranteed.

Relatedly, the results obtained for G1ocean-albedo were to some extent by design. The objective of G1ocean-albedo was to achieve net top-of-atmosphere radiative flux balance, which resulted in warming. Conceivably, one could define an objective of no global temperature change, implying a net negative radiative flux at the top-of-atmosphere. It is unclear whether, unlike G1ocean-albedo, that alternate approach would result in transient behavior that lasts longer than a few years. Such an experiment could be accomplished using feedback methods that have been introduced to geoengineering research in recent years (e.g., MacMartin et al., 2014; Kravitz et al., 2016).

The results presented here have several features that were not necessarily expected from the outset. Kravitz et al. (2013c) found that determining whether the climate system was in balance took up to 30 years of simulation. However, once that balance is achieved, the climate does not change appreciably after the initial rapid adjustment. Potential future work could investigate these results, shedding light on timescales of climate response and potential thresholds, e.g., how large does the energy imbalance need to be to trigger slower adjustments?

Related to this issue of different timescales of adjustment is the traditional separation of climate response into rapid adjustment and slow response components (e.g., Andrews and Forster, 2010; Sherwood et al., 2015). The rapid adjustment is often defined as the climate response unassociated with global mean temperature change, and the slow response describes a transient temperature change with a large component due to climate system feedbacks. The results from G1ocean-albedo, like those of G1 (Kravitz et al., 2013b), show an initial rapid change and no appreciable slower change. However, in G1ocean-albedo, that initial change is associated with a temperature increase, which in principle should excite a slow adjustment through climate system feedbacks. These results are somewhat inconsistent with the traditional definitions of rapid adjustment and slow response. Additionally, this sustained temperature increase is to some extent decoupled from net energy imbalances in the climate system, as ΔR_{TOA} and ΔS (Equation 4) are both

approximately zero. Reconciling all of these features suggests a potentially rich research topic focused on understanding the relationships between radiative flux changes, temperature changes, and the circumstances under which climate feedbacks are excited.

G1ocean-albedo may be more apposite to the impact of geoengineering via "ocean microbubbles," whereby surfactants are added to the ocean surface, promoting the formation of microscopic, highly reflective bubbles (Seitz, 2011; Robock, 2011). An area of investigation we did not undertake, yet one that repeatedly emerges in discussions of microbubbles, is the effect on the ocean mixed layer. By reflecting more solar radiation, microbubbles have the potential to inhibit vertical mixing and available light in the euphotic zone, which could have profound effects on marine biota. This implies that another useful future area of investigation for the G1ocean-albedo simulation is an analysis of the marine carbon cycle.

There are numerous potential areas of research prompted by this study. The stark land/ocean contrast in warming has potential implications for ocean circulation patterns, including the meridional overturning circulation and Western boundary ocean currents, with consequent implications for marine ecosystems. This contrast also has implications for the terrestrial biosphere, including ecosystem services and the land and ocean carbon cycles. Although we did not evaluate seasonal changes in this manuscript, such investigations could prove fruitful for more detailed assessments of variability, such as monsoon precipitation, extreme events, and sea ice extent.

Despite being informative for MCB, there are limits as to the applicability of this idealized approach. There are important differences in boundary layer stability changes from surface albedo increases versus marine stratocumulus cloud top brightening. Also, it appears impossible for marine cloud brightening to be conducted over all ocean regions and with a sufficient magnitude to offset the radiative forcing from a quadrupling of the CO_2 concentration. The purpose of this manuscript is to describe the broad features of change under a uniform ocean albedo increase, and some of these changes are likely to be present with more realistic scenarios of marine cloud brightening. We anticipate that future research can more deeply explore the applicability of this simulation to marine cloud brightening.

Acknowledgments. We thank Jón Egill Kristjánsson, who tragically passed away, for invaluable comments on an earlier version of this manuscript. We acknowledge the World Climate Research Programme's Working Group on Coupled Modelling, which is responsible for CMIP, and we thank the climate modeling groups for producing and making available their model output. For CMIP the U.S. Department of Energy's Program for Climate Model Diagnosis and Intercomparison provides coordinating support and led development of software infrastructure in partnership with the Global Organization for Earth System Science Portals. We thank all participants of the Geoengineering Model Intercomparison Project and their model

development teams, CLIVAR/WCRP Working Group on Coupled Modeling for endorsing GeoMIP, and the scientists managing the Earth System Grid data nodes who have assisted with making GeoMIP output available. The Pacific Northwest National Laboratory is operated for the U.S. Department of Energy by Battelle Memorial Institute under contract DE-AC05-76RL01830. Simulations performed by Ben Kravitz were supported by the NASA High-End Computing (HEC) Program through the NASA Center for Climate Simulation (NCCS) at Goddard Space Flight Center. Alan Robock is supported by NSF grants AGS-1157525 and GEO-1240507. Andy Jones was supported by the Joint UK DECC/Defra Met Office Hadley Centre Climate Programme (GA01101). Olivier Boucher acknowledges HPC resources from CCRT under the allocation 2015-t2012012201 made by GENCI (Grand Equipement National de Calcul Intensif). This research was supported under the Australian Research Council's Special Research Initiative for the Antarctic Gateway Partnership (project SR140300001).

551 **References**
552
553 Alterskjær, K., J. E. Kristjansson, and Ø. Seland (2012), Sensitivity to deliberate sea
554 salt seeding of marine clouds – observations and model simulations, *Atmos.*
555 *Chem. Phys.*, *12*, 2795-2807 doi:10.5194/acp-12-2795-2012.
556 Alterskjær, K., J. E. Kristjánsson, O. Boucher, H. Muri, U. Niemeier, H. Schmidt, M.
557 Schulz, and C. Timmreck (2013), Sea-salt injections into the low-latitude
558 marine boundary layer: The transient response in three Earth system
559 models, *J. Geophys. Res. Atmos., 118*, 12,195–12,206,
560 doi:10.1002/2013JD020432.
561 Andrews, T., and P. M. Forster (2010), The transient response of global-mean
562 precipitation to increasing carbon dioxide levels, *Environ. Res. Lett.*, *5*,
563 025212, doi:10.1088/1748-9326/5/2/025212.
564 Armour, K. C., C. M. Bitz, and G. H. Roe (2013), Time-varying climate sensitivity from
565 regional feedbacks, *J. Climate, 26*, 4518–4534, doi:10.1175/JCLI-D-12-
566 00544.1.
567 Arora, V. K., J. F. Scinocca, G. J. Boer, J. R. Christian, K. L. Denman, G. M. Flato, V. V.
568 Kharin, W. G. Lee, and W. J. Merryfield (2011), Carbon emission limits
569 required to satisfy future representative concentration pathways of
570 greenhouse gases, *Geophys. Res. Lett.*, *38*, L05805,
571 doi:10.1029/2010GL046270.
572 Bala, G., K. Caldeira, and R. Nemani (2010), Fast versus slow response in climate
573 change: Implications for the global hydrological cycle, *Clim. Dyn.*, *35*, 423-
574 434, doi:10.1007/s00382-009-0583-y.
575 Collins, W. J., N. Bellouin, M. Doutriaux-Boucher, N. Gedney, P. Halloran, T. Hinton, J.
576 Hughes, C. D. Jones, M. Joshi, S. Liddicoat, G. Martin, F. O'Connor, J. Rae, C.
577 Senior, S. Sitch, I. Totterdell, A. Wiltshire, and S. Woodward (2011),
578 Development and evaluation of an Earth-System model—HadGEM2, *Geosci.*
579 *Model Dev.*, *4*, 1051-1075, doi:10.5194/gmd-4-1051-2011.
580 Crook, J. A., L. S. Jackson, S. M. Osprey, and P. M. Forster (2015), A comparison of
581 temperature and precipitation responses to different Earth radiation
582 management geoengineering schemes, *J. Geophys. Res., 120*, 9352-9373,
583 doi:10.1002/2015JD023269.
584 Curry, C. L., J. Sillmann, D. Bronaugh, K. Alterskjær, J. N. S. Cole, B. Kravitz., J. E.
585 Kristjánsson, H. Muri, U. Niemeier, A. Robock, and S. Tilmes (2014), A multi-
586 model examination of climate extremes in an idealized geoengineering
587 experiment, *Journal of Geophysical Research*, *119*, 3900-3923,
588 doi:10.1002/2013JD020648.
589 Dufresne, J.-L., M.-A. Foujols, S. Denvil, A. Caubel, O. Marti, O. Aumont, Y. Balkanski, S.
590 Bekki, H. Bellenger, R. Benshila, S. Bony, L. Bopp, P. Braconnot, P. Brockmann,
591 P. Cadule, F. Cheruy, F. Codron, A. Cozic, D. Cugnet, N. de Noblet, J.-P. Duvel, C.
592 Ethé, L. Fairhead, T. Fichefet, S. Flavoni, P. Friedlingstein, J.-Y. Grandpeix, L.
593 Guez, E. Guilyardi, D. Hauglustaine, F. Hourdin, A. Idelkadi, J. Ghattas, S.
594 Joussaume, M. Kageyama, G. Krinner, S. Labetoulle, A. Lahellec, M.-P.
595 Lefebvre, F. Lefevre, C. Levy, Z. X. Li, J. Lloyd, F. Lott, G. Madec, M. Mancip, M.
596 Marchand, S. Masson, Y. Meurdesoif, J. Mignot, I. Musat, S. Parouty, J. Polcher,

C. Rio, M. Schulz, D. Swingedouw, S. Szopa, C. Talandier, P. Terray, N. Viovy, and N. Vuichard (2013), Climate change projections using the IPSL-CM5 Earth System Model: From CMIP3 to CMIP5, *Clim. Dynam.*, *40*, 2123-2165 doi:10.1007/s00382-012-1636-1.

Geoffroy, O., D. Saint-Martin, and A. Voldoire (2015), Land-sea warming contrast: the role of the horizontal energy transport, *Clim. Dynam.*, *45*, 3493-3511, doi:10.1007/s00382-015-2552-y.

Giorgetta, M. A., Johann Jungclaus, Christian H. Reick, Stephanie Legutke, Jürgen Bader, Michael Böttinger, Victor Brovkin, Traute Crueger, Monika Esch, Kerstin Fieg, Ksenia Glushak, Veronika Gayler, Helmuth Haak, Heinz-Dieter Hollweg, Tatiana Ilyina, Stefan Kinne, Luis Kornblueh, Daniela Matei, Thorsten Mauritsen, Uwe Mikolajewicz, Wolfgang Mueller, Dirk Notz, Felix Pithan, Thomas Raddatz, Sebastian Rast, Rene Redler, Erich Roeckner, Hauke Schmidt, Reiner Schnur, Joachim Segschneider, Katharina D. Six, Martina Stockhause, Claudia Timmreck, Jörg Wegner, Heinrich Widmann, Karl-H. Wieners, Martin Claussen, Jochem Marotzke, and Bjorn Stevens (2013), Climate and carbon cycle changes from 1850 to 2100 in MPI-ESM simulations for the Coupled Model Intercomparison Project Phase 5, *J. Adv. Model. Earth Syst.*, *5*, 572-597, doi:10.1002/jame.20038.

Glienke, S., P. J. Irvine, and M. G. Lawrence (2015), The impact of geoengineering on vegetation in experiment G1 of the GeoMIP, *Journal of Geophysical Research*, *120*, 10196-10213, doi:10.1002/2015JD024202.

Gregory, J. M., W. J. Ingram, M. A. Palmer, G. S. Jones, P. A. Stott, R. B. Thorpe, J. A. Lowe, T. C. Johns, and K. D. Williams (2004), A new method for diagnosing radiative forcing and climate sensitivity, *Geophys. Res. Lett., 31*, L03205, doi:10.1029/2003GL018747.

Hansen, J., M. Sato, R. Ruedy, L. Nazarenko, A. Lacis, G. A. Schmidt, G. Russell, I. Aleinov, M. Bauer, S. Bauer, N. Bell, B. Cairns, V. Canuto, M. Chandler, Y. Cheng, A. Del Genio, G. Faluvegi, E. Fleming, A. Friend, T. Hall, C. Jackman, M. Kelley, N. Kiang, D. Koch, J. Lean, J. Lerner, K. Lo, S. Menon, R. Miller, P. Minnis, T. Novakov, V. Oinas, Ja. Perlwitz, Ju. Perlwitz, D. Rind, A. Romanou, D. Shindell, P. Stone, S. Sun, N. Tausnev, D. Thresher, B. Wielicki, T. Wong, M. Yao, and S. Zhang (2005), Efficacy of climate forcings, *J. Geophys. Res., 110*, D18104, doi:10.1029/2005JD005776.

Hazeleger, W., X. Wang, C. Severijns, S. Ştefănescu, R. Bintanja, A. Sterl, K. Wyser, T. Semmler, S. Yang, B. van den Hurk, T. van Noije, E. van der Linden, and K. van der Wiel (2011), EC-Earth V2.2: Description and validation of a new seamless Earth system prediction model, *Clim. Dynam., 39*(11), 2611-2629, doi:10.1007/s00382-011-1228-5.

Hurrell, J. W., M. M. Holland, P. R. Gent, S. Ghan, J. E. Kay, P. J. Kushner, J.-F. Lamarque, W. G. Large, D. Lawrence, K. Lindsay, W. H. Lipscomb, M. C. Long, N. Mahowald, D. R. Marsh, R. B. Neale, P. Rasch, S. Vavrus, M. Vertenstein, D. Bader, W. D. Collins, J. J. Hack, J. Kiehl, and S. Marshall (2013), The Community Earth System Model: A framework for collaborative research, *Bull. Amer. Meteor. Soc.*, *94*, 1339-1360, doi:10.1175/BAMS-D-12-00121.1.

643 Ji, D., L. Wang, J. Feng, Q. Wu, H. Cheng, Q. Zhang, J. Yang, W. Dong, Y. Dai, D. Gong, R.-
644 H. Zhang, X. Wang, J. Liu, J. C. Moore, D. Chen, and M. Zhou (2014),
645 Description and basic evaluation of Beijing Normal University Earth System
646 Model (BNU-ESM) version 1, *Geosci. Model. Dev.*, *7*, 2039-2064,
647 10.5194/gmd-7-2039-2014.
648 Kalidindi, S., G. Bala, A. Modak, and K. Caldeira (2015), Modeling of solar radiation
649 management: a comparison of simulations using reduced solar constant and
650 stratospheric sulphate aerosols, *Clim. Dynam.*, *44*, 2909-2925,
651 doi:10.1007/s00382-014-2240-3.
652 Kravitz, B., A. Robock, O. Boucher, H. Schmidt, K. E. Taylor, G. Stenchikov, and M.
653 Schulz (2011), The Geoengineering Model Intercomparison Project
654 (GeoMIP), *Atm. Sci. Lett.*, *12,* 162-167, doi:10.1002/asl.316.
655 Kravitz, B., K. Caldeira, O. Boucher, A. Robock, P. J. Rasch, K. Alterskjær, D. Bou
656 Karam, J. N. S. Cole, C. L. Curry, J. M. Haywood, P. J. Irvine, D. Ji, A. Jones, J. E.
657 Kristjánsson, D. J. Lunt, J. Moore, U. Niemeier, H. Schmidt, M. Schulz, B. Singh,
658 S. Tilmes, S. Watanabe, S. Yang, and J.-H. Yoon (2013a), Climate model
659 response from the Geoengineering Model Intercomparison Project (GeoMIP),
660 *Journal of Geophysical Research*, *118*(15), 8320-8332,
661 doi:10.1002/jgrd.50646.
662 Kravitz, B., P. J. Rasch, P. M. Forster, T. Andrews, J. N. S. Cole, P. J. Irvine, D. Ji, J. E.
663 Kristjánsson, J. C. Moore, H. Muri, U. Niemeier, A. Robock, B. Singh, S. Tilmes,
664 S. Watanabe, and J.-H. Yoon (2013b), An energetic perspective on
665 hydrological cycle changes in the Geoengineering Model Intercomparison
666 Project (GeoMIP), *Journal of Geophysical Research*, *118*, 13087-13102,
667 doi:10.1002/2013JD020502.
668 Kravitz, B., P. M. Forster, A. Jones, A. Robock, K. Alterskjær, O. Boucher, A. K. L.
669 Jenkins, H. Korhonen, J. E. Kristjánsson, H. Muri, U. Niemeier, A.-I. Partanen, P.
670 J. Rasch, H. Wang, and S. Watanabe (2013c), Sea spray geoengineering
671 experiments in the Geoengineering Model Intercomparison Project
672 (GeoMIP): Experimental design and preliminary results, *Journal of*
673 *Geophysical Research*, *118*(19), 11175-11186, doi:10.1002/jgrd.50856.
674 Kravitz, B., D. G. MacMartin, P. J. Rasch, and A. J. Jarvis (2015), A new method of
675 comparing forcing agents in climate models, *J. Climate, 28*, 8203–8218,
676 doi:10.1175/JCLI-D-14-00663.1.
677 Kravitz, B., D. G. MacMartin, H. Wang, and P. J. Rasch (2016), Geoengineering as a
678 design problem, *Earth System Dynamics, 7*, 469-497, doi:10.5194/esd-7-469-
679 2016.
680 Latham, J. (1990), Control of global warming? *Nature*, *347*, 339–340.
681 MacMartin, D.G., B. Kravitz, D. W. Keith, and A. Jarvis (2014), Dynamics of the
682 coupled human-climate system resulting from closed-loop control of solar
683 geoengineering, *Clim. Dynam., 43*, 243-258, doi:10.1007/s00382-013-1822-9.
684 Mitchell, D. L. and W. Finnegan (2009), Modification of cirrus clouds to reduce global
685 warming, *Environ. Res. Lett.*, *4*, 045102, doi:10.1088/1748-
686 9326/4/4/045102.
687 Moore, J. C., A. Rinke, X. Yu, D. Ji, X. Cui, Y. Li, K. Alterskjær, J. E. Kristjánsson, O.
688 Boucher, N. Huneeus, B. Kravitz, A. Robock, U. Niemeier, H. Schmidt, M.

689 Schulz, S. Tilmes, and S. Watanabe (2014), Arctic sea ice and atmospheric
690 circulation under the GeoMIP G1 scenario, *J. Geophys. Res., 119*, 567-583,
691 doi:10.1002/2013JD021060.
692 NAS (2015a), Climate Intervention: Carbon Dioxide Removal and Reliable
693 Sequestration, National Research Council, The National Academies Press,
694 Washington, DC, 141 pp.
695 NAS (2015b), Climate Intervention: Reflecting Sunlight to Cool Earth, National
696 Research Council, The National Academies Press, Washington, DC, 235 pp.
697 Niemeier, U., H. Schmidt, K. Alterskjær, and J. E. Kristjánsson (2013), Solar
698 irradiance reduction via climate engineering--impact of different techniques
699 on the energy balance and the hydrological cycle, *Journal of Geophysical*
700 *Research*, *118*, 11905-11917, doi:10.1002/2013JD020445.
701 Oreopoulos, L. and S. Platnick (2008), Radiative susceptibility of cloudy
702 atmospheres to droplet number perturbations: 2. Global analysis from
703 MODIS, *J. Geophys. Res.*, *113*, D14S21, doi:10.1029/2007JD009655.
704 Pandey, D. K., R. B. Lee III, and J. Paden (1995), Effects of atmospheric emissivity on
705 clear sky temperatures, *Atmos. Environ.*, *29*, 2201-2204, doi:10.1016/1352-
706 2310(94)00243-E.
707 Phipps, S. J., L. D. Rotstayn, H. B. Gordon, J. L. Roberts, A. C. Hirst, and W. F. Budd
708 (2011), The CSIRO Mk3L climate system model version 1.0 – Part 1:
709 Description and evaluation, *Geosci. Model Dev.*, *4*, 483-509, 10.5194/gmd-4-
710 483-2011.
711 Robock, Alan (2011), Bubble, bubble, toil and trouble. An editorial comment.
712 *Climatic Change*, *105*, 383-385, doi:10.1007/s10584-010-0017-1.
713 Schmidt, H., K. Alterskjær, D. Bou Karam, O. Boucher, A. Jones, J. E. Kristjánsson, U.
714 Niemeier, M. Schulz, A. Aaheim, F. Benduhn, M. Lawrence, and C. Timmreck
715 (2012), Solar irradiance reduction to counteract radiative forcing from a
716 quadrupling of CO_2: Climate responses simulated by four Earth system
717 models, *Earth System Dynamics, 3*, 63-78, doi:10.5194/esd-3-63-2012.
718 Schmidt, Gavin A., Max Kelley, Larissa Nazarenko, Reto Ruedy, Gary L. Russell, Igor
719 Aleinov, Mike Bauer, Susanne E. Bauer, Maharaj K. Bhat, Rainer Bleck,
720 Vittorio Canuto, Yong-Hua Chen, Ye Cheng, Thomas L. Clune, Anthony Del
721 Genio, Rosalinda de Fainchtein, Greg Faluvegi, James E. Hansen, Richard J.
722 Healy, Nancy Y. Kiang, Dorothy Koch, Andy A. Lacis, Allegra N. LeGrande, Jean
723 Lerner, Ken K. Lo, Elaine E. Matthews, Surabi Menon, Ron L. Miller, Valdar
724 Oinas, Amidu O. Oloso, Jan P. Perlwitz, Michael J. Puma, William M. Putman,
725 David Rind, Anastasia Romanou, Makiko Sato, Drew T. Shindell, Shan Sun,
726 Rahman A. Syed, Nick Tausnev, Kostas Tsigaridis, Nadine Unger, Apostolos
727 Voulgarakis, Mao-Sung Yao, and Jinlun Zhang (2014), Configuration and
728 assessment of the GISS ModelE2 contributions to the CMIP5 archive, *J. Adv.*
729 *Model. Earth Syst., 6*, 141–184, doi:10.1002/2013MS000265.
730 Seitz, R. (2011), Bright water: hydrosols, water conservation and climate change,
731 *Climatic Change*, *105*, 365-381, doi:10.1007/s10584-010-9965-8.
732 Shepherd, J., K. Caldeira, P. Cox, J. Haigh, K. Keith, B. Launder, G. Mace, G. MacKerron,
733 J. Pyle, S. Rayner, C. Redgwell, and A. Watson (2009), Geoengineering the

climate: Science, governance, and uncertainty, Royal Society Policy document 10/09, 82 pp.

Sherwood, S. C., S. Bony, O. Boucher, C. Bretherton, P. M. Forster, J. M. Gregory, and B. Stevens (2015), Adjustments in the forcing-feedback framework for understanding climate change, *Bull. Amer. Meteor. Soc., 96*, 217–228, doi:10.1175/BAMS-D-13-00167.1.

Stephens, G. L., D. O'Brien, P. J. Webster, P. Pilewski, S. Kato, and J.-L. Li (2015), The albedo of Earth, *Rev. Geophys.*, *53*, 141-163, doi:10.1002/2014RG000449.

Taylor, K. E., R. J. Stouffer, and G. A. Meehl (2012), An overview of CMIP5 and the experiment design, *Bull. Amer. Meteor. Soc.*, *93*, 485-498, doi:10.1175/BAMS-D-11-00094.1.

Tilmes, S., J. Fasullo, J.-F. Lamarque, D. R. Marsch, M. Mills, K. Alterskjær, O. Boucher, J. N. S. Cole, C. L. Curry, J. M. Haywood, P. J. Irvine, D. Ji, A. Jones, D. B. Karam, B. Kravitz, J. E. Kristjánsson, J. C. Moore, H. O. Muri, U. Niemeier, P. J. Rasch, A. Robock, H. Schmidt, M. Schulz, B. Singh, S. Watanabe, S. Yang, and J.-H. Yoon (2013), The hydrological impact of geoengineering in the Geoengineering Model Intercomparison Project (GeoMIP), *Journal of Geophysical Research*, *118*(19), 11036-11058, doi:10.1002/jgrd.50868.

Watanabe, S., T. Hajima, K. Sudo, T. Nagashima, T. Takemura, H. Okajima, T. Nozawa, H. Kawase, M. Abe, T. Yokohata, T. Ise, H. Sato, E. Kato, K. Takata, S. Emori, and M. Kawamiya (2011), MIROC-ESM 2010: Model description and basic results of CMIP5-20c3m experiments, *Geosci. Mod. Dev.*, *4*, 845-872, doi:10.5194/gmd-4-845-2011.

758 **Table 1.** Description of the 11 models participating in this study. Column 1 gives
759 the standard model name. Columns 2 and 3 give the default and perturbed surface
760 ocean albedo, defined as upward shortwave divided by downward shortwave
761 radiative flux at the surface, both averaged over ocean regions and over years 11-50
762 of simulation. Column 4 is the ratio of column 3 to column 2. Column 5 gives the
763 factor (δ) by which the model default ocean albedo was multiplied to achieve
764 negligible top-of-atmosphere radiative flux changes under an abrupt4xCO2
765 simulation (described in greater detail by Kravitz et al., 2015). Column 6 gives a
766 relevant reference for each model. All values are rounded to two decimal places.
767

Model name	piControl ocean albedo	G1OA ocean albedo	Ratio	δ	Reference
BNU-ESM	0.12	0.17	1.48	2.50	Ji et al. (2014)
CanESM2	0.11	0.19	1.73	2.45	Arora et al. (2011)
CESM-CAM5.1-FV	0.10	0.18	1.79	2.70	Hurrell et al. (2013)
CSIRO-Mk3L-1.2	0.12	0.19	1.61	2.04	Phipps et al. (2011)
EC-Earth	0.10	0.19	1.97	3.17	Hazeleger et al. (2011)
GISS-E2-R	0.08	0.16	1.95	2.53	Schmidt et al. (2014)
HadGEM2-ES	0.10	0.17	1.83	2.44	Collins et al. (2011)
IPSL-CM5A-LR	0.10	0.17	1.78	2.33	Dufresne et al. (2013)
MIROC-ESM	0.10	0.20	2.00	3.10	Watanabe et al. (2011)
MPI-ESM-LR	0.09	0.23	2.40	5.42	Giorgetta et al. (2013)
NorESM1-M	0.09	0.18	1.95	2.77	Alterskjær et al. (2012)

Table 2. Parameters used in different runs with the simple one-dimensional radiative equilibrium model (Section 3.2). Surface ΔT (in Kelvin) for the Global runs are with respect to Control (Global) and for the Ocean runs are with respect to Control (Ocean).

Run	**Emissivity in each model layer**	**Surface albedo**	**Surface ΔT**
Control (Global)	0.80	0.3	0
abrupt4xCO2 (Global)	0.8265	0.3	4.4189
Albedo increase (Global)	0.80	0.3395	-4.0165
G1ocean-albedo (Global)	0.8265	0.3395	0.3674
Control (Ocean)	0.80	0.1	0
abrupt4xCO2 (Ocean)	0.8265	0.1	4.7251
Albedo increase (Ocean)	0.80	0.1863	-7.3806
G1ocean-albedo (Ocean)	0.8265	0.1863	-2.7730

Table 3. Feedback parameters (Section 3.3; units W m^{-2}) for global, land, and ocean averages, calculated via the "Gregory method" (Gregory et al., 2004), where annual mean top-of-atmosphere net radiative flux is regressed against annual mean temperature.

	λ_g	λ_ℓ	λ_o
BNU-ESM	0.9019	0.7181	0.9838
CanESM2	1.1539	1.1898	1.1260
CESM-CAM5.1-FV	1.1435	1.0357	1.1591
CSIRO-Mk3L-1.2	1.0192	0.9300	0.8034
EC-Earth	1.2124	1.1937	1.3155
GISS-E2-R	2.2440	1.9751	2.3560
HadGEM2-ES	0.8411	0.8363	0.8351
IPSL-CM5A-LR	0.8367	1.2891	0.5894
MIROC-ESM	1.0378	0.8736	1.0383
MPI-ESM-LR	1.3701	1.0573	1.3986
NorESM1-M	1.4285	1.8828	1.6063

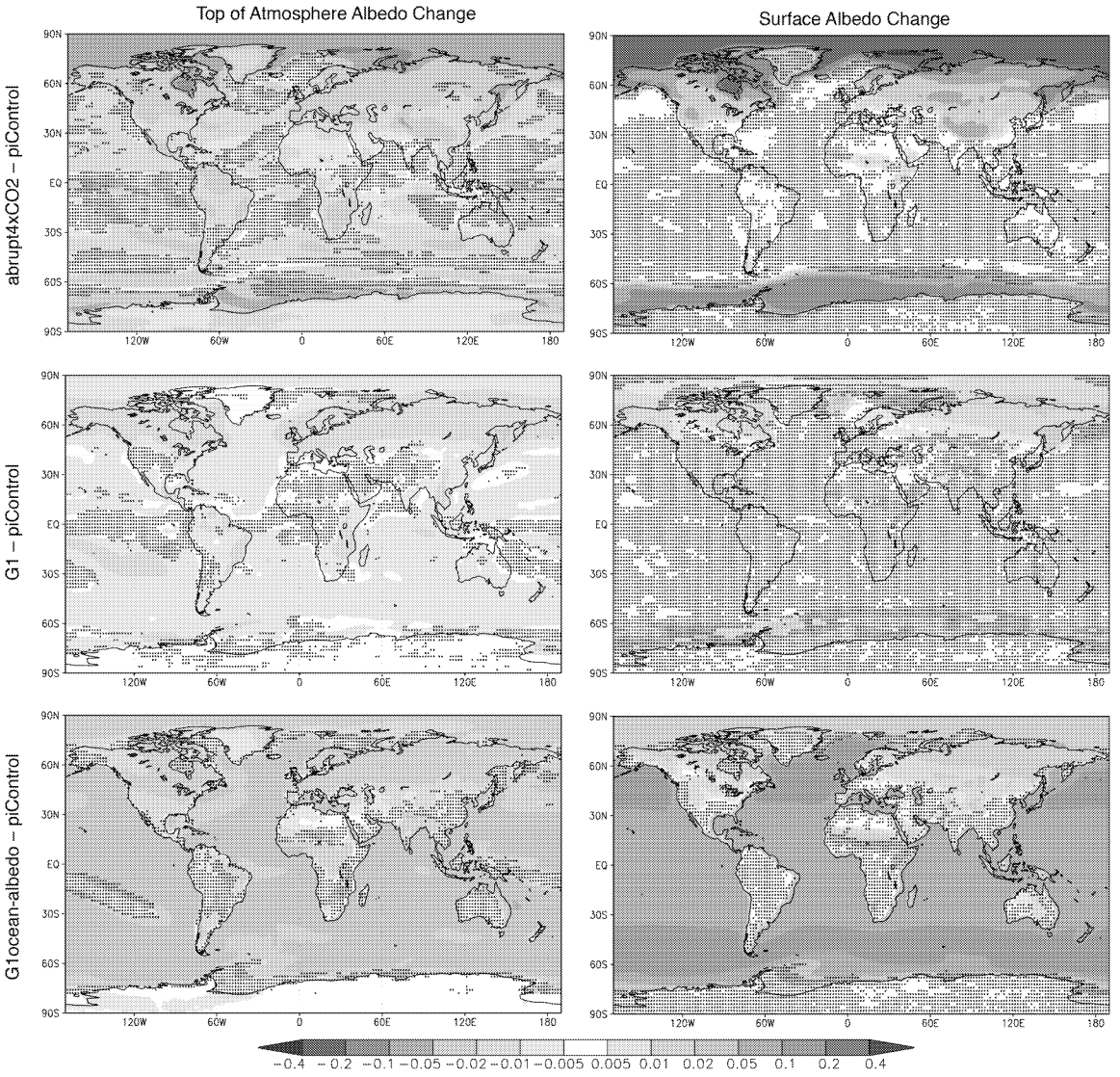

Figure 1. Top-of-atmosphere (TOA) and surface albedo differences (relative to piControl) for the abrupt4xCO2, G1, and G1ocean-albedo experiments. Albedo here is calculated as the ratio of upwelling to downwelling all-sky shortwave radiative flux, either at TOA or at the surface. Values are averages over years 11-50 of simulation. Stippling indicates where fewer than 8 out of 11 models agree on the sign of the response.

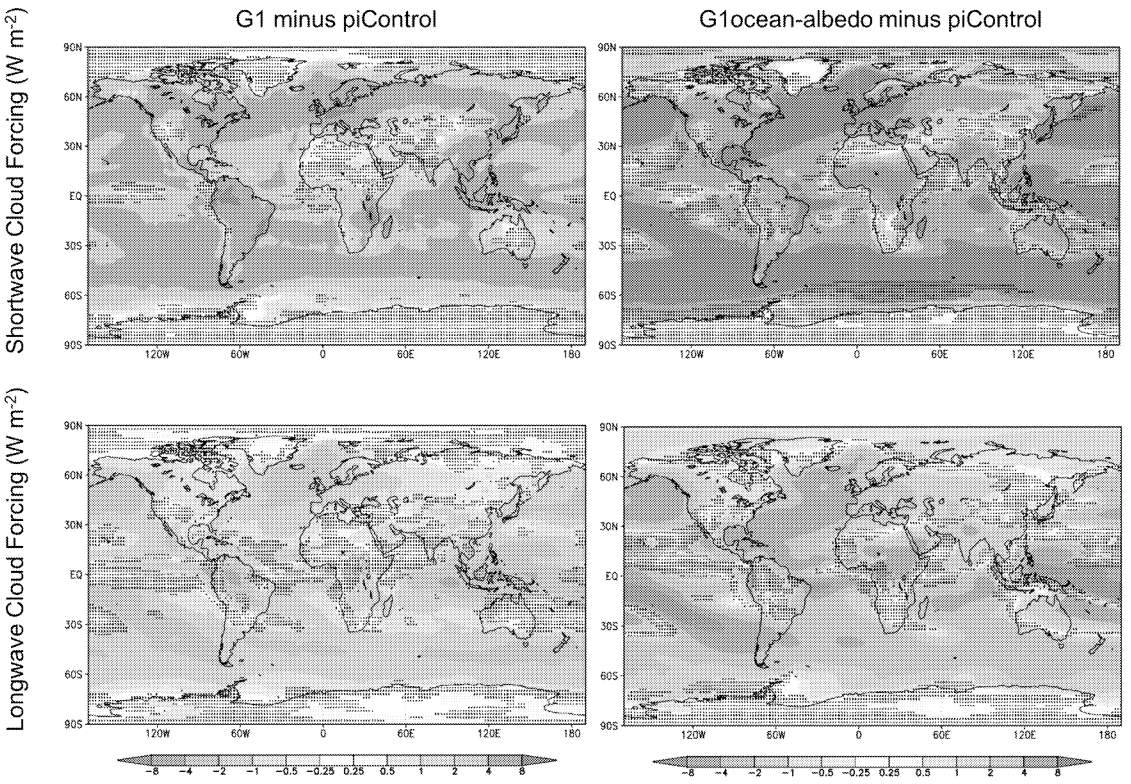

Figure 2. Shortwave (top) and longwave (bottom) cloud forcing changes due to the G1 (left) and G1ocean-albedo perturbations. Cloud forcing is defined as all-sky minus clear-sky radiative flux at the top of the atmosphere.

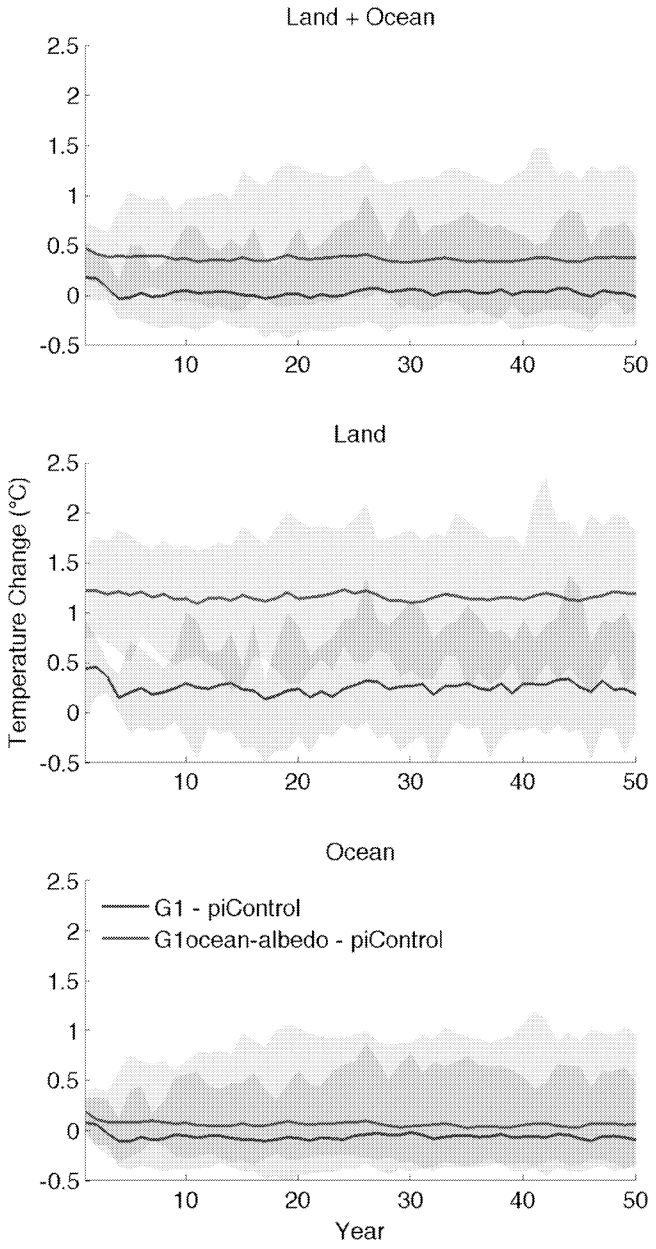

794
795
796 **Figure 3.** Global (top), land (middle), and ocean (bottom) average temperature
797 change for the G1 (blue) and G1ocean-albedo (red) simulations. Lines show the all-
798 model ensemble mean, and shading shows model spread (smallest to largest
799 values).

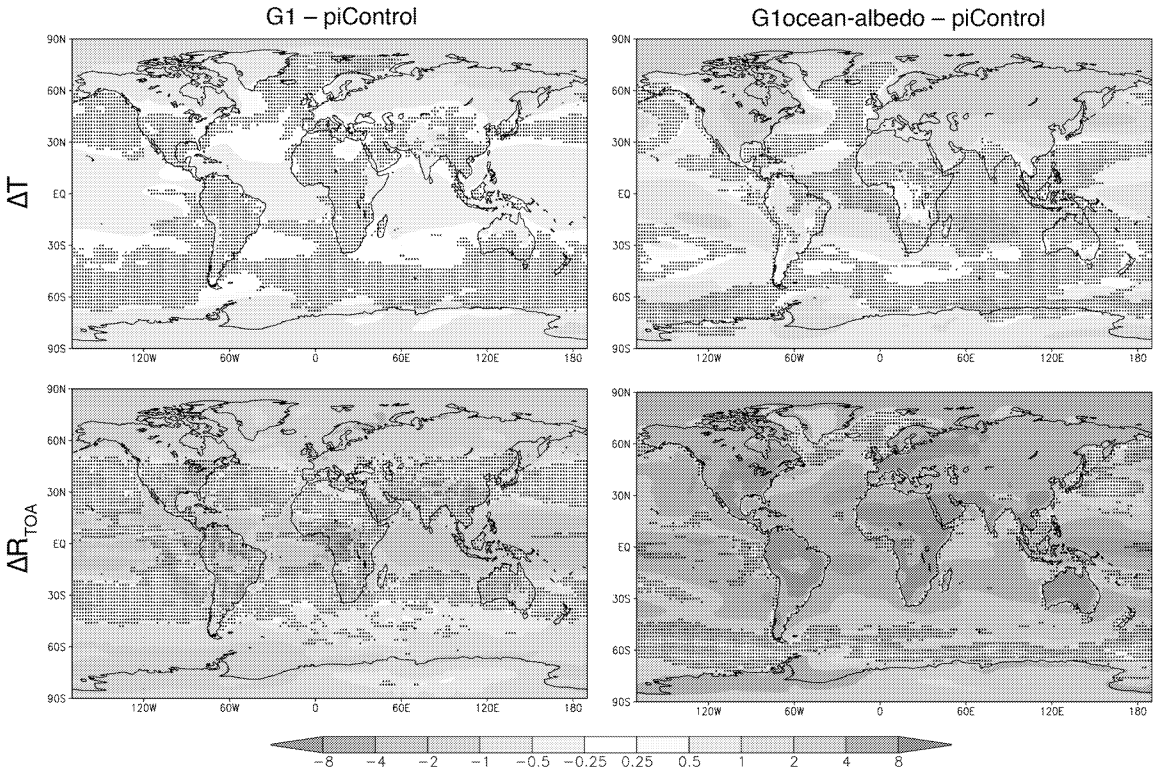

Figure 4. Surface air temperature (top row; K) and TOA net radiative flux (bottom row; W m^{-2}) changes for experiments G1 (left) and G1ocean-albedo (right). Values are averages over years 11-50 of simulation. Stippling indicates where fewer than 8 out of 11 models agree on the sign of the response.

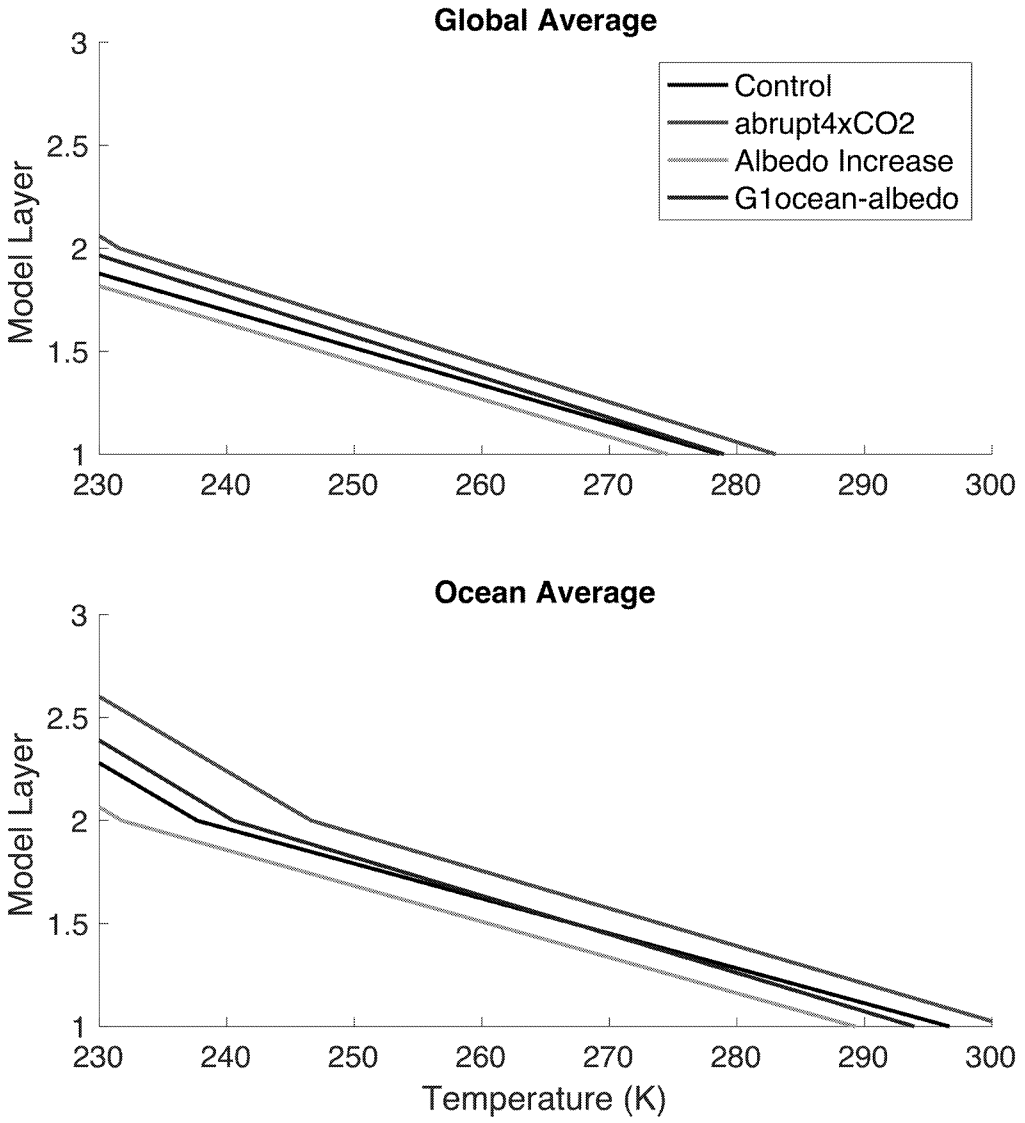

806
807
808 **Figure 5.** Temperature results for calculations with a one-dimensional radiative
809 equilibrium model with 15 vertical layers (only the bottom three layers are shown).
810 Specifications for all of the simulations are provided in Table 2.

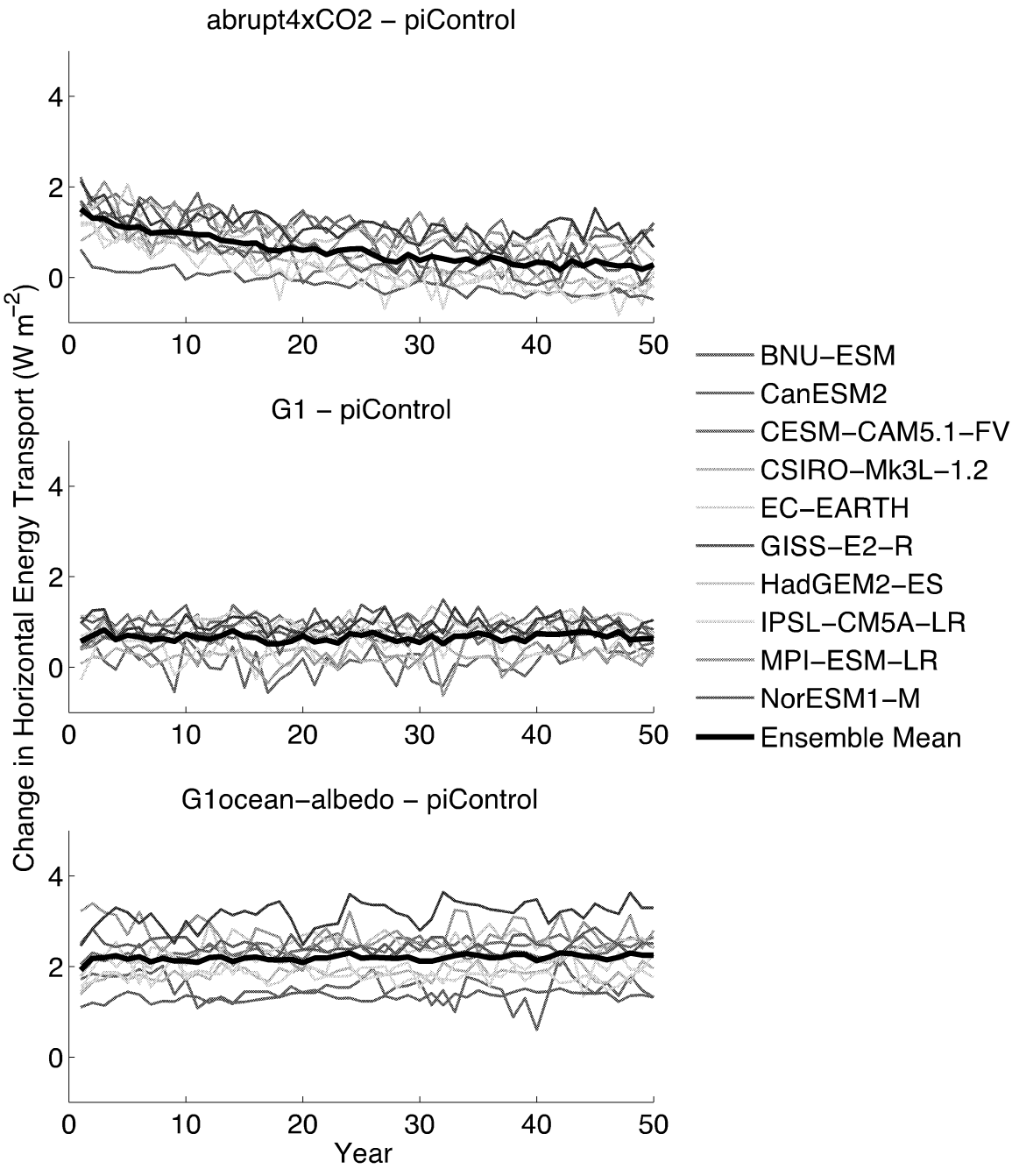

Figure 6. Annual mean change in land-ocean energy transport (Section 3.4; W m^{-2}) from piControl. See Equation 3 for a formal definition.

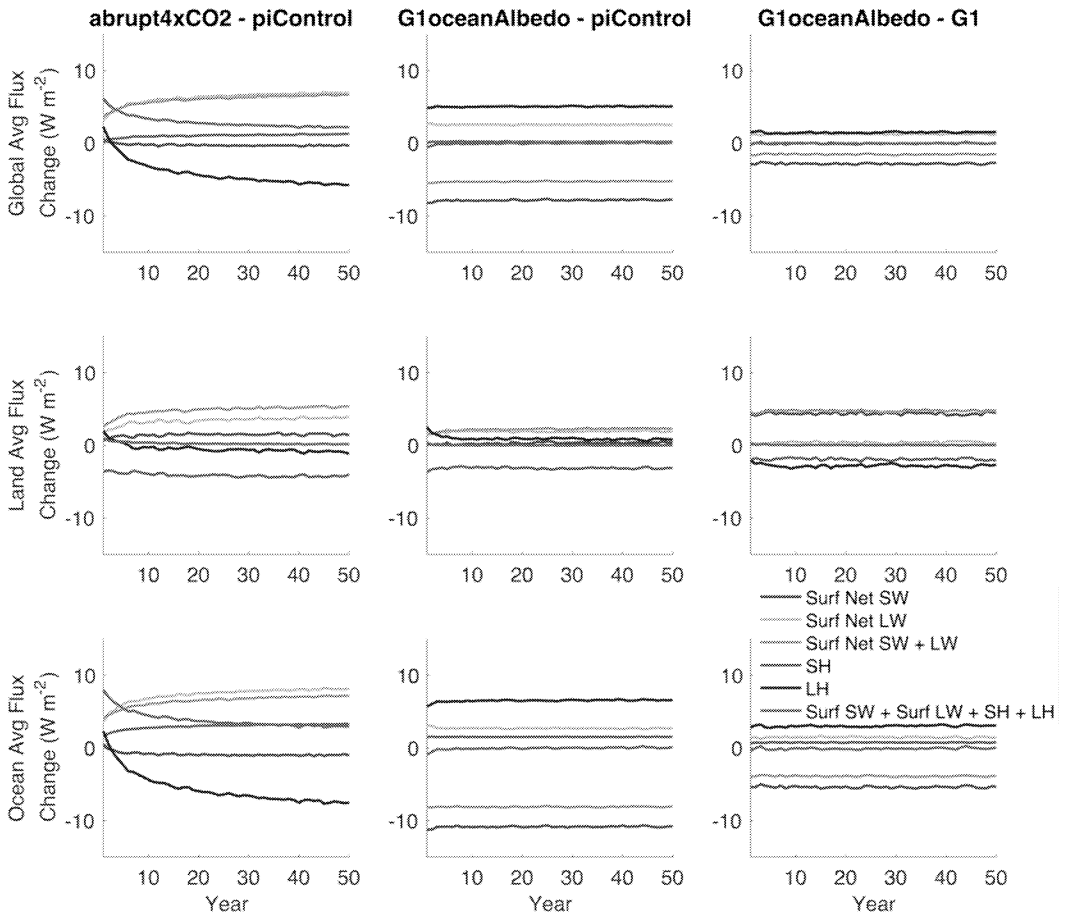

Figure 7. Annual mean time series of all-model mean surface fluxes (terms in Equation 4) for global averages (top), land averages (middle), and ocean averages (bottom). All fluxes are positive in the downward direction.

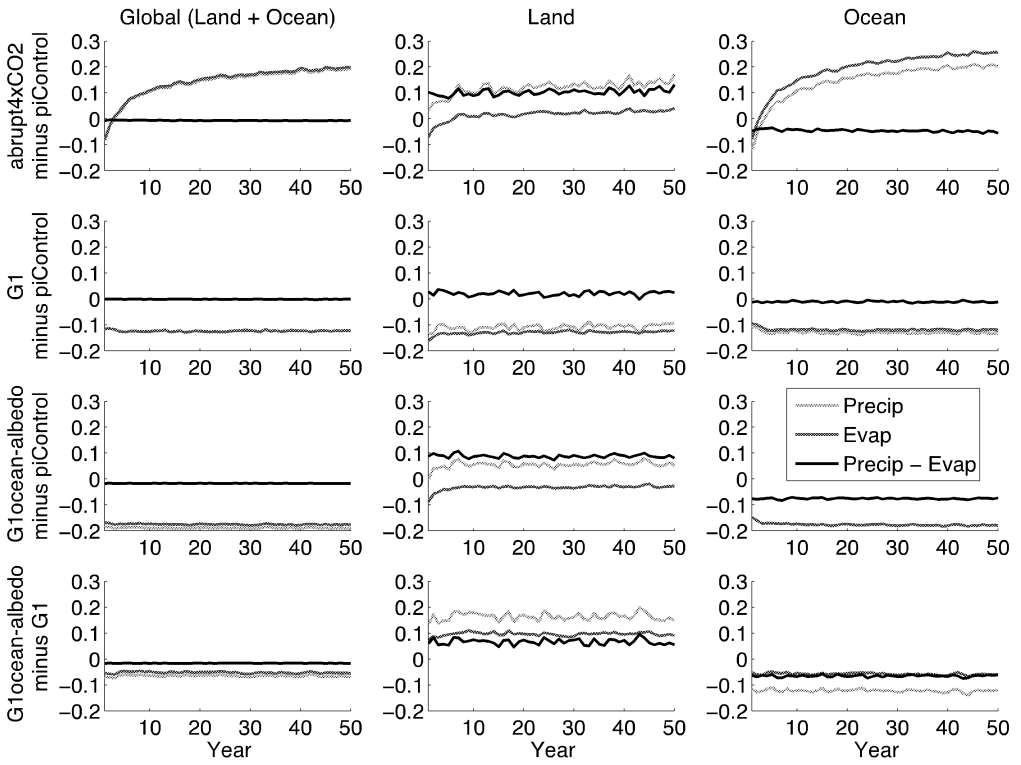

Figure 8. Annual mean time series of hydrological cycle changes (all in mm day^{-1}). Green lines show precipitation changes, red lines show evaporation changes, and black lines show precipitation minus evaporation. When no green line is evident, it is obscured by either the red or black lines.

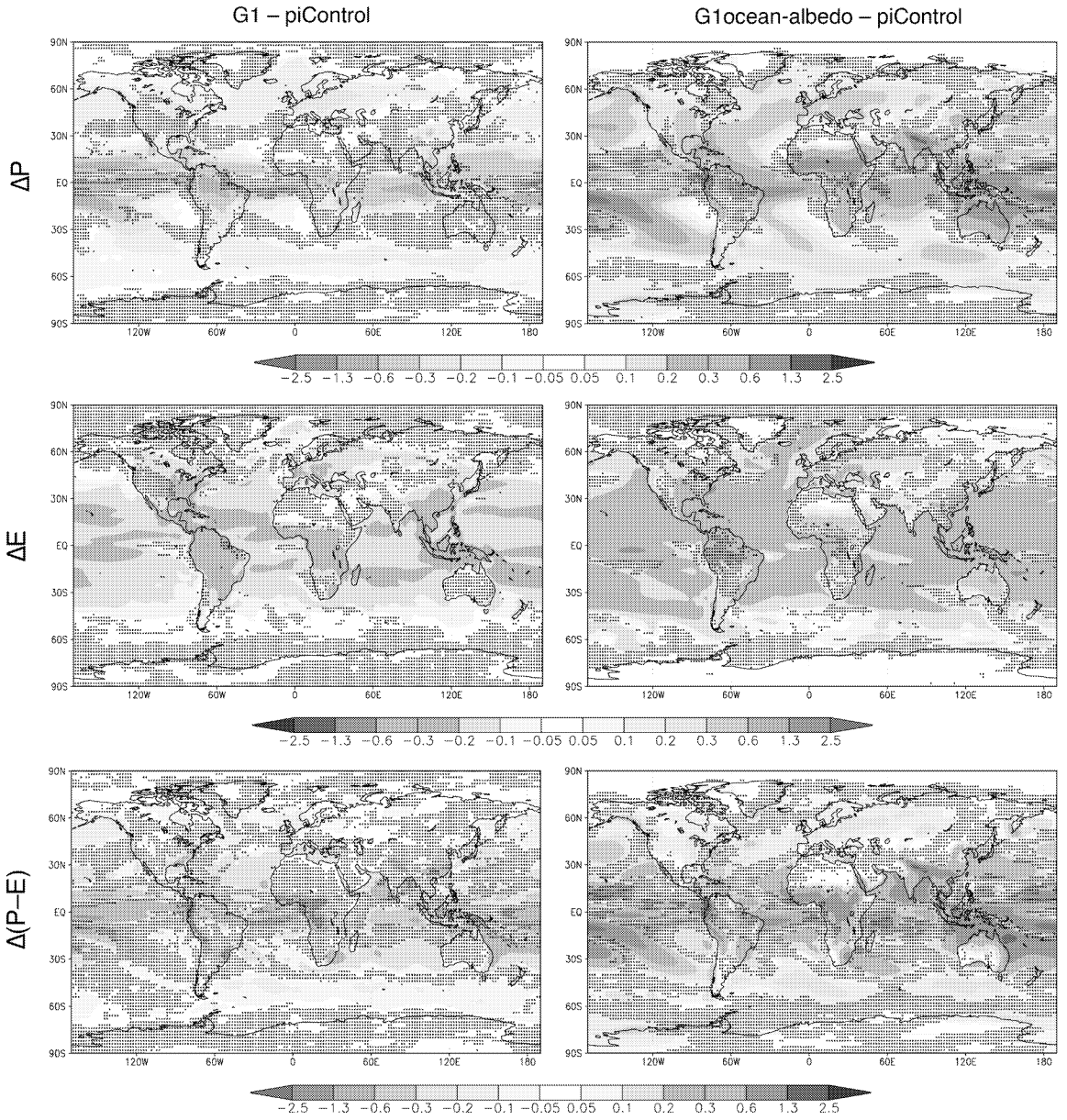

826
827

828 **Figure 9.** Precipitation (top row), evaporation (middle row), and precipitation
829 minus evaporation (bottom row) changes (all panels have units mm day^{-1}) for
830 experiments G1 and G1ocean-albedo. Values are averages over years 11-50 of
831 simulation. Stippling indicates where fewer than 8 out of 11 models agree on the
832 sign of the response.
833

The climate effects of increasing ocean albedo: An idealized representation of solar geoengineering

Ben Kravitz,[1*] Philip J. Rasch,[1] Hailong Wang,[1] Alan Robock,[2] Corey Gabriel,[3] Olivier Boucher,[4] Jason N. S. Cole,[5] Jim Haywood,[6,7] Duoying Ji,[8] Andy Jones,[6] Andrew Lenton,[9] John C. Moore,[8] Helene Muri,[10] Ulrike Niemeier,[11] Steven Phipps,[12,13] Hauke Schmidt,[11] Shingo Watanabe,[14] Shuting Yang,[15] and Jin-Ho Yoon[16]

[1]Atmospheric Sciences and Global Change Division, Pacific Northwest National Laboratory, Richland, WA, USA
[2]Department of Environmental Sciences, Rutgers University, New Brunswick, NJ, USA
[3]Scripps Institution of Oceanography, La Jolla, CA, USA
[4]~~Laboratoire de Météorologie Dynamique,~~ Institut Pierre-Simon Laplace, CNRS / ~~Université P. et M. Curie~~Sorbonne Université, Paris, France
[5]Environment and Climate Change Canada, Toronto, Canada
[6]Met Office Hadley Centre, Exeter, UK
[7]College of Engineering, Mathematics, and Physical Sciences, University of Exeter, Exeter, UK
[8]State Key Laboratory of Earth Surface Processes and Resource Ecology, College of Global Change and Earth System Science, Beijing Normal University, Beijing, China
[9]CSIRO Oceans and Atmosphere, Hobart, Tasmania, Australia
[10]Department of Geosciences, University of Oslo, Oslo, Norway
[11]Max Planck Institute for Meteorology, Hamburg, Germany
[12]Climate Change Research Centre, University of New South Wales, Sydney, Australia
[13]Institute for Marine and Antarctic Studies, University of Tasmania, Hobart, Tasmania, Australia
[14]Japan Agency for Marine-Earth Science and Technology, Yokohama, Japan
[15]Danish Meteorological Institute, Copenhagen, Denmark
[16]Gwangju Institute of Science and Technology, Gwangju, South Korea

Submission to *Atmospheric Chemistry and Physics*
Special Issue: The Geoengineering Model Intercomparison Project

[*]To whom correspondence should be addressed: P.O. Box 999, MSIN K9-30, Richland, WA 99352, USA. E-mail: ben.kravitz@pnnl.gov.

Abstract. Marine cloud brightening has been proposed as a means of geoengineering, or deliberately altering the climate system to offset climate change. As an idealized representation of marine cloud brightening, this paper discusses experiment G1ocean-albedo of the Geoengineering Model Intercomparison Project (GeoMIP), involving an abrupt quadrupling of the CO_2 concentration and an instantaneous increase in ocean albedo to maintain approximate net top-of-atmosphere radiative flux balance. Eleven Earth System Models are relatively consistent in their temperature, radiative flux, and hydrological cycle responses to this experiment. Due to the imposed forcing, the land surface warms by 1.14°C, while most of the ocean cools. Some parts of the near-surface air temperature over ocean warm due to heat transport from land to ocean. These changes generally resolve within a few years, indicating that changes in ocean heat content play at most a small role in the warming over the oceans. The hydrological cycle response is a general slowing down, with little net change in large-scale precipitation minus evaporation, but also with substantial heterogeneity. While idealized, these results have important implications for marine cloud brightening or any other method of geoengineering involving spatially heterogeneous forcing, particularly if that forcing has a strong land/ocean contrast.

Main points:

1) Under an increase in the CO_2 concentration and ocean albedo, the climate transitions to a new, warmer steady state.
2) The land surface warms substantially, and oceans near the land warm due to heat transport
3) The hydrological cycle slows down, with regional heterogeneity in the response

Suggested reviewers:

Tim Andrews
Olivier Geoffroy
Govindasamy Bala

Commenté [o1]: Rephrase. Is this over land only ? why just look at large-scale precip ?

Commenté [o2]: Or even any forcing with a land/sea contrast. What about aerosols over land ?

Commenté [o3]: Needs to say that this is at fixed global energy budget ?

1. Introduction

Geoengineering (also called "climate intervention") describes a set of technological approaches to reduce the effects of climate change by deliberately intervening in the climate system (e.g., Shepherd et al., 2009). There are two broad categories of geoengineering that are commonly discussed: solar geoengineering (modifying the amount of shortwave radiation incident at the surface; NAS, 2015a) and carbon dioxide removal (NAS, 2015b). There are also proposals, such as cirrus cloud thinning (Mitchell and Finnegan, 2009) that do not fit neatly into either of these two categories. In all subsequent discussions in this manuscript, we only discuss solar geoengineering methods.

Two of the most commonly proposed methods of global geoengineering are stratospheric sulfate aerosol injection (SAI) and marine cloud brightening (MCB). Comparison of the different climate effects of these two methods (e.g., Niemeier et al., 2013; Crook et al., 2015) reveals that, among other things, the spatial distributions of the applied forcings strongly affect the climate effects. Many of the effects of SAI can be reasonably well approximated by a uniform reduction in shortwave radiative flux reaching the surface (Kalidindi et al., 2015). Conversely, MCB targets low clouds over oceans (Latham, 1990), which are not ubiquitous. In addition, there are higher order effects due to the altitude at which the shortwave scattering occurs, including multiple scattering effects, infrared absorption of shortwave and longwave radiative flux by sulfate aerosols or cloud particles, and absorption of shortwave radiative flux by atmospheric CO_2 and water vapor (e.g., Kravitz et al., 2013b).

Idealized simulations of solar geoengineering are useful in the context of multi-model intercomparisons, in that they capture many of the effects of more complicated methods of representing geoengineering, yet can be performed by a wide variety of models. In simulations conducted under the Geoengineering Model Intercomparison Project (GeoMIP; Kravitz et al., 2011), an idealized method of representing SAI is via reductions in total solar irradiance; experiment G1 involved offsetting the global radiative flux imbalance from a quadrupling of the CO_2 concentration via solar reduction. Thus far, 15 models have participated in this simulation, providing information about model commonalities and differences in the global climate response, including effects on temperature, the hydrological cycle, cryosphere, terrestrial biosphere, and extreme events (Schmidt et al., 2012; Kravitz et al., 2013a, 2013b; Tilmes et al. 2013; Moore et al., 2014; Glienke et al., 2015; Curry et al., 2014; among numerous other studies). The GeoMIP website (http://climate.envsci.rutgers.edu/GeoMIP/) provides an up-to-date list of publications using GeoMIP model output.

While total solar irradiance reductions are straightforward to simulate in all models, this idealization is not a good approximation of MCB. The dominant effect of MCB is an increase in albedo in and near marine low clouds through "direct" and "indirect" effects. Changes in the albedo near the surface can produce different signatures

from reductions in energy input at the top of the atmosphere. There are also likely to be differences in the spatial distribution of the energy reduction. While some forms of albedo modification like SAI operate over broad areas (on a hemispheric or larger scale), albedo changes produced are likely to operate on smaller spatial scales and be concentrated over particular oceanic regions. Previous studies suggest that the clouds that are most susceptible to albedo modification are located on the western side of ocean basins in the subtropics, in regions dominated by stratocumulus clouds (Oreopoulos and Platnick, 2008). So, rather than considering a reduction of solar input operating uniformly over both land and ocean, an idealized representation of MCB that better approximates the effects is to increase the albedo only over ocean surfaces, as described by Kravitz et al. (2013c). This method can also be used to assess some effects of geoengineering by creating microbubbles at the ocean surface to increase reflectivity (e.g., Seitz, 2011).

In this study, we investigate the climate effects of using ocean albedo increases to offset CO_2 warming and compare those effects with those of total solar irradiance reduction (experiments are described in more detail in the following section). All simulations were conducted under the auspices of GeoMIP, allowing us to characterize a range of model responses to these different idealized methods of representing solar geoengineering.

2. Methodology and Description

Our analyses focus on four simulations: (1) a preindustrial control simulation (piControl), (2) a simulation in which the CO_2 concentration is abruptly quadrupled from its preindustrial value (abrupt4xCO2), (3) a simulation in which the net radiative flux imbalance in abrupt4xCO2 is offset by a reduction in total solar irradiance (G1), and (4) a simulation in which the net radiative flux imbalance in abrupt4xCO2 is offset by an increase in ocean albedo everywhere by a uniform factor (G1ocean-albedo). piControl and abrupt4xCO2 are standard experiments in the Coupled Model Intercomparison Project Phase 5 (CMIP5; Taylor et al., 2012). G1 is described further by Kravitz et al. (2011). The protocol for G1ocean-albedo is described in more detail by Kravitz et al. (2013c). Table 1 lists the models participating in this study, including relevant references and the required change in albedo to meet the objectives of experiment G1ocean-albedo. A similar table for experiment G1 is given by Kravitz et al. (2013a). One of the advantages of G1ocean-albedo is that, like G1, all models can conduct this simulation fairly easily. Supplemental Table S1 quantifies how well each model achieved radiative balance in the G1 and G1ocean-albedo experiments.

Kravitz et al. (2013c) found that in test simulations, one could only determine whether the objectives of G1ocean-albedo were met after several decades of simulation. However, as our analysis will show, once the proper value of ocean albedo increase is ascertained, the climate response reaches steady state in a few years, as in experiment G1 (Kravitz et al., 2013a). Supplemental Table S2 quantifies temperature trends in each participating model over years 11-50 of simulation. The

Commenté [o4]: I think it is important to restate that we aim for a balanced TOA budget over the first 10 years, right ? plus the fact that the albedo is increase proportionally

mean model trend over this period is approximately zero (to four decimal places), and with little exception, the trends in G1 and G1ocean-albedo are an order of magnitude smaller than the trends in the abrupt4xCO2 simulation. As such, for the purpose of analysis, we assume that "slow responses," i.e., responses operating on time scales longer than a few years (e.g., Andrews and Forster, 2010; Sherwood et al., 2015) are negligible in the G1 and G1ocean-albedo simulations. We do not separate results into rapid adjustment and slow response timescales, and with the exception of time series plots, all figures show averages over the years 11-50 of simulation, which we take as a sufficient indication of the dominant climate response after the transient response has resolved.

Except where indicated, all plots show the mean model response. All values in the text are reported as mean (min to max), where mean indicates the all-model mean for that particular quantity, min is the lower bound of the range of model responses, and max is the upper bound of the range of model responses. In all maps, stippling indicates where fewer than 75% of the models agree on the sign of the response. All models in Table 1 were able to provide output for all variables except for cloud radiative forcing. The models included in cloud forcing analyses are BNU-ESM, CanESM2, CESM-CAM5.1-FV, HadGEM2-ES, IPSL-CM5A-LR, and MPI-ESM-LR. Supplemental Tables S1-S15 provide more quantitative information for all of the analyses presented in this study.

3. Results

3.1. Albedo and Temperature

Figure 1 shows the change in albedo at the top-of-atmosphere and at the surface for the abrupt4xCO2, G1, and G1ocean-albedo simulations, where albedo is defined as the ratio of upwelling to downwelling all-sky shortwave radiative flux. Quantitative values are given in Supplemental Tables S3 and S4. Results for abrupt4xCO2 and G1 are consistent with known responses of an increase in absorbed shortwave by carbon dioxide, reduced cloud cover, and reduced snow and sea ice cover (e.g., Schmidt et al., 2012; Kravitz et al., 2013b). These result in a broad decrease in albedo at the top of atmosphere and a decrease in surface albedo in many regions with substantial snow and ice cover. G1ocean-albedo retains many of these local high latitude features, but with large albedo increases over ocean, consistent with the experimental design and imposed forcing.

Figure 2 expands upon this picture by showing changes in shortwave and longwave cloud forcing in G1 and G1ocean-albedo, where cloud forcing is defined as all-sky minus clear-sky radiative flux measured at the top of the atmosphere. Positive shortwave values and negative longwave values in Figure 2 generally indicate less cloud cover. As was shown by Kravitz et al. (2013b), cloud cover in G1 tends to be reduced, which is consistent with what is depicted in Figure 2. For G1ocean-albedo, cloud cover is reduced over most ocean regions and large portions of land. Exceptions include an increase in cloudiness over the Arctic, much of Africa, South

Asia, Australia, and the leeward side of the Andes. These changes in cloudiness have implications for the hydrologic cycle, which we revisit in Section 3.5.

Figure 3 shows changes in global mean, land mean, and ocean mean surface air temperature for the G1 and G1ocean-albedo multi-model ensembles. Quantitative values are provided in Supplemental Table S5. Whereas the G1 simulation largely offsets temperature changes due to increased CO_2 concentration, G1ocean-albedo is approximately 0.36°C (-0.12 to 1.20) warmer than the control simulation. This is predominantly due to warming over land by 1.14°C (0.41 to 1.83). The temperature results in Figure 3 indicate that the temperature change happens within the first few years, and while some models show a slight trend in temperature over the 50-year G1ocean-albedo simulation (Supplemental Table S2), in general, any such trends are small, especially as compared to the warming in the abrupt4xCO2 simulation. This lack of substantial transient behavior after an initial fast response indicates that G1ocean-albedo has entered a new approximate steady state.

Figure 4 shows spatial patterns of change in temperature and top-of-atmosphere net radiative flux. (Also see Supplemental Tables S5 and S6.) The temperature changes are broadly consistent with the net radiative flux changes in the respective experiments. As was discussed by Kravitz et al. (2013a), G1 results in an "overcooling" of the tropics and an "undercooling" of the poles, consistent with offsetting the ubiquitous longwave forcing from CO_2 with a latitudinally dependent reduction in shortwave. G1ocean-albedo shows warming at high latitudes, over land regions, and in some ocean regions near or downwind of large continents, with the remaining ocean regions generally showing cooling. Because net top-of-atmosphere radiative flux is approximately zero in G1ocean-albedo, these temperature changes cannot be the result of energy being added to or subtracted from the climate system, and instead must be the result of energy redistribution. Hypotheses for why these temperature change patterns look the way they do (which will be tested in subsequent sections) include

Commenté [o5]: This needs to come earlier

1) The global average warming experienced in G1ocean-albedo is primarily due to increased heating over land.

2) Most warming over oceanic regions is due to transport of heat from land to ocean.

3) Any contributions to temperature or radiative flux changes from changes in ocean heat content are small on the timescales being evaluated here.

3.2. Hypothesis 1: Increased heating over land drives global average warming in G1ocean-albedo

The first hypothesis is fairly straightforward to argue based on first principles. To do so, we employ a one-dimensional radiative equilibrium model with 15 vertical layers extending from the surface to the nominal top-of-atmosphere. In the model,

Commenté [o6]: Has the model two compartments for ocean and land ? should you show a schematic of the model ?

each layer behaves as a gray body with a specified emissivity, and the model computes radiative transfer between each layer via Planck radiation (the Stefan-Boltzmann equation). Although this model represents a gross oversimplification of the vertical profile of temperature response to idealized forcing, it is useful here for understanding differences between land and ocean temperature changes in response to the forcing imposed in G1ocean-albedo.

Figure 5 shows temperature profiles calculated using this model for four experiments: a control simulation, an abrupt4xCO2-like simulation (modeled as an increase in the emissivity of each model layer), a simulation with increased surface albedo, and G1ocean-albedo-like simulation involving an increase in emissivity and an increase in surface albedo. These simulations were conducted separately for global average and ocean-only regions.

Values of emissivity in the control simulation were prescribed to be 0.80 at all layers, consistent with a gray body (Pandey et al., 1995). The emissivity in the abrupt4xCO2 simulation was calculated to be the value such that global mean temperature change in the first model layer is approximately 4.42 K (Supplemental Table S5), yielding an emissivity value of 0.8265. In the control simulations, the surface albedos for the global and ocean-only simulations are 0.3 and 0.1, respectively, consistent with estimates provided by Stephens et al. (2015) and the values given in Table 1. In the global average simulation, the albedo increase in the G1-ocean albedo simulation was calculated to be the value such that global mean temperature change in the first model layer is approximately 0.36 K (Supplemental Table S5). In the ocean average simulation, the albedo increase is the all-model average of the required albedo increase in Table 1, which is a multiplication factor of 1.8627.

The results in Figure 5 show that under reasonable assumptions around atmospheric emissivity and surface albedo, oceanic cooling is expected in the G1ocean-albedo simulation. Based on these results, any increase in global average temperature must be due to warming over land. The oceanic temperature change in this simple model's simulation of G1ocean-albedo is -2.77 K, which is far too large in magnitude as compared to the results from the Earth System Models. Figure 2 indicates that changes in cloud cover in G1ocean-albedo are more likely to increase the magnitude of this temperature change than decrease it. In subsequent sections, we discuss some additional mediating factors that could act to reduce the magnitude of this change, such as land-ocean energy transport or reduced net ocean heat uptake. Nevertheless, the dominant radiative effects in G1ocean-albedo are to cause cooling over the oceans, as is seen in Figure 4.

3.3. Hypothesis 2: The role of Land-Ocean Energy Transport (LOET)

Although the air over the ocean warms somewhat in G1ocean-albedo, it does not warm uniformly. Figure 4 shows that much of the warming over the ocean is in areas near land, indicating the potential for some of the heating energy over land to

be transported to ocean regions. This can be quantified via calculating what Geoffroy et al. (2015) call horizontal energy transport, and which we call land-ocean energy transport (LOET), as it represents an aggregate transport of energy from the atmosphere over the land (averaged over all land regions) to the atmosphere over the ocean (averaged over all ocean regions). They provide a more detailed description, calculation, and validation of this concept using a three-box energy balance model that can be fitted to changes in land/ocean temperature and TOA energy imbalance such that the model captures the relevant energy transport dynamics; we repeat here only the calculations germane to our discussions.

Gregory et al. (2004) describe a method of estimating adjusted radiative forcing and the aggregate strength of global feedbacks via linear regression of the net global, annual mean TOA radiative flux imbalance (ΔR) against the global, annual mean temperature change (ΔT) in response to a forcing. The *y*-intercept of the regression line gives an estimate of adjusted radiative forcing ($\boldsymbol{\mathcal{F}}$), and the negative of the slope of the regression line gives the feedback parameter (λ). Similarly, one can perform regression just over land-averaged quantities (denoted with the subscript ℓ) or just over ocean quantities (subscript o). Feedback parameter values are provided in Table 3.

In addition, one can regress ΔT_ℓ against ΔT_o to obtain a *y*-intercept of

$$\boldsymbol{\mathcal{F}}_\ell/(\lambda_\ell+\alpha_\ell/f_\ell) \quad (1)$$

where α_ℓ is the land heat transport parameter and f_ℓ is the land fraction (approximately 0.3). The slope is

$$(\alpha_o/f_\ell)/(\lambda_\ell+\alpha_\ell/f_\ell) \quad (2)$$

If one solves these two equations for α_ℓ and α_o, then one can define

$$\Delta A= \alpha_\ell \Delta T_\ell - \alpha_o \Delta T_o \quad (3)$$

The quantity ΔA is the time-dependent LOET (units of W m^{-2}).

Figure 7 provides calculations of LOET for the simulations presented here. See Supplemental Table S7 for more details on individual model values. In the abrupt4xCO2 simulation, changes in LOET are positive (indicating an increase in heat transport from the land to the ocean) and decrease in magnitude steadily over the course of the simulation; these results are discussed in more detail by Geoffroy et al. (2015).

In Experiment G1, LOET increases by a model-dependent constant value and remains relatively unchanged over the course of the simulation. Although the air temperature over land in G1 increases slightly, and the air temperature over ocean decreases slightly (Kravitz et al., 2013a), the temperature changes in G1 are more

latitude-dependent than representative of a clear land-ocean contrast (Figure 4), so it is perhaps not unexpected that LOET would be small.

Experiment G1ocean-albedo exhibits a strong land-ocean contrast in temperature (Figure 4), and the response is in steady state after a few years. As such, consistent with the behavior of other fluxes, LOET in G1ocean-albedo does not show transient behavior. LOET in G1ocean-albedo is approximately 2.20 (1.35 to 3.21) W m^{-2}, which is larger than in the other experiments examined here.

Converting LOET into temperature change is not necessarily straightforward, but an approximate change in temperature can be calculated by combining values of ΔA (Supplemental Table S7) with feedback parameter calculations (Table 3). More specifically, the temperature "added" to the air over the oceans by LOET can be calculated as $\Delta A/\lambda_o$, and the temperature "subtracted" from the air over land by LOET can be calculated as $\Delta A/\lambda_l$. Performing these calculations, LOET in the G1ocean-albedo experiment contributes 1.87°C (0.57 to 3.06) to ocean temperature and "subtracts" 2.03°C (0.68 to 3.06) from land temperature. We caution that this naïve calculation is somewhat circular, and it inherently includes in the ocean calculations both regions unaffected by LOET (e.g., tropical oceans) and regions strongly affected by LOET (e.g., Northeast Atlantic and Pacific Oceans).

Based on the calculations in Section 3.2 and the present section, it seems unlikely that LOET can on average transport enough energy from the land to the ocean to offset the radiative deficit due to an ocean albedo increase. However, locally, LOET appears to be able not only to offset these radiative changes, but also result in net warming.

3.4. Hypothesis 3: Atmospheric Column Energetics and Net Energy Flux into the Oceans

An additional potential source of energy to the atmosphere is a reduction in net ocean heat uptake. Calculating changes in ocean heat uptake are challenging and not particularly revealing in this case for three reasons:

1) It is possible that the models used in simulating G1ocean-albedo were not entirely spun up to steady state. As such, any remaining imbalances could manifest as changes in ocean heat content. In principle, one could subtract off the preindustrial control value, which likely has a similar trend in ocean heat content arising from spinup. However, this would not remove the influence of nonlinearities (state dependence), so there is no way to guarantee that the signal is entirely due to the G1ocean-albedo forcing.
2) As is seen in Supplemental Table S1, not all models were able to achieve top-of-atmosphere net radiative flux balance over the course of the simulation. These small changes can lead to large changes in ocean heat content over the course of a 50-year simulation. For example, a 0.1 W m^{-2} imbalance over a 50-year period can lead to an additional 5.5 x $\times$$10^{22}$ J of energy

incident at the ocean surface. As such, we are unable to properly assess the degree to which ocean heat content changes may be due to small imbalances.

3) Ocean heat content requires a depth threshold for calculation, meaning calculations of it are sensitive to redistribution of heat to/from lower depths, obscuring the signal of the forcing.

As an alternative, we calculate net energy exchange across the surface in terms of changes in radiative and turbulent fluxes. Kravitz et al. (2013b) calculated energetics changes in the entire atmospheric column. However, because we are only interested in net surface fluxes, we calculate

$$\Delta S = \Delta R_{surf} + \Delta SH + \Delta LH \quad (1)$$

where ΔR_{surf} is the change in net surface radiative flux (shortwave and longwave), ΔSH is change in sensible heat flux from the atmosphere to the surface, and ΔLH is change in latent heat flux from the atmosphere to the surface. By convention, all fluxes are positive downward unless specifically noted. Calculations of individual terms in this budget, as well as of ΔS, are provided in Supplemental Tables S8-S12. Because these calculations are performed at the surface, no advection term (e.g., LOET) is needed, and ΔS is well defined as a land or ocean average.

Figure 7 shows the all-model mean for all of the terms in Equation 4. Several clear conclusions emerge. The first is that ΔS is approximately zero globally, over land, and over ocean for nearly the entire 50-year period, after an initial rapid adjustment that resolves within a few years. With the exception of latent heat over land, this is true of all fluxes for G1ocean-albedo in Figure 7, and even latent heat flux over land reaches an approximate steady state within ten years. If ΔS indeed serves as a useful proxy for net energy flux into or out of the ocean, then these results indicate that there is no sizable contribution to atmospheric energetics by changes in ocean heat content. Moreover, even if ΔS were not zero over ocean, ocean heat content changes would still be an insufficient explanation for temperature changes due to incongruent timescales. The oceanic mixed layer operates on an approximately decadal timescale, but all transient behavior in these simulations is resolved well before ten years. The transient response is much more consistent with a land surface time scale, which is on the order of 1-3 years. As such, it seems plausible that the temperature changes over ocean in G1ocean-albedo are due to land processes rather than ocean heat content changes. This is not to say that the ocean plays no role in the observed temperature changes. Rather, given the discussions in this section and the two previous sections, the role of the ocean heat content in causing temperature changes over the ocean in G1ocean-albedo is likely small.

The remainder of the results in Figure 7 are consistent with the applied forcing. There is a large sensible heat flux increase from the land to the atmosphere of 2.87 (-0.99 to 6.00) W m^{-2}, with a comparatively smaller sensible heat flux decrease from the ocean to the atmosphere of 1.47 (0.34 to 2.20) W m^{-2}. Over the ocean, latent heat flux from the surface to the atmosphere is 6.71 (4.95 to 7.89) W m^{-2} lower in

399 G1ocean-albedo than in the preindustrial control simulation. These results indicate
400 a greater shift of energy away from evaporating water and toward increasing land
401 temperature. Large differences in flux magnitude between G1 and G1ocean-albedo
402 can be found over land for net shortwave flux and latent heat flux, and differences in
403 sign can be found over land for total radiative flux. These features are consistent
404 with the applied forcing being different over land and ocean.
405
406 **3.5. Hydrological cycle changes**
407
408 Introducing a strong land-ocean energy and temperature gradient, as in G1ocean-
409 albedo, will undoubtedly impact the hydrological cycle. Although the simulation is
410 idealized, more realistic representations of MCB have shown important hydrological
411 cycle impacts, including secondary circulation patterns that shift precipitation onto
412 land in the tropics and extratropics (Bala et al., 2010), changes in the monsoon
413 (Alterskjær et al., 2013), and changes in the Walker circulation (Niemeier et al.,
414 2013). Here we evaluate the large-scale hydrological cycle changes in G1ocean-
415 albedo, with possible applicability to other realizations of MCB.
416
417 Figure 8 shows global, land, and ocean averaged precipitation, evaporation, and
418 precipitation minus evaporation (P–E) for all of the simulations considered in this
419 manuscript; quantitative descriptions are given in Tables S13–15. The abrupt4xCO2
420 simulation is the only one with a distinct rapid adjustment and slow response. Over
421 both land and ocean, G1 shows decreases in precipitation and evaporation of
422 approximately equal magnitude, resulting in net changes in P–E of 0.02 (-0.05 to
423 0.11) mm day^{-1} over land and -0.01 (-0.04 to 0.01) mm day^{-1} over ocean. In
424 G1ocean-albedo, global precipitation and evaporation both decrease by
425 approximately 0.19 (0.11 to 0.26) mm day^{-1} to yield little net change in P–E.
426 However, this net small change is due to differential effects over land and ocean.
427 Over land, precipitation remains relatively unchanged, but evaporation decreases,
428 resulting in a net change in P–E by 0.09 (-0.18 to 0.18) mm day^{-1}. Over the ocean,
429 both precipitation and evaporation decrease, with a net negative P–E of -0.06 (-0.19
430 to -0.01) mm day^{-1}.
431
432 Annual mean land/ocean contrasts in precipitation and evaporation changes tend to
433 be more uniform in sign in experiment G1 (Figure 9), resulting in few large regions
434 of change in P–E with the exception of the tropics (mostly driven by a southward
435 shift in the intertropical convergence zone; Kravitz et al., 2013a). In G1ocean-
436 albedo, precipitation and evaporation over the oceans are reduced in most regions,
437 consistent with the applied forcing. Over land, the signs of precipitation and
438 evaporation changes are regionally heterogeneous, yet the precipitation and
439 evaporation changes are concordant, e.g., land regions with increased precipitation
440 also generally show increased evaporation. The net P–E map is highly
441 heterogeneous, but in general, tropical land areas are projected to have more
442 available moisture (as measured by P–E) under G1ocean-albedo, and midlatitude
443 land areas are projected to have less. The implications of these changes for people
444 and ecosystems ~~is~~ are an important area of future research.

4. Discussion and Conclusions

The results presented here indicate that even though experiments G1 and G1ocean-albedo both achieve approximate net top-of-atmosphere radiative flux balance, the climate system responses differ dramatically between the two experiments. The idea that global energy balance can still result in local changes is perhaps not surprising, as feedback operate locally (Armour et al., 2013). These different climate responses for the same forcing are effectively an illustration of different efficacies (Hansen et al., 2005). Even in the absence of slow responses, forcings with different efficacies can cause different climate system changes (Kravitz et al., 2015). G1ocean-albedo serves as an excellent reminder not to conflate small net top-of-atmosphere radiative flux imbalance with small temperature change; a clear relationship between those two quantities is not guaranteed.

Relatedly, the results obtained for G1ocean-albedo were to some extent by design. The objective of G1ocean-albedo was to achieve net top-of-atmosphere radiative flux balance, which resulted in warming. Conceivably, one could define an objective of no global temperature change, implying a net negative radiative flux at the top-of-atmosphere. It is unclear whether, unlike G1ocean-albedo, that alternate approach would result in transient behavior that lasts longer than a few years. Such an experiment could be accomplished using feedback methods that have been introduced to geoengineering research in recent years (e.g., MacMartin et al., 2014; Kravitz et al., 2016).

Commenté [o7]: Or no global land temperature change

The results presented here have several features that were not necessarily expected from the outset. Kravitz et al. (2013c) found that determining whether the climate system was in balance took up to 30 years of simulation. However, once that balance is achieved, the climate does not change appreciably after the initial rapid adjustment. Potential future work could investigate these results, shedding light on timescales of climate response and potential thresholds, e.g., how large does the energy imbalance need to be to trigger slower adjustments?

Related to this issue of different timescales of adjustment is the traditional separation of climate response into rapid adjustment and slow response components (e.g., Andrews and Forster, 2010; Sherwood et al., 2015). The rapid adjustment is often defined as the climate response unassociated with global mean temperature change, and the slow response describes a transient temperature change with a large component due to climate system feedbacks. The results from G1ocean-albedo, like those of G1 (Kravitz et al., 2013b), show an initial rapid change and no appreciable slower change. However, in G1ocean-albedo, that initial change is associated with a temperature increase, which in principle should excite ~~a~~ slow ~~adjustment through~~ climate system feedbacks. These results are somewhat inconsistent with the traditional definitions of rapid adjustment and slow response. Additionally, this sustained temperature increase is to some extent decoupled from net energy imbalances in the climate system, as ΔR_{TOA} and ΔS (Equation 4) are both

Commenté [o8]: Ummmh, not sure I understand here

approximately zero. Reconciling all of these features suggests a potentially rich research topic focused on understanding the relationships between radiative flux changes, temperature changes, and the circumstances under which climate feedbacks are excited.

G1ocean-albedo may be more apposite to the impact of geoengineering via "ocean microbubbles," whereby surfactants are added to the ocean surface, promoting the formation of microscopic, highly reflective bubbles (Seitz, 2011; Robock, 2011). An area of investigation we did not undertake, yet one that repeatedly emerges in discussions of microbubbles, is the effects on the ocean mixed layer. By reflecting more solar radiation, microbubbles have the potential to inhibit vertical mixing and available light in the euphotic zone, which could have profound effects on marine biota. This implies that another useful future area of investigation for the G1ocean-albedo simulation is an analysis of the marine carbon cycle.

Commenté [o9]: Temperature, depth, radiation, ...

There are numerous potential areas of research prompted by this study. The stark land/ocean contrast in warming has potential implications for ocean circulation patterns, including the meridional overturning circulation and Western boundary ocean currents, with consequent implications for marine ecosystems. This contrast also has implications for the terrestrial biosphere, including ecosystem services and the land and ocean carbon cycles. Although we did not evaluate seasonal changes in this manuscript, such investigations could prove fruitful for more detailed assessments of variability, such as monsoon precipitation, extreme events, and sea ice extent.

Despite being informative for MCB, there are limits as to the applicability of this idealized approach. There are important differences in boundary layer stability changes from surface albedo increases versus marine stratocumulus cloud top brightening. Also, it appears impossible for marine cloud brightening to be conducted over all ocean regions and with a sufficient magnitude to offset the radiative forcing from a quadrupling of the CO_2 concentration. The purpose of this manuscript is to describe the broad features of change under a uniform ocean albedo increase, and some of these changes are likely to be present with more realistic scenarios of marine cloud brightening. We anticipate that future research can more deeply explore the applicability of this simulation to marine cloud brightening.

Acknowledgments. We thank Jón Egill Kristjánsson, who tragically passed away, for invaluable comments on an earlier version of this manuscript. We acknowledge the World Climate Research Programme's Working Group on Coupled Modelling, which is responsible for CMIP, and we thank the climate modeling groups for producing and making available their model output. For CMIP the U.S. Department of Energy's Program for Climate Model Diagnosis and Intercomparison provides coordinating support and led development of software infrastructure in partnership with the Global Organization for Earth System Science Portals. We thank all participants of the Geoengineering Model Intercomparison Project and their model

development teams, CLIVAR/WCRP Working Group on Coupled Modeling for endorsing GeoMIP, and the scientists managing the Earth System Grid data nodes who have assisted with making GeoMIP output available. The Pacific Northwest National Laboratory is operated for the U.S. Department of Energy by Battelle Memorial Institute under contract DE-AC05-76RL01830. Simulations performed by Ben Kravitz were supported by the NASA High-End Computing (HEC) Program through the NASA Center for Climate Simulation (NCCS) at Goddard Space Flight Center. Alan Robock is supported by NSF grants AGS-1157525 and GEO-1240507. Andy Jones was supported by the Joint UK DECC/Defra Met Office Hadley Centre Climate Programme (GA01101). Olivier Boucher acknowledges HPC resources from CCRT under the allocation 2015-t2012012201 made by GENCI (Grand Equipement National de Calcul Intensif). This research was supported under the Australian Research Council's Special Research Initiative for the Antarctic Gateway Partnership (project SR140300001).

551 **References**
552
553 Alterskjær, K., J. E. Kristjansson, and Ø. Seland (2012), Sensitivity to deliberate sea
554 salt seeding of marine clouds – observations and model simulations, *Atmos.*
555 *Chem. Phys.*, *12*, 2795-2807 doi:10.5194/acp-12-2795-2012.
556 Alterskjær, K., J. E. Kristjánsson, O. Boucher, H. Muri, U. Niemeier, H. Schmidt, M.
557 Schulz, and C. Timmreck (2013), Sea-salt injections into the low-latitude
558 marine boundary layer: The transient response in three Earth system
559 models, *J. Geophys. Res. Atmos., 118*, 12,195–12,206,
560 doi:10.1002/2013JD020432.
561 Andrews, T., and P. M. Forster (2010), The transient response of global-mean
562 precipitation to increasing carbon dioxide levels, *Environ. Res. Lett.*, *5*,
563 025212, doi:10.1088/1748-9326/5/2/025212.
564 Armour, K. C., C. M. Bitz, and G. H. Roe (2013), Time-varying climate sensitivity from
565 regional feedbacks, *J. Climate, 26*, 4518–4534, doi:10.1175/JCLI-D-12-
566 00544.1.
567 Arora, V. K., J. F. Scinocca, G. J. Boer, J. R. Christian, K. L. Denman, G. M. Flato, V. V.
568 Kharin, W. G. Lee, and W. J. Merryfield (2011), Carbon emission limits
569 required to satisfy future representative concentration pathways of
570 greenhouse gases, *Geophys. Res. Lett.*, *38*, L05805,
571 doi:10.1029/2010GL046270.
572 Bala, G., K. Caldeira, and R. Nemani (2010), Fast versus slow response in climate
573 change: Implications for the global hydrological cycle, *Clim. Dyn.*, *35*, 423-
574 434, doi:10.1007/s00382-009-0583-y.
575 Collins, W. J., N. Bellouin, M. Doutriaux-Boucher, N. Gedney, P. Halloran, T. Hinton, J.
576 Hughes, C. D. Jones, M. Joshi, S. Liddicoat, G. Martin, F. O'Connor, J. Rae, C.
577 Senior, S. Sitch, I. Totterdell, A. Wiltshire, and S. Woodward (2011),
578 Development and evaluation of an Earth-System model—HadGEM2, *Geosci.*
579 *Model Dev.*, *4*, 1051-1075, doi:10.5194/gmd-4-1051-2011.
580 Crook, J. A., L. S. Jackson, S. M. Osprey, and P. M. Forster (2015), A comparison of
581 temperature and precipitation responses to different Earth radiation
582 management geoengineering schemes, *J. Geophys. Res., 120*, 9352-9373,
583 doi:10.1002/2015JD023269.
584 Curry, C. L., J. Sillmann, D. Bronaugh, K. Alterskjær, J. N. S. Cole, B. Kravitz., J. E.
585 Kristjánsson, H. Muri, U. Niemeier, A. Robock, and S. Tilmes (2014), A multi-
586 model examination of climate extremes in an idealized geoengineering
587 experiment, *Journal of Geophysical Research*, *119*, 3900-3923,
588 doi:10.1002/2013JD020648.
589 Dufresne, J.-L., M.-A. Foujols, S. Denvil, A. Caubel, O. Marti, O. Aumont, Y. Balkanski, S.
590 Bekki, H. Bellenger, R. Benshila, S. Bony, L. Bopp, P. Braconnot, P. Brockmann,
591 P. Cadule, F. Cheruy, F. Codron, A. Cozic, D. Cugnet, N. de Noblet, J.-P. Duvel, C.
592 Ethé, L. Fairhead, T. Fichefet, S. Flavoni, P. Friedlingstein, J.-Y. Grandpeix, L.
593 Guez, E. Guilyardi, D. Hauglustaine, F. Hourdin, A. Idelkadi, J. Ghattas, S.
594 Joussaume, M. Kageyama, G. Krinner, S. Labetoulle, A. Lahellec, M.-P.
595 Lefebvre, F. Lefevre, C. Levy, Z. X. Li, J. Lloyd, F. Lott, G. Madec, M. Mancip, M.
596 Marchand, S. Masson, Y. Meurdesoif, J. Mignot, I. Musat, S. Parouty, J. Polcher,

C. Rio, M. Schulz, D. Swingedouw, S. Szopa, C. Talandier, P. Terray, N. Viovy, and N. Vuichard (2013), Climate change projections using the IPSL-CM5 Earth System Model: From CMIP3 to CMIP5, *Clim. Dynam.*, *40*, 2123-2165 doi:10.1007/s00382-012-1636-1.

Geoffroy, O., D. Saint-Martin, and A. Voldoire (2015), Land-sea warming contrast: the role of the horizontal energy transport, *Clim. Dynam.*, *45*, 3493-3511, doi:10.1007/s00382-015-2552-y.

Giorgetta, M. A., Johann Jungclaus, Christian H. Reick, Stephanie Legutke, Jürgen Bader, Michael Böttinger, Victor Brovkin, Traute Crueger, Monika Esch, Kerstin Fieg, Ksenia Glushak, Veronika Gayler, Helmuth Haak, Heinz-Dieter Hollweg, Tatiana Ilyina, Stefan Kinne, Luis Kornblueh, Daniela Matei, Thorsten Mauritsen, Uwe Mikolajewicz, Wolfgang Mueller, Dirk Notz, Felix Pithan, Thomas Raddatz, Sebastian Rast, Rene Redler, Erich Roeckner, Hauke Schmidt, Reiner Schnur, Joachim Segschneider, Katharina D. Six, Martina Stockhause, Claudia Timmreck, Jörg Wegner, Heinrich Widmann, Karl-H. Wieners, Martin Claussen, Jochem Marotzke, and Bjorn Stevens (2013), Climate and carbon cycle changes from 1850 to 2100 in MPI-ESM simulations for the Coupled Model Intercomparison Project Phase 5, *J. Adv. Model. Earth Syst.*, *5*, 572-597, doi:10.1002/jame.20038.

Glienke, S., P. J. Irvine, and M. G. Lawrence (2015), The impact of geoengineering on vegetation in experiment G1 of the GeoMIP, *Journal of Geophysical Research*, *120*, 10196-10213, doi:10.1002/2015JD024202.

Gregory, J. M., W. J. Ingram, M. A. Palmer, G. S. Jones, P. A. Stott, R. B. Thorpe, J. A. Lowe, T. C. Johns, and K. D. Williams (2004), A new method for diagnosing radiative forcing and climate sensitivity, *Geophys. Res. Lett., 31*, L03205, doi:10.1029/2003GL018747.

Hansen, J., M. Sato, R. Ruedy, L. Nazarenko, A. Lacis, G. A. Schmidt, G. Russell, I. Aleinov, M. Bauer, S. Bauer, N. Bell, B. Cairns, V. Canuto, M. Chandler, Y. Cheng, A. Del Genio, G. Faluvegi, E. Fleming, A. Friend, T. Hall, C. Jackman, M. Kelley, N. Kiang, D. Koch, J. Lean, J. Lerner, K. Lo, S. Menon, R. Miller, P. Minnis, T. Novakov, V. Oinas, Ja. Perlwitz, Ju. Perlwitz, D. Rind, A. Romanou, D. Shindell, P. Stone, S. Sun, N. Tausnev, D. Thresher, B. Wielicki, T. Wong, M. Yao, and S. Zhang (2005), Efficacy of climate forcings, *J. Geophys. Res., 110*, D18104, doi:10.1029/2005JD005776.

Hazeleger, W., X. Wang, C. Severijns, S. Ştefănescu, R. Bintanja, A. Sterl, K. Wyser, T. Semmler, S. Yang, B. van den Hurk, T. van Noije, E. van der Linden, and K. van der Wiel (2011), EC-Earth V2.2: Description and validation of a new seamless Earth system prediction model, *Clim. Dynam., 39*(11), 2611-2629, doi:10.1007/s00382-011-1228-5.

Hurrell, J. W., M. M. Holland, P. R. Gent, S. Ghan, J. E. Kay, P. J. Kushner, J.-F. Lamarque, W. G. Large, D. Lawrence, K. Lindsay, W. H. Lipscomb, M. C. Long, N. Mahowald, D. R. Marsh, R. B. Neale, P. Rasch, S. Vavrus, M. Vertenstein, D. Bader, W. D. Collins, J. J. Hack, J. Kiehl, and S. Marshall (2013), The Community Earth System Model: A framework for collaborative research, *Bull. Amer. Meteor. Soc.*, *94*, 1339-1360, doi:10.1175/BAMS-D-12-00121.1.

643 Ji, D., L. Wang, J. Feng, Q. Wu, H. Cheng, Q. Zhang, J. Yang, W. Dong, Y. Dai, D. Gong, R.-
644 H. Zhang, X. Wang, J. Liu, J. C. Moore, D. Chen, and M. Zhou (2014),
645 Description and basic evaluation of Beijing Normal University Earth System
646 Model (BNU-ESM) version 1, *Geosci. Model. Dev.*, *7*, 2039-2064,
647 10.5194/gmd-7-2039-2014.
648 Kalidindi, S., G. Bala, A. Modak, and K. Caldeira (2015), Modeling of solar radiation
649 management: a comparison of simulations using reduced solar constant and
650 stratospheric sulphate aerosols, *Clim. Dynam.*, *44*, 2909-2925,
651 doi:10.1007/s00382-014-2240-3.
652 Kravitz, B., A. Robock, O. Boucher, H. Schmidt, K. E. Taylor, G. Stenchikov, and M.
653 Schulz (2011), The Geoengineering Model Intercomparison Project
654 (GeoMIP), *Atm. Sci. Lett.*, *12,* 162-167, doi:10.1002/asl.316.
655 Kravitz, B., K. Caldeira, O. Boucher, A. Robock, P. J. Rasch, K. Alterskjær, D. Bou
656 Karam, J. N. S. Cole, C. L. Curry, J. M. Haywood, P. J. Irvine, D. Ji, A. Jones, J. E.
657 Kristjánsson, D. J. Lunt, J. Moore, U. Niemeier, H. Schmidt, M. Schulz, B. Singh,
658 S. Tilmes, S. Watanabe, S. Yang, and J.-H. Yoon (2013a), Climate model
659 response from the Geoengineering Model Intercomparison Project (GeoMIP),
660 *Journal of Geophysical Research*, *118*(15), 8320-8332,
661 doi:10.1002/jgrd.50646.
662 Kravitz, B., P. J. Rasch, P. M. Forster, T. Andrews, J. N. S. Cole, P. J. Irvine, D. Ji, J. E.
663 Kristjánsson, J. C. Moore, H. Muri, U. Niemeier, A. Robock, B. Singh, S. Tilmes,
664 S. Watanabe, and J.-H. Yoon (2013b), An energetic perspective on
665 hydrological cycle changes in the Geoengineering Model Intercomparison
666 Project (GeoMIP), *Journal of Geophysical Research*, *118*, 13087-13102,
667 doi:10.1002/2013JD020502.
668 Kravitz, B., P. M. Forster, A. Jones, A. Robock, K. Alterskjær, O. Boucher, A. K. L.
669 Jenkins, H. Korhonen, J. E. Kristjánsson, H. Muri, U. Niemeier, A.-I. Partanen, P.
670 J. Rasch, H. Wang, and S. Watanabe (2013c), Sea spray geoengineering
671 experiments in the Geoengineering Model Intercomparison Project
672 (GeoMIP): Experimental design and preliminary results, *Journal of*
673 *Geophysical Research*, *118*(19), 11175-11186, doi:10.1002/jgrd.50856.
674 Kravitz, B., D. G. MacMartin, P. J. Rasch, and A. J. Jarvis (2015), A new method of
675 comparing forcing agents in climate models, *J. Climate, 28*, 8203–8218,
676 doi:10.1175/JCLI-D-14-00663.1.
677 Kravitz, B., D. G. MacMartin, H. Wang, and P. J. Rasch (2016), Geoengineering as a
678 design problem, *Earth System Dynamics, 7*, 469-497, doi:10.5194/esd-7-469-
679 2016.
680 Latham, J. (1990), Control of global warming? *Nature*, *347*, 339–340.
681 MacMartin, D.G., B. Kravitz, D. W. Keith, and A. Jarvis (2014), Dynamics of the
682 coupled human-climate system resulting from closed-loop control of solar
683 geoengineering, *Clim. Dynam., 43*, 243-258, doi:10.1007/s00382-013-1822-9.
684 Mitchell, D. L. and W. Finnegan (2009), Modification of cirrus clouds to reduce global
685 warming, *Environ. Res. Lett.*, *4*, 045102, doi:10.1088/1748-
686 9326/4/4/045102.
687 Moore, J. C., A. Rinke, X. Yu, D. Ji, X. Cui, Y. Li, K. Alterskjær, J. E. Kristjánsson, O.
688 Boucher, N. Huneeus, B. Kravitz, A. Robock, U. Niemeier, H. Schmidt, M.

Schulz, S. Tilmes, and S. Watanabe (2014), Arctic sea ice and atmospheric circulation under the GeoMIP G1 scenario, *J. Geophys. Res., 119*, 567-583, doi:10.1002/2013JD021060.

NAS (2015a), Climate Intervention: Carbon Dioxide Removal and Reliable Sequestration, National Research Council, The National Academies Press, Washington, DC, 141 pp.

NAS (2015b), Climate Intervention: Reflecting Sunlight to Cool Earth, National Research Council, The National Academies Press, Washington, DC, 235 pp.

Niemeier, U., H. Schmidt, K. Alterskjær, and J. E. Kristjánsson (2013), Solar irradiance reduction via climate engineering--impact of different techniques on the energy balance and the hydrological cycle, *Journal of Geophysical Research*, *118*, 11905-11917, doi:10.1002/2013JD020445.

Oreopoulos, L. and S. Platnick (2008), Radiative susceptibility of cloudy atmospheres to droplet number perturbations: 2. Global analysis from MODIS, *J. Geophys. Res.*, *113*, D14S21, doi:10.1029/2007JD009655.

Pandey, D. K., R. B. Lee III, and J. Paden (1995), Effects of atmospheric emissivity on clear sky temperatures, *Atmos. Environ.*, *29*, 2201-2204, doi:10.1016/1352-2310(94)00243-E.

Phipps, S. J., L. D. Rotstayn, H. B. Gordon, J. L. Roberts, A. C. Hirst, and W. F. Budd (2011), The CSIRO Mk3L climate system model version 1.0 – Part 1: Description and evaluation, *Geosci. Model Dev.*, *4*, 483-509, 10.5194/gmd-4-483-2011.

Robock, Alan (2011), Bubble, bubble, toil and trouble. An editorial comment. *Climatic Change*, *105*, 383-385, doi:10.1007/s10584-010-0017-1.

Schmidt, H., K. Alterskjær, D. Bou Karam, O. Boucher, A. Jones, J. E. Kristjánsson, U. Niemeier, M. Schulz, A. Aaheim, F. Benduhn, M. Lawrence, and C. Timmreck (2012), Solar irradiance reduction to counteract radiative forcing from a quadrupling of CO_2: Climate responses simulated by four Earth system models, *Earth System Dynamics, 3*, 63-78, doi:10.5194/esd-3-63-2012.

Schmidt, Gavin A., Max Kelley, Larissa Nazarenko, Reto Ruedy, Gary L. Russell, Igor Aleinov, Mike Bauer, Susanne E. Bauer, Maharaj K. Bhat, Rainer Bleck, Vittorio Canuto, Yong-Hua Chen, Ye Cheng, Thomas L. Clune, Anthony Del Genio, Rosalinda de Fainchtein, Greg Faluvegi, James E. Hansen, Richard J. Healy, Nancy Y. Kiang, Dorothy Koch, Andy A. Lacis, Allegra N. LeGrande, Jean Lerner, Ken K. Lo, Elaine E. Matthews, Surabi Menon, Ron L. Miller, Valdar Oinas, Amidu O. Oloso, Jan P. Perlwitz, Michael J. Puma, William M. Putman, David Rind, Anastasia Romanou, Makiko Sato, Drew T. Shindell, Shan Sun, Rahman A. Syed, Nick Tausnev, Kostas Tsigaridis, Nadine Unger, Apostolos Voulgarakis, Mao-Sung Yao, and Jinlun Zhang (2014), Configuration and assessment of the GISS ModelE2 contributions to the CMIP5 archive, *J. Adv. Model. Earth Syst., 6*, 141–184, doi:10.1002/2013MS000265.

Seitz, R. (2011), Bright water: hydrosols, water conservation and climate change, *Climatic Change*, *105*, 365-381, doi:10.1007/s10584-010-9965-8.

Shepherd, J., K. Caldeira, P. Cox, J. Haigh, K. Keith, B. Launder, G. Mace, G. MacKerron, J. Pyle, S. Rayner, C. Redgwell, and A. Watson (2009), Geoengineering the

climate: Science, governance, and uncertainty, Royal Society Policy document 10/09, 82 pp.

Sherwood, S. C., S. Bony, O. Boucher, C. Bretherton, P. M. Forster, J. M. Gregory, and B. Stevens (2015), Adjustments in the forcing-feedback framework for understanding climate change, *Bull. Amer. Meteor. Soc., 96*, 217–228, doi:10.1175/BAMS-D-13-00167.1.

Stephens, G. L., D. O'Brien, P. J. Webster, P. Pilewski, S. Kato, and J.-L. Li (2015), The albedo of Earth, *Rev. Geophys.*, *53*, 141-163, doi:10.1002/2014RG000449.

Taylor, K. E., R. J. Stouffer, and G. A. Meehl (2012), An overview of CMIP5 and the experiment design, *Bull. Amer. Meteor. Soc.*, *93*, 485-498, doi:10.1175/BAMS-D-11-00094.1.

Tilmes, S., J. Fasullo, J.-F. Lamarque, D. R. Marsch, M. Mills, K. Alterskjær, O. Boucher, J. N. S. Cole, C. L. Curry, J. M. Haywood, P. J. Irvine, D. Ji, A. Jones, D. B. Karam, B. Kravitz, J. E. Kristjánsson, J. C. Moore, H. O. Muri, U. Niemeier, P. J. Rasch, A. Robock, H. Schmidt, M. Schulz, B. Singh, S. Watanabe, S. Yang, and J.-H. Yoon (2013), The hydrological impact of geoengineering in the Geoengineering Model Intercomparison Project (GeoMIP), *Journal of Geophysical Research*, *118*(19), 11036-11058, doi:10.1002/jgrd.50868.

Watanabe, S., T. Hajima, K. Sudo, T. Nagashima, T. Takemura, H. Okajima, T. Nozawa, H. Kawase, M. Abe, T. Yokohata, T. Ise, H. Sato, E. Kato, K. Takata, S. Emori, and M. Kawamiya (2011), MIROC-ESM 2010: Model description and basic results of CMIP5-20c3m experiments, *Geosci. Mod. Dev.*, *4*, 845-872, doi:10.5194/gmd-4-845-2011.

Table 1. Description of the 11 models participating in this study. Column 1 gives the standard model name. Columns 2 and 3 give the default and perturbed surface ocean albedo, defined as upward shortwave divided by downward shortwave radiative flux at the surface, both averaged over ocean regions and over years 11-50 of simulation. Column 4 is the ratio of column 3 to column 2. Column 5 gives the factor (δ) by which the model default ocean albedo was multiplied to achieve negligible top-of-atmosphere radiative flux changes under an abrupt4xCO2 simulation (described in greater detail by Kravitz et al., 2015). Column 6 gives a relevant reference for each model. All values are rounded to two decimal places.

Model name	piControl ocean albedo	G1OA ocean albedo	Ratio	δ	Reference
BNU-ESM	0.12	0.17	1.48	2.50	Ji et al. (2014)
CanESM2	0.11	0.19	1.73	2.45	Arora et al. (2011)
CESM-CAM5.1-FV	0.10	0.18	1.79	2.70	Hurrell et al. (2013)
CSIRO-Mk3L-1.2	0.12	0.19	1.61	2.04	Phipps et al. (2011)
EC-Earth	0.10	0.19	1.97	3.17	Hazeleger et al. (2011)
GISS-E2-R	0.08	0.16	1.95	2.53	Schmidt et al. (2014)
HadGEM2-ES	0.10	0.17	1.83	2.44	Collins et al. (2011)
IPSL-CM5A-LR	0.10	0.17	1.78	2.33	Dufresne et al. (2013)
MIROC-ESM	0.10	0.20	2.00	3.10	Watanabe et al. (2011)
MPI-ESM-LR	0.09	0.23	2.40	5.42	Giorgetta et al. (2013)
NorESM1-M	0.09	0.18	1.95	2.77	Alterskjær et al. (2012)

Table 2. Parameters used in different runs with the simple one-dimensional radiative equilibrium model (Section 3.2). Surface ΔT (in Kkelvin) for the Global runs are with respect to Control (Global) and for the Ocean runs are with respect to Control (Ocean).

Run	Emissivity in each model layer	Surface albedo	Surface ΔT
Control (Global)	0.80	0.3	0
abrupt4xCO2 (Global)	0.8265	0.3	4.4189
Albedo increase (Global)	0.80	0.3395	-4.0165
G1ocean-albedo (Global)	0.8265	0.3395	0.3674
Control (Ocean)	0.80	0.1	0
abrupt4xCO2 (Ocean)	0.8265	0.1	4.7251
Albedo increase (Ocean)	0.80	0.1863	-7.3806
G1ocean-albedo (Ocean)	0.8265	0.1863	-2.7730

Table 3. Feedback parameters (Section 3.3; units W m^{-2}) for global, land, and ocean averages, calculated via the "Gregory method" (Gregory et al., 2004), where annual mean top-of-atmosphere net radiative flux is regressed against annual mean temperature.

	λ_g	λ_ℓ	λ_o
BNU-ESM	0.9019	0.7181	0.9838
CanESM2	1.1539	1.1898	1.1260
CESM-CAM5.1-FV	1.1435	1.0357	1.1591
CSIRO-Mk3L-1.2	1.0192	0.9300	0.8034
EC-Earth	1.2124	1.1937	1.3155
GISS-E2-R	2.2440	1.9751	2.3560
HadGEM2-ES	0.8411	0.8363	0.8351
IPSL-CM5A-LR	0.8367	1.2891	0.5894
MIROC-ESM	1.0378	0.8736	1.0383
MPI-ESM-LR	1.3701	1.0573	1.3986
NorESM1-M	1.4285	1.8828	1.6063

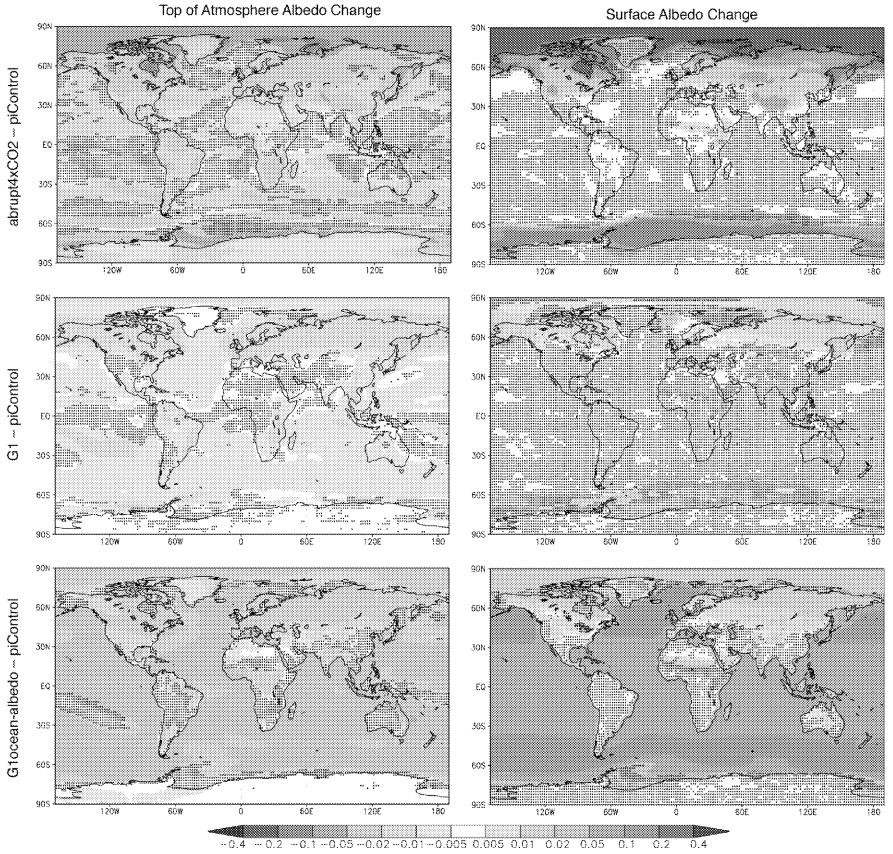

Figure 1. Top-of-atmosphere (TOA) and surface albedo differences (relative to piControl) for the abrupt4xCO2, G1, and G1ocean-albedo experiments. Albedo here is calculated as the ratio of upwelling to downwelling all-sky shortwave radiative flux, either at TOA or at the surface. Values are averages over years 11-50 of simulation. Stippling indicates where fewer than 8 out of 11 models agree on the sign of the response.

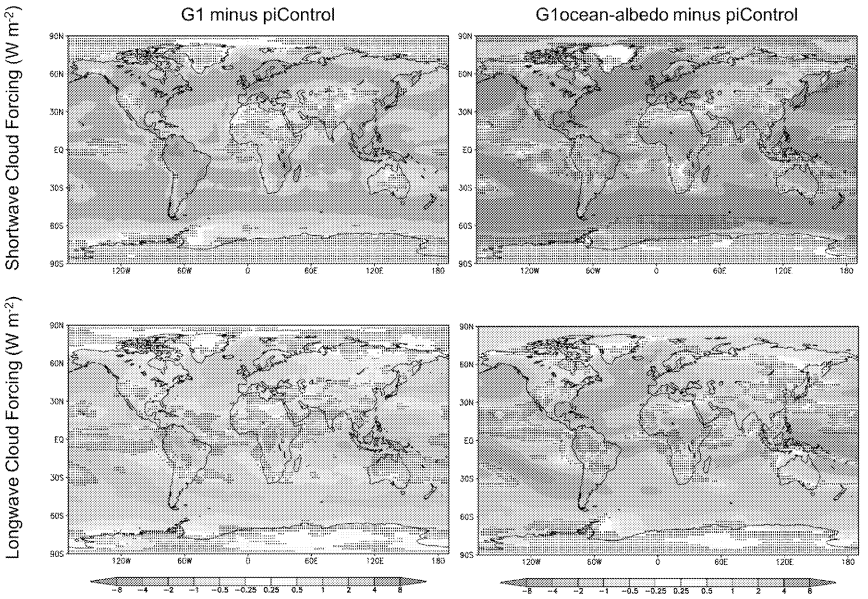

Figure 2. Shortwave (top) and longwave (bottom) cloud forcing changes due to the G1 (left) and G1ocean-albedo perturbations. Cloud forcing is defined as all-sky minus clear-sky radiative flux at the top of the atmosphere.

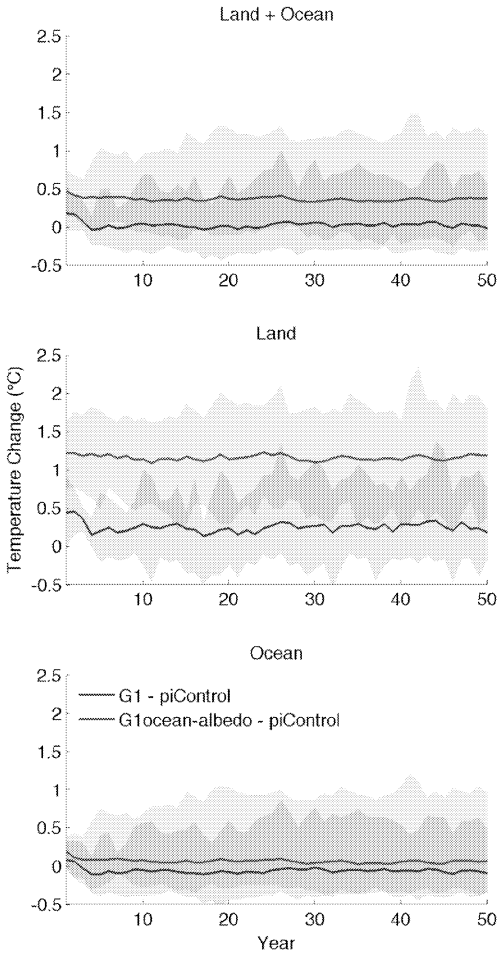

Figure 3. Global (top), land (middle), and ocean (bottom) average temperature change for the G1 (blue) and G1ocean-albedo (red) simulations. Lines show the all-model ensemble mean, and shading shows model spread (smallest to largest values).

Commenté [o10]: Ypu have a mix of °C and K for the T change

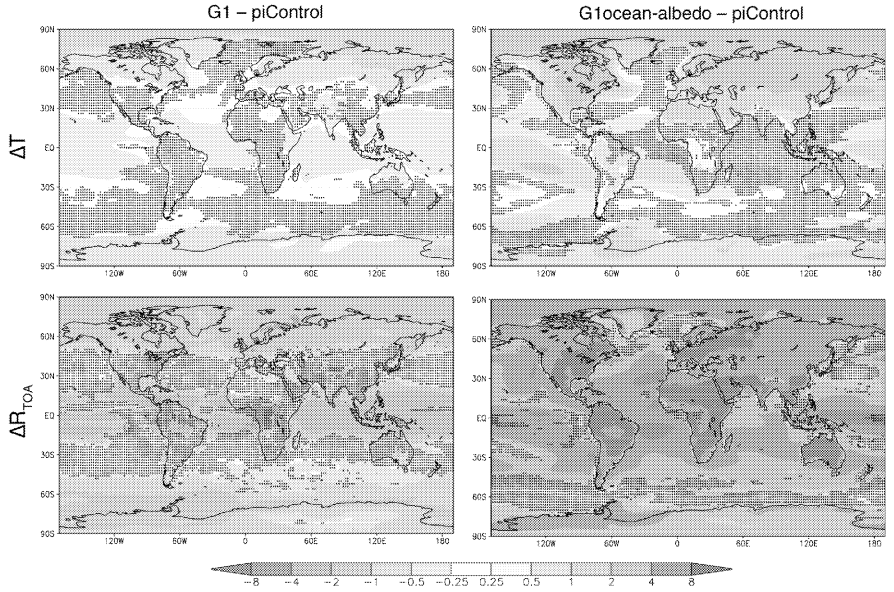

Figure 4. Surface air temperature (top row; K) and TOA net radiative flux (bottom row; W m^{-2}) changes for experiments G1 (left) and G1ocean-albedo (right). Values are averages over years 11-50 of simulation. Stippling indicates where fewer than 8 out of 11 models agree on the sign of the response.

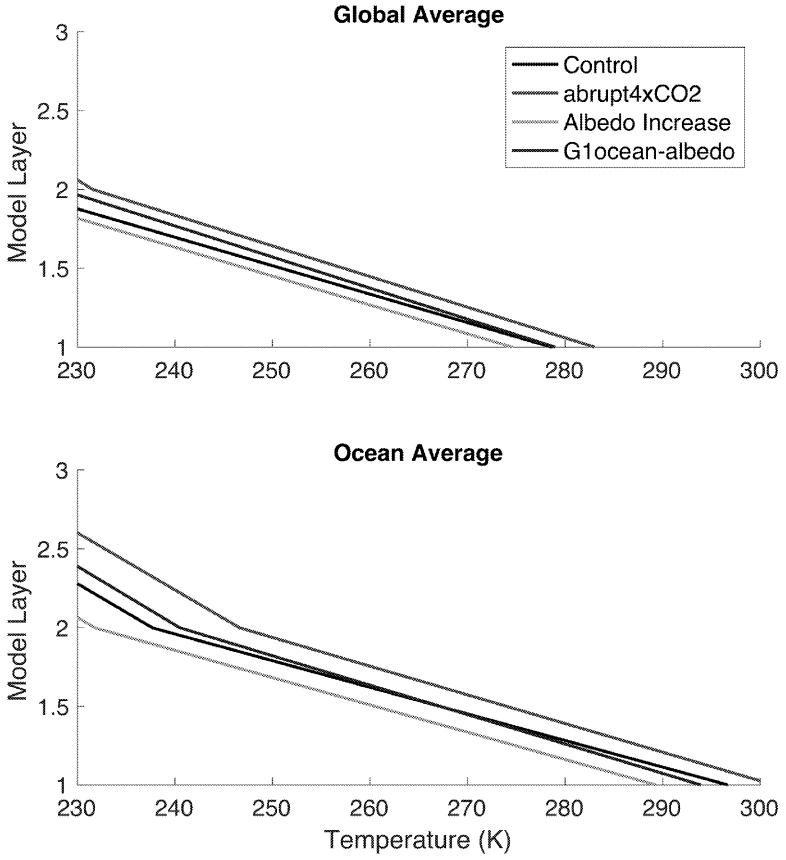

806
807
808 **Figure 5.** Temperature results for calculations with a one-dimensional radiative
809 equilibrium model with 15 vertical layers (only the bottom three layers are shown).
810 Specifications for all of the simulations are provided in Table 2.

Commenté [o11]: ??

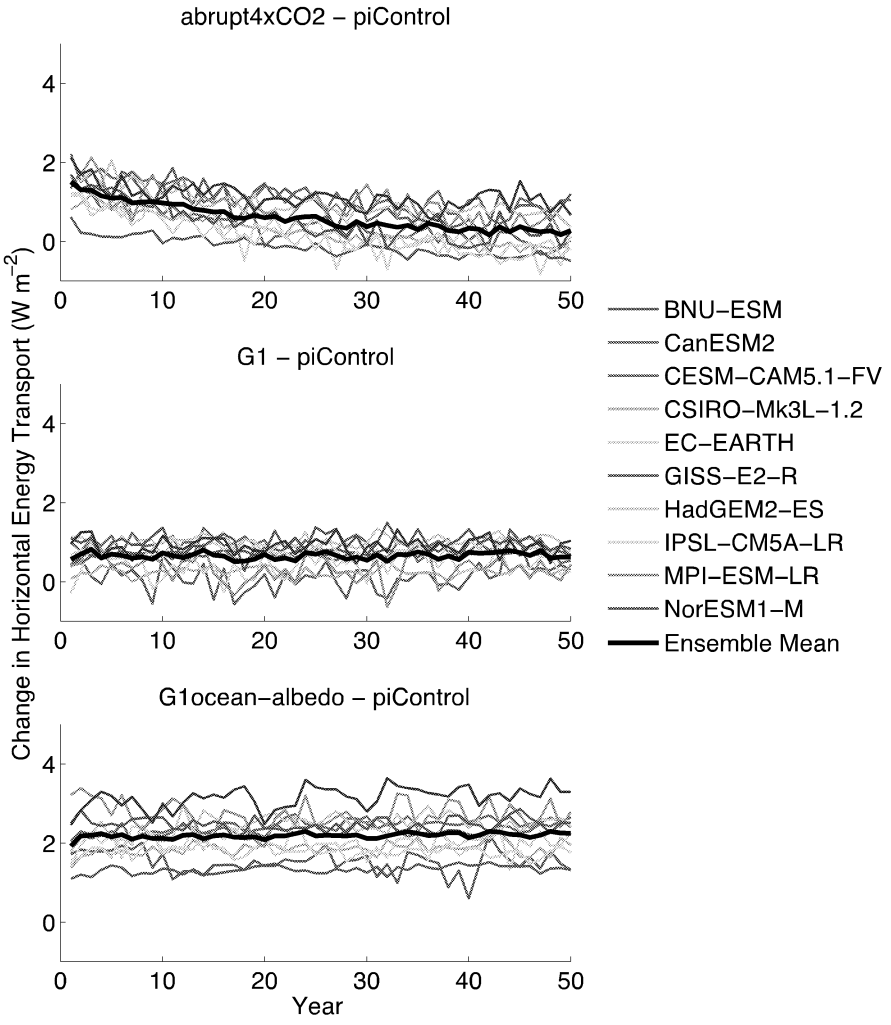

Figure 6. Annual mean change in land-ocean energy transport (Section 3.4; W m^{-2}) from piControl. See Equation 3 for a formal definition.

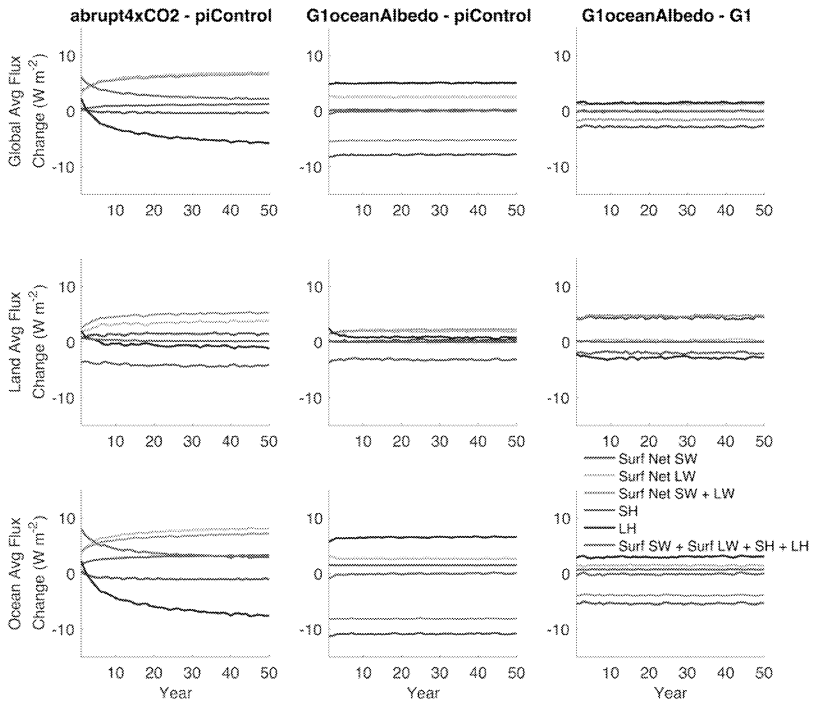

Figure 7. Annual mean time series of all-model mean surface fluxes (terms in Equation 4) for global averages (top), land averages (middle), and ocean averages (bottom). All fluxes are positive in the downward direction.

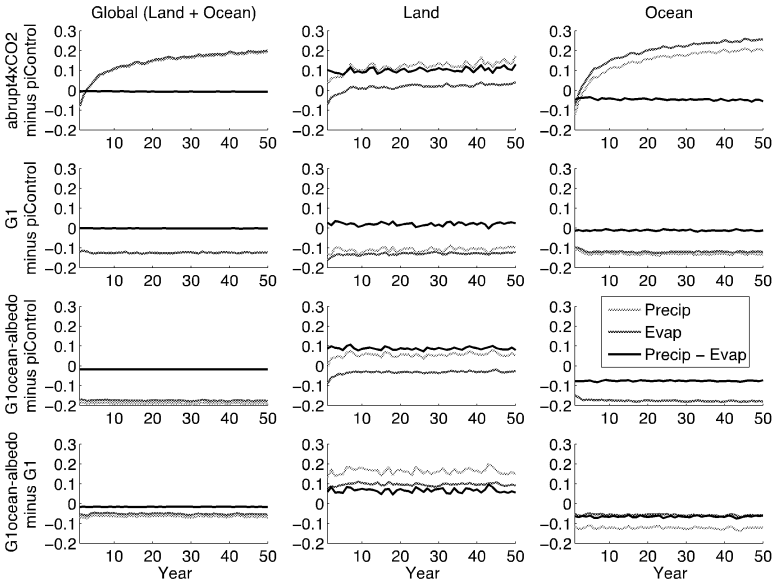

Figure 8. Annual mean time series of hydrological cycle changes (all in mm day^{-1}). Green lines show precipitation changes, red lines show evaporation changes, and black lines show precipitation minus evaporation. When no green line is evident, it is obscured by either the red or black lines.

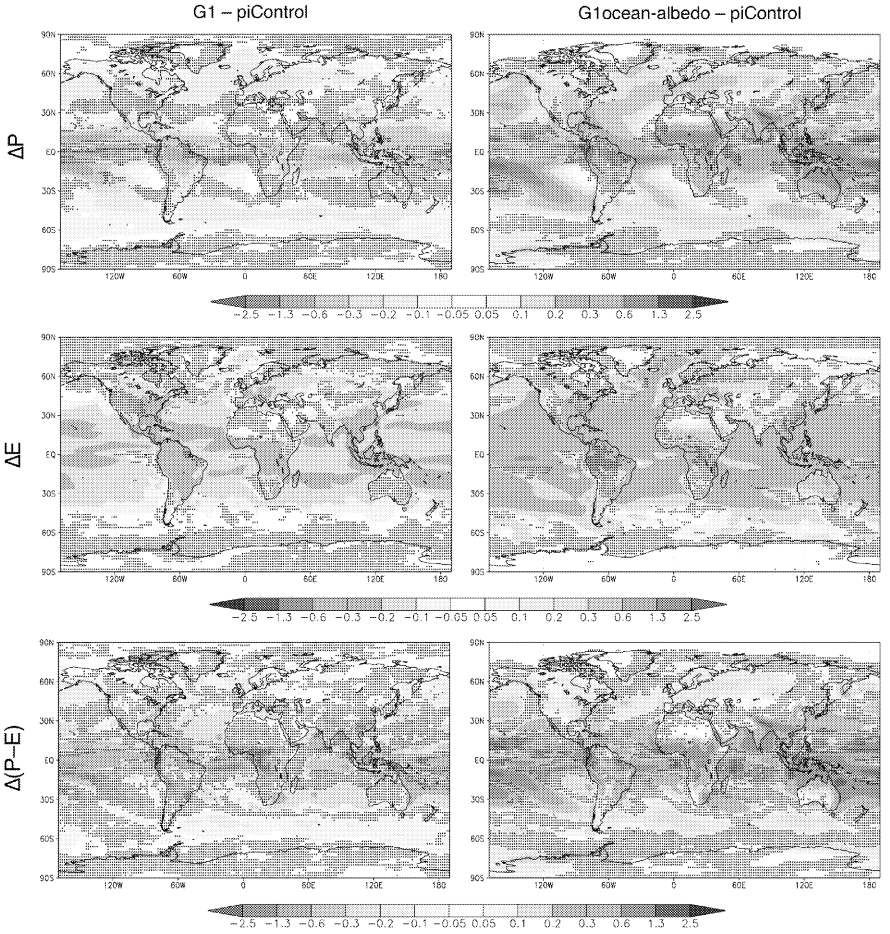

826
827
828 **Figure 9.** Precipitation (top row), evaporation (middle row), and precipitation
829 minus evaporation (bottom row) changes (all panels have units mm day^{-1}) for
830 experiments G1 and G1ocean-albedo. Values are averages over years 11-50 of
831 simulation. Stippling indicates where fewer than 8 out of 11 models agree on the
832 sign of the response.
833

The climate effects of increasing ocean albedo: An idealized representation of solar geoengineering

Ben Kravitz,[1*] Philip J. Rasch,[1] Hailong Wang,[1] Alan Robock,[2] Corey Gabriel,[3] Olivier Boucher,[4] Jason N. S. Cole,[5] Jim Haywood,[6,7] Duoying Ji,[8] Andy Jones,[6] Andrew Lenton,[9] John C. Moore,[8] Helene Muri,[10] Ulrike Niemeier,[11] Steven Phipps,[12,13] Hauke Schmidt,[11] Shingo Watanabe,[14] Shuting Yang,[15] and Jin-Ho Yoon[16]

[1]Atmospheric Sciences and Global Change Division, Pacific Northwest National Laboratory, Richland, WA, USA
[2]Department of Environmental Sciences, Rutgers University, New Brunswick, NJ, USA
[3]Scripps Institution of Oceanography, La Jolla, CA, USA
[4]~~Laboratoire de Météorologie Dynamique,~~ Institut Pierre-Simon Laplace, CNRS / ~~Université P. et M. Curie~~Sorbonne Université, Paris, France
[5]Environment and Climate Change Canada, Toronto, Canada
[6]Met Office Hadley Centre, Exeter, UK
[7]College of Engineering, Mathematics, and Physical Sciences, University of Exeter, Exeter, UK
[8]State Key Laboratory of Earth Surface Processes and Resource Ecology, College of Global Change and Earth System Science, Beijing Normal University, Beijing, China
[9]CSIRO Oceans and Atmosphere, Hobart, Tasmania, Australia
[10]Department of Geosciences, University of Oslo, Oslo, Norway
[11]Max Planck Institute for Meteorology, Hamburg, Germany
[12]Climate Change Research Centre, University of New South Wales, Sydney, Australia
[13]Institute for Marine and Antarctic Studies, University of Tasmania, Hobart, Tasmania, Australia
[14]Japan Agency for Marine-Earth Science and Technology, Yokohama, Japan
[15]Danish Meteorological Institute, Copenhagen, Denmark
[16]Gwangju Institute of Science and Technology, Gwangju, South Korea

Submission to *Atmospheric Chemistry and Physics*
Special Issue: The Geoengineering Model Intercomparison Project

[*]To whom correspondence should be addressed: P.O. Box 999, MSIN K9-30, Richland, WA 99352, USA. E-mail: ben.kravitz@pnnl.gov.

Abstract. Marine cloud brightening has been proposed as a means of ~~geoengineering~~climate intervention, or deliberately altering the climate system to offset anthropogenic climate change. As an idealized representation of marine cloud brightening, this paper discusses experiment G1ocean-albedo of the Geoengineering Model Intercomparison Project ~~(GeoMIP)~~, involving an abrupt quadrupling of the CO_2 concentration and an instantaneous increase in ocean albedo to maintain approximate net top-of-atmosphere radiative flux balance. Eleven Earth System Models are relatively consistent in their temperature, radiative flux, and hydrological cycle responses to this experiment. Due to the imposed forcing, the land surface warms by 1.14~~°C~~ K, while most of the ocean cools. Some parts of the near-surface air temperature over ocean warm due to heat transport from land to ocean. These changes generally resolve within a few years, indicating that changes in ocean heat content play at most a small role in the warming over the oceans. The hydrological cycle response is a general slowing down, with little net change in large-scale precipitation minus evaporation, but also with substantial heterogeneity. While idealized, these results have important implications for marine cloud brightening or any other method of geoengineering involving spatially heterogeneous forcing, particularly if that forcing has a strong land/ocean contrast.

Main points:

1) Under an increase in the CO_2 concentration and ocean albedo, the global? climate transitions to a new, warmer steady state.

2) The land surface warms substantially, and oceans near the land warm due to heat transport

3) The hydrological cycle slows down, with regional heterogeneity in the response

Suggested reviewers:

Tim Andrews

Olivier Geoffroy

Govindasamy Bala

Commenté [AR1]: Add error bars? Or make less precise.

Mis en forme : Surlignage

Commenté [o2]: Rephrase. Is this over land only ? why just look at large-scale precip ?

Commenté [o3]: Or even any forcing with a land/sea contrast. What about aerosols over land ?

Commenté [o4]: Needs to say that this is at fixed global energy budget ?

Mis en forme : Surlignage

Commenté [AR5]: Add because of cloud feedbacks?

1. Introduction

Geoengineering (also called "climate intervention") describes a set of technological approaches to reduce the effects of climate change by deliberately intervening in the climate system (e.g., Shepherd et al., 2009). There are two broad categories of geoengineering that are commonly discussed: solar geoengineering (modifying the amount of shortwave radiation incident at the surface; NAS, 2015a) and carbon dioxide removal (NAS, 2015b). There are also proposals, such as cirrus cloud thinning (Mitchell and Finnegan, 2009) that do not fit neatly into either of these two categories. In all subsequent discussions in this manuscript, we only discuss solar geoengineering methods.

Two of the most commonly proposed methods of global geoengineering are stratospheric sulfate aerosol injection (SAI) and marine cloud brightening (MCB). Comparison of the different climate effects of these two methods (e.g., Niemeier et al., 2013; Crook et al., 2015) reveals that, among other things, the spatial distributions of the applied forcings strongly affect the climate effects. Many of the effects of SAI can be reasonably well approximated by a uniform reduction in shortwave radiative flux reaching the surface (Kalidindi et al., 2015). Conversely, MCB targets low clouds over oceans (Latham, 1990), which are not ubiquitous. In addition, there are higher order effects due to the altitude at which the shortwave scattering occurs, including multiple scattering effects, infrared absorption of shortwave and longwave radiative flux by sulfate aerosols or cloud particles, and absorption of shortwave radiative flux by atmospheric CO_2 and water vapor (e.g., Kravitz et al., 2013b).

Idealized simulations of solar geoengineering are useful in the context of multi-model intercomparisons, in that they capture many of the effects of more complicated methods of representing geoengineering, yet can be performed by a wide variety of models. In simulations conducted under the Geoengineering Model Intercomparison Project (GeoMIP; Kravitz et al., 2011), an idealized method of representing SAI is via reductions in total solar irradiance; experiment G1 involved offsetting the global radiative flux imbalance from a quadrupling of the CO_2 concentration via solar reduction. Thus far, 15 models have participated in this simulation, providing information about model commonalities and differences in the global climate response, including effects on temperature, the hydrological cycle, cryosphere, terrestrial biosphere, and extreme events (Schmidt et al., 2012; Kravitz et al., 2013a, 2013b; Tilmes et al. 2013; Moore et al., 2014; Glienke et al., 2015; Curry et al., 2014; among numerous other studies). The GeoMIP website (http://climate.envsci.rutgers.edu/GeoMIP/) provides an up-to-date list of publications using GeoMIP model output.

While total solar irradiance reductions are straightforward to simulate in all models, this idealization is not a good approximation of MCB. The dominant effect of MCB ~~is~~ would be an increase in albedo in and near marine low clouds through "direct" and "indirect" effects. Changes in the albedo near the surface can produce different

signatures from reductions in energy input at the top of the atmosphere. There are also likely to be differences in the spatial distribution of the energy reduction. While some forms of albedo modification like SAI operate over broad areas (on a hemispheric or larger scale), albedo changes produced by MCB ~~are likely to~~would operate on smaller spatial scales and be concentrated over particular oceanic regions. Previous studies suggest that the clouds that are most susceptible to albedo modification are located on the ~~w~~eastern side of ocean basins in the subtropics, in regions dominated by stratocumulus clouds (Oreopoulos and Platnick, 2008). So, rather than considering a reduction of solar input operating uniformly over both land and ocean, an idealized representation of MCB that better approximates the effects is to increase the albedo only over ocean surfaces, as described by Kravitz et al. (2013c). This method can also be used to assess some effects of geoengineering by creating microbubbles at the ocean surface to increase reflectivity (e.g., Seitz, 2011; Robock, 2011; Gabriel et al., 2017).

In this study, we investigate the climate effects of using ocean albedo increases to offset CO_2 warming and compare those effects with those of total solar irradiance reduction (experiments are described in more detail in the following section). All simulations were conducted under the auspices of GeoMIP, allowing us to characterize a range of model responses to these different idealized methods of representing solar geoengineering.

2. Methodology and Description

Our analyses focus on four simulations: (1) a preindustrial control simulation (piControl), (2) a simulation in which the CO_2 concentration is abruptly quadrupled from its preindustrial value (abrupt4xCO2), (3) a simulation in which the net radiative flux imbalance in abrupt4xCO2 is offset by a reduction in total solar irradiance (G1), and (4) a simulation in which the net radiative flux imbalance in abrupt4xCO2 is offset by an increase in ocean albedo everywhere by a uniform factor (G1ocean-albedo). piControl and abrupt4xCO2 are standard experiments in the Coupled Model Intercomparison Project Phase 5 (CMIP5; Taylor et al., 2012). G1 is described further by Kravitz et al. (2011). The protocol for G1ocean-albedo is described in more detail by Kravitz et al. (2013c). Table 1 lists the models participating in this study, including relevant references and the required change in albedo to meet the objectives of experiment G1ocean-albedo. A similar table for experiment G1 is given by Kravitz et al. (2013a). One of the advantages of G1ocean-albedo is that, like G1, all models can conduct this simulation fairly easily. Supplemental Table S1 quantifies how well each model achieved radiative balance in the G1 and G1ocean-albedo experiments.

Commenté [o6]: I think it is important to restate that we aim for a balanced TOA budget over the first 10 years, right ? plus the fact that the albedo is increase proportionally

Kravitz et al. (2013c) found that in test simulations, one could only determine whether the objectives of G1ocean-albedo were met after several decades of simulation. However, as our analysis will show, once the proper value of ocean albedo increase is ascertained, the climate response reaches steady state in a few years, as in experiment G1 (Kravitz et al., 2013a). Supplemental Table S2 quantifies

temperature trends in each participating model over years 11-50 of simulation. The mean model trend over this period is approximately zero (to four decimal places), and with little exception, the trends in G1 and G1ocean-albedo are an order of magnitude smaller than the trends in the abrupt4xCO2 simulation. As such, for the purpose of analysis, we assume that "slow responses," i.e., responses operating on time scales longer than a few years (e.g., Andrews and Forster, 2010; Sherwood et al., 2015) are negligible in the G1 and G1ocean-albedo simulations. We do not separate results into rapid adjustment and slow response timescales, and with the exception of time series plots, all figures show averages over the years 11-50 of simulation, which we take as a sufficient indication of the dominant climate response after the transient response has resolved.

Commenté [AR7]: In what units?

Except where indicated, all plots show the mean model response. All values in the text are reported as mean (min to max), where mean indicates the all-model mean for that particular quantity, min is the lower bound of the range of model responses, and max is the upper bound of the range of model responses. In all maps, stippling indicates where fewer than 75% of the models agree on the sign of the response. All models in Table 1 were able to provide output for all variables except for cloud radiative forcing. The models included in cloud forcing analyses are BNU-ESM, CanESM2, CESM-CAM5.1-FV, HadGEM2-ES, IPSL-CM5A-LR, and MPI-ESM-LR. Supplemental Tables S1-S15 provide more quantitative information for all of the analyses presented in this study.

3. Results

3.1. Albedo and Temperature

Figure 1 shows the change in albedo at the top-of-atmosphere and at the surface for the abrupt4xCO2, G1, and G1ocean-albedo simulations, where albedo is defined as the ratio of upwelling to downwelling all-sky shortwave radiative flux. Quantitative values are given in Supplemental Tables S3 and S4. Results for abrupt4xCO2 and G1 are consistent with known responses of an increase in absorbed shortwave by carbon dioxide, reduced cloud cover, and reduced snow and sea ice cover (e.g., Schmidt et al., 2012; Kravitz et al., 2013b). These result in a broad decrease in albedo at the top of atmosphere and a decrease in surface albedo in many regions with substantial snow and ice cover. G1ocean-albedo retains many of these local high latitude features, but with large albedo increases over ocean, consistent with the experimental design and imposed forcing.

Figure 2 expands upon this picture by showing changes in shortwave and longwave cloud forcing in G1 and G1ocean-albedo, where cloud forcing is defined as all-sky minus clear-sky radiative flux measured at the top of the atmosphere. Positive shortwave values and negative longwave values in Figure 2 generally indicate less cloud cover. As was shown by Kravitz et al. (2013b), cloud cover in G1 tends to be reduced, which is consistent with what is depicted in Figure 2. For G1ocean-albedo, cloud cover is reduced over most ocean regions and large portions of land.

Exceptions include an increase in cloudiness over the Arctic, much of Africa, South Asia, Australia, and the leeward side of the Andes. These changes in cloudiness have implications for the hydrologic cycle, which we revisit in Section 3.5.

Figure 3 shows changes in global mean, land mean, and ocean mean surface air temperature for the G1 and G1ocean-albedo multi-model ensembles. Quantitative values are provided in Supplemental Table S5. Whereas the G1 simulation largely offsets temperature changes due to increased CO_2 concentration, G1ocean-albedo is approximately 0.36°C K (-0.12 to 1.20) warmer than the control simulation. This is predominantly due to warming over land by 1.14°C K (0.41 to 1.83). The temperature results in Figure 3 indicate that the temperature change happens within the first few years, and while some models show a slight trend in temperature over the 50-year G1ocean-albedo simulation (Supplemental Table S2), in general, any such trends are small, especially as compared to the warming in the abrupt4xCO2 simulation. This lack of substantial transient behavior after an initial fast response indicates that G1ocean-albedo has entered a new approximate steady state.

Figure 4 shows spatial patterns of change in temperature and top-of-atmosphere net radiative flux. (Also see Supplemental Tables S5 and S6.) The temperature changes are broadly consistent with the net radiative flux changes in the respective experiments. As was discussed by Kravitz et al. (2013a), G1 results in an "overcooling" of the tropics and an "undercooling" of the poles, consistent with offsetting the ubiquitous longwave forcing from CO_2 with a latitudinally dependent reduction in shortwave. G1ocean-albedo shows warming at high latitudes, over land regions, and in some ocean regions near or downwind of large continents, with the remaining ocean regions generally showing cooling. Because net top-of-atmosphere radiative flux is approximately zero in G1ocean-albedo, these temperature changes cannot be the result of energy being added to or subtracted from the climate system, and instead must be the result of energy redistribution. Hypotheses for why these temperature change patterns look the way they do (which will be tested in subsequent sections) include

Commenté [o8]: This needs to come earlier

1) The global average warming experienced in G1ocean-albedo is primarily due to increased heating over land.

2) Most warming over oceanic regions is due to transport of heat from land to ocean.

3) Any contributions to temperature or radiative flux changes from changes in ocean heat content are small on the timescales being evaluated here.

3.2. Hypothesis 1: Increased heating over land drives global average warming in G1ocean-albedo

The first hypothesis is fairly straightforward to argue based on first principles. To do so, we employ a one-dimensional radiative equilibrium model with 15 vertical layers extending from the surface to the nominal top-of-atmosphere. In the model, each layer behaves as a gray body with a specified emissivity, and the model computes radiative transfer between each layer via Planck radiation (the Stefan-Boltzmann equation). Although this model represents a gross oversimplification of the vertical profile of temperature response to idealized forcing, it is useful here for understanding differences between land and ocean temperature changes in response to the forcing imposed in G1ocean-albedo.

Figure 5 shows temperature profiles calculated using this model for four experiments: a control simulation, an abrupt4xCO2-like simulation (modeled as an increase in the emissivity of each model layer), a simulation with increased surface albedo, and G1ocean-albedo-like simulation involving an increase in emissivity and an increase in surface albedo. These simulations were conducted separately for global average and ocean-only regions.

Values of emissivity in the control simulation were prescribed to be 0.80 at all layers, consistent with a gray body (Pandey et al., 1995). The emissivity in the abrupt4xCO2 simulation was calculated to be the value such that global mean temperature change in the first model layer is approximately 4.42 K (Supplemental Table S5), yielding an emissivity value of 0.8265. In the control simulations, the surface albedos for the global and ocean-only simulations are 0.3 and 0.1, respectively, consistent with estimates provided by Stephens et al. (2015) and the values given in Table 1. In the global average simulation, the albedo increase in the G1-ocean albedo simulation was calculated to be the value such that global mean temperature change in the first model layer is approximately 0.36 K (Supplemental Table S5). In the ocean average simulation, the albedo increase is the all-model average of the required albedo increase in Table 1, which is a multiplication factor of 1.8627.

The results in Figure 5 show that under reasonable assumptions around atmospheric emissivity and surface albedo, oceanic cooling is expected in the G1ocean-albedo simulation. Based on these results, any increase in global average temperature must be due to warming over land. The oceanic temperature change in this simple model's simulation of G1ocean-albedo is -2.77 K, which is far too large in magnitude as compared to the results from the Earth System Models. Figure 2 indicates that changes in cloud cover in G1ocean-albedo are more likely to increase the magnitude of this temperature change than decrease it. In subsequent sections, we discuss some additional mediating factors that could act to reduce the magnitude of this change, such as land-ocean energy transport or reduced net ocean heat uptake. Nevertheless, the dominant radiative effects in G1ocean-albedo are to cause cooling over the oceans, as is seen in Figure 4.

3.3. Hypothesis 2: The role of Land-Ocean Energy Transport (LOET)

Commenté [o9]: Has the model two compartments for ocean and land ? should you show a schematic of the model ?

Commenté [AR10]: Certainly true if you ignore convection. Why use such an unrealistic representation? And why 15 layers?

Although the air over the ocean warms somewhat in G1ocean-albedo, it does not warm uniformly. Figure 4 shows that much of the warming over the ocean is in areas near land, indicating the potential for some of the heating energy over land to be transported to ocean regions. This can be quantified via calculating what Geoffroy et al. (2015) call horizontal energy transport, and which we call land-ocean energy transport (LOET), as it represents an aggregate transport of energy from the atmosphere over the land (averaged over all land regions) to the atmosphere over the ocean (averaged over all ocean regions). They provide a more detailed description, calculation, and validation of this concept using a three-box energy balance model that can be fitted to changes in land/ocean temperature and TOA energy imbalance such that the model captures the relevant energy transport dynamics; we repeat here only the calculations germane to our discussions.

Gregory et al. (2004) describe a method of estimating adjusted radiative forcing and the aggregate strength of global feedbacks via linear regression of the net global, annual mean TOA radiative flux imbalance (ΔR) against the global, annual mean temperature change (ΔT) in response to a forcing. The y-intercept of the regression line gives an estimate of adjusted radiative forcing ($\mathcal{F}$), and the negative of the slope of the regression line gives the feedback parameter (λ). Similarly, one can perform regression just over land-averaged quantities (denoted with the subscript ℓ) or just over ocean quantities (subscript o). Feedback parameter values are provided in Table 3.

In addition, one can regress ΔT_ℓ against ΔT_o to obtain a y-intercept of

$$\mathcal{F}_\ell/(\lambda_\ell+\alpha_\ell/f_\ell) \quad (1)$$

where α_ℓ is the land heat transport parameter and f_ℓ is the land fraction (approximately 0.3). The slope is

$$(\alpha_o/f_\ell)/(\lambda_\ell+\alpha_\ell/f_\ell) \quad (2)$$

If one solves these two equations for α_ℓ and α_o, then one can define

$$\Delta A = \alpha_\ell \Delta T_\ell - \alpha_o \Delta T_o \quad (3)$$

The quantity ΔA is the time-dependent LOET (units of W m^{-2}).

Figure 7 provides calculations of LOET for the simulations presented here. See Supplemental Table S7 for more details on individual model values. In the abrupt4xCO2 simulation, changes in LOET are positive (indicating an increase in heat transport from the land to the ocean) and decrease in magnitude steadily over the course of the simulation; these results are discussed in more detail by Geoffroy et al. (2015).

Mis en forme : Police :Italique
Mis en forme : Police :Italique
Mis en forme : Police :Italique
Commenté [AR11]: Are you sure you want to use alpha? Some will confuse this with albedo.
Mis en forme : Police :Italique
Mis en forme : Police :Italique
Mis en forme : Police :Italique
Mis en forme : Police :Italique
Mis en forme : Police :Italique
Mis en forme : Police :Italique
Mis en forme : Police :Italique

In Experiment G1, LOET increases by a model-dependent constant value and remains relatively unchanged over the course of the simulation. Although the air temperature over land in G1 increases slightly, and the air temperature over ocean decreases slightly (Kravitz et al., 2013a), the temperature changes in G1 are more latitude-dependent than representative of a clear land-ocean contrast (Figure 4), so it is perhaps not unexpected that LOET would be small.

Experiment G1ocean-albedo exhibits a strong land-ocean contrast in temperature (Figure 4), and the response is in steady state after a few years. As such, consistent with the behavior of other fluxes, LOET in G1ocean-albedo does not show transient behavior. LOET in G1ocean-albedo is approximately 2.20 (1.35 to 3.21) W m^{-2}, which is larger than in the other experiments examined here.

Converting LOET into temperature change is not necessarily straightforward, but an approximate change in temperature can be calculated by combining values of ΔA (Supplemental Table S7) with feedback parameter calculations (Table 3). More specifically, the temperature "added" to the air over the oceans by LOET can be calculated as $\Delta A/\lambda_o$, and the temperature "subtracted" from the air over land by LOET can be calculated as $\Delta A/\lambda_l$. Performing these calculations, LOET in the G1ocean-albedo experiment contributes 1.87°C K (0.57 to 3.06) to ocean temperature and "subtracts" 2.03°C K (0.68 to 3.06) from land temperature. We caution that this naïve calculation is somewhat circular, and it inherently includes in the ocean calculations both regions unaffected by LOET (e.g., tropical oceans) and regions strongly affected by LOET (e.g., Northeast Atlantic and Pacific Oceans).

Mis en forme : Police :Italique

Mis en forme : Police :Non Italique

Mis en forme : Police :Non Italique

Based on the calculations in Section 3.2 and the present section, it seems unlikely that LOET can on average transport enough energy from the land to the ocean to offset the radiative deficit due to an ocean albedo increase. However, locally, LOET appears to be able not only to offset these radiative changes, but also result in net warming.

3.4. Hypothesis 3: Atmospheric Column Energetics and Net Energy Flux into the Oceans

An additional potential source of energy to the atmosphere is a reduction in net ocean heat uptake. Calculating changes in ocean heat uptake are challenging and not particularly revealing in this case for three reasons:

1) It is possible that the models used in simulating G1ocean-albedo were not entirely spun up to steady state. As such, any remaining imbalances could manifest as changes in ocean heat content. In principle, one could subtract off the preindustrial control value, which likely has a similar trend in ocean heat content arising from spinup. However, this would not remove the influence of nonlinearities (state dependence), so there is no way to guarantee that the signal is entirely due to the G1ocean-albedo forcing.

2) As is seen in Supplemental Table S1, not all models were able to achieve top-of-atmosphere net radiative flux balance over the course of the simulation. These small changes can lead to large changes in ocean heat content over the course of a 50-year simulation. For example, a 0.1 W m^{-2} imbalance over a 50-year period can lead to an additional 5.5 x $\times$$10^{22}$ J of energy incident at the ocean surface. As such, we are unable to properly assess the degree to which ocean heat content changes may be due to small imbalances.
3) Ocean heat content requires a depth threshold for calculation, meaning calculations of it are sensitive to redistribution of heat to/from lower depths, obscuring the signal of the forcing.

As an alternative, we calculate net energy exchange across the surface in terms of changes in radiative and turbulent fluxes. Kravitz et al. (2013b) calculated energetics changes in the entire atmospheric column. However, because we are only interested in net surface fluxes, we calculate

$$\Delta S = \Delta R_{\text{surf}} + \Delta SH + \Delta LH \quad (1)$$

where ΔR_{surf} is the change in net surface radiative flux (shortwave and longwave), ΔSH is change in sensible heat flux from the atmosphere to the surface, and ΔLH is change in latent heat flux from the atmosphere to the surface. By convention, all fluxes are positive downward unless specifically noted. Calculations of individual terms in this budget, as well as of ΔS, are provided in Supplemental Tables S8-S12. Because these calculations are performed at the surface, no advection term (e.g., LOET) is needed, and ΔS is well defined as a land or ocean average.

Figure 7 shows the all-model mean for all of the terms in Equation 4. Several clear conclusions emerge. The first is that ΔS is approximately zero globally, over land, and over ocean for nearly the entire 50-year period, after an initial rapid adjustment that resolves within a few years. With the exception of latent heat over land, this is true of all fluxes for G1ocean-albedo in Figure 7, and even latent heat flux over land reaches an approximate steady state within ten years. If ΔS indeed serves as a useful proxy for net energy flux into or out of the ocean, then these results indicate that there is no sizable contribution to atmospheric energetics by changes in ocean heat content. Moreover, even if ΔS were not zero over ocean, ocean heat content changes would still be an insufficient explanation for temperature changes due to incongruent timescales. The oceanic mixed layer operates on an approximately decadal timescale, but all transient behavior in these simulations is resolved well before ten years. The transient response is much more consistent with a land surface time scale, which is on the order of 1-3 years. As such, it seems plausible that the temperature changes over ocean in G1ocean-albedo are due to land processes rather than ocean heat content changes. This is not to say that the ocean plays no role in the observed temperature changes. Rather, given the discussions in this section and the two previous sections, the role of the ocean heat content in causing temperature changes over the ocean in G1ocean-albedo is likely small.

Mis en forme : Police :Italique
Mis en forme : Police :Italique
Mis en forme : Police :Italique
Mis en forme : Police :Italique
Mis en forme : Police :Italique
Mis en forme : Police :Italique
Mis en forme : Police :Italique
Mis en forme : Police :Italique
Mis en forme : Police :Italique
Mis en forme : Police :Italique
Mis en forme : Police :Italique

The remainder of the results in Figure 7 are consistent with the applied forcing. There is a large sensible heat flux increase from the land to the atmosphere of 2.87 (-0.99 to 6.00) W m^{-2}, with a comparatively smaller sensible heat flux decrease from the ocean to the atmosphere of 1.47 (0.34 to 2.20) W m^{-2}. Over the ocean, latent heat flux from the surface to the atmosphere is 6.71 (4.95 to 7.89) W m^{-2} lower in G1ocean-albedo than in the preindustrial control simulation. These results indicate a greater shift of energy away from evaporating water and toward increasing land temperature. Large differences in flux magnitude between G1 and G1ocean-albedo can be found over land for net shortwave flux and latent heat flux, and differences in sign can be found over land for total radiative flux. These features are consistent with the applied forcing being different over land and ocean.

3.5. Hydrological cycle changes

Introducing a strong land-ocean energy and temperature gradient, as in G1ocean-albedo, will undoubtedly impact the hydrological cycle. Although the simulation is idealized, more realistic representations of MCB have shown important hydrological cycle impacts, including secondary circulation patterns that shift precipitation onto land in the tropics and extratropics (Bala et al., 2010), changes in the monsoon (Alterskjær et al., 2013), and changes in the Walker circulation (Niemeier et al., 2013). Here we evaluate the large-scale hydrological cycle changes in G1ocean-albedo, with possible applicability to other realizations of MCB.

Figure 8 shows global, land, and ocean averaged precipitation, evaporation, and precipitation minus evaporation ($P-E$) for all of the simulations considered in this manuscript; quantitative descriptions are given in Tables S13–15. The abrupt4xCO2 simulation is the only one with a distinct rapid adjustment and slow response. Over both land and ocean, G1 shows decreases in precipitation and evaporation of approximately equal magnitude, resulting in net changes in $P-E$ of 0.02 (-0.05 to 0.11) mm day^{-1} over land and -0.01 (-0.04 to 0.01) mm day^{-1} over ocean. In G1ocean-albedo, global precipitation and evaporation both decrease by approximately 0.19 (0.11 to 0.26) mm day^{-1} to yield little net change in $P-E$. However, this net small change is due to differential effects over land and ocean. Over land, precipitation remains relatively unchanged, but evaporation decreases, resulting in a net change in $P-E$ by 0.09 (-0.18 to 0.18) mm day^{-1}. Over the ocean, both precipitation and evaporation decrease, with a net negative $P-E$ of -0.06 (-0.19 to -0.01) mm day^{-1}.

Annual mean land/ocean contrasts in precipitation and evaporation changes tend to be more uniform in sign in experiment G1 (Figure 9), resulting in few large regions of change in P–E with the exception of the tropics (mostly driven by a southward shift in the intertropical convergence zone; Kravitz et al., 2013a). In G1ocean-albedo, precipitation and evaporation over the oceans are reduced in most regions, consistent with the applied forcing. Over land, the signs of precipitation and evaporation changes are regionally heterogeneous, yet the precipitation and evaporation changes are concordant, e.g., land regions with increased precipitation

Mis en forme : Police :Italique
Mis en forme : Police :Italique
Mis en forme : Police :Italique
Mis en forme : Police :Italique
Mis en forme : Police :Italique
Mis en forme : Police :Italique
Mis en forme : Police :Italique
Mis en forme : Police :Italique
Mis en forme : Police :Italique
Mis en forme : Police :Italique

also generally show increased evaporation. The net P–E map is highly heterogeneous, but in general, tropical land areas are projected to have more available moisture (as measured by P–E) under G1ocean-albedo, and midlatitude land areas are projected to have less. The implications of these changes for people and ecosystems ~~is~~ are an important area of future research.

Mis en forme : Police :Italique

Mis en forme : Police :Italique

Mis en forme : Police :Italique

Mis en forme : Police :Italique

4. Discussion and Conclusions

The results presented here indicate that even though experiments G1 and G1ocean-albedo both achieve approximate net top-of-atmosphere radiative flux balance, the climate system responses differ dramatically between the two experiments. The idea that global energy balance can still result in local changes is perhaps not surprising, as feedback operate locally (Armour et al., 2013). These different climate responses for the same forcing are effectively an illustration of different efficacies (Hansen et al., 2005). Even in the absence of slow responses, forcings with different efficacies can cause different climate system changes (Kravitz et al., 2015). G1ocean-albedo serves as an excellent reminder not to conflate small net top-of-atmosphere radiative flux imbalance with small temperature change; a clear relationship between those two quantities is not guaranteed.

Relatedly, the results obtained for G1ocean-albedo were to some extent by design. The objective of G1ocean-albedo was to achieve net top-of-atmosphere radiative flux balance, which resulted in warming. Conceivably, one could define an objective of no global temperature change, implying a net negative radiative flux at the top-of-atmosphere. It is unclear whether, unlike G1ocean-albedo, that alternate approach would result in transient behavior that lasts longer than a few years. Such an experiment could be accomplished using feedback methods that have been introduced to geoengineering research in recent years (e.g., MacMartin et al., 2014; Kravitz et al., 2016).

Commenté [o12]: Or no global land temperature change

The results presented here have several features that were not necessarily expected from the outset. Kravitz et al. (2013c) found that determining whether the climate system was in balance took up to 30 years of simulation. However, once that balance is achieved, the climate does not change appreciably after the initial rapid adjustment. Potential future work could investigate these results, shedding light on timescales of climate response and potential thresholds, e.g., how large does the energy imbalance need to be to trigger slower adjustments?

Related to this issue of different timescales of adjustment is the traditional separation of climate response into rapid adjustment and slow response components (e.g., Andrews and Forster, 2010; Sherwood et al., 2015). The rapid adjustment is often defined as the climate response unassociated with global mean temperature change, and the slow response describes a transient temperature change with a large component due to climate system feedbacks. The results from G1ocean-albedo, like those of G1 (Kravitz et al., 2013b), show an initial rapid change and no appreciable slower change. However, in G1ocean-albedo, that initial change

is associated with a temperature increase, which in principle should excite ~~a~~ slow ~~adjustment through~~ climate system feedbacks. These results are somewhat inconsistent with the traditional definitions of rapid adjustment and slow response. Additionally, this sustained temperature increase is to some extent decoupled from net energy imbalances in the climate system, as ΔR_{TOA} and ΔS (Equation 4) are both approximately zero. Reconciling all of these features suggests a potentially rich research topic focused on understanding the relationships between radiative flux changes, temperature changes, and the circumstances under which climate feedbacks are excited.

G1ocean-albedo may be more apposite to the impact of geoengineering via "ocean microbubbles," whereby surfactants are added to the ocean surface, promoting the formation of microscopic, highly reflective bubbles (Seitz, 2011; Robock, 2011; Gabriel et al., 2017). An area of investigation we did not undertake, yet one that repeatedly emerges in discussions of microbubbles, is the effects on the ocean mixed layer. By reflecting more solar radiation, microbubbles have the potential to inhibit vertical mixing and available light in the euphotic zone, which could have profound effects on marine biota. This implies that another useful future area of investigation for the G1ocean-albedo simulation is an analysis of the marine carbon cycle (Robock, 2011; Gabriel et al., 2017).

There are numerous potential areas of research prompted by this study. The stark land/ocean contrast in warming has potential implications for ocean circulation patterns, including the meridional overturning circulation and Western boundary ocean currents, with consequent implications for marine ecosystems. This contrast also has implications for the terrestrial biosphere, including ecosystem services and the land and ocean carbon cycles. Although we did not evaluate seasonal changes in this manuscript, such investigations could prove fruitful for more detailed assessments of variability, such as monsoon precipitation, extreme events, and sea ice extent.

Despite being informative for MCB, there are limits as to the applicability of this idealized approach. There are important differences in boundary layer stability changes from surface albedo increases versus marine stratocumulus cloud top brightening. Also, it appears impossible for marine cloud brightening to be conducted over all ocean regions and with a sufficient magnitude to offset the radiative forcing from a quadrupling of the CO_2 concentration. The purpose of this manuscript is to describe the broad features of change under a uniform ocean albedo increase, and some of these changes are likely to be present with more realistic scenarios of marine cloud brightening. We anticipate that future research can more deeply explore the applicability of this simulation to marine cloud brightening.

Acknowledgments. We thank Jón Egill Kristjánsson, who tragically passed away, for invaluable comments on an earlier version of this manuscript. We acknowledge the World Climate Research Programme's Working Group on Coupled Modelling,

Commenté [o13]: Ummmh, not sure I understand here

Commenté [o14]: Temperature, depth, radiation, …

which is responsible for CMIP, and we thank the climate modeling groups for producing and making available their model output. For CMIP the U.S. Department of Energy's Program for Climate Model Diagnosis and Intercomparison provides coordinating support and led development of software infrastructure in partnership with the Global Organization for Earth System Science Portals. We thank all participants of the Geoengineering Model Intercomparison Project and their model development teams, CLIVAR/WCRP Working Group on Coupled Modeling for endorsing GeoMIP, and the scientists managing the Earth System Grid data nodes who have assisted with making GeoMIP output available. The Pacific Northwest National Laboratory is operated for the U.S. Department of Energy by Battelle Memorial Institute under contract DE-AC05-76RL01830. Simulations performed by Ben Kravitz were supported by the NASA High-End Computing (HEC) Program through the NASA Center for Climate Simulation (NCCS) at Goddard Space Flight Center. Alan Robock is supported by NSF grants AGS-1157525 and GEO-1240507 AGS-1617844. Andy Jones was supported by the Joint UK DECC/Defra Met Office Hadley Centre Climate Programme (GA01101). Olivier Boucher acknowledges HPC resources from CCRT under the allocation 2015-t2012012201 made by GENCI (Grand Equipement National de Calcul Intensif). This research was supported under the Australian Research Council's Special Research Initiative for the Antarctic Gateway Partnership (project SR140300001).

554 **References**
555
556 Alterskjær, K., J. E. Kristjansson, and Ø. Seland (2012), Sensitivity to deliberate sea
557 salt seeding of marine clouds – observations and model simulations, *Atmos.*
558 *Chem. Phys.*, *12*, 2795-2807 doi:10.5194/acp-12-2795-2012.

559 Alterskjær, K., J. E. Kristjánsson, O. Boucher, H. Muri, U. Niemeier, H. Schmidt, M.
560 Schulz, and C. Timmreck (2013), Sea-salt injections into the low-latitude marine
561 boundary layer: The transient response in three Earth system models, *J. Geophys.*
562 *Res. Atmos., 118*, 12,195–12,206, doi:10.1002/2013JD020432.

563 Andrews, T., and P. M. Forster (2010), The transient response of global-mean
564 precipitation to increasing carbon dioxide levels, *Environ. Res. Lett.*, *5*, 025212,
565 doi:10.1088/1748-9326/5/2/025212.

566 Armour, K. C., C. M. Bitz, and G. H. Roe (2013), Time-varying climate sensitivity from
567 regional feedbacks, *J. Climate, 26*, 4518–4534, doi:10.1175/JCLI-D-12-00544.1.

568 Arora, V. K., J. F. Scinocca, G. J. Boer, J. R. Christian, K. L. Denman, G. M. Flato, V. V.
569 Kharin, W. G. Lee, and W. J. Merryfield (2011), Carbon emission limits required
570 to satisfy future representative concentration pathways of greenhouse gases,
571 *Geophys. Res. Lett.*, *38*, L05805, doi:10.1029/2010GL046270.

572 Bala, G., K. Caldeira, and R. Nemani (2010), Fast versus slow response in climate
573 change: Implications for the global hydrological cycle, *Clim. Dyn.*, *35*, 423-434,
574 doi:10.1007/s00382-009-0583-y.

575 Collins, W. J., N. Bellouin, M. Doutriaux-Boucher, N. Gedney, P. Halloran, T. Hinton, J.
576 Hughes, C. D. Jones, M. Joshi, S. Liddicoat, G. Martin, F. O'Connor, J. Rae, C. Senior,
577 S. Sitch, I. Totterdell, A. Wiltshire, and S. Woodward (2011), Development and
578 evaluation of an Earth-System model—HadGEM2, *Geosci. Model Dev.*, *4*, 1051-
579 1075, doi:10.5194/gmd-4-1051-2011.

580 Crook, J. A., L. S. Jackson, S. M. Osprey, and P. M. Forster (2015), A comparison of
581 temperature and precipitation responses to different Earth radiation
582 management geoengineering schemes, *J. Geophys. Res., 120*, 9352-9373,
583 doi:10.1002/2015JD023269.

584 Curry, C. L., J. Sillmann, D. Bronaugh, K. Alterskjær, J. N. S. Cole, B. Kravitz., J. E.
585 Kristjánsson, H. Muri, U. Niemeier, A. Robock, and S. Tilmes (2014), A multi-
586 model examination of climate extremes in an idealized geoengineering
587 experiment, *Journal of Geophysical Research*, *119*, 3900-3923,
588 doi:10.1002/2013JD020648.

589 Dufresne, J.-L., M.-A. Foujols, S. Denvil, A. Caubel, O. Marti, O. Aumont, Y. Balkanski, S.
590 Bekki, H. Bellenger, R. Benshila, S. Bony, L. Bopp, P. Braconnot, P. Brockmann, P.
591 Cadule, F. Cheruy, F. Codron, A. Cozic, D. Cugnet, N. de Noblet, J.-P. Duvel, C. Ethé,
592 L. Fairhead, T. Fichefet, S. Flavoni, P. Friedlingstein, J.-Y. Grandpeix, L. Guez, E.
593 Guilyardi, D. Hauglustaine, F. Hourdin, A. Idelkadi, J. Ghattas, S. Joussaume, M.
594 Kageyama, G. Krinner, S. Labetoulle, A. Lahellec, M.-P. Lefebvre, F. Lefevre, C.
595 Levy, Z. X. Li, J. Lloyd, F. Lott, G. Madec, M. Mancip, M. Marchand, S. Masson, Y.

Mis en forme : Espace Après : 6 pt

Meurdesoif, J. Mignot, I. Musat, S. Parouty, J. Polcher, C. Rio, M. Schulz, D. Swingedouw, S. Szopa, C. Talandier, P. Terray, N. Viovy, and N. Vuichard (2013), Climate change projections using the IPSL-CM5 Earth System Model: From CMIP3 to CMIP5, *Clim. Dynam.*, *40*, 2123-2165 doi:10.1007/s00382-012-1636-1.

Gabriel, C. J., A. Robock, L. Xia, B. Zambri, and B. Kravitz (201), The G4Foam experiment: Global climate impacts of regional ocean albedo modification, *Atmos. Chem. Phys., 17*, 595-613, doi:10.5194/acp-17-595-2017.

Geoffroy, O., D. Saint-Martin, and A. Voldoire (2015), Land-sea warming contrast: the role of the horizontal energy transport, *Clim. Dynam.*, *45*, 3493-3511, doi:10.1007/s00382-015-2552-y.

Giorgetta, M. A., Johann Jungclaus, Christian H. Reick, Stephanie Legutke, Jürgen Bader, Michael Böttinger, Victor Brovkin, Traute Crueger, Monika Esch, Kerstin Fieg, Ksenia Glushak, Veronika Gayler, Helmuth Haak, Heinz-Dieter Hollweg, Tatiana Ilyina, Stefan Kinne, Luis Kornblueh, Daniela Matei, Thorsten Mauritsen, Uwe Mikolajewicz, Wolfgang Mueller, Dirk Notz, Felix Pithan, Thomas Raddatz, Sebastian Rast, Rene Redler, Erich Roeckner, Hauke Schmidt, Reiner Schnur, Joachim Segschneider, Katharina D. Six, Martina Stockhause, Claudia Timmreck, Jörg Wegner, Heinrich Widmann, Karl-H. Wieners, Martin Claussen, Jochem Marotzke, and Bjorn Stevens (2013), Climate and carbon cycle changes from 1850 to 2100 in MPI-ESM simulations for the Coupled Model Intercomparison Project Phase 5, *J. Adv. Model. Earth Syst.*, *5*, 572-597, doi:10.1002/jame.20038.

Glienke, S., P. J. Irvine, and M. G. Lawrence (2015), The impact of geoengineering on vegetation in experiment G1 of the GeoMIP, *Journal of Geophysical Research*, *120*, 10196-10213, doi:10.1002/2015JD024202.

Gregory, J. M., W. J. Ingram, M. A. Palmer, G. S. Jones, P. A. Stott, R. B. Thorpe, J. A. Lowe, T. C. Johns, and K. D. Williams (2004), A new method for diagnosing radiative forcing and climate sensitivity, *Geophys. Res. Lett., 31*, L03205, doi:10.1029/2003GL018747.

Hansen, J., M. Sato, R. Ruedy, L. Nazarenko, A. Lacis, G. A. Schmidt, G. Russell, I. Aleinov, M. Bauer, S. Bauer, N. Bell, B. Cairns, V. Canuto, M. Chandler, Y. Cheng, A. Del Genio, G. Faluvegi, E. Fleming, A. Friend, T. Hall, C. Jackman, M. Kelley, N. Kiang, D. Koch, J. Lean, J. Lerner, K. Lo, S. Menon, R. Miller, P. Minnis, T. Novakov, V. Oinas, Ja. Perlwitz, Ju. Perlwitz, D. Rind, A. Romanou, D. Shindell, P. Stone, S. Sun, N. Tausnev, D. Thresher, B. Wielicki, T. Wong, M. Yao, and S. Zhang (2005), Efficacy of climate forcings, *J. Geophys. Res., 110*, D18104, doi:10.1029/2005JD005776.

Hazeleger, W., X. Wang, C. Severijns, S. Ştefănescu, R. Bintanja, A. Sterl, K. Wyser, T. Semmler, S. Yang, B. van den Hurk, T. van Noije, E. van der Linden, and K. van der Wiel (2011), EC-Earth V2.2: Description and validation of a new seamless Earth system prediction model, *Clim. Dynam., 39*(11), 2611-2629, doi:10.1007/s00382-011-1228-5.

Mis en forme : Police :Italique

Mis en forme : Police :Italique

637 Hurrell, J. W., M. M. Holland, P. R. Gent, S. Ghan, J. E. Kay, P. J. Kushner, J.-F.
638 Lamarque, W. G. Large, D. Lawrence, K. Lindsay, W. H. Lipscomb, M. C. Long,
639 N. Mahowald, D. R. Marsh, R. B. Neale, P. Rasch, S. Vavrus, M. Vertenstein, D.
640 Bader, W. D. Collins, J. J. Hack, J. Kiehl, and S. Marshall (2013), The Community
641 Earth System Model: A framework for collaborative research, *Bull. Amer. Meteor.*
642 *Soc.*, *94*, 1339-1360, doi:10.1175/BAMS-D-12-00121.1.

643 Ji, D., L. Wang, J. Feng, Q. Wu, H. Cheng, Q. Zhang, J. Yang, W. Dong, Y. Dai, D. Gong, R.-
644 H. Zhang, X. Wang, J. Liu, J. C. Moore, D. Chen, and M. Zhou (2014), Description
645 and basic evaluation of Beijing Normal University Earth System Model (BNU-
646 ESM) version 1, *Geosci. Model. Dev.*, *7*, 2039-2064, 10.5194/gmd-7-2039-2014.

647 Kalidindi, S., G. Bala, A. Modak, and K. Caldeira (2015), Modeling of solar radiation
648 management: a comparison of simulations using reduced solar constant and
649 stratospheric sulphate aerosols, *Clim. Dynam.*, *44*, 2909-2925,
650 doi:10.1007/s00382-014-2240-3.

651 Kravitz, B., A. Robock, O. Boucher, H. Schmidt, K. E. Taylor, G. Stenchikov, and M.
652 Schulz (2011), The Geoengineering Model Intercomparison Project (GeoMIP),
653 *Atm. Sci. Lett.*, *12,* 162-167, doi:10.1002/asl.316.

654 Kravitz, B., K. Caldeira, O. Boucher, A. Robock, P. J. Rasch, K. Alterskjær, D. Bou
655 Karam, J. N. S. Cole, C. L. Curry, J. M. Haywood, P. J. Irvine, D. Ji, A. Jones, J. E.
656 Kristjánsson, D. J. Lunt, J. Moore, U. Niemeier, H. Schmidt, M. Schulz, B. Singh, S.
657 Tilmes, S. Watanabe, S. Yang, and J.-H. Yoon (2013a), Climate model response
658 from the Geoengineering Model Intercomparison Project (GeoMIP), *Journal of*
659 *Geophysical Research*, *118*(15), 8320-8332, doi:10.1002/jgrd.50646.

660 Kravitz, B., P. J. Rasch, P. M. Forster, T. Andrews, J. N. S. Cole, P. J. Irvine, D. Ji, J. E.
661 Kristjánsson, J. C. Moore, H. Muri, U. Niemeier, A. Robock, B. Singh, S. Tilmes, S.
662 Watanabe, and J.-H. Yoon (2013b), An energetic perspective on hydrological
663 cycle changes in the Geoengineering Model Intercomparison Project (GeoMIP),
664 *Journal of Geophysical Research*, *118*, 13087-13102, doi:10.1002/2013JD020502.

665 Kravitz, B., P. M. Forster, A. Jones, A. Robock, K. Alterskjær, O. Boucher, A. K. L.
666 Jenkins, H. Korhonen, J. E. Kristjánsson, H. Muri, U. Niemeier, A.-I. Partanen, P. J.
667 Rasch, H. Wang, and S. Watanabe (2013c), Sea spray geoengineering
668 experiments in the Geoengineering Model Intercomparison Project (GeoMIP):
669 Experimental design and preliminary results, *Journal of Geophysical Research*,
670 *118*(19), 11175-11186, doi:10.1002/jgrd.50856.

671 Kravitz, B., D. G. MacMartin, P. J. Rasch, and A. J. Jarvis (2015), A new method of
672 comparing forcing agents in climate models, *J. Climate, 28*, 8203–8218,
673 doi:10.1175/JCLI-D-14-00663.1.

674 Kravitz, B., D. G. MacMartin, H. Wang, and P. J. Rasch (2016), Geoengineering as a
675 design problem, *Earth System Dynamics, 7*, 469-497, doi:10.5194/esd-7-469-
676 2016.

677 Latham, J. (1990), Control of global warming? *Nature*, *347*, 339–340.

MacMartin, D.G., B. Kravitz, D. W. Keith, and A. Jarvis (2014), Dynamics of the coupled human-climate system resulting from closed-loop control of solar geoengineering, *Clim. Dynam., 43*, 243-258, doi:10.1007/s00382-013-1822-9.

Mitchell, D. L. and W. Finnegan (2009), Modification of cirrus clouds to reduce global warming, *Environ. Res. Lett.*, *4*, 045102, doi:10.1088/1748-9326/4/4/045102.

Moore, J. C., A. Rinke, X. Yu, D. Ji, X. Cui, Y. Li, K. Alterskjær, J. E. Kristjánsson, O. Boucher, N. Huneeus, B. Kravitz, A. Robock, U. Niemeier, H. Schmidt, M. Schulz, S. Tilmes, and S. Watanabe (2014), Arctic sea ice and atmospheric circulation under the GeoMIP G1 scenario, *J. Geophys. Res., 119*, 567-583, doi:10.1002/2013JD021060.

NAS (2015a), Climate Intervention: Carbon Dioxide Removal and Reliable Sequestration, National Research Council, The National Academies Press, Washington, DC, 141 pp.

NAS (2015b), Climate Intervention: Reflecting Sunlight to Cool Earth, National Research Council, The National Academies Press, Washington, DC, 235 pp.

Niemeier, U., H. Schmidt, K. Alterskjær, and J. E. Kristjánsson (2013), Solar irradiance reduction via climate engineering--impact of different techniques on the energy balance and the hydrological cycle, *Journal of Geophysical Research*, *118*, 11905-11917, doi:10.1002/2013JD020445.

Oreopoulos, L. and S. Platnick (2008), Radiative susceptibility of cloudy atmospheres to droplet number perturbations: 2. Global analysis from MODIS, *J. Geophys. Res.*, *113*, D14S21, doi:10.1029/2007JD009655.

Pandey, D. K., R. B. Lee III, and J. Paden (1995), Effects of atmospheric emissivity on clear sky temperatures, *Atmos. Environ.*, *29*, 2201-2204, doi:10.1016/1352-2310(94)00243-E.

Phipps, S. J., L. D. Rotstayn, H. B. Gordon, J. L. Roberts, A. C. Hirst, and W. F. Budd (2011), The CSIRO Mk3L climate system model version 1.0 – Part 1: Description and evaluation, *Geosci. Model Dev.*, *4*, 483-509, 10.5194/gmd-4-483-2011.

Robock, Alan A. (2011), Bubble, bubble, toil and trouble. An editorial comment. *Climatic Change*, *105*, 383-385, doi:10.1007/s10584-010-0017-1.

Schmidt, H., K. Alterskjær, D. Bou Karam, O. Boucher, A. Jones, J. E. Kristjánsson, U. Niemeier, M. Schulz, A. Aaheim, F. Benduhn, M. Lawrence, and C. Timmreck (2012), Solar irradiance reduction to counteract radiative forcing from a quadrupling of CO_2: Climate responses simulated by four Earth system models, *Earth System Dynamics, 3*, 63-78, doi:10.5194/esd-3-63-2012.

Schmidt, Gavin A., Max Kelley, Larissa Nazarenko, Reto Ruedy, Gary L. Russell, Igor Aleinov, Mike Bauer, Susanne E. Bauer, Maharaj K. Bhat, Rainer Bleck, Vittorio Canuto, Yong-Hua Chen, Ye Cheng, Thomas L. Clune, Anthony Del Genio, Rosalinda de Fainchtein, Greg Faluvegi, James E. Hansen, Richard J. Healy, Nancy Y. Kiang, Dorothy Koch, Andy A. Lacis, Allegra N. LeGrande, Jean Lerner, Ken K. Lo, Elaine E. Matthews, Surabi Menon, Ron L. Miller, Valdar Oinas, Amidu O.

719 Oloso, Jan P. Perlwitz, Michael J. Puma, William M. Putman, David Rind, Anastasia
720 Romanou, Makiko Sato, Drew T. Shindell, Shan Sun, Rahman A. Syed, Nick
721 Tausnev, Kostas Tsigaridis, Nadine Unger, Apostolos Voulgarakis, Mao-Sung Yao,
722 and Jinlun Zhang (2014), Configuration and assessment of the GISS ModelE2
723 contributions to the CMIP5 archive, *J. Adv. Model. Earth Syst., 6*, 141–184,
724 doi:10.1002/2013MS000265.

725 Seitz, R. (2011), Bright water: hydrosols, water conservation and climate change,
726 *Climatic Change*, *105*, 365-381, doi:10.1007/s10584-010-9965-8.

727 Shepherd, J., K. Caldeira, P. Cox, J. Haigh, K. Keith, B. Launder, G. Mace, G. MacKerron,
728 J. Pyle, S. Rayner, C. Redgwell, and A. Watson (2009), Geoengineering the climate:
729 Science, governance, and uncertainty, Royal Society Policy document 10/09, 82
730 pp.

731 Sherwood, S. C., S. Bony, O. Boucher, C. Bretherton, P. M. Forster, J. M. Gregory, and B.
732 Stevens (2015), Adjustments in the forcing-feedback framework for
733 understanding climate change, *Bull. Amer. Meteor. Soc., 96*, 217–228,
734 doi:10.1175/BAMS-D-13-00167.1.

735 Stephens, G. L., D. O'Brien, P. J. Webster, P. Pilewski, S. Kato, and J.-L. Li (2015), The
736 albedo of Earth, *Rev. Geophys.*, *53*, 141-163, doi:10.1002/2014RG000449.

737 Taylor, K. E., R. J. Stouffer, and G. A. Meehl (2012), An overview of CMIP5 and the
738 experiment design, *Bull. Amer. Meteor. Soc.*, *93*, 485-498, doi:10.1175/BAMS-D-
739 11-00094.1.

740 Tilmes, S., J. Fasullo, J.-F. Lamarque, D. R. Marsch, M. Mills, K. Alterskjær, O. Boucher,
741 J. N. S. Cole, C. L. Curry, J. M. Haywood, P. J. Irvine, D. Ji, A. Jones, D. B. Karam, B.
742 Kravitz, J. E. Kristjánsson, J. C. Moore, H. O. Muri, U. Niemeier, P. J. Rasch, A.
743 Robock, H. Schmidt, M. Schulz, B. Singh, S. Watanabe, S. Yang, and J.-H. Yoon
744 (2013), The hydrological impact of geoengineering in the Geoengineering Model
745 Intercomparison Project (GeoMIP), *Journal of Geophysical Research*, *118*(19),
746 11036-11058, doi:10.1002/jgrd.50868.

747 Watanabe, S., T. Hajima, K. Sudo, T. Nagashima, T. Takemura, H. Okajima, T. Nozawa,
748 H. Kawase, M. Abe, T. Yokohata, T. Ise, H. Sato, E. Kato, K. Takata, S. Emori, and M.
749 Kawamiya (2011), MIROC-ESM 2010: Model description and basic results of
750 CMIP5-20c3m experiments, *Geosci. Mod. Dev.*, *4*, 845-872, doi:10.5194/gmd-4-
751 845-2011.

752

Table 1. Description of the 11 models participating in this study. Column 1 gives the standard model name. Columns 2 and 3 give the default and perturbed surface ocean albedo, defined as upward shortwave divided by downward shortwave radiative flux at the surface, both averaged over ocean regions and over years 11-50 of simulation. Column 4 is the ratio of column 3 to column 2. Column 5 gives the factor (δ) by which the model default ocean albedo was multiplied to achieve negligible top-of-atmosphere radiative flux changes under an abrupt4xCO2 simulation (described in greater detail by Kravitz et al., 2015). The differences between Ratio and δ are caused by cloud responses. Column 6 gives a relevant reference for each model. All values are rounded to two decimal places.

Model name	piControl ocean albedo	G1OA ocean albedo	Ratio	δ	Reference
BNU-ESM	0.12	0.17	1.48	2.50	Ji et al. (2014)
CanESM2	0.11	0.19	1.73	2.45	Arora et al. (2011)
CESM-CAM5.1-FV	0.10	0.18	1.79	2.70	Hurrell et al. (2013)
CSIRO-Mk3L-1.2	0.12	0.19	1.61	2.04	Phipps et al. (2011)
EC-Earth	0.10	0.19	1.97	3.17	Hazeleger et al. (2011)
GISS-E2-R	0.08	0.16	1.95	2.53	Schmidt et al. (2014)
HadGEM2-ES	0.10	0.17	1.83	2.44	Collins et al. (2011)
IPSL-CM5A-LR	0.10	0.17	1.78	2.33	Dufresne et al. (2013)
MIROC-ESM	0.10	0.20	2.00	3.10	Watanabe et al. (2011)
MPI-ESM-LR	0.09	0.23	2.40	5.42	Giorgetta et al. (2013)
NorESM1-M	0.09	0.18	1.95	2.77	Alterskjær et al. (2012)

Table 2. Parameters used in different runs with the simple one-dimensional radiative equilibrium model (Section 3.2). Surface ΔT ~~(in Kkelvin)~~ for the Global runs are with respect to Control (Global) and for the Ocean runs are with respect to Control (Ocean).

Run	Emissivity in each model layer	Surface albedo	Surface ΔT (K)
Control (Global)	0.80	0.3	0
abrupt4xCO2 (Global)	0.8265	0.3	4.4189
Albedo increase (Global)	0.80	0.3395	-4.0165
G1ocean-albedo (Global)	0.8265	0.3395	0.3674
Control (Ocean)	0.80	0.1	0
abrupt4xCO2 (Ocean)	0.8265	0.1	4.7251
Albedo increase (Ocean)	0.80	0.1863	-7.3806
G1ocean-albedo (Ocean)	0.8265	0.1863	-2.7730

Mis en forme : Centré
Tableau mis en forme
Mis en forme : Centré
Mis en forme : Centré
Mis en forme : Centré
Mis en forme : Centré
Mis en forme : Centré
Mis en forme : Centré
Mis en forme : Centré
Mis en forme : Centré

Table 3. Feedback parameters (Section 3.3; units W m^{-2}) for global, land, and ocean averages, calculated via the "Gregory method" (Gregory et al., 2004), where annual mean top-of-atmosphere net radiative flux is regressed against annual mean temperature.

	λ_g	λ_ℓ	λ_o
BNU-ESM	0.9019	0.7181	0.9838
CanESM2	1.1539	1.1898	1.1260
CESM-CAM5.1-FV	1.1435	1.0357	1.1591
CSIRO-Mk3L-1.2	1.0192	0.9300	0.8034
EC-Earth	1.2124	1.1937	1.3155
GISS-E2-R	2.2440	1.9751	2.3560
HadGEM2-ES	0.8411	0.8363	0.8351
IPSL-CM5A-LR	0.8367	1.2891	0.5894
MIROC-ESM	1.0378	0.8736	1.0383
MPI-ESM-LR	1.3701	1.0573	1.3986
NorESM1-M	1.4285	1.8828	1.6063

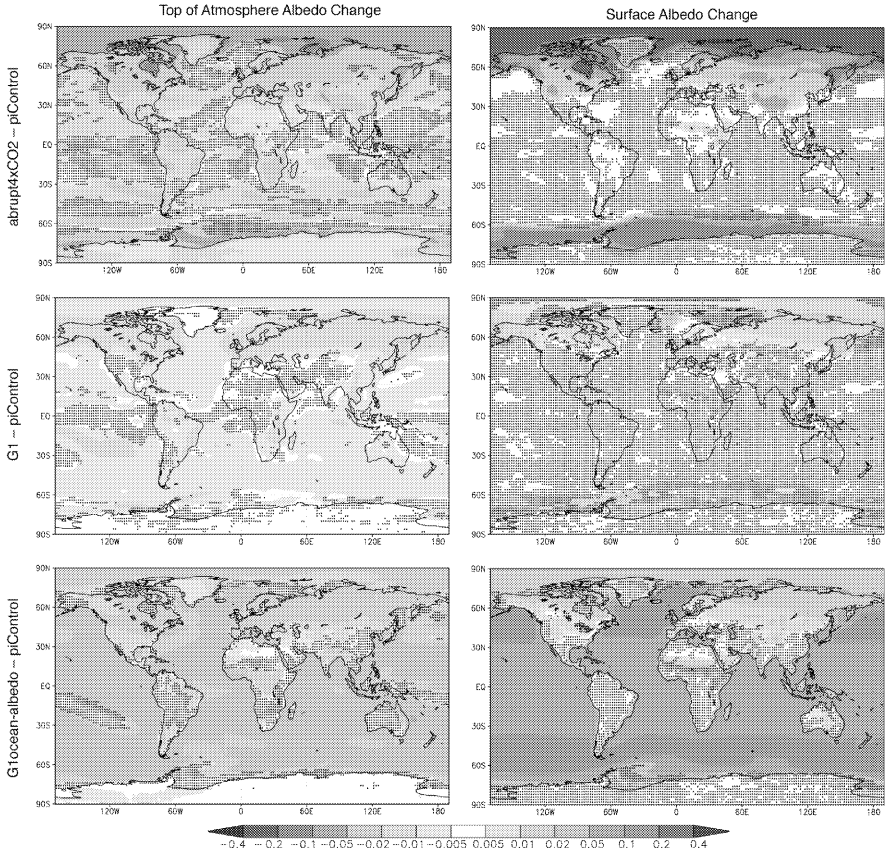

Figure 1. Top-of-atmosphere (TOA) and surface albedo differences (relative to piControl) for the abrupt4xCO2, G1, and G1ocean-albedo experiments. Albedo here is calculated as the ratio of upwelling to downwelling all-sky shortwave radiative flux, either at TOA or at the surface. Values are averages over years 11-50 of simulation. Stippling indicates where fewer than 8 out of 11 models agree on the sign of the response.

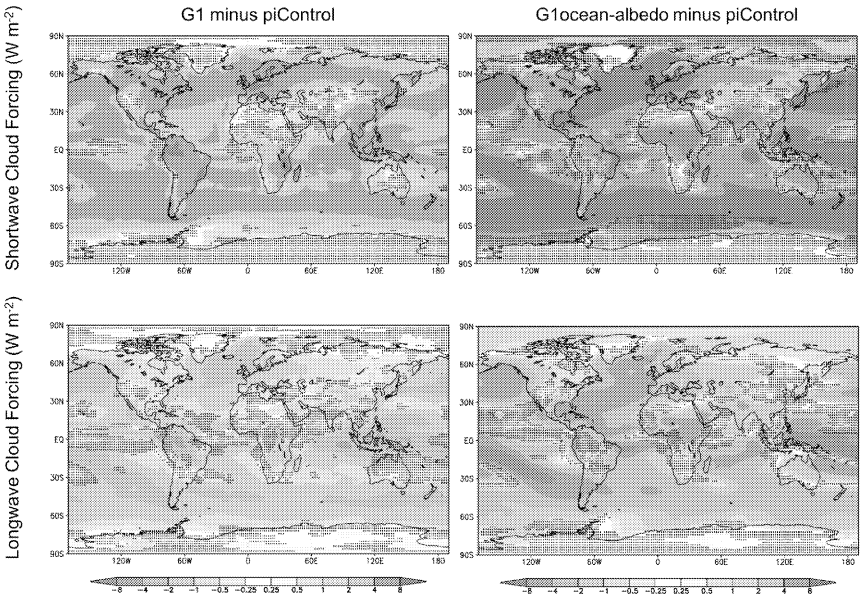

785
786
787 **Figure 2.** Shortwave (top) and longwave (bottom) cloud forcing changes due to the
788 G1 (left) and G1ocean-albedo perturbations. Cloud forcing is defined as all-sky
789 minus clear-sky radiative flux at the top of the atmosphere.

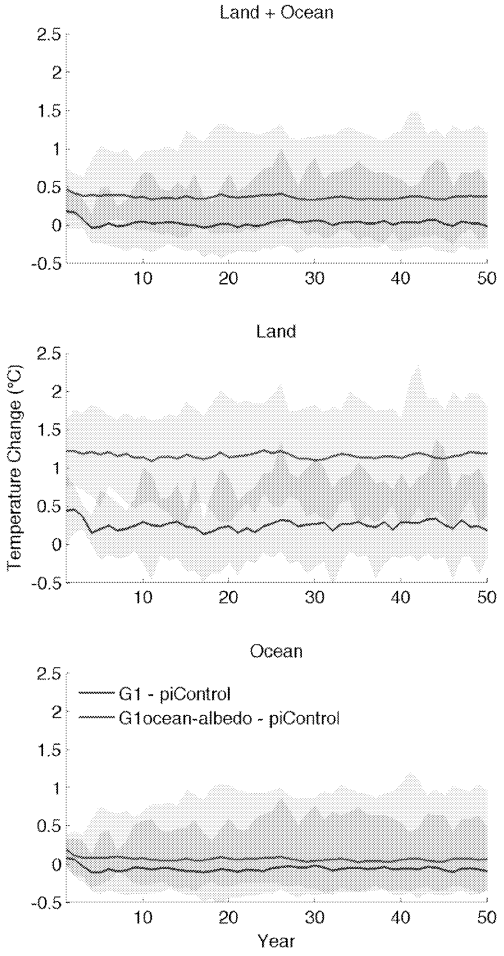

Figure 3. Global (top), land (middle), and ocean (bottom) average temperature change for the G1 (blue) and G1ocean-albedo (red) simulations. Lines show the all-model ensemble mean, and shading shows model spread (smallest to largest values).

Commenté [o15]: You have a mix of °C and K for the T change

Commenté [AR16R15]: Yes, make it all K. Formally, temperature change anyway should be C°.

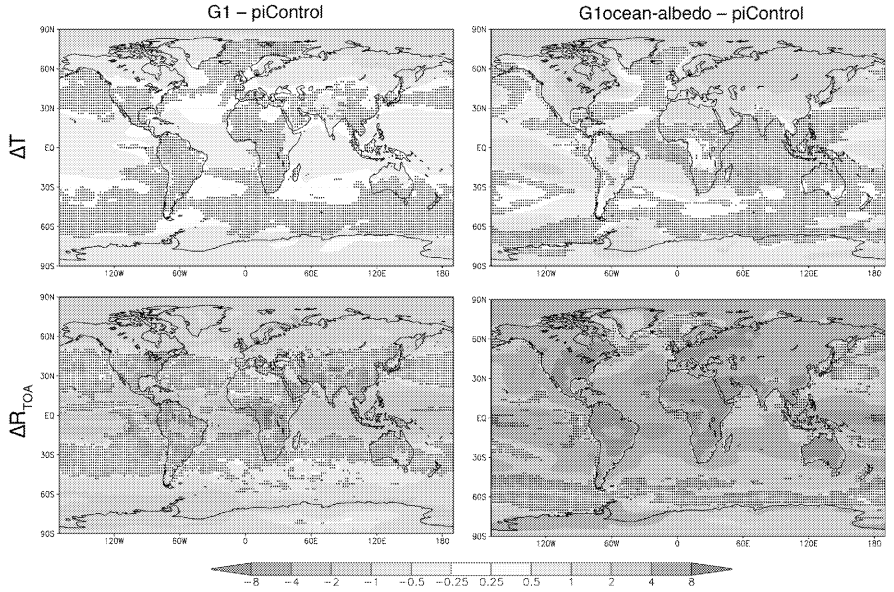

Figure 4. Surface air temperature (top row; K) and TOA net radiative flux (bottom row; W m^{-2}) changes for experiments G1 (left) and G1ocean-albedo (right). Values are averages over years 11-50 of simulation. Stippling indicates where fewer than 8 out of 11 models agree on the sign of the response.

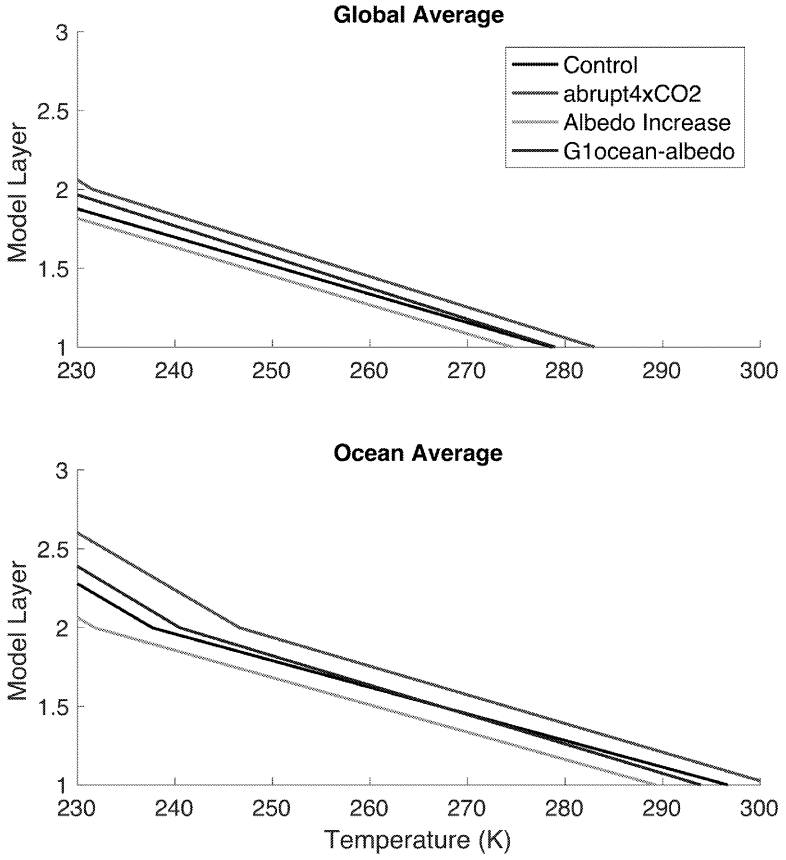

Figure 5. Temperature results for calculations with a one-dimensional radiative equilibrium model with 15 vertical layers (only the bottom three layers are shown). Specifications for all of the simulations are provided in Table 2.

Commenté [o17]: ??

Commenté [AR18R17]: Is layer 1 the surface or the lowest atmospheric model layer?

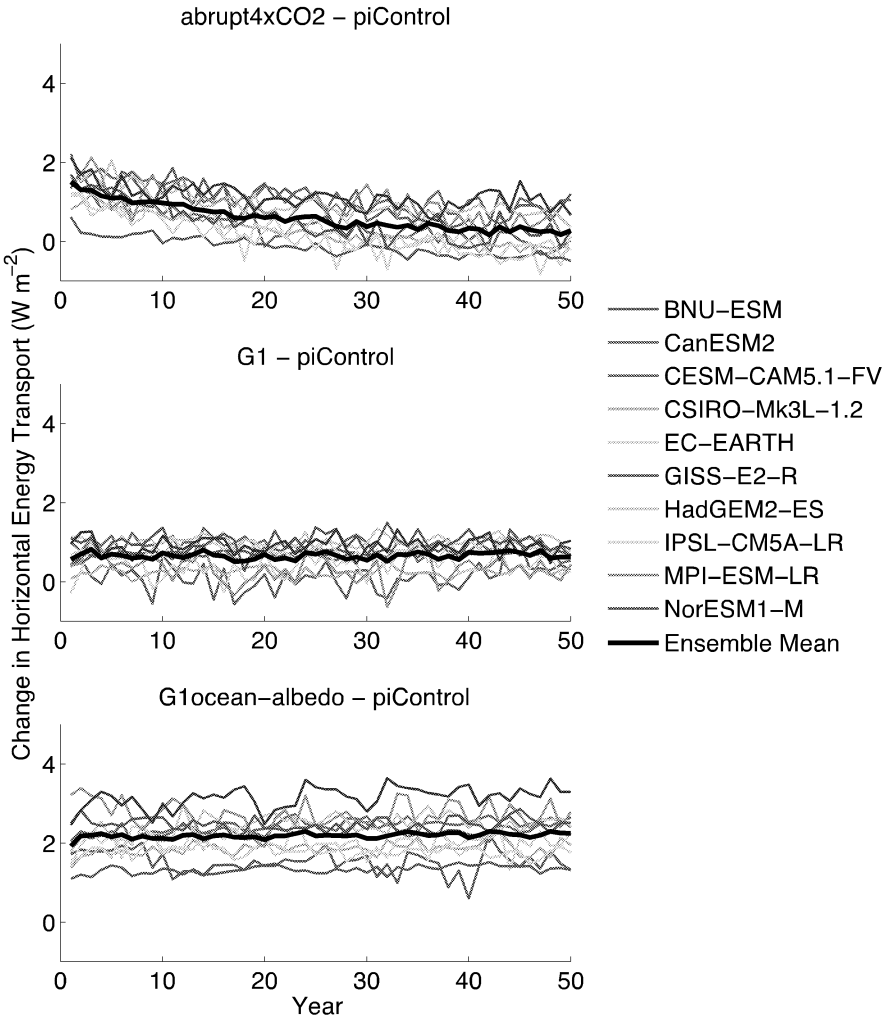

Figure 6. Annual mean change in land-ocean energy transport (Section 3.4; W m^{-2}) from piControl. See Equation 3 for a formal definition.

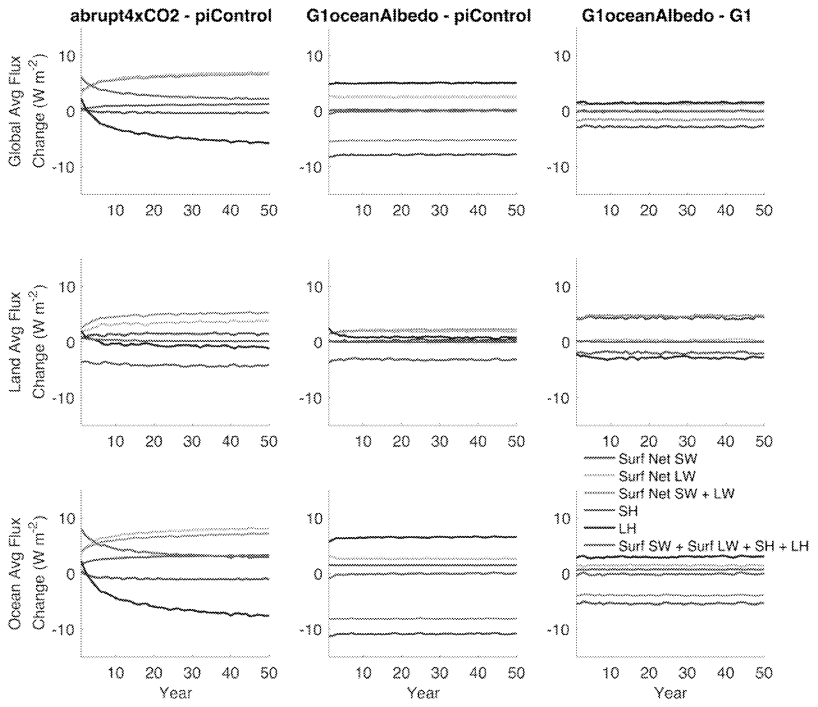

Commenté [AR19]: Make the legend with the same notation as in Eq. (1). Should all these terms start with Δ? Is the last term actually ΔS?

Figure 7. Annual mean time series of all-model mean surface fluxes (terms in Equation 4) for global averages (top), land averages (middle), and ocean averages (bottom). All fluxes are positive in the downward direction.

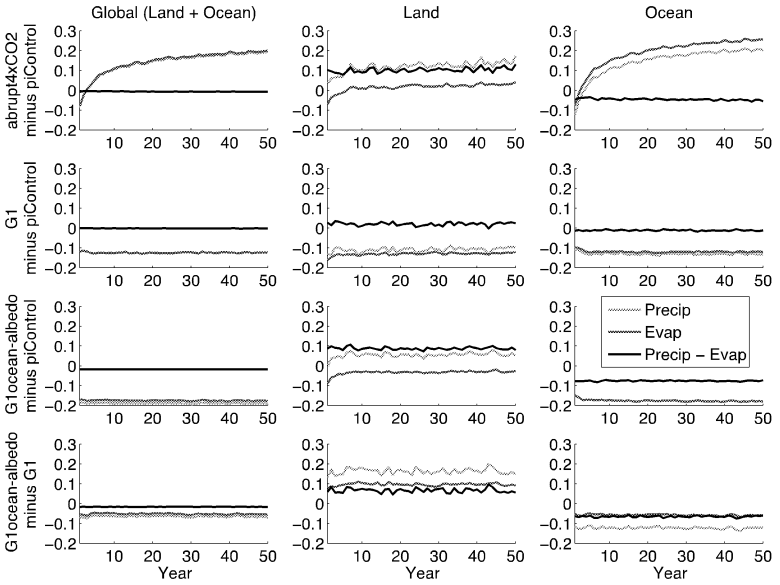

Figure 8. Annual mean time series of hydrological cycle changes (all in mm day^{-1}). Green lines show precipitation changes, red lines show evaporation changes, and black lines show precipitation minus evaporation. When no green line is evident, it is obscured by either the red or black lines.

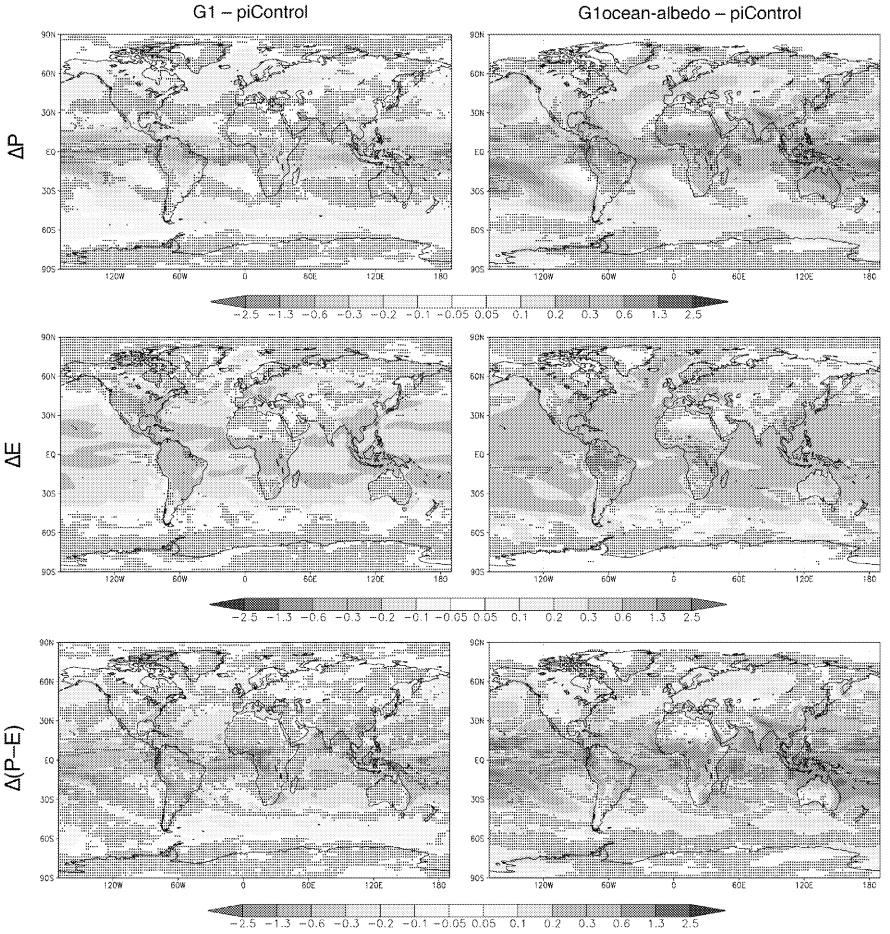

822
823
824 **Figure 9.** Precipitation (top row), evaporation (middle row), and precipitation
825 minus evaporation (bottom row) changes (all panels have units mm day^{-1}) for
826 experiments G1 and G1ocean-albedo. Values are averages over years 11-50 of
827 simulation. Stippling indicates where fewer than 8 out of 11 models agree on the
828 sign of the response.
829

The climate effects of increasing ocean albedo: An idealized representation of solar geoengineering

Ben Kravitz,[1*] Philip J. Rasch,[1] Hailong Wang,[1] Alan Robock,[2] Corey Gabriel,[3] Olivier Boucher,[4] Jason N. S. Cole,[5] Jim Haywood,[6,7] Duoying Ji,[8] Andy Jones,[6] Andrew Lenton,[9] John C. Moore,[8] Helene Muri,[10] Ulrike Niemeier,[11] Steven Phipps,[12,13] Hauke Schmidt,[11] Shingo Watanabe,[14] Shuting Yang,[15] and Jin-Ho Yoon[16]

[1]Atmospheric Sciences and Global Change Division, Pacific Northwest National Laboratory, Richland, WA, USA
[2]Department of Environmental Sciences, Rutgers University, New Brunswick, NJ, USA
[3]Scripps Institution of Oceanography, La Jolla, CA, USA
[4]~~Laboratoire de Météorologie Dynamique,~~ Institut Pierre-Simon Laplace, CNRS / ~~Université P. et M. Curie~~Sorbonne Université, Paris, France
[5]Environment and Climate Change Canada, Toronto, Canada
[6]Met Office Hadley Centre, Exeter, UK
[7]College of Engineering, Mathematics, and Physical Sciences, University of Exeter, Exeter, UK
[8]State Key Laboratory of Earth Surface Processes and Resource Ecology, College of Global Change and Earth System Science, Beijing Normal University, Beijing, China
[9]CSIRO Oceans and Atmosphere, Hobart, Tasmania, Australia
[10]Department of Geosciences, University of Oslo, Oslo, Norway
[11]Max Planck Institute for Meteorology, Hamburg, Germany
[12]Climate Change Research Centre, University of New South Wales, Sydney, Australia
[13]Institute for Marine and Antarctic Studies, University of Tasmania, Hobart, Tasmania, Australia
[14]Japan Agency for Marine-Earth Science and Technology, Yokohama, Japan
[15]Danish Meteorological Institute, Copenhagen, Denmark
[16]Gwangju Institute of Science and Technology, Gwangju, South Korea

Submission to *Atmospheric Chemistry and Physics*
Special Issue: The Geoengineering Model Intercomparison Project

[*]To whom correspondence should be addressed: P.O. Box 999, MSIN K9-30, Richland, WA 99352, USA. E-mail: ben.kravitz@pnnl.gov.

Abstract. Marine cloud brightening has been proposed as a means of ~~geoengineering~~climate intervention, or deliberately altering the climate system to offset anthropogenic climate change. As an idealized representation of marine cloud brightening, this paper discusses experiment G1ocean-albedo of the Geoengineering Model Intercomparison Project ~~(GeoMIP)~~, involving an abrupt quadrupling of the CO_2 concentration and an instantaneous increase in ocean albedo to maintain approximate net top-of-atmosphere radiative flux balance. Eleven Earth System Models are relatively consistent in their temperature, radiative flux, and hydrological cycle responses to this experiment. Due to the imposed forcing, the land surface warms by 1.14~~°C~~ K, while most of the ocean cools. Some parts of the near-surface air temperature over ocean warm due to heat transport from land to ocean. These changes generally resolve within a few years, indicating that changes in ocean heat content play at most a small role in the warming over the oceans. The hydrological cycle response is a general slowing down, with little net change in large-scale precipitation minus evaporation, but also with substantial heterogeneity. While idealized, these results have important implications for marine cloud brightening or any other method of geoengineering involving spatially heterogeneous forcing, particularly if that forcing has a strong land/ocean contrast.

Main points:

1) Under an increase in the CO_2 concentration and ocean albedo, the global? climate transitions to a new, warmer steady state.

2) The land surface warms substantially, and oceans near the land warm due to heat transport

3) The hydrological cycle slows down, with regional heterogeneity in the response

Suggested reviewers:

Tim Andrews

Olivier Geoffroy

Govindasamy Bala

Commenté [AR1]: Add error bars? Or make less precise.

Mis en forme : Surlignage

Commenté [o2]: Rephrase. Is this over land only ? why just look at large-scale precip ?

Commenté [o3]: Or even any forcing with a land/sea contrast. What about aerosols over land ?

Commenté [o4]: Needs to say that this is at fixed global energy budget ?

Mis en forme : Surlignage

Commenté [AR5]: Add because of cloud feedbacks?

1. Introduction

Geoengineering (also called "climate intervention") describes a set of technological approaches to reduce the effects of climate change by deliberately intervening in the climate system (e.g., Shepherd et al., 2009). There are two broad categories of geoengineering that are commonly discussed: solar geoengineering (modifying the amount of shortwave radiation incident at the surface; NAS, 2015a) and carbon dioxide removal (NAS, 2015b). There are also proposals, such as cirrus cloud thinning (Mitchell and Finnegan, 2009) that do not fit neatly into either of these two categories. In all subsequent discussions in this manuscript, we only discuss solar geoengineering methods.

Two of the most commonly proposed methods of global geoengineering are stratospheric sulfate aerosol injection (SAI) and marine cloud brightening (MCB). Comparison of the different climate effects of these two methods (e.g., Niemeier et al., 2013; Crook et al., 2015) reveals that, among other things, the spatial distributions of the applied forcings strongly affect the climate effects. Many of the effects of SAI can be reasonably well approximated by a uniform reduction in shortwave radiative flux reaching the surface (Kalidindi et al., 2015). Conversely, MCB targets low clouds over oceans (Latham, 1990), which are not ubiquitous. In addition, there are higher order effects due to the altitude at which the shortwave scattering occurs, including multiple scattering effects, infrared absorption of shortwave and longwave radiative flux by sulfate aerosols or cloud particles, and absorption of shortwave radiative flux by atmospheric CO_2 and water vapor (e.g., Kravitz et al., 2013b).

Idealized simulations of solar geoengineering are useful in the context of multi-model intercomparisons, in that they capture many of the effects of more complicated methods of representing geoengineering, yet can be performed by a wide variety of models. In simulations conducted under the Geoengineering Model Intercomparison Project (GeoMIP; Kravitz et al., 2011), an idealized method of representing SAI is via reductions in total solar irradiance; experiment G1 involved offsetting the global radiative flux imbalance from a quadrupling of the CO_2 concentration via solar reduction. Thus far, 15 models have participated in this simulation, providing information about model commonalities and differences in the global climate response, including effects on temperature, the hydrological cycle, cryosphere, terrestrial biosphere, and extreme events (Schmidt et al., 2012; Kravitz et al., 2013a, 2013b; Tilmes et al. 2013; Moore et al., 2014; Glienke et al., 2015; Curry et al., 2014; among numerous other studies). The GeoMIP website (http://climate.envsci.rutgers.edu/GeoMIP/) provides an up-to-date list of publications using GeoMIP model output.

Commenté [HS6]: For me, the main purpose of idealization is the attempt to facilitate understanding.

While total solar irradiance reductions are straightforward to simulate in all models, this idealization is not a good approximation of MCB. The dominant effect of MCB ~~is~~ would be an increase in albedo in and near marine low clouds through "direct" and "indirect" effects. Changes in the albedo near the surface can produce different

signatures from reductions in energy input at the top of the atmosphere. There are also likely to be differences in the spatial distribution of the energy reduction. While some forms of albedo modification like SAI operate over broad areas (on a hemispheric or larger scale), albedo changes produced by MCB ~~are likely to~~would operate on smaller spatial scales and be concentrated over particular oceanic regions. Previous studies suggest that the clouds that are most susceptible to albedo modification are located on the ~~w~~eastern side of ocean basins in the subtropics, in regions dominated by stratocumulus clouds (Oreopoulos and Platnick, 2008). So, rather than considering a reduction of solar input operating uniformly over both land and ocean, an idealized representation of MCB that better approximates the effects is to increase the albedo only over ocean surfaces, as described by Kravitz et al. (2013c). This method can also be used to assess some effects of geoengineering by creating microbubbles at the ocean surface to increase reflectivity (e.g., Seitz, 2011; Robock, 2011; Gabriel et al., 2017).

In this study, we investigate the climate effects of using ocean albedo increases to offset CO_2 warming and compare those effects with those of total solar irradiance reduction (experiments are described in more detail in the following section). All simulations were conducted under the auspices of GeoMIP, allowing us to characterize a range of model responses to these different idealized methods of representing solar geoengineering.

2. Methodology and Description

Our analyses focus on four simulations: (1) a preindustrial control simulation (piControl), (2) a simulation in which the CO_2 concentration is abruptly quadrupled from its preindustrial value (abrupt4xCO2), (3) a simulation in which the net radiative flux imbalance in abrupt4xCO2 is offset by a reduction in total solar irradiance (G1), and (4) a simulation in which the net radiative flux imbalance in abrupt4xCO2 is offset by an increase in ocean albedo everywhere by a uniform factor (G1ocean-albedo). piControl and abrupt4xCO2 are standard experiments in the Coupled Model Intercomparison Project Phase 5 (CMIP5; Taylor et al., 2012). G1 is described further by Kravitz et al. (2011). The protocol for G1ocean-albedo is described in more detail by Kravitz et al. (2013c). Table 1 lists the models participating in this study, including relevant references and the required change in albedo to meet the objectives of experiment G1ocean-albedo. A similar table for experiment G1 is given by Kravitz et al. (2013a). One of the advantages of G1ocean-albedo is that, like G1, all models can conduct this simulation fairly easily. Supplemental Table S1 quantifies how well each model achieved radiative balance in the G1 and G1ocean-albedo experiments.

Kravitz et al. (2013c) found that in test simulations, one could only determine whether the objectives of G1ocean-albedo were met after several decades of simulation. However, as our analysis will show, once the proper value of ocean albedo increase is ascertained, the climate response reaches steady state in a few years, as in experiment G1 (Kravitz et al., 2013a). Supplemental Table S2 quantifies

Commenté [HS7]: "So" doesn't really fit, because in our experiment we don't care where the clouds are most susceptible.

Commenté [o8]: I think it is important to restate that we aim for a balanced TOA budget over the first 10 years, right ? plus the fact that the albedo is increase proportionally

Commenté [HS9R8]: Actually the balanced budget was requested for years 21-30, although I don't know if people have really followed the protocol and if that matters much.

temperature trends in each participating model over years 11-50 of simulation. The mean model trend over this period is approximately zero (to four decimal places), and with little exception, the trends in G1 and G1ocean-albedo are an order of magnitude smaller than the trends in the abrupt4xCO2 simulation. As such, for the purpose of analysis, we assume that "slow responses," i.e., responses operating on time scales longer than a few years (e.g., Andrews and Forster, 2010; Sherwood et al., 2015) are negligible in the G1 and G1ocean-albedo simulations. We do not separate results into rapid adjustment and slow response timescales, and with the exception of time series plots, all figures show averages over the years 11-50 of simulation, which we take as a sufficient indication of the dominant climate response after the transient response has resolved.

Commenté [AR10]: In what units?

Except where indicated, all plots show the mean model response. All values in the text are reported as mean (min to max), where mean indicates the all-model mean for that particular quantity, min is the lower bound of the range of model responses, and max is the upper bound of the range of model responses. In all maps, stippling indicates where fewer than 75% of the models agree on the sign of the response. All models in Table 1 were able to provide output for all variables except for cloud radiative forcing. The models included in cloud forcing analyses are BNU-ESM, CanESM2, CESM-CAM5.1-FV, HadGEM2-ES, IPSL-CM5A-LR, and MPI-ESM-LR. Supplemental Tables S1-S15 provide more quantitative information for all of the analyses presented in this study.

3. Results

3.1. Albedo and Temperature

Figure 1 shows the change in albedo at the top-of-atmosphere and at the surface for the abrupt4xCO2, G1, and G1ocean-albedo simulations, where albedo is defined as the ratio of upwelling to downwelling all-sky shortwave radiative flux. Quantitative values are given in Supplemental Tables S3 and S4. Results for abrupt4xCO2 and G1 are consistent with known responses of an increase in absorbed shortwave by carbon dioxide, reduced cloud cover, and reduced snow and sea ice cover (e.g., Schmidt et al., 2012; Kravitz et al., 2013b). These result in a broad decrease in albedo at the top of atmosphere and a decrease in surface albedo in many regions with substantial snow and ice cover. G1ocean-albedo retains many of these local high latitude features, but with large albedo increases over ocean, consistent with the experimental design and imposed forcing.

Figure 2 expands upon this picture by showing changes in shortwave and longwave cloud forcing in G1 and G1ocean-albedo, where cloud forcing is defined as all-sky minus clear-sky radiative flux measured at the top of the atmosphere. Positive shortwave values and negative longwave values in Figure 2 generally indicate less cloud cover. As was shown by Kravitz et al. (2013b), cloud cover in G1 tends to be reduced, which is consistent with what is depicted in Figure 2. For G1ocean-albedo, cloud cover is reduced over most ocean regions and large portions of land.

Exceptions include an increase in cloudiness over the Arctic, much of Africa, South Asia, Australia, and the leeward side of the Andes. These changes in cloudiness have implications for the hydrologic cycle, which we revisit in Section 3.5.

Figure 3 shows changes in global mean, land mean, and ocean mean surface air temperature for the G1 and G1ocean-albedo multi-model ensembles. Quantitative values are provided in Supplemental Table S5. Whereas the G1 simulation largely offsets temperature changes due to increased CO_2 concentration, G1ocean-albedo is approximately 0.36~~°C~~ K (-0.12 to 1.20) warmer than the control simulation. This is predominantly due to warming over land by 1.14~~°C~~ K (0.41 to 1.83). The temperature results in Figure 3 indicate that the temperature change happens within the first few years, and while some models show a slight trend in temperature over the 50-year G1ocean-albedo simulation (Supplemental Table S2), in general, any such trends are small, especially as compared to the warming in the abrupt4xCO2 simulation. This lack of substantial transient behavior after an initial fast response indicates that G1ocean-albedo has entered a new approximate steady state.

Figure 4 shows spatial patterns of change in temperature and top-of-atmosphere net radiative flux. (Also see Supplemental Tables S5 and S6.) The temperature changes are broadly consistent with the net radiative flux changes in the respective experiments. As was discussed by Kravitz et al. (2013a), G1 results in an "overcooling" of the tropics and an "undercooling" of the poles, consistent with offsetting the ubiquitous longwave forcing from CO_2 with a latitudinally dependent reduction in shortwave. G1ocean-albedo shows warming at high latitudes, over land regions, and in some ocean regions near or downwind of large continents, with the remaining ocean regions generally showing cooling. Because net top-of-atmosphere radiative flux is approximately zero in G1ocean-albedo, these temperature changes cannot be the result of energy being added to or subtracted from the climate system, and instead must be the result of energy redistribution. Hypotheses for why these temperature change patterns look the way they do (which will be tested in subsequent sections) include

1) The global average warming experienced in G1ocean-albedo is primarily due to increased heating over land.

2) Most warming over oceanic regions is due to transport of heat from land to ocean.

3) Any contributions to temperature or radiative flux changes from changes in ocean heat content are small on the timescales being evaluated here.

3.2. Hypothesis 1: Increased heating over land drives global average warming in G1ocean-albedo

Commenté [HS11]: Are these really exceptions, I guess the map projection may fool us. Most of Africa + tropical and subtropical Asia + Australia is a fairly large fraction of the land surface

Commenté [HS12]: The multi-model mean temperature increase in G1OA must happen actually very rapidly. It is apparently there already in the first year.

Commenté [o13]: This needs to come earlier

The first hypothesis is fairly straightforward to argue based on first principles. To do so, we employ a one-dimensional radiative equilibrium model with 15 vertical layers extending from the surface to the nominal top-of-atmosphere. In the model, each layer behaves as a gray body with a specified emissivity, and the model computes radiative transfer between each layer via Planck radiation (the Stefan-Boltzmann equation). Although this model represents a gross oversimplification of the vertical profile of temperature response to idealized forcing, it is useful here for understanding differences between land and ocean temperature changes in response to the forcing imposed in G1ocean-albedo.

Figure 5 shows temperature profiles calculated using this model for four experiments: a control simulation, an abrupt4xCO2-like simulation (modeled as an increase in the emissivity of each model layer), a simulation with increased surface albedo, and G1ocean-albedo-like simulation involving an increase in emissivity and an increase in surface albedo. These simulations were conducted separately for global average and ocean-only regions.

Values of emissivity in the control simulation were prescribed to be 0.80 at all layers, consistent with a gray body (Pandey et al., 1995). The emissivity in the abrupt4xCO2 simulation was calculated to be the value such that global mean temperature change in the first model layer is approximately 4.42 K (Supplemental Table S5), yielding an emissivity value of 0.8265. In the control simulations, the surface albedos for the global and ocean-only simulations are 0.3 and 0.1, respectively, consistent with estimates provided by Stephens et al. (2015) and the values given in Table 1. In the global average simulation, the albedo increase in the G1-ocean albedo simulation was calculated to be the value such that global mean temperature change in the first model layer is approximately 0.36 K (Supplemental Table S5). In the ocean average simulation, the albedo increase is the all-model average of the required albedo increase in Table 1, which is a multiplication factor of 1.8627.

The results in Figure 5 show that under reasonable assumptions around atmospheric emissivity and surface albedo, oceanic cooling is expected in the G1ocean-albedo simulation. Based on these results, any increase in global average temperature must be due to warming over land. The oceanic temperature change in this simple model's simulation of G1ocean-albedo is -2.77 K, which is far too large in magnitude as compared to the results from the Earth System Models. Figure 2 indicates that changes in cloud cover in G1ocean-albedo are more likely to increase the magnitude of this temperature change than decrease it. In subsequent sections, we discuss some additional mediating factors that could act to reduce the magnitude of this change, such as land-ocean energy transport or reduced net ocean heat uptake. Nevertheless, the dominant radiative effects in G1ocean-albedo are to cause cooling over the oceans, as is seen in Figure 4.

3.3. Hypothesis 2: The role of Land-Ocean Energy Transport (LOET)

Commenté [o14]: Has the model two compartments for ocean and land ? should you show a schematic of the model ?

Commenté [HS15]: I don't really understand what the model is supposed to tell me. If the main result is that we expect the atmosphere above oceans to cool, I guess we would have expected that without the model. Doing G1 ocean albedo in a connected two-column (one ocean, one land) RCE model could be useful.

Commenté [AR16]: Certainly true if you ignore convection. Why use such an unrealistic representation? And why 15 layers?

Although the air over the ocean warms somewhat in G1ocean-albedo, it does not warm uniformly. Figure 4 shows that much of the warming over the ocean is in areas near land, indicating the potential for some of the heating energy over land to be transported to ocean regions. This can be quantified via calculating what Geoffroy et al. (2015) call horizontal energy transport, and which we call land-ocean energy transport (LOET), as it represents an aggregate transport of energy from the atmosphere over the land (averaged over all land regions) to the atmosphere over the ocean (averaged over all ocean regions). They provide a more detailed description, calculation, and validation of this concept using a three-box energy balance model that can be fitted to changes in land/ocean temperature and TOA energy imbalance such that the model captures the relevant energy transport dynamics; we repeat here only the calculations germane to our discussions.

Gregory et al. (2004) describe a method of estimating adjusted radiative forcing and the aggregate strength of global feedbacks via linear regression of the net global, annual mean TOA radiative flux imbalance (ΔR) against the global, annual mean temperature change (ΔT) in response to a forcing. The y-intercept of the regression line gives an estimate of adjusted radiative forcing ($\mathcal{F}$), and the negative of the slope of the regression line gives the feedback parameter (λ). Similarly, one can perform regression just over land-averaged quantities (denoted with the subscript ℓ) or just over ocean quantities (subscript o). Feedback parameter values are provided in Table 3.

In addition, one can regress ΔT_ℓ against ΔT_o to obtain a y-intercept of

$$\mathcal{F}_\ell/(\lambda_\ell+\alpha_\ell/f_\ell) \quad (1)$$

where α_ℓ is the land heat transport parameter and f_ℓ is the land fraction (approximately 0.3). The slope is

$$(\alpha_o/f_\ell)/(\lambda_\ell+\alpha_\ell/f_\ell) \quad (2)$$

If one solves these two equations for α_ℓ and α_o, then one can define

$$\Delta A = \alpha_\ell \Delta T_\ell - \alpha_o \Delta T_o \quad (3)$$

The quantity ΔA is the time-dependent LOET (units of W m^{-2}).

Figure 7 provides calculations of LOET for the simulations presented here. See Supplemental Table S7 for more details on individual model values. In the abrupt4xCO2 simulation, changes in LOET are positive (indicating an increase in heat transport from the land to the ocean) and decrease in magnitude steadily over the course of the simulation; these results are discussed in more detail by Geoffroy et al. (2015).

Mis en forme : Police :Italique
Mis en forme : Police :Italique
Mis en forme : Police :Italique
Commenté [AR17]: Are you sure you want to use alpha? Some will confuse this with albedo.
Mis en forme : Police :Italique
Mis en forme : Police :Italique
Mis en forme : Police :Italique
Commenté [HS18]: (1) And (2) are not equations. Geoffroy et al. don't derive equation 3 but assume it.
Mis en forme : Police :Italique
Mis en forme : Police :Italique
Mis en forme : Police :Italique
Mis en forme : Police :Italique

In Experiment G1, LOET increases by a model-dependent constant value and remains relatively unchanged over the course of the simulation. Although the air temperature over land in G1 increases slightly, and the air temperature over ocean decreases slightly (Kravitz et al., 2013a), the temperature changes in G1 are more latitude-dependent than representative of a clear land-ocean contrast (Figure 4), so it is perhaps not unexpected that LOET would be small.

Experiment G1ocean-albedo exhibits a strong land-ocean contrast in temperature (Figure 4), and the response is in steady state after a few years. As such, consistent with the behavior of other fluxes, LOET in G1ocean-albedo does not show transient behavior. LOET in G1ocean-albedo is approximately 2.20 (1.35 to 3.21) W m^{-2}, which is larger than in the other experiments examined here.

Converting LOET into temperature change is not necessarily straightforward, but an approximate change in temperature can be calculated by combining values of ΔA (Supplemental Table S7) with feedback parameter calculations (Table 3). More specifically, the temperature "added" to the air over the oceans by LOET can be calculated as $\Delta A/\lambda_o$, and the temperature "subtracted" from the air over land by LOET can be calculated as $\Delta A/\lambda_l$. Performing these calculations, LOET in the G1ocean-albedo experiment contributes 1.87°C K (0.57 to 3.06) to ocean temperature and "subtracts" 2.03°C K (0.68 to 3.06) from land temperature. We caution that this naïve calculation is somewhat circular, and it inherently includes in the ocean calculations both regions unaffected by LOET (e.g., tropical oceans) and regions strongly affected by LOET (e.g., Northeast Atlantic and Pacific Oceans).

Mis en forme : Police :Italique

Mis en forme : Police :Non Italique

Mis en forme : Police :Non Italique

Based on the calculations in Section 3.2 and the present section, it seems unlikely that LOET can on average transport enough energy from the land to the ocean to offset the radiative deficit due to an ocean albedo increase. However, locally, LOET appears to be able not only to offset these radiative changes, but also result in net warming.

3.4. Hypothesis 3: Atmospheric Column Energetics and Net Energy Flux into the Oceans

An additional potential source of energy to the atmosphere is a reduction in net ocean heat uptake. Calculating changes in ocean heat uptake are challenging and not particularly revealing in this case for three reasons:

1) It is possible that the models used in simulating G1ocean-albedo were not entirely spun up to steady state. As such, any remaining imbalances could manifest as changes in ocean heat content. In principle, one could subtract off the preindustrial control value, which likely has a similar trend in ocean heat content arising from spinup. However, this would not remove the influence of nonlinearities (state dependence), so there is no way to guarantee that the signal is entirely due to the G1ocean-albedo forcing.

2) As is seen in Supplemental Table S1, not all models were able to achieve top-of-atmosphere net radiative flux balance over the course of the simulation. These small changes can lead to large changes in ocean heat content over the course of a 50-year simulation. For example, a 0.1 W m^{-2} imbalance over a 50-year period can lead to an additional 5.5 x $\times$$10^{22}$ J of energy incident at the ocean surface. As such, we are unable to properly assess the degree to which ocean heat content changes may be due to small imbalances.
3) Ocean heat content requires a depth threshold for calculation, meaning calculations of it are sensitive to redistribution of heat to/from lower depths, obscuring the signal of the forcing.

As an alternative, we calculate net energy exchange across the surface in terms of changes in radiative and turbulent fluxes. Kravitz et al. (2013b) calculated energetics changes in the entire atmospheric column. However, because we are only interested in net surface fluxes, we calculate

$$\Delta S = \Delta R_{\text{surf}} + \Delta SH + \Delta LH \quad (1)$$

where ΔR_{surf} is the change in net surface radiative flux (shortwave and longwave), ΔSH is change in sensible heat flux from the atmosphere to the surface, and ΔLH is change in latent heat flux from the atmosphere to the surface. By convention, all fluxes are positive downward unless specifically noted. Calculations of individual terms in this budget, as well as of ΔS, are provided in Supplemental Tables S8-S12. Because these calculations are performed at the surface, no advection term (e.g., LOET) is needed, and ΔS is well defined as a land or ocean average.

Figure 7 shows the all-model mean for all of the terms in Equation 4. Several clear conclusions emerge. The first is that ΔS is approximately zero globally, over land, and over ocean for nearly the entire 50-year period, after an initial rapid adjustment that resolves within a few years. With the exception of latent heat over land, this is true of all fluxes for G1ocean-albedo in Figure 7, and even latent heat flux over land reaches an approximate steady state within ten years. If ΔS indeed serves as a useful proxy for net energy flux into or out of the ocean, then these results indicate that there is no sizable contribution to atmospheric energetics by changes in ocean heat content. Moreover, even if ΔS were not zero over ocean, ocean heat content changes would still be an insufficient explanation for temperature changes due to incongruent timescales. The oceanic mixed layer operates on an approximately decadal timescale, but all transient behavior in these simulations is resolved well before ten years. The transient response is much more consistent with a land surface time scale, which is on the order of 1-3 years. As such, it seems plausible that the temperature changes over ocean in G1ocean-albedo are due to land processes rather than ocean heat content changes. This is not to say that the ocean plays no role in the observed temperature changes. Rather, given the discussions in this section and the two previous sections, the role of the ocean heat content in causing temperature changes over the ocean in G1ocean-albedo is likely small.

Mis en forme : Police :Italique
Mis en forme : Police :Italique
Mis en forme : Police :Italique
Mis en forme : Police :Italique
Mis en forme : Police :Italique
Mis en forme : Police :Italique
Mis en forme : Police :Italique
Mis en forme : Police :Italique
Mis en forme : Police :Italique
Mis en forme : Police :Italique
Mis en forme : Police :Italique
Commenté [HS19]: True, so why discuss the energy flux changes over years 11 to 50 at all? The energy flux we are after has to happen in the first year of the simulation.

The remainder of the results in Figure 7 are consistent with the applied forcing. There is a large sensible heat flux increase from the land to the atmosphere of 2.87 (-0.99 to 6.00) W m^{-2}, with a comparatively smaller sensible heat flux decrease from the ocean to the atmosphere of 1.47 (0.34 to 2.20) W m^{-2}. Over the ocean, latent heat flux from the surface to the atmosphere is 6.71 (4.95 to 7.89) W m^{-2} lower in G1ocean-albedo than in the preindustrial control simulation. These results indicate a greater shift of energy away from evaporating water and toward increasing land temperature. Large differences in flux magnitude between G1 and G1ocean-albedo can be found over land for net shortwave flux and latent heat flux, and differences in sign can be found over land for total radiative flux. These features are consistent with the applied forcing being different over land and ocean.

3.5. Hydrological cycle changes

Introducing a strong land-ocean energy and temperature gradient, as in G1ocean-albedo, will undoubtedly impact the hydrological cycle. Although the simulation is idealized, more realistic representations of MCB have shown important hydrological cycle impacts, including secondary circulation patterns that shift precipitation onto land in the tropics and extratropics (Bala et al., 2010), changes in the monsoon (Alterskjær et al., 2013), and changes in the Walker circulation (Niemeier et al., 2013). Here we evaluate the large-scale hydrological cycle changes in G1ocean-albedo, with possible applicability to other realizations of MCB.

Figure 8 shows global, land, and ocean averaged precipitation, evaporation, and precipitation minus evaporation ($P-E$) for all of the simulations considered in this manuscript; quantitative descriptions are given in Tables S13–15. The abrupt4xCO2 simulation is the only one with a distinct rapid adjustment and slow response. Over both land and ocean, G1 shows decreases in precipitation and evaporation of approximately equal magnitude, resulting in net changes in $P-E$ of 0.02 (-0.05 to 0.11) mm day^{-1} over land and -0.01 (-0.04 to 0.01) mm day^{-1} over ocean. In G1ocean-albedo, global precipitation and evaporation both decrease by approximately 0.19 (0.11 to 0.26) mm day^{-1} to yield little net change in $P-E$. However, this net small change is due to differential effects over land and ocean. Over land, precipitation remains relatively unchanged, but evaporation decreases, resulting in a net change in $P-E$ by 0.09 (-0.18 to 0.18) mm day^{-1}. Over the ocean, both precipitation and evaporation decrease, with a net negative $P-E$ of -0.06 (-0.19 to -0.01) mm day^{-1}.

Annual mean land/ocean contrasts in precipitation and evaporation changes tend to be more uniform in sign in experiment G1 (Figure 9), resulting in few large regions of change in P–E with the exception of the tropics (mostly driven by a southward shift in the intertropical convergence zone; Kravitz et al., 2013a). In G1ocean-albedo, precipitation and evaporation over the oceans are reduced in most regions, consistent with the applied forcing. Over land, the signs of precipitation and evaporation changes are regionally heterogeneous, yet the precipitation and evaporation changes are concordant, e.g., land regions with increased precipitation

Mis en forme : Police :Italique
Mis en forme : Police :Italique
Mis en forme : Police :Italique
Mis en forme : Police :Italique
Commenté [HS20]: Actually, averaged over long time scales, global P-E change should be zero. Otherwise we would change the water content of the atmosphere.
Mis en forme : Police :Italique
Mis en forme : Police :Italique
Mis en forme : Police :Italique
Mis en forme : Police :Italique
Mis en forme : Police :Italique
Mis en forme : Police :Italique

also generally show increased evaporation. The net P–E map is highly heterogeneous, but in general, tropical land areas are projected to have more available moisture (as measured by P–E) under G1ocean-albedo, and midlatitude land areas are projected to have less. The implications of these changes for people and ecosystems ~~is~~ are an important area of future research.

4. Discussion and Conclusions

The results presented here indicate that even though experiments G1 and G1ocean-albedo both achieve approximate net top-of-atmosphere radiative flux balance, the climate system responses differ dramatically between the two experiments. The idea that global energy balance can still result in local changes is perhaps not surprising, as feedbacks operate locally (Armour et al., 2013). These different climate responses for the same forcing are effectively an illustration of different efficacies (Hansen et al., 2005). Even in the absence of slow responses, forcings with different efficacies can cause different climate system changes (Kravitz et al., 2015). G1ocean-albedo serves as an excellent reminder not to conflate small net top-of-atmosphere radiative flux imbalance with small temperature change; a clear relationship between those two quantities is not guaranteed.

Relatedly, the results obtained for G1ocean-albedo were to some extent by design. The objective of G1ocean-albedo was to achieve net top-of-atmosphere radiative flux balance, which resulted in warming. Conceivably, one could define an objective of no global temperature change, implying a net negative radiative flux at the top-of-atmosphere. It is unclear whether, unlike G1ocean-albedo, that alternate approach would result in transient behavior that lasts longer than a few years. Such an experiment could be accomplished using feedback methods that have been introduced to geoengineering research in recent years (e.g., MacMartin et al., 2014; Kravitz et al., 2016).

The results presented here have several features that were not necessarily expected from the outset. Kravitz et al. (2013c) found that determining whether the climate system was in balance took up to 30 years of simulation. However, once that balance is achieved, the climate does not change appreciably after the initial rapid adjustment. Potential future work could investigate these results, shedding light on timescales of climate response and potential thresholds, e.g., how large does the energy imbalance need to be to trigger slower adjustments?

Related to this issue of different timescales of adjustment is the traditional separation of climate response into rapid adjustment and slow response components (e.g., Andrews and Forster, 2010; Sherwood et al., 2015). The rapid adjustment is often defined as the climate response unassociated with global mean temperature change, and the slow response describes a transient temperature change with a large component due to climate system feedbacks. The results from G1ocean-albedo, like those of G1 (Kravitz et al., 2013b), show an initial rapid change and no appreciable slower change. However, in G1ocean-albedo, that initial change

Mis en forme : Police :Italique

Mis en forme : Police :Italique

Mis en forme : Police :Italique

Mis en forme : Police :Italique

Commenté [HS21]: I think we are confusing local and global responses, here. Hansen's efficacies are global if I remember correctly.

Commenté [o22]: Or no global land temperature change

is associated with a temperature increase, which in principle should excite ~~a~~ slow ~~adjustment through~~ climate system feedbacks. These results are somewhat inconsistent with the traditional definitions of rapid adjustment and slow response. Additionally, this sustained temperature increase is to some extent decoupled from net energy imbalances in the climate system, as ΔR_{TOA} and ΔS (Equation 4) are both approximately zero. Reconciling all of these features suggests a potentially rich research topic focused on understanding the relationships between radiative flux changes, temperature changes, and the circumstances under which climate feedbacks are excited.

G1ocean-albedo may be more apposite to the impact of geoengineering via "ocean microbubbles," whereby surfactants are added to the ocean surface, promoting the formation of microscopic, highly reflective bubbles (Seitz, 2011; Robock, 2011; Gabriel et al., 2017). An area of investigation we did not undertake, yet one that repeatedly emerges in discussions of microbubbles, is the effects on the ocean mixed layer. By reflecting more solar radiation, microbubbles have the potential to inhibit vertical mixing and available light in the euphotic zone, which could have profound effects on marine biota. This implies that another useful future area of investigation for the G1ocean-albedo simulation is an analysis of the marine carbon cycle (Robock, 2011; Gabriel et al., 2017).

There are numerous potential areas of research prompted by this study. The stark land/ocean contrast in warming has potential implications for ocean circulation patterns, including the meridional overturning circulation and Western boundary ocean currents, with consequent implications for marine ecosystems. This contrast also has implications for the terrestrial biosphere, including ecosystem services and the land and ocean carbon cycles. Although we did not evaluate seasonal changes in this manuscript, such investigations could prove fruitful for more detailed assessments of variability, such as monsoon precipitation, extreme events, and sea ice extent.

Despite being informative for MCB, there are limits as to the applicability of this idealized approach. There are important differences in boundary layer stability changes from surface albedo increases versus marine stratocumulus cloud top brightening. Also, it appears impossible for marine cloud brightening to be conducted over all ocean regions and with a sufficient magnitude to offset the radiative forcing from a quadrupling of the CO_2 concentration. The purpose of this manuscript is to describe the broad features of change under a uniform ocean albedo increase, and some of these changes are likely to be present with more realistic scenarios of marine cloud brightening. We anticipate that future research can more deeply explore the applicability of this simulation to marine cloud brightening.

Acknowledgments. We thank Jón Egill Kristjánsson, who tragically passed away, for invaluable comments on an earlier version of this manuscript. We acknowledge the World Climate Research Programme's Working Group on Coupled Modelling,

Commenté [o23]: Ummmh, not sure I understand here

Commenté [o24]: Temperature, depth, radiation, …

which is responsible for CMIP, and we thank the climate modeling groups for producing and making available their model output. For CMIP the U.S. Department of Energy's Program for Climate Model Diagnosis and Intercomparison provides coordinating support and led development of software infrastructure in partnership with the Global Organization for Earth System Science Portals. We thank all participants of the Geoengineering Model Intercomparison Project and their model development teams, CLIVAR/WCRP Working Group on Coupled Modeling for endorsing GeoMIP, and the scientists managing the Earth System Grid data nodes who have assisted with making GeoMIP output available. The Pacific Northwest National Laboratory is operated for the U.S. Department of Energy by Battelle Memorial Institute under contract DE-AC05-76RL01830. Simulations performed by Ben Kravitz were supported by the NASA High-End Computing (HEC) Program through the NASA Center for Climate Simulation (NCCS) at Goddard Space Flight Center. Alan Robock is supported by NSF grants AGS-1157525 and GEO-1240507 AGS-1617844. Andy Jones was supported by the Joint UK DECC/Defra Met Office Hadley Centre Climate Programme (GA01101). Olivier Boucher acknowledges HPC resources from CCRT under the allocation 2015-t2012012201 made by GENCI (Grand Equipement National de Calcul Intensif). This research was supported under the Australian Research Council's Special Research Initiative for the Antarctic Gateway Partnership (project SR140300001).

554 **References**
555
556 Alterskjær, K., J. E. Kristjansson, and Ø. Seland (2012), Sensitivity to deliberate sea
557 salt seeding of marine clouds – observations and model simulations, *Atmos.*
558 *Chem. Phys.*, *12*, 2795-2807 doi:10.5194/acp-12-2795-2012.

559 Alterskjær, K., J. E. Kristjánsson, O. Boucher, H. Muri, U. Niemeier, H. Schmidt, M.
560 Schulz, and C. Timmreck (2013), Sea-salt injections into the low-latitude marine
561 boundary layer: The transient response in three Earth system models, *J. Geophys.*
562 *Res. Atmos., 118*, 12,195–12,206, doi:10.1002/2013JD020432.

563 Andrews, T., and P. M. Forster (2010), The transient response of global-mean
564 precipitation to increasing carbon dioxide levels, *Environ. Res. Lett.*, *5*, 025212,
565 doi:10.1088/1748-9326/5/2/025212.

566 Armour, K. C., C. M. Bitz, and G. H. Roe (2013), Time-varying climate sensitivity from
567 regional feedbacks, *J. Climate, 26*, 4518–4534, doi:10.1175/JCLI-D-12-00544.1.

568 Arora, V. K., J. F. Scinocca, G. J. Boer, J. R. Christian, K. L. Denman, G. M. Flato, V. V.
569 Kharin, W. G. Lee, and W. J. Merryfield (2011), Carbon emission limits required
570 to satisfy future representative concentration pathways of greenhouse gases,
571 *Geophys. Res. Lett.*, *38*, L05805, doi:10.1029/2010GL046270.

572 Bala, G., K. Caldeira, and R. Nemani (2010), Fast versus slow response in climate
573 change: Implications for the global hydrological cycle, *Clim. Dyn.*, *35*, 423-434,
574 doi:10.1007/s00382-009-0583-y.

575 Collins, W. J., N. Bellouin, M. Doutriaux-Boucher, N. Gedney, P. Halloran, T. Hinton, J.
576 Hughes, C. D. Jones, M. Joshi, S. Liddicoat, G. Martin, F. O'Connor, J. Rae, C. Senior,
577 S. Sitch, I. Totterdell, A. Wiltshire, and S. Woodward (2011), Development and
578 evaluation of an Earth-System model—HadGEM2, *Geosci. Model Dev.*, *4*, 1051-
579 1075, doi:10.5194/gmd-4-1051-2011.

580 Crook, J. A., L. S. Jackson, S. M. Osprey, and P. M. Forster (2015), A comparison of
581 temperature and precipitation responses to different Earth radiation
582 management geoengineering schemes, *J. Geophys. Res., 120*, 9352-9373,
583 doi:10.1002/2015JD023269.

584 Curry, C. L., J. Sillmann, D. Bronaugh, K. Alterskjær, J. N. S. Cole, B. Kravitz., J. E.
585 Kristjánsson, H. Muri, U. Niemeier, A. Robock, and S. Tilmes (2014), A multi-
586 model examination of climate extremes in an idealized geoengineering
587 experiment, *Journal of Geophysical Research*, *119*, 3900-3923,
588 doi:10.1002/2013JD020648.

589 Dufresne, J.-L., M.-A. Foujols, S. Denvil, A. Caubel, O. Marti, O. Aumont, Y. Balkanski, S.
590 Bekki, H. Bellenger, R. Benshila, S. Bony, L. Bopp, P. Braconnot, P. Brockmann, P.
591 Cadule, F. Cheruy, F. Codron, A. Cozic, D. Cugnet, N. de Noblet, J.-P. Duvel, C. Ethé,
592 L. Fairhead, T. Fichefet, S. Flavoni, P. Friedlingstein, J.-Y. Grandpeix, L. Guez, E.
593 Guilyardi, D. Hauglustaine, F. Hourdin, A. Idelkadi, J. Ghattas, S. Joussaume, M.
594 Kageyama, G. Krinner, S. Labetoulle, A. Lahellec, M.-P. Lefebvre, F. Lefevre, C.
595 Levy, Z. X. Li, J. Lloyd, F. Lott, G. Madec, M. Mancip, M. Marchand, S. Masson, Y.

Mis en forme : Espace Après : 6 pt

Meurdesoif, J. Mignot, I. Musat, S. Parouty, J. Polcher, C. Rio, M. Schulz, D. Swingedouw, S. Szopa, C. Talandier, P. Terray, N. Viovy, and N. Vuichard (2013), Climate change projections using the IPSL-CM5 Earth System Model: From CMIP3 to CMIP5, *Clim. Dynam.*, *40*, 2123-2165 doi:10.1007/s00382-012-1636-1.

Gabriel, C. J., A. Robock, L. Xia, B. Zambri, and B. Kravitz (201), The G4Foam experiment: Global climate impacts of regional ocean albedo modification, *Atmos. Chem. Phys., 17*, 595-613, doi:10.5194/acp-17-595-2017.

Geoffroy, O., D. Saint-Martin, and A. Voldoire (2015), Land-sea warming contrast: the role of the horizontal energy transport, *Clim. Dynam.*, *45*, 3493-3511, doi:10.1007/s00382-015-2552-y.

Giorgetta, M. A., Johann Jungclaus, Christian H. Reick, Stephanie Legutke, Jürgen Bader, Michael Böttinger, Victor Brovkin, Traute Crueger, Monika Esch, Kerstin Fieg, Ksenia Glushak, Veronika Gayler, Helmuth Haak, Heinz-Dieter Hollweg, Tatiana Ilyina, Stefan Kinne, Luis Kornblueh, Daniela Matei, Thorsten Mauritsen, Uwe Mikolajewicz, Wolfgang Mueller, Dirk Notz, Felix Pithan, Thomas Raddatz, Sebastian Rast, Rene Redler, Erich Roeckner, Hauke Schmidt, Reiner Schnur, Joachim Segschneider, Katharina D. Six, Martina Stockhause, Claudia Timmreck, Jörg Wegner, Heinrich Widmann, Karl-H. Wieners, Martin Claussen, Jochem Marotzke, and Bjorn Stevens (2013), Climate and carbon cycle changes from 1850 to 2100 in MPI-ESM simulations for the Coupled Model Intercomparison Project Phase 5, *J. Adv. Model. Earth Syst.*, *5*, 572-597, doi:10.1002/jame.20038.

Glienke, S., P. J. Irvine, and M. G. Lawrence (2015), The impact of geoengineering on vegetation in experiment G1 of the GeoMIP, *Journal of Geophysical Research*, *120*, 10196-10213, doi:10.1002/2015JD024202.

Gregory, J. M., W. J. Ingram, M. A. Palmer, G. S. Jones, P. A. Stott, R. B. Thorpe, J. A. Lowe, T. C. Johns, and K. D. Williams (2004), A new method for diagnosing radiative forcing and climate sensitivity, *Geophys. Res. Lett., 31*, L03205, doi:10.1029/2003GL018747.

Hansen, J., M. Sato, R. Ruedy, L. Nazarenko, A. Lacis, G. A. Schmidt, G. Russell, I. Aleinov, M. Bauer, S. Bauer, N. Bell, B. Cairns, V. Canuto, M. Chandler, Y. Cheng, A. Del Genio, G. Faluvegi, E. Fleming, A. Friend, T. Hall, C. Jackman, M. Kelley, N. Kiang, D. Koch, J. Lean, J. Lerner, K. Lo, S. Menon, R. Miller, P. Minnis, T. Novakov, V. Oinas, Ja. Perlwitz, Ju. Perlwitz, D. Rind, A. Romanou, D. Shindell, P. Stone, S. Sun, N. Tausnev, D. Thresher, B. Wielicki, T. Wong, M. Yao, and S. Zhang (2005), Efficacy of climate forcings, *J. Geophys. Res., 110*, D18104, doi:10.1029/2005JD005776.

Hazeleger, W., X. Wang, C. Severijns, S. Ştefănescu, R. Bintanja, A. Sterl, K. Wyser, T. Semmler, S. Yang, B. van den Hurk, T. van Noije, E. van der Linden, and K. van der Wiel (2011), EC-Earth V2.2: Description and validation of a new seamless Earth system prediction model, *Clim. Dynam., 39*(11), 2611-2629, doi:10.1007/s00382-011-1228-5.

Mis en forme : Police :Italique

Mis en forme : Police :Italique

637 Hurrell, J. W., M. M. Holland, P. R. Gent, S. Ghan, J. E. Kay, P. J. Kushner, J.-F.
638 Lamarque, W. G. Large, D. Lawrence, K. Lindsay, W. H. Lipscomb, M. C. Long,
639 N. Mahowald, D. R. Marsh, R. B. Neale, P. Rasch, S. Vavrus, M. Vertenstein, D.
640 Bader, W. D. Collins, J. J. Hack, J. Kiehl, and S. Marshall (2013), The Community
641 Earth System Model: A framework for collaborative research, *Bull. Amer. Meteor.*
642 *Soc.*, *94*, 1339-1360, doi:10.1175/BAMS-D-12-00121.1.

643 Ji, D., L. Wang, J. Feng, Q. Wu, H. Cheng, Q. Zhang, J. Yang, W. Dong, Y. Dai, D. Gong, R.-
644 H. Zhang, X. Wang, J. Liu, J. C. Moore, D. Chen, and M. Zhou (2014), Description
645 and basic evaluation of Beijing Normal University Earth System Model (BNU-
646 ESM) version 1, *Geosci. Model. Dev.*, *7*, 2039-2064, 10.5194/gmd-7-2039-2014.

647 Kalidindi, S., G. Bala, A. Modak, and K. Caldeira (2015), Modeling of solar radiation
648 management: a comparison of simulations using reduced solar constant and
649 stratospheric sulphate aerosols, *Clim. Dynam.*, *44*, 2909-2925,
650 doi:10.1007/s00382-014-2240-3.

651 Kravitz, B., A. Robock, O. Boucher, H. Schmidt, K. E. Taylor, G. Stenchikov, and M.
652 Schulz (2011), The Geoengineering Model Intercomparison Project (GeoMIP),
653 *Atm. Sci. Lett.*, *12,* 162-167, doi:10.1002/asl.316.

654 Kravitz, B., K. Caldeira, O. Boucher, A. Robock, P. J. Rasch, K. Alterskjær, D. Bou
655 Karam, J. N. S. Cole, C. L. Curry, J. M. Haywood, P. J. Irvine, D. Ji, A. Jones, J. E.
656 Kristjánsson, D. J. Lunt, J. Moore, U. Niemeier, H. Schmidt, M. Schulz, B. Singh, S.
657 Tilmes, S. Watanabe, S. Yang, and J.-H. Yoon (2013a), Climate model response
658 from the Geoengineering Model Intercomparison Project (GeoMIP), *Journal of*
659 *Geophysical Research*, *118*(15), 8320-8332, doi:10.1002/jgrd.50646.

660 Kravitz, B., P. J. Rasch, P. M. Forster, T. Andrews, J. N. S. Cole, P. J. Irvine, D. Ji, J. E.
661 Kristjánsson, J. C. Moore, H. Muri, U. Niemeier, A. Robock, B. Singh, S. Tilmes, S.
662 Watanabe, and J.-H. Yoon (2013b), An energetic perspective on hydrological
663 cycle changes in the Geoengineering Model Intercomparison Project (GeoMIP),
664 *Journal of Geophysical Research*, *118*, 13087-13102, doi:10.1002/2013JD020502.

665 Kravitz, B., P. M. Forster, A. Jones, A. Robock, K. Alterskjær, O. Boucher, A. K. L.
666 Jenkins, H. Korhonen, J. E. Kristjánsson, H. Muri, U. Niemeier, A.-I. Partanen, P. J.
667 Rasch, H. Wang, and S. Watanabe (2013c), Sea spray geoengineering
668 experiments in the Geoengineering Model Intercomparison Project (GeoMIP):
669 Experimental design and preliminary results, *Journal of Geophysical Research*,
670 *118*(19), 11175-11186, doi:10.1002/jgrd.50856.

671 Kravitz, B., D. G. MacMartin, P. J. Rasch, and A. J. Jarvis (2015), A new method of
672 comparing forcing agents in climate models, *J. Climate, 28*, 8203–8218,
673 doi:10.1175/JCLI-D-14-00663.1.

674 Kravitz, B., D. G. MacMartin, H. Wang, and P. J. Rasch (2016), Geoengineering as a
675 design problem, *Earth System Dynamics, 7*, 469-497, doi:10.5194/esd-7-469-
676 2016.

677 Latham, J. (1990), Control of global warming? *Nature*, *347*, 339–340.

MacMartin, D.G., B. Kravitz, D. W. Keith, and A. Jarvis (2014), Dynamics of the coupled human-climate system resulting from closed-loop control of solar geoengineering, *Clim. Dynam., 43*, 243-258, doi:10.1007/s00382-013-1822-9.

Mitchell, D. L. and W. Finnegan (2009), Modification of cirrus clouds to reduce global warming, *Environ. Res. Lett.*, *4*, 045102, doi:10.1088/1748-9326/4/4/045102.

Moore, J. C., A. Rinke, X. Yu, D. Ji, X. Cui, Y. Li, K. Alterskjær, J. E. Kristjánsson, O. Boucher, N. Huneeus, B. Kravitz, A. Robock, U. Niemeier, H. Schmidt, M. Schulz, S. Tilmes, and S. Watanabe (2014), Arctic sea ice and atmospheric circulation under the GeoMIP G1 scenario, *J. Geophys. Res., 119*, 567-583, doi:10.1002/2013JD021060.

NAS (2015a), Climate Intervention: Carbon Dioxide Removal and Reliable Sequestration, National Research Council, The National Academies Press, Washington, DC, 141 pp.

NAS (2015b), Climate Intervention: Reflecting Sunlight to Cool Earth, National Research Council, The National Academies Press, Washington, DC, 235 pp.

Niemeier, U., H. Schmidt, K. Alterskjær, and J. E. Kristjánsson (2013), Solar irradiance reduction via climate engineering--impact of different techniques on the energy balance and the hydrological cycle, *Journal of Geophysical Research*, *118*, 11905-11917, doi:10.1002/2013JD020445.

Oreopoulos, L. and S. Platnick (2008), Radiative susceptibility of cloudy atmospheres to droplet number perturbations: 2. Global analysis from MODIS, *J. Geophys. Res.*, *113*, D14S21, doi:10.1029/2007JD009655.

Pandey, D. K., R. B. Lee III, and J. Paden (1995), Effects of atmospheric emissivity on clear sky temperatures, *Atmos. Environ.*, *29*, 2201-2204, doi:10.1016/1352-2310(94)00243-E.

Phipps, S. J., L. D. Rotstayn, H. B. Gordon, J. L. Roberts, A. C. Hirst, and W. F. Budd (2011), The CSIRO Mk3L climate system model version 1.0 – Part 1: Description and evaluation, *Geosci. Model Dev.*, *4*, 483-509, 10.5194/gmd-4-483-2011.

Robock, Alan A. (2011), Bubble, bubble, toil and trouble. An editorial comment. *Climatic Change*, *105*, 383-385, doi:10.1007/s10584-010-0017-1.

Schmidt, H., K. Alterskjær, D. Bou Karam, O. Boucher, A. Jones, J. E. Kristjánsson, U. Niemeier, M. Schulz, A. Aaheim, F. Benduhn, M. Lawrence, and C. Timmreck (2012), Solar irradiance reduction to counteract radiative forcing from a quadrupling of CO_2: Climate responses simulated by four Earth system models, *Earth System Dynamics, 3*, 63-78, doi:10.5194/esd-3-63-2012.

Schmidt, Gavin A., Max Kelley, Larissa Nazarenko, Reto Ruedy, Gary L. Russell, Igor Aleinov, Mike Bauer, Susanne E. Bauer, Maharaj K. Bhat, Rainer Bleck, Vittorio Canuto, Yong-Hua Chen, Ye Cheng, Thomas L. Clune, Anthony Del Genio, Rosalinda de Fainchtein, Greg Faluvegi, James E. Hansen, Richard J. Healy, Nancy Y. Kiang, Dorothy Koch, Andy A. Lacis, Allegra N. LeGrande, Jean Lerner, Ken K. Lo, Elaine E. Matthews, Surabi Menon, Ron L. Miller, Valdar Oinas, Amidu O.

719 Oloso, Jan P. Perlwitz, Michael J. Puma, William M. Putman, David Rind, Anastasia
720 Romanou, Makiko Sato, Drew T. Shindell, Shan Sun, Rahman A. Syed, Nick
721 Tausnev, Kostas Tsigaridis, Nadine Unger, Apostolos Voulgarakis, Mao-Sung Yao,
722 and Jinlun Zhang (2014), Configuration and assessment of the GISS ModelE2
723 contributions to the CMIP5 archive, *J. Adv. Model. Earth Syst., 6*, 141–184,
724 doi:10.1002/2013MS000265.

725 Seitz, R. (2011), Bright water: hydrosols, water conservation and climate change,
726 *Climatic Change*, *105*, 365-381, doi:10.1007/s10584-010-9965-8.

727 Shepherd, J., K. Caldeira, P. Cox, J. Haigh, K. Keith, B. Launder, G. Mace, G. MacKerron,
728 J. Pyle, S. Rayner, C. Redgwell, and A. Watson (2009), Geoengineering the climate:
729 Science, governance, and uncertainty, Royal Society Policy document 10/09, 82
730 pp.

731 Sherwood, S. C., S. Bony, O. Boucher, C. Bretherton, P. M. Forster, J. M. Gregory, and B.
732 Stevens (2015), Adjustments in the forcing-feedback framework for
733 understanding climate change, *Bull. Amer. Meteor. Soc., 96*, 217–228,
734 doi:10.1175/BAMS-D-13-00167.1.

735 Stephens, G. L., D. O'Brien, P. J. Webster, P. Pilewski, S. Kato, and J.-L. Li (2015), The
736 albedo of Earth, *Rev. Geophys.*, *53*, 141-163, doi:10.1002/2014RG000449.

737 Taylor, K. E., R. J. Stouffer, and G. A. Meehl (2012), An overview of CMIP5 and the
738 experiment design, *Bull. Amer. Meteor. Soc.*, *93*, 485-498, doi:10.1175/BAMS-D-
739 11-00094.1.

740 Tilmes, S., J. Fasullo, J.-F. Lamarque, D. R. Marsch, M. Mills, K. Alterskjær, O. Boucher,
741 J. N. S. Cole, C. L. Curry, J. M. Haywood, P. J. Irvine, D. Ji, A. Jones, D. B. Karam, B.
742 Kravitz, J. E. Kristjánsson, J. C. Moore, H. O. Muri, U. Niemeier, P. J. Rasch, A.
743 Robock, H. Schmidt, M. Schulz, B. Singh, S. Watanabe, S. Yang, and J.-H. Yoon
744 (2013), The hydrological impact of geoengineering in the Geoengineering Model
745 Intercomparison Project (GeoMIP), *Journal of Geophysical Research*, *118*(19),
746 11036-11058, doi:10.1002/jgrd.50868.

747 Watanabe, S., T. Hajima, K. Sudo, T. Nagashima, T. Takemura, H. Okajima, T. Nozawa,
748 H. Kawase, M. Abe, T. Yokohata, T. Ise, H. Sato, E. Kato, K. Takata, S. Emori, and M.
749 Kawamiya (2011), MIROC-ESM 2010: Model description and basic results of
750 CMIP5-20c3m experiments, *Geosci. Mod. Dev.*, *4*, 845-872, doi:10.5194/gmd-4-
751 845-2011.

752

Table 1. Description of the 11 models participating in this study. Column 1 gives the standard model name. Columns 2 and 3 give the default and perturbed surface ocean albedo, defined as upward shortwave divided by downward shortwave radiative flux at the surface, both averaged over ocean regions and over years 11-50 of simulation. Column 4 is the ratio of column 3 to column 2. Column 5 gives the factor (δ) by which the model default ocean albedo was multiplied to achieve negligible top-of-atmosphere radiative flux changes under an abrupt4xCO2 simulation (described in greater detail by Kravitz et al., 2015). The differences between Ratio and δ are caused by cloud responses. Column 6 gives a relevant reference for each model. All values are rounded to two decimal places.

Model name	piControl ocean albedo	G1OA ocean albedo	Ratio	δ	Reference
BNU-ESM	0.12	0.17	1.48	2.50	Ji et al. (2014)
CanESM2	0.11	0.19	1.73	2.45	Arora et al. (2011)
CESM-CAM5.1-FV	0.10	0.18	1.79	2.70	Hurrell et al. (2013)
CSIRO-Mk3L-1.2	0.12	0.19	1.61	2.04	Phipps et al. (2011)
EC-Earth	0.10	0.19	1.97	3.17	Hazeleger et al. (2011)
GISS-E2-R	0.08	0.16	1.95	2.53	Schmidt et al. (2014)
HadGEM2-ES	0.10	0.17	1.83	2.44	Collins et al. (2011)
IPSL-CM5A-LR	0.10	0.17	1.78	2.33	Dufresne et al. (2013)
MIROC-ESM	0.10	0.20	2.00	3.10	Watanabe et al. (2011)
MPI-ESM-LR	0.09	0.23	2.40	5.42	Giorgetta et al. (2013)
NorESM1-M	0.09	0.18	1.95	2.77	Alterskjær et al. (2012)

Commenté [HS25]: The SOM has many tables. I'm not sure if we need all of them, but if we want to provide detailed information on the individual models I would suggest to also put average changes in T, P , and P-E for global, land and ocean.

Table 2. Parameters used in different runs with the simple one-dimensional radiative equilibrium model (Section 3.2). Surface ΔT ~~(in Kkelvin)~~ for the Global runs are with respect to Control (Global) and for the Ocean runs are with respect to Control (Ocean).

Run	Emissivity in each model layer	Surface albedo	Surface ΔT (K)
Control (Global)	0.80	0.3	0
abrupt4xCO2 (Global)	0.8265	0.3	4.4189
Albedo increase (Global)	0.80	0.3395	-4.0165
G1ocean-albedo (Global)	0.8265	0.3395	0.3674
Control (Ocean)	0.80	0.1	0
abrupt4xCO2 (Ocean)	0.8265	0.1	4.7251
Albedo increase (Ocean)	0.80	0.1863	-7.3806
G1ocean-albedo (Ocean)	0.8265	0.1863	-2.7730

Mis en forme : Centré
Tableau mis en forme
Mis en forme : Centré
Mis en forme : Centré
Mis en forme : Centré
Mis en forme : Centré
Mis en forme : Centré
Mis en forme : Centré
Mis en forme : Centré
Mis en forme : Centré

Table 3. Feedback parameters (Section 3.3; units W m^{-2}) for global, land, and ocean averages, calculated via the "Gregory method" (Gregory et al., 2004), where annual mean top-of-atmosphere net radiative flux is regressed against annual mean temperature.

	λ_g	λ_ℓ	λ_o
BNU-ESM	0.9019	0.7181	0.9838
CanESM2	1.1539	1.1898	1.1260
CESM-CAM5.1-FV	1.1435	1.0357	1.1591
CSIRO-Mk3L-1.2	1.0192	0.9300	0.8034
EC-Earth	1.2124	1.1937	1.3155
GISS-E2-R	2.2440	1.9751	2.3560
HadGEM2-ES	0.8411	0.8363	0.8351
IPSL-CM5A-LR	0.8367	1.2891	0.5894
MIROC-ESM	1.0378	0.8736	1.0383
MPI-ESM-LR	1.3701	1.0573	1.3986
NorESM1-M	1.4285	1.8828	1.6063

Commenté [HS26]: We should reduce the number of digits in many of the tables (in particular in the SOM) in order to facilitate reading.

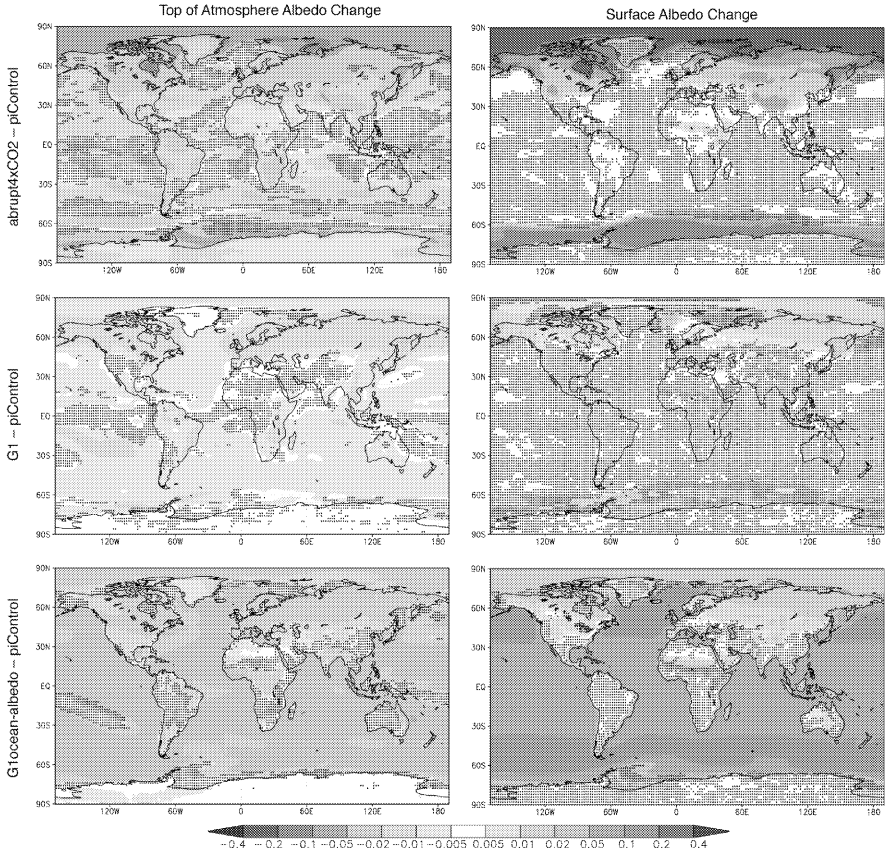

Figure 1. Top-of-atmosphere (TOA) and surface albedo differences (relative to piControl) for the abrupt4xCO2, G1, and G1ocean-albedo experiments. Albedo here is calculated as the ratio of upwelling to downwelling all-sky shortwave radiative flux, either at TOA or at the surface. Values are averages over years 11-50 of simulation. Stippling indicates where fewer than 8 out of 11 models agree on the sign of the response.

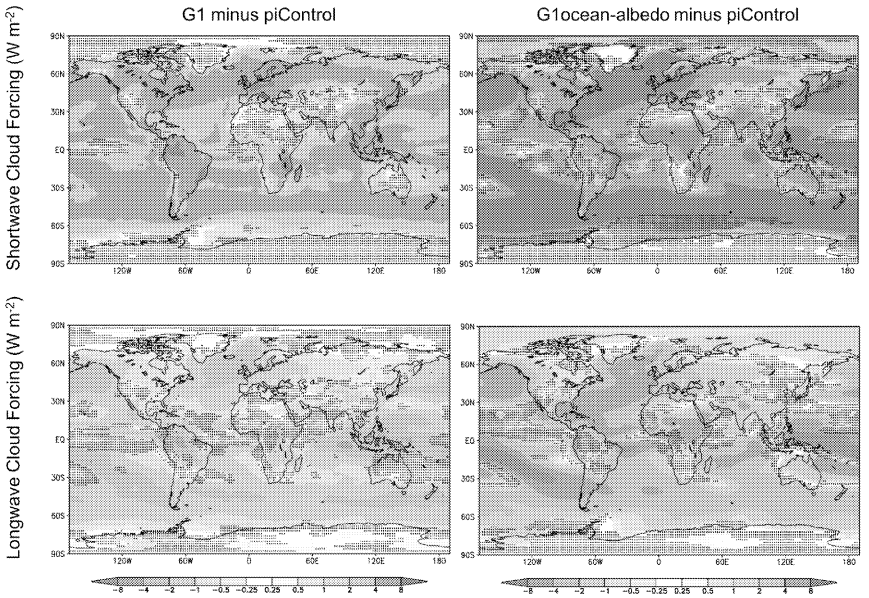

Figure 2. Shortwave (top) and longwave (bottom) cloud forcing changes due to the G1 (left) and G1ocean-albedo perturbations. Cloud forcing is defined as all-sky minus clear-sky radiative flux at the top of the atmosphere.

Commenté [HS27]: What means stippling in this figure?

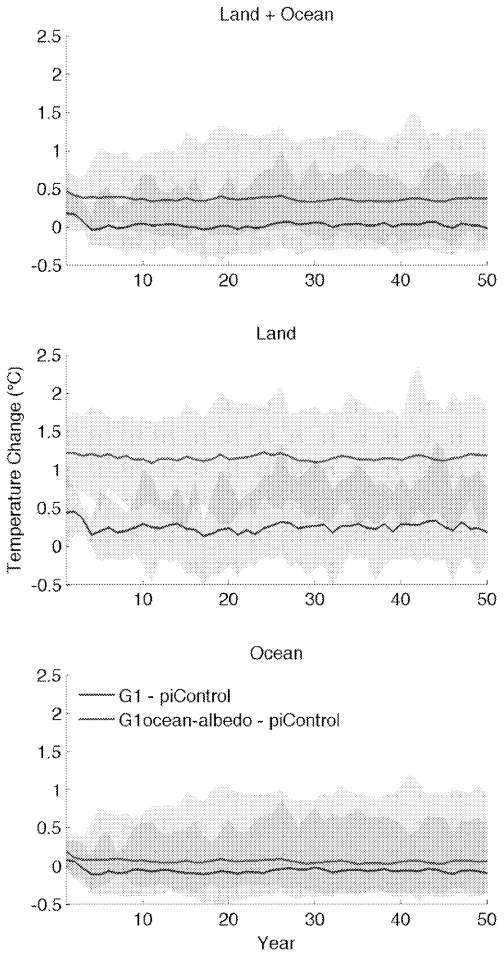

Figure 3. Global (top), land (middle), and ocean (bottom) average temperature change for the G1 (blue) and G1ocean-albedo (red) simulations. Lines show the all-model ensemble mean, and shading shows model spread (smallest to largest values).

Commenté [o28]: You have a mix of °C and K for the T change

Commenté [AR29R28]: Yes, make it all K. Formally, temperature change anyway should be C°.

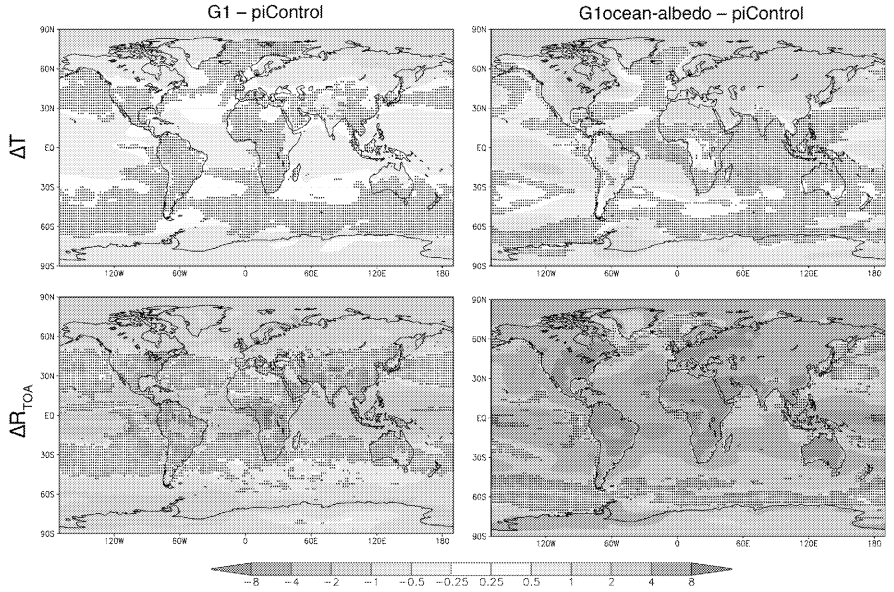

796
797
798 **Figure 4.** Surface air temperature (top row; K) and TOA net radiative flux (bottom
799 row; W m^{-2}) changes for experiments G1 (left) and G1ocean-albedo (right). Values
800 are averages over years 11-50 of simulation. Stippling indicates where fewer than 8
801 out of 11 models agree on the sign of the response.

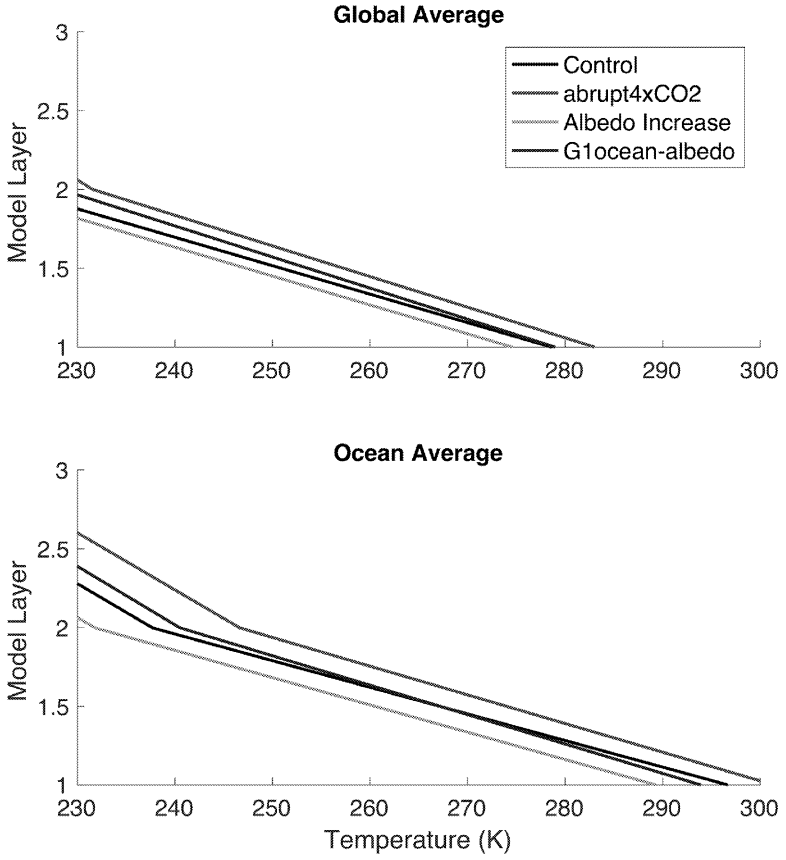

Figure 5. Temperature results for calculations with a one-dimensional radiative equilibrium model with 15 vertical layers (only the bottom three layers are shown). Specifications for all of the simulations are provided in Table 2.

Commenté [o30]: ??

Commenté [AR31R30]: Is layer 1 the surface or the lowest atmospheric model layer?

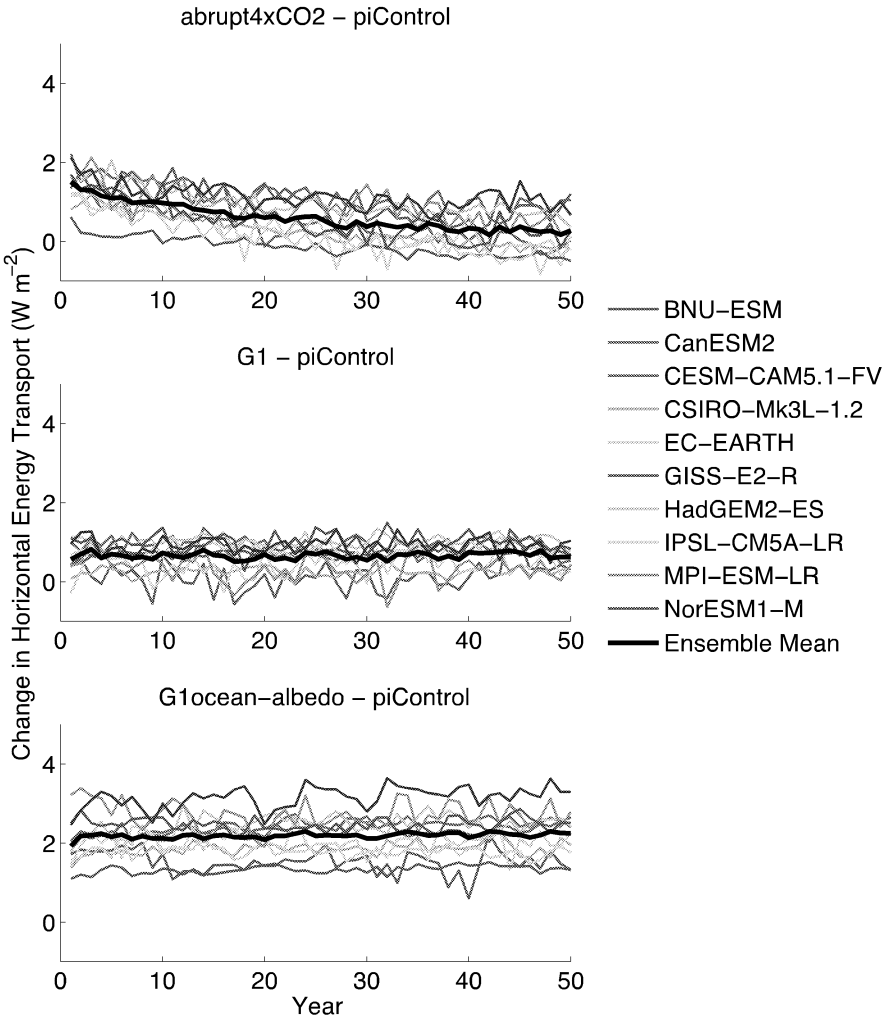

Figure 6. Annual mean change in land-ocean energy transport (Section 3.4; W m^{-2}) from piControl. See Equation 3 for a formal definition.

Commenté [HS32]: Fig. 6 is not referred to in the manuscript.

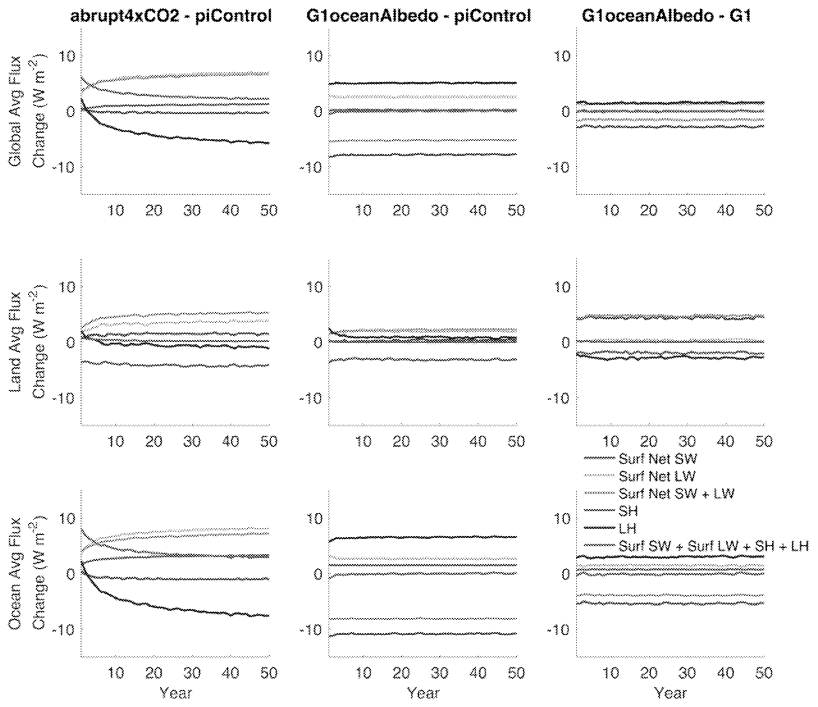

Commenté [AR33]: Make the legend with the same notation as in Eq. (1). Should all these terms start with Δ? Is the last term actually ΔS?

Figure 7. Annual mean time series of all-model mean surface fluxes (terms in Equation 4) for global averages (top), land averages (middle), and ocean averages (bottom). All fluxes are positive in the downward direction.

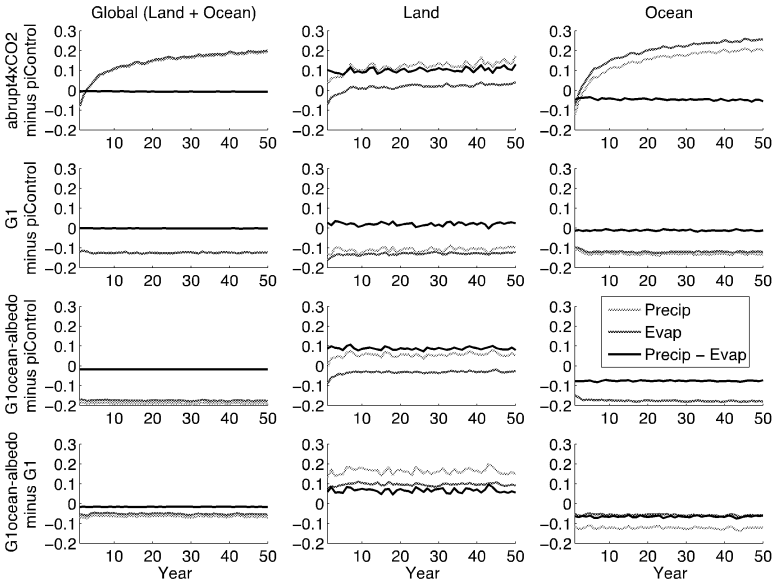

Figure 8. Annual mean time series of hydrological cycle changes (all in mm day^{-1}). Green lines show precipitation changes, red lines show evaporation changes, and black lines show precipitation minus evaporation. When no green line is evident, it is obscured by either the red or black lines.

Commenté [HS34]: In the case of ocean precip in G1OA-picontrol the green line should be out of the range.

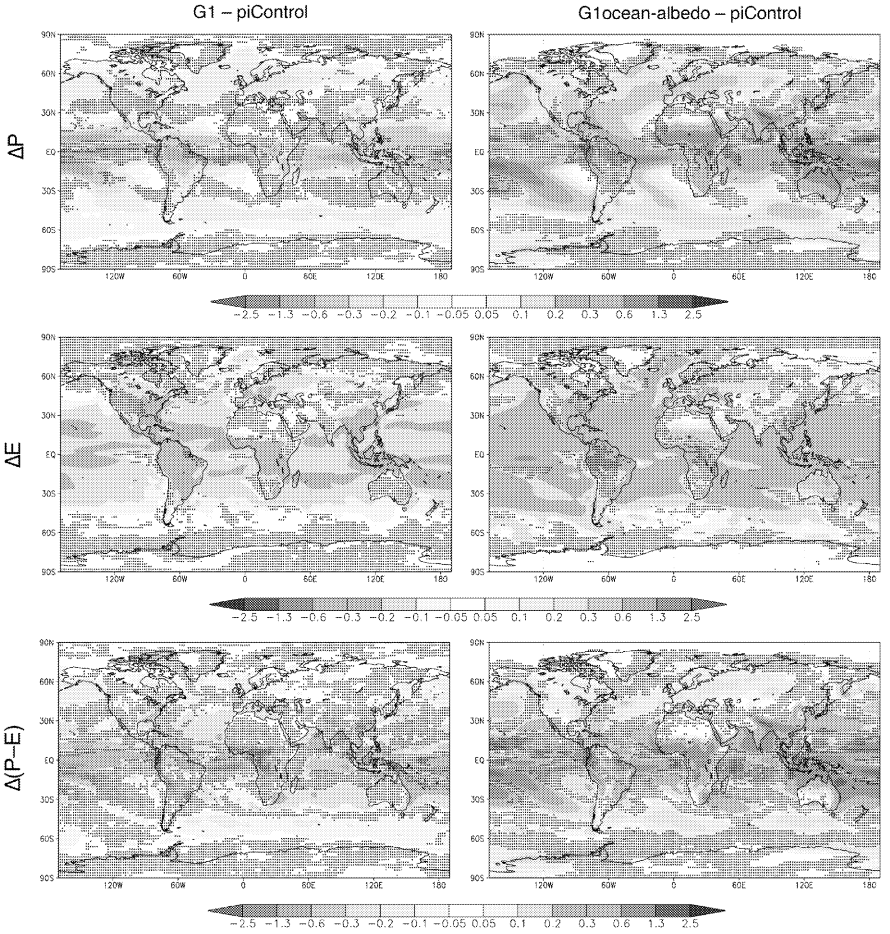

822
823
824 **Figure 9.** Precipitation (top row), evaporation (middle row), and precipitation
825 minus evaporation (bottom row) changes (all panels have units mm day^{-1}) for
826 experiments G1 and G1ocean-albedo. Values are averages over years 11-50 of
827 simulation. Stippling indicates where fewer than 8 out of 11 models agree on the
828 sign of the response.
829

The climate effects of increasing ocean albedo: An idealized representation of solar geoengineering

Ben Kravitz,[1*] Philip J. Rasch,[1] Hailong Wang,[1] Alan Robock,[2] Corey Gabriel,[3] Olivier Boucher,[4] Jason N. S. Cole,[5] Jim Haywood,[6,7] Duoying Ji,[8] Andy Jones,[6] Andrew Lenton,[9] John C. Moore,[8] Helene Muri,[10] Ulrike Niemeier,[11] Steven Phipps,[12,13] Hauke Schmidt,[11] Shingo Watanabe,[14] Shuting Yang,[15] and Jin-Ho Yoon[16]

[1]Atmospheric Sciences and Global Change Division, Pacific Northwest National Laboratory, Richland, WA, USA
[2]Department of Environmental Sciences, Rutgers University, New Brunswick, NJ, USA
[3]Scripps Institution of Oceanography, La Jolla, CA, USA
[4]Laboratoire de Météorologie Dynamique, CNRS / Sorbonne Université, Paris, France
[5]Environment and Climate Change Canada, Toronto, Canada
[6]Met Office Hadley Centre, Exeter, UK
[7]College of Engineering, Mathematics, and Physical Sciences, University of Exeter, Exeter, UK
[8]State Key Laboratory of Earth Surface Processes and Resource Ecology, College of Global Change and Earth System Science, Beijing Normal University, Beijing, China
[9]CSIRO Oceans and Atmosphere, Hobart, Tasmania, Australia
[10]Department of Geosciences, University of Oslo, Oslo, Norway
[11]Max Planck Institute for Meteorology, Hamburg, Germany
[12]Climate Change Research Centre, University of New South Wales, Sydney, Australia
[13]Institute for Marine and Antarctic Studies, University of Tasmania, Hobart, Tasmania, Australia
[14]Japan Agency for Marine-Earth Science and Technology, Yokohama, Japan
[15]Danish Meteorological Institute, Copenhagen, Denmark
[16] School of Earth Sciences and Environmental Engineering, Gwangju Institute of Science and Technology, Gwangju, South Korea

Submission to *Atmospheric Chemistry and Physics*
Special Issue: The Geoengineering Model Intercomparison Project

[*]To whom correspondence should be addressed: P.O. Box 999, MSIN K9-30, Richland, WA 99352, USA. E-mail: ben.kravitz@pnnl.gov.

Abstract. Marine cloud brightening has been proposed as a means of geoengineering/climate intervention, or deliberately altering the climate system to offset anthropogenic climate change. As an idealized representation of marine cloud brightening, this paper discusses experiment G1ocean-albedo of the Geoengineering Model Intercomparison Project (GeoMIP), involving an abrupt quadrupling of the CO_2 concentration and an instantaneous increase in ocean albedo to maintain approximate net top-of-atmosphere radiative flux balance. Eleven Earth System Models are relatively consistent in their temperature, radiative flux, and hydrological cycle responses to this experiment. Due to the imposed forcing, the land surface warms by a model average of 1.14 K, while most of the ocean cools. Some parts of the near-surface air temperature over ocean warm due to heat transport from land to ocean. These changes generally resolve within a few years, indicating that changes in ocean heat content play at most a small role in the warming over the oceans. The hydrological cycle response is a general slowing down, with high heterogeneity in the response, particularly in the tropics. While idealized, these results have important implications for marine cloud brightening, or any other method of geoengineering involving spatially heterogeneous forcing, or any other forcing in general with a strong land/ocean contrast. It also reinforces previous findings that keeping top-of-atmosphere net radiative flux constant is not sufficient for preventing changes in global mean temperature.

Main points:

1) Under an increase in the CO_2 concentration and ocean albedo (at global energy balance), the global climate transitions to a new, warmer steady state.
2) The land surface warms substantially, and oceans near the land warm due to heat transport
3) The hydrological cycle slows down, with regional heterogeneity in the response

Suggested reviewers:

Tim Andrews
Olivier Geoffroy
Govindasamy Bala

1. Introduction

Geoengineering (also called "climate intervention") describes a set of technological approaches to reduce the effects of climate change by deliberately intervening in the climate system (e.g., Shepherd et al., 2009). There are two broad categories of geoengineering that are commonly discussed: solar geoengineering (modifying the amount of shortwave radiation incident at the surface; NAS, 2015a) and carbon dioxide removal (NAS, 2015b). There are also proposals, such as cirrus cloud thinning (Mitchell and Finnegan, 2009) that do not fit neatly into either of these two categories. In all subsequent discussions in this manuscript, we only discuss solar geoengineering methods.

Two of the most commonly proposed methods of global geoengineering are stratospheric sulfate aerosol geoengineering and marine cloud brightening (MCB). Comparison of the different climate effects of these two methods (e.g., Niemeier et al., 2013; Crook et al., 2015) reveals that, among other things, the spatial distributions of the applied forcings strongly affect the climate effects. Many of the effects of sulfate geoengineering can be reasonably well approximated by a uniform reduction in shortwave radiative flux reaching the surface (Kalidindi et al., 2015). Conversely, MCB targets low clouds over oceans (Latham, 1990), which are not ubiquitous. In addition, there are higher order effects due to the altitude at which the shortwave scattering occurs, including multiple scattering effects, infrared absorption of shortwave and longwave radiative flux by sulfate aerosols or cloud particles, and absorption of shortwave radiative flux by atmospheric CO_2 and water vapor (e.g., Kravitz et al., 2013b).

Idealized simulations of solar geoengineering are useful in the context of multi-model intercomparisons, in that they capture many of the effects of more complicated methods of representing geoengineering, yet can be performed by a wide variety of models. In simulations conducted under the Geoengineering Model Intercomparison Project (GeoMIP; Kravitz et al., 2011), an idealized method of representing stratospheric sulfate aerosol geoengineering is via reductions in total solar irradiance. As an example of this representation, experiment G1 involved offsetting the global radiative flux imbalance from a quadrupling of the CO_2 concentration via solar reduction. Thus far, 15 models have participated in this simulation, providing information about model commonalities and differences in the global climate response, including effects on temperature, the hydrological cycle, cryosphere, terrestrial biosphere, and extreme events (Schmidt et al., 2012; Kravitz et al., 2013a, 2013b; Tilmes et al. 2013; Moore et al., 2014; Glienke et al., 2015; Curry et al., 2014; among numerous other studies). The GeoMIP website (http://climate.envsci.rutgers.edu/GeoMIP/) provides an up-to-date list of publications using GeoMIP model output.

While total solar irradiance reductions are straightforward to simulate in all models, this idealization is not a good approximation of MCB. The dominant effect of MCB would be an increase in albedo in and near marine low clouds through aerosol

effects. Changes in the albedo near the surface can produce different signatures from reductions in energy input at the top of the atmosphere, particularly in terms of spatial distribution. While some forms of albedo modification like stratospheric sulfate aerosol geoengineering operate over broad areas (on a hemispheric or larger scale), albedo changes produced by MCB would operate on smaller spatial scales and be concentrated over particular oceanic regions. Previous studies suggest that the clouds that are most susceptible to albedo modification are located on the eastern side of ocean basins in the subtropics, in regions dominated by stratocumulus clouds (Oreopoulos and Platnick, 2008). So, rather than considering a reduction of solar input operating uniformly over both land and ocean, an idealized representation of MCB that better approximates the effects is to increase the albedo only over ocean surfaces, as described by Kravitz et al. (2013c). This method can also be used to assess some effects of geoengineering by creating microbubbles at the ocean surface to increase reflectivity (e.g., Seitz, 2011; Robock, 2011; Gabriel et al., 2017).

In this study, we investigate the climate effects of using ocean albedo increases to offset CO_2 warming and compare those effects with those of total solar irradiance reduction (experiments are described in more detail in the following section). All simulations were conducted under the auspices of GeoMIP, allowing us to characterize a range of model responses to these different idealized methods of representing solar geoengineering.

2. Methodology and Description

Our analyses focus on four simulations: (1) a preindustrial control simulation (piControl), (2) a simulation in which the CO_2 concentration is abruptly quadrupled from its preindustrial value (abrupt4xCO2), (3) a simulation in which the net radiative flux imbalance in abrupt4xCO2 is offset by a reduction in total solar irradiance (G1), and (4) a simulation in which the net radiative flux imbalance in abrupt4xCO2 is offset by an increase in ocean albedo everywhere by a uniform factor (G1ocean-albedo). piControl and abrupt4xCO2 are standard experiments in the Coupled Model Intercomparison Project Phase 5 (CMIP5; Taylor et al., 2012). G1 is described further by Kravitz et al. (2011), and many of the gross features of the results are described by Kravitz et al. (2013a). All models participating in experiment G1 needed to reduce model total solar irradiance by 3.5-5.0% to offset the radiative forcing from a quadrupling of the CO_2 concentration. In G1ocean-albedo, the ocean surface albedo was increased abruptly at the start of the simulation such that net top-of-atmosphere radiative flux perturbation was within ± 0.1 W m^{-2} of the piControl value in an average over years 21-30 of simulation. Based on preliminary simulations described by Kravitz et al. (2013c), it took approximately 20 years for the climate to reach steady state after an abrupt simultaneous change in the CO_2 concentration and the ocean albedo. As will be shown in subsequent sections, once the appropriate value of ocean albedo increase is found and imposed, the climate system adjusts rapidly, requiring at most a few years to reach steady state (as was the case in experiment G1). Table 1 lists the

models participating in this study, including relevant references and the required change in albedo to meet the objectives of experiment G1ocean-albedo. A similar table for experiment G1 is given by Kravitz et al. (2013a). One of the advantages of G1ocean-albedo is that, like G1, all models can conduct this simulation fairly easily. Supplemental Table S1 quantifies how well each model achieved radiative balance in the G1 and G1ocean-albedo experiments.

Kravitz et al. (2013c) found that in test simulations, one could only determine whether the objectives of G1ocean-albedo were met after several decades of simulation. However, as our analysis will show, once the proper value of ocean albedo increase is ascertained, the climate response reaches steady state in a few years, as in experiment G1 (Kravitz et al., 2013a). Supplemental Table S2 quantifies temperature trends in each participating model over years 11-50 of simulation. The mean model trend over this period is approximately zero K/decade (to four decimal places), and with little exception, the trends in G1 and G1ocean-albedo are an order of magnitude smaller than the trends in the abrupt4xCO2 simulation. As such, for the purpose of analysis, we assume that "slow responses," i.e., responses operating on time scales longer than a few years (e.g., Andrews and Forster, 2010; Sherwood et al., 2015) are negligible in the G1 and G1ocean-albedo simulations. We do not separate results into rapid adjustment and slow response timescales, and with the exception of time series plots, all figures show averages over the years 11-50 of simulation, which we take as a sufficient indication of the dominant climate response after the transient response has resolved.

Except where indicated, all plots show the mean model response. All values in the text are reported as mean (min to max), where mean indicates the all-model mean for that particular quantity, min is the lower bound of the range of model responses, and max is the upper bound of the range of model responses. In all maps, stippling indicates where fewer than 75% of the models agree on the sign of the response. All models in Table 1 were able to provide output for all variables except for cloud radiative forcing. The models included in cloud forcing analyses are BNU-ESM, CanESM2, CESM-CAM5.1-FV, HadGEM2-ES, IPSL-CM5A-LR, and MPI-ESM-LR. Supplemental Tables S1-S15 provide more quantitative information for all of the analyses presented in this study.

3. Results

3.1. Albedo and Temperature

Figure 1 shows the change in albedo at the top-of-atmosphere and at the surface for the abrupt4xCO2, G1, and G1ocean-albedo simulations, where albedo is defined as the ratio of upwelling to downwelling all-sky shortwave radiative flux. Quantitative values are given in Supplemental Tables S3 and S4. Results for abrupt4xCO2 and G1 are consistent with known responses of an increase in absorbed shortwave by carbon dioxide, reduced cloud cover, and reduced snow and sea ice cover (e.g., Schmidt et al., 2012; Kravitz et al., 2013b). These result in a broad decrease in

albedo at the top of atmosphere and a decrease in surface albedo in many regions with substantial snow and ice cover. G1ocean-albedo retains many of these local high latitude features, but with large albedo increases over ocean, consistent with the experimental design and imposed forcing.

Figure 2 expands upon this picture by showing changes in shortwave and longwave cloud forcing in G1 and G1ocean-albedo, where cloud forcing is defined as all-sky minus clear-sky radiative flux measured at the top of the atmosphere. Positive shortwave values and negative longwave values in Figure 2 generally indicate less cloud cover. As was shown by Kravitz et al. (2013b), cloud cover in G1 tends to be reduced, which is consistent with what is depicted in Figure 2. For G1ocean-albedo, cloud cover is reduced over most ocean regions and large portions of land. Exceptions include an increase in cloudiness over the Arctic, much of Africa, South Asia, Australia, and the leeward side of the Andes. These changes in cloudiness have implications for the hydrologic cycle, which we revisit in Section 3.4.

Figure 3 shows changes in global mean, land mean, and ocean mean surface air temperature for the G1 and G1ocean-albedo multi-model ensembles. Quantitative values are provided in Supplemental Table S5. Whereas the G1 simulation largely offsets global temperature changes due to increased CO_2 concentration, G1ocean-albedo is approximately 0.36 K (-0.12 to 1.20) warmer than the control simulation. This is predominantly due to warming over land by 1.14 K (0.41 to 1.83). The temperature results in Figure 3 indicate that the temperature change happens within the first few years, and while some models show a slight trend in temperature over the 50-year G1ocean-albedo simulation (Supplemental Table S2), in general, any such trends are small, especially as compared to the warming in the abrupt4xCO2 simulation. This lack of substantial transient behavior after an initial fast response indicates that G1ocean-albedo has entered a new approximate steady state.

Figure 4 shows spatial patterns of change in temperature and top-of-atmosphere net radiative flux. (Also see Supplemental Tables S5 and S6.) The temperature changes are broadly consistent with the net radiative flux changes in the respective experiments. As was discussed by Kravitz et al. (2013a), G1 results in an "overcooling" of the tropics and an "undercooling" of the poles, consistent with offsetting the ubiquitous longwave forcing from CO_2 with a latitudinally dependent reduction in shortwave. G1ocean-albedo shows warming at high latitudes, over land regions, and in some ocean regions near or downwind of large continents, with the remaining ocean regions generally showing cooling.

While the warming over land is easily explainable from first principles, the warming over the ocean is heterogeneous and perhaps somewhat counterintuitive, requiring additional explanation. Because net top-of-atmosphere radiative flux is approximately zero in G1ocean-albedo, these oceanic temperature changes cannot be the result of energy being added to or subtracted from the climate system, and instead must be the result of energy redistribution. Two hypotheses for why these

temperature change patterns look the way they do (which will be tested in subsequent sections) include

1) Most warming over oceanic regions is due to transport of heat from land to ocean.

2) Any contributions to temperature or radiative flux changes from changes in ocean heat content are small on the timescales being evaluated here.

3.2. Hypothesis 1: The role of Land-Ocean Energy Transport (LOET)

Although the air over the ocean warms somewhat in G1ocean-albedo, it does not warm uniformly. Figure 4 shows that much of the warming over the ocean is in areas near land, indicating the potential for some of the heating energy over land to be transported to ocean regions. Indeed, the oceans far from land experience cooling, which is consistent with expectations for a large increase in albedo (Table 1).

Transport of heating energy from land to ocean can be quantified via calculating what Geoffroy et al. (2015) call horizontal energy transport, and which we call land-ocean energy transport (LOET), as it represents an aggregate transport of energy from the atmosphere over the land (averaged over all land regions) to the atmosphere over the ocean (averaged over all ocean regions). Geoffroy et al. (2015) provide a more detailed description, calculation, and validation of this concept using a three-box energy balance model that can be fitted to changes in land/ocean temperature and TOA energy imbalance such that the model captures the relevant energy transport dynamics; we repeat here only the calculations germane to our discussions.

Gregory et al. (2004) describe a method of estimating adjusted radiative forcing and the aggregate strength of global feedbacks via linear regression of the net global, annual mean TOA radiative flux imbalance (ΔR) against the global, annual mean temperature change (ΔT) in response to a forcing. The y-intercept of the regression line gives an estimate of adjusted radiative forcing ($\boldsymbol{\mathcal{F}}$), and the negative of the slope of the regression line gives the feedback parameter (λ). Similarly, one can perform regression just over land-averaged quantities (denoted with the subscript ℓ) or just over ocean quantities (subscript o). Feedback parameter values are provided in Table 2.

In addition, one can regress ΔT_ℓ against ΔT_o to obtain the equation

$$\Delta T_\ell = (\alpha_o/f_\ell)/(\lambda_\ell+\alpha_\ell/f_\ell)\Delta T_o+\boldsymbol{\mathcal{F}}_\ell/(\lambda_\ell+\alpha_\ell/f_\ell) \quad (1)$$

where α_ℓ is the land heat transport parameter and f_ℓ is the land fraction (approximately 0.3). If one solves this equation for α_ℓ and α_o, then one can define

$$\Delta A = \alpha_\ell \Delta T_\ell - \alpha_o \Delta T_o \quad (2)$$

The quantity ΔA is the time-dependent LOET (units of W m^{-2}).

Figure 5 provides calculations of LOET for the simulations presented here. See Supplemental Table S7 for more details on individual model values. In the abrupt4xCO2 simulation, changes in LOET are positive (indicating an increase in heat transport from the land to the ocean) and decrease in magnitude steadily over the course of the simulation; these results are discussed in more detail by Geoffroy et al. (2015).

In Experiment G1, LOET increases by a model-dependent constant value and remains relatively unchanged over the course of the simulation. Although the air temperature over land in G1 increases slightly, and the air temperature over ocean decreases slightly (Kravitz et al., 2013a), the temperature changes in G1 are more latitude-dependent than representative of a clear land-ocean contrast (Figure 4), so it is perhaps not unexpected that LOET would be small.

Experiment G1ocean-albedo exhibits a strong land-ocean contrast in temperature (Figure 4), and the response is in steady state after a few years. As such, consistent with the behavior of other fluxes, LOET in G1ocean-albedo does not show transient behavior. LOET in G1ocean-albedo is approximately 2.20 (1.35 to 3.21) W m^{-2}, which is larger than in the other experiments examined here.

Converting LOET into temperature change is not necessarily straightforward, but an approximate change in temperature can be calculated by combining values of ΔA (Supplemental Table S7) with feedback parameter calculations (Table 2). More specifically, the temperature "added" to the air over the oceans by LOET can be calculated as $\Delta A/\lambda_o$, and the temperature "subtracted" from the air over land by LOET can be calculated as $\Delta A/\lambda_l$. Performing these calculations, LOET in the G1ocean-albedo experiment contributes 1.87 K (0.57 to 3.06) to ocean temperature and "subtracts" 2.03 K (0.68 to 3.06) from land temperature. We caution that this naïve calculation is somewhat circular, and it inherently includes in the ocean calculations both regions unaffected by LOET (e.g., tropical oceans) and regions strongly affected by LOET (e.g., Northeast Atlantic and Pacific Oceans).

Based on the calculations in the present section, it seems unlikely that LOET can on average transport enough energy from the land to the ocean to offset the radiative deficit over the ocean due to an ocean albedo increase. However, locally, LOET appears to be able not only to offset these radiative changes, but also result in net warming.

3.3. Hypothesis 2: Atmospheric Column Energetics and Net Energy Flux into the Oceans

An additional potential source of energy to the atmosphere is a reduction in net ocean heat uptake. Calculating changes in ocean heat uptake are challenging and not particularly revealing in this study for three reasons:

1) It is possible that the models used in simulating G1ocean-albedo were not entirely spun up to steady state. As such, any remaining imbalances could manifest as changes in ocean heat content. In principle, one could subtract off the preindustrial control value, which likely has a similar trend in ocean heat content arising from spinup. However, this would not remove the influence of nonlinearities (state dependence), so there is no way to guarantee that the signal is entirely due to the G1ocean-albedo forcing.
2) As is seen in Supplemental Table S1, not all models were able to achieve top-of-atmosphere net radiative flux balance over the course of the simulation. These small changes can lead to large changes in ocean heat content over the course of a 50-year simulation. For example, a 0.1 W m^{-2} imbalance over a 50-year period can lead to an additional 5.5×10^{22} J of energy incident at the ocean surface. As such, we are unable to properly assess the degree to which ocean heat content changes may be due to small imbalances.
3) Ocean heat content requires a depth threshold for calculation, meaning calculations of it are sensitive to redistribution of heat to/from lower depths, obscuring the signal of the forcing.

As an alternative, we calculate net energy exchange across the surface in terms of changes in radiative and turbulent fluxes. Kravitz et al. (2013b) calculated energetics changes in the entire atmospheric column. However, because we are only interested in net surface fluxes, we calculate

$$\Delta S = \Delta R_{surf} + \Delta SH + \Delta LH \quad (3)$$

where ΔR_{surf} is the change in net surface radiative flux (shortwave and longwave), ΔSH is change in sensible heat flux from the atmosphere to the surface, and ΔLH is change in latent heat flux from the atmosphere to the surface. By convention, all fluxes are positive downward unless specifically noted. Calculations of individual terms in this budget, as well as of ΔS, are provided in Supplemental Tables S8-S12. Because these calculations are performed at the surface, no advection term (e.g., LOET) is needed, and ΔS is well defined as a land or ocean average.

Figure 6 shows the all-model mean for all of the terms in Equation 3. Several clear conclusions emerge. The first is that ΔS is approximately zero globally, over land, and over ocean for nearly the entire 50-year period, after an initial rapid adjustment that resolves within a few years. With the exception of latent heat over land, this is true of all fluxes for G1ocean-albedo in Figure 6, and even latent heat flux over land

reaches an approximate steady state within ten years. If ΔS indeed serves as a useful proxy for net energy flux into or out of the ocean, then these results indicate that there is no sizable contribution to atmospheric energetics by changes in ocean heat content. Moreover, even if ΔS were not zero over ocean, ocean heat content changes would still be an insufficient explanation for temperature changes due to incongruent timescales. The oceanic mixed layer operates on an approximately decadal timescale, but all transient behavior in these simulations is resolved well before ten years. The transient response is much more consistent with a land surface time scale, which is on the order of 1-3 years. As such, it seems plausible that the temperature changes over ocean in G1ocean-albedo are due to land processes rather than ocean heat content changes. This is not to say that the ocean plays no role in the observed temperature changes. Rather, given the discussions in this section and the two previous sections, the role of the ocean heat content in causing temperature changes over the ocean in G1ocean-albedo (over the timescales being analyzed here) is likely small.

The remainder of the results in Figure 6 are consistent with the applied forcing. There is a large sensible heat flux increase from the land to the atmosphere of 2.87 (-0.99 to 6.00) W m^{-2}, with a comparatively smaller sensible heat flux decrease from the ocean to the atmosphere of 1.47 (0.34 to 2.20) W m^{-2}. Over the ocean, latent heat flux from the surface to the atmosphere is 6.71 (4.95 to 7.89) W m^{-2} lower in G1ocean-albedo than in the preindustrial control simulation. These results indicate a greater shift of energy away from evaporating water and toward increasing land temperature. Large differences in flux magnitude between G1 and G1ocean-albedo can be found over land for net shortwave flux and latent heat flux, and differences in sign can be found over land for total radiative flux. These features are consistent with the applied forcing being different over land and ocean.

3.4. Hydrological cycle changes

Introducing a strong land-ocean energy and temperature gradient, as in G1ocean-albedo, will undoubtedly impact the hydrological cycle. Although the G1ocean-albedo simulation is idealized, more realistic representations of MCB have shown important hydrological cycle impacts, including secondary circulation patterns that shift precipitation onto land in the tropics and extratropics (Bala et al., 2010), changes in the monsoon (Alterskjær et al., 2013), and changes in the Walker circulation (Niemeier et al., 2013). Here we evaluate the large-scale hydrological cycle changes in G1ocean-albedo, with possible applicability to other realizations of MCB.

Figure 7 shows global, land, and ocean averaged precipitation, evaporation, and precipitation minus evaporation (P–E) for all of the simulations considered in this manuscript; quantitative descriptions are given in Tables S13–15. The abrupt4xCO2 simulation is the only one with a distinct rapid adjustment and slow response. Over both land and ocean, G1 shows decreases in precipitation and evaporation of approximately equal magnitude, resulting in net changes in P–E of 0.02 (-0.05 to

0.11) mm day^{-1} over land and -0.01 (-0.04 to 0.01) mm day^{-1} over ocean. In G1ocean-albedo, global precipitation and evaporation both decrease by approximately 0.19 (0.11 to 0.26) mm day^{-1} to yield little net change in *P–E*. However, this net small change is due to differential effects over land and ocean. Over land, precipitation remains relatively unchanged, but evaporation decreases, resulting in a net change in *P–E* by 0.09 (-0.18 to 0.18) mm day^{-1}. Over the ocean, both precipitation and evaporation decrease, with a net negative *P–E* of -0.06 (-0.19 to -0.01) mm day^{-1}.

Annual mean land/ocean contrasts in precipitation and evaporation changes tend to be more uniform in sign in experiment G1 (Figure 8), resulting in few large regions of change in P–E with the exception of the tropics (mostly driven by a southward shift in the intertropical convergence zone; Kravitz et al., 2013a). In G1ocean-albedo, precipitation and evaporation over the oceans are reduced in most regions, consistent with the applied forcing. Over land, the signs of precipitation and evaporation changes are regionally heterogeneous, yet the precipitation and evaporation changes are concordant, e.g., land regions with increased precipitation also generally show increased evaporation. The net *P–E* map is highly heterogeneous, but in general, tropical land areas are projected to have more available moisture (as measured by *P–E*) under G1ocean-albedo, and midlatitude land areas are projected to have less. The implications of these changes for people and ecosystems are important to research.

4. Discussion and Conclusions

The results presented here indicate that even though experiments G1 and G1ocean-albedo both achieve approximate net top-of-atmosphere radiative flux balance, the climate system responses differ dramatically between the two experiments. The idea that global energy balance can still result in local changes is perhaps not surprising, as feedbacks operate locally (Armour et al., 2013). These different climate responses for the same forcing are effectively an illustration of different efficacies (Hansen et al., 2005). Even in the absence of slow responses, forcings with different efficacies can cause different climate system changes (Kravitz et al., 2015). G1ocean-albedo serves as an excellent reminder not to conflate small net top-of-atmosphere radiative flux imbalance with small temperature change; a clear relationship between those two quantities is not guaranteed.

Relatedly, the results obtained for G1ocean-albedo were to some extent by design. The objective of G1ocean-albedo was to achieve net top-of-atmosphere radiative flux balance, which resulted in warming. Conceivably, one could define an objective of no global temperature change, implying a net negative radiative flux at the top-of-atmosphere, or no global land temperature change, requiring adjustments over the oceans to make up the imbalance. It is unclear whether, unlike G1ocean-albedo, such alternate approaches would result in transient behavior that lasts longer than a few years. Such an experiment could be accomplished using feedback methods that

have been introduced to geoengineering research in recent years (e.g., MacMartin et al., 2014; Kravitz et al., 2016).

Related to this discussion, Supplemental Figures S1-S3 show monthly differences (from piControl) of net top-of-atmosphere radiative flux change and temperature change for the abrupt4xCO2, G1, and G1ocean-albedo simulations. These were calculated by naively subtracting each monthly value of the three perturbed experiments from the monthly values of the corresponding piControl simulation, so all differences are subject to noise introduced by chaos. G1 shows an indication of slight transient behavior, starting out with positive temperature anomaly that relaxes to near-zero within a few years. G1ocean-albedo does not show any discernible anomaly, in that it starts out slightly warmer (globally) than piControl and stays slightly warm. The Gregory plot for G1ocean-albedo similarly shows no discernible trend, unlike the abrupt4xCO2 simulation. There are several possibilities of explanations for this behavior. One is that the adjustments are happening on a short enough timescale in G1ocean-albedo that any transient response is difficult to detect with only monthly averages (Cao et al., 2012). Another possibility is that the noise introduced by chaos on the timescales of interest (months to a few years) obscures our ability to detect any transient behavior. An ensemble of shorter simulations (e.g., Wan et al., 2014) might be well equipped to reveal transience in the response on these timescales. A third option is model artifact related to how the climate models treat energy conservation, indicating that experiments like G1ocean-albedo could be useful in testing models beyond their originally conceived application space. While it is beyond the scope of the present manuscript to fully assess all of these possibilities, it becomes clear that G1ocean-albedo and simulations of geoengineering in general are useful for improving understanding about climate modeling and climate science.

The results presented here have several features that were not necessarily expected from the outset. Kravitz et al. (2013c) found that determining whether the climate system was in balance took up to 30 years of simulation. However, once that balance is achieved, the climate does not change appreciably after the initial rapid adjustment. Potential future work could investigate these results, shedding light on timescales of climate response and potential thresholds, e.g., how large does the energy imbalance need to be to trigger slower adjustments?

Related to this issue of different timescales of adjustment is the traditional separation of climate response into rapid adjustment and slow response components (e.g., Andrews and Forster, 2010; Sherwood et al., 2015). The rapid adjustment is often defined as the climate response unassociated with global mean temperature change, and the slow response describes a transient response due to temperature change, largely as a result of climate system feedbacks. The results from G1ocean-albedo, like those of G1 (Kravitz et al., 2013b), show an initial rapid change and no appreciable slower change. However, in G1ocean-albedo, there is a sustained temperature increase without appreciable transient behavior. Thus, G1ocean-albedo represents an experiment that does not cleanly delineate into the

traditional definitions of rapid adjustment and slow response. Additionally, this sustained temperature increase is to some extent decoupled from net energy imbalances in the climate system, as ΔR_{TOA} and ΔS (Equation 3) are both approximately zero. Reconciling all of these features suggests a potentially rich research topic focused on understanding the relationships between radiative flux changes, temperature changes, and the circumstances under which climate feedbacks are excited, particularly for forcings with strong land/ocean contrast (e.g., anthropogenic aerosols).

The results presented here are broadly relevant to more sophisticated representations of MCB, such as increasing cloud droplet number concentration or directly injecting sea salt aerosols into the marine boundary layer. Stjern et al. (2018) analyzed a multi-model ensemble of simulations of G4cdnc (Kravitz et al., 2013c), involving a 50% increase in cloud droplet number concentration in all marine low clouds, wherever the model forms those clouds. Although smaller in magnitude, they found similar patterns of top-of-atmosphere radiative flux change as in G1ocean-albedo. Also similar between the two experiments was an increase in land precipitation and a decrease in ocean precipitation. Perhaps an even more realistic representation is G4sea-salt (Ahlm et al., 2017), involving direct injection of sea salt into the marine boundary layer between 30°S and 30°N to achieve an effective radiative forcing of -2.0 W m^{-2}. In the injection area (the tropics), this experiment also showed similar patterns of net top-of-atmosphere radiative flux perturbation and hydrologic cycle response. As such, while G1ocean-albedo is highly idealized and exerts a perhaps unrealistically large forcing, it has relevance for other global representations of MCB or sea spray geoengineering.

G1ocean-albedo may be more apposite to the impact of geoengineering via "ocean microbubbles," whereby surfactants are added to the ocean surface, promoting the formation of microscopic, highly reflective bubbles (Seitz, 2011; Robock, 2011). An area of investigation we did not undertake, yet one that repeatedly emerges in discussions of microbubbles, is the resulting effects of surface albedo increase on the ocean mixed layer. By reflecting more solar radiation, microbubbles have the potential to inhibit vertical mixing and available light in the euphotic zone, which could have profound effects on marine biota. This implies that another useful future area of investigation for the G1ocean-albedo simulation is an analysis of the marine carbon cycle.

There are numerous potential areas of research prompted by this study. The stark land/ocean contrast in warming has potential implications for ocean circulation patterns, including the meridional overturning circulation and Western boundary ocean currents, with consequent implications for marine ecosystems. This contrast also has implications for the terrestrial biosphere, including ecosystem services and the land and ocean carbon cycles. Although we did not evaluate seasonal changes in this manuscript, such investigations could prove fruitful for more detailed assessments of variability, such as monsoon precipitation, extreme events, and sea ice extent.

Despite being informative for MCB, there are limits as to the applicability of this idealized approach. There are important differences in boundary layer stability changes from surface albedo increases versus marine stratocumulus cloud top brightening. Also, it appears impossible for marine cloud brightening to be conducted over all ocean regions and with a sufficient magnitude to offset the radiative forcing from a quadrupling of the CO_2 concentration. The purpose of this manuscript is to describe the broad features of change under a uniform ocean albedo increase, and some of these changes are likely to be present with more realistic scenarios of marine cloud brightening. We anticipate that future research can more deeply explore the applicability of this simulation to marine cloud brightening.

Acknowledgments. We thank Jón Egill Kristjánsson, who tragically passed away, for invaluable comments on an earlier version of this manuscript. We acknowledge the World Climate Research Programme's Working Group on Coupled Modelling, which is responsible for CMIP, and we thank the climate modeling groups for producing and making available their model output. For CMIP the U.S. Department of Energy's Program for Climate Model Diagnosis and Intercomparison provides coordinating support and led development of software infrastructure in partnership with the Global Organization for Earth System Science Portals. We thank all participants of the Geoengineering Model Intercomparison Project and their model development teams, CLIVAR/WCRP Working Group on Coupled Modeling for endorsing GeoMIP, and the scientists managing the Earth System Grid data nodes who have assisted with making GeoMIP output available. The Pacific Northwest National Laboratory is operated for the U.S. Department of Energy by Battelle Memorial Institute under contract DE-AC05-76RL01830. Simulations performed by Ben Kravitz were supported by the NASA High-End Computing (HEC) Program through the NASA Center for Climate Simulation (NCCS) at Goddard Space Flight Center. Alan Robock is supported by NSF grant AGS-1617844. Olivier Boucher acknowledges HPC resources from CCRT under the allocation 2015-t2012012201 made by GENCI (Grand Equipement National de Calcul Intensif). This research was supported under the Australian Research Council's Special Research Initiative for the Antarctic Gateway Partnership (project SR140300001). Jin-Ho Yoon was supported by the National Strategic Project – Find particle of the National Research of Korea (NRF) funded by the Ministry of Science and ICT (MSIT), the Ministry of Environment (ME), and the Ministry of Health and Welfare (MOHW) NRF-2017M3D8A1092022.

571 **References**
572
573 Ahlm, L., A. Jones, C. W. Stjern, H. Muri, B. Kravitz, and J. E. Kristjánsson (2017),
574 Marine cloud brightening – as effective without clouds, *Atmos. Chem. Phys.*,
575 *17*, 13071-13087, doi:10.5194/acp-17-13071-2017.
576 Alterskjær, K., J. E. Kristjansson, and Ø. Seland (2012), Sensitivity to deliberate sea
577 salt seeding of marine clouds – observations and model simulations, *Atmos.*
578 *Chem. Phys.*, *12*, 2795-2807 doi:10.5194/acp-12-2795-2012.
579 Alterskjær, K., J. E. Kristjánsson, O. Boucher, H. Muri, U. Niemeier, H. Schmidt, M.
580 Schulz, and C. Timmreck (2013), Sea-salt injections into the low-latitude
581 marine boundary layer: The transient response in three Earth system
582 models, *J. Geophys. Res. Atmos., 118*, 12,195–12,206,
583 doi:10.1002/2013JD020432.
584 Andrews, T., and P. M. Forster (2010), The transient response of global-mean
585 precipitation to increasing carbon dioxide levels, *Environ. Res. Lett.*, *5*,
586 025212, doi:10.1088/1748-9326/5/2/025212.
587 Armour, K. C., C. M. Bitz, and G. H. Roe (2013), Time-varying climate sensitivity from
588 regional feedbacks, *J. Climate, 26*, 4518–4534, doi:10.1175/JCLI-D-12-
589 00544.1.
590 Arora, V. K., J. F. Scinocca, G. J. Boer, J. R. Christian, K. L. Denman, G. M. Flato, V. V.
591 Kharin, W. G. Lee, and W. J. Merryfield (2011), Carbon emission limits
592 required to satisfy future representative concentration pathways of
593 greenhouse gases, *Geophys. Res. Lett.*, *38*, L05805,
594 doi:10.1029/2010GL046270.
595 Bala, G., K. Caldeira, and R. Nemani (2010), Fast versus slow response in climate
596 change: Implications for the global hydrological cycle, *Clim. Dyn.*, *35*, 423-
597 434, doi:10.1007/s00382-009-0583-y.
598 Collins, W. J., N. Bellouin, M. Doutriaux-Boucher, N. Gedney, P. Halloran, T. Hinton, J.
599 Hughes, C. D. Jones, M. Joshi, S. Liddicoat, G. Martin, F. O'Connor, J. Rae, C.
600 Senior, S. Sitch, I. Totterdell, A. Wiltshire, and S. Woodward (2011),
601 Development and evaluation of an Earth-System model—HadGEM2, *Geosci.*
602 *Model Dev.*, *4*, 1051-1075, doi:10.5194/gmd-4-1051-2011.
603 Crook, J. A., L. S. Jackson, S. M. Osprey, and P. M. Forster (2015), A comparison of
604 temperature and precipitation responses to different Earth radiation
605 management geoengineering schemes, *J. Geophys. Res., 120*, 9352-9373,
606 doi:10.1002/2015JD023269.
607 Curry, C. L., J. Sillmann, D. Bronaugh, K. Alterskjær, J. N. S. Cole, B. Kravitz., J. E.
608 Kristjánsson, H. Muri, U. Niemeier, A. Robock, and S. Tilmes (2014), A multi-
609 model examination of climate extremes in an idealized geoengineering
610 experiment, *Journal of Geophysical Research*, *119*, 3900-3923,
611 doi:10.1002/2013JD020648.
612 Dufresne, J.-L., M.-A. Foujols, S. Denvil, A. Caubel, O. Marti, O. Aumont, Y. Balkanski, S.
613 Bekki, H. Bellenger, R. Benshila, S. Bony, L. Bopp, P. Braconnot, P. Brockmann,
614 P. Cadule, F. Cheruy, F. Codron, A. Cozic, D. Cugnet, N. de Noblet, J.-P. Duvel, C.
615 Ethé, L. Fairhead, T. Fichefet, S. Flavoni, P. Friedlingstein, J.-Y. Grandpeix, L.
616 Guez, E. Guilyardi, D. Hauglustaine, F. Hourdin, A. Idelkadi, J. Ghattas, S.

Joussaume, M. Kageyama, G. Krinner, S. Labetoulle, A. Lahellec, M.-P. Lefebvre, F. Lefevre, C. Levy, Z. X. Li, J. Lloyd, F. Lott, G. Madec, M. Mancip, M. Marchand, S. Masson, Y. Meurdesoif, J. Mignot, I. Musat, S. Parouty, J. Polcher, C. Rio, M. Schulz, D. Swingedouw, S. Szopa, C. Talandier, P. Terray, N. Viovy, and N. Vuichard (2013), Climate change projections using the IPSL-CM5 Earth System Model: From CMIP3 to CMIP5, *Clim. Dynam.*, *40*, 2123-2165 doi:10.1007/s00382-012-1636-1.

Gabriel, C. J., A. Robock, L. Xia, B. Zambri, and B. Kravitz (2017), The G4Foam experiment: Global climate impacts of regional ocean albedo modification. *Atmos. Chem. Phys.*, *17*, 595-613, doi:10.5194/acp-17-595-2017.

Geoffroy, O., D. Saint-Martin, and A. Voldoire (2015), Land-sea warming contrast: the role of the horizontal energy transport, *Clim. Dynam.*, *45*, 3493-3511, doi:10.1007/s00382-015-2552-y.

Giorgetta, M. A., Johann Jungclaus, Christian H. Reick, Stephanie Legutke, Jürgen Bader, Michael Böttinger, Victor Brovkin, Traute Crueger, Monika Esch, Kerstin Fieg, Ksenia Glushak, Veronika Gayler, Helmuth Haak, Heinz-Dieter Hollweg, Tatiana Ilyina, Stefan Kinne, Luis Kornblueh, Daniela Matei, Thorsten Mauritsen, Uwe Mikolajewicz, Wolfgang Mueller, Dirk Notz, Felix Pithan, Thomas Raddatz, Sebastian Rast, Rene Redler, Erich Roeckner, Hauke Schmidt, Reiner Schnur, Joachim Segschneider, Katharina D. Six, Martina Stockhause, Claudia Timmreck, Jörg Wegner, Heinrich Widmann, Karl-H. Wieners, Martin Claussen, Jochem Marotzke, and Bjorn Stevens (2013), Climate and carbon cycle changes from 1850 to 2100 in MPI-ESM simulations for the Coupled Model Intercomparison Project Phase 5, *J. Adv. Model. Earth Syst.*, *5*, 572-597, doi:10.1002/jame.20038.

Glienke, S., P. J. Irvine, and M. G. Lawrence (2015), The impact of geoengineering on vegetation in experiment G1 of the GeoMIP, *Journal of Geophysical Research*, *120*, 10196-10213, doi:10.1002/2015JD024202.

Gregory, J. M., W. J. Ingram, M. A. Palmer, G. S. Jones, P. A. Stott, R. B. Thorpe, J. A. Lowe, T. C. Johns, and K. D. Williams (2004), A new method for diagnosing radiative forcing and climate sensitivity, *Geophys. Res. Lett., 31*, L03205, doi:10.1029/2003GL018747.

Hansen, J., M. Sato, R. Ruedy, L. Nazarenko, A. Lacis, G. A. Schmidt, G. Russell, I. Aleinov, M. Bauer, S. Bauer, N. Bell, B. Cairns, V. Canuto, M. Chandler, Y. Cheng, A. Del Genio, G. Faluvegi, E. Fleming, A. Friend, T. Hall, C. Jackman, M. Kelley, N. Kiang, D. Koch, J. Lean, J. Lerner, K. Lo, S. Menon, R. Miller, P. Minnis, T. Novakov, V. Oinas, Ja. Perlwitz, Ju. Perlwitz, D. Rind, A. Romanou, D. Shindell, P. Stone, S. Sun, N. Tausnev, D. Thresher, B. Wielicki, T. Wong, M. Yao, and S. Zhang (2005), Efficacy of climate forcings, *J. Geophys. Res., 110*, D18104, doi:10.1029/2005JD005776.

Hazeleger, W., X. Wang, C. Severijns, S. Ştefănescu, R. Bintanja, A. Sterl, K. Wyser, T. Semmler, S. Yang, B. van den Hurk, T. van Noije, E. van der Linden, and K. van der Wiel (2011), EC-Earth V2.2: Description and validation of a new seamless Earth system prediction model, *Clim. Dynam., 39*(11), 2611-2629, doi:10.1007/s00382-011-1228-5.

Hurrell, J. W., M. M. Holland, P. R. Gent, S. Ghan, J. E. Kay, P. J. Kushner, J.-F. Lamarque, W. G. Large, D. Lawrence, K. Lindsay, W. H. Lipscomb, M. C. Long, N. Mahowald, D. R. Marsh, R. B. Neale, P. Rasch, S. Vavrus, M. Vertenstein, D. Bader, W. D. Collins, J. J. Hack, J. Kiehl, and S. Marshall (2013), The Community Earth System Model: A framework for collaborative research, *Bull. Amer. Meteor. Soc.*, *94*, 1339-1360, doi:10.1175/BAMS-D-12-00121.1.

Ji, D., L. Wang, J. Feng, Q. Wu, H. Cheng, Q. Zhang, J. Yang, W. Dong, Y. Dai, D. Gong, R.-H. Zhang, X. Wang, J. Liu, J. C. Moore, D. Chen, and M. Zhou (2014), Description and basic evaluation of Beijing Normal University Earth System Model (BNU-ESM) version 1, *Geosci. Model. Dev.*, *7*, 2039-2064, 10.5194/gmd-7-2039-2014.

Kalidindi, S., G. Bala, A. Modak, and K. Caldeira (2015), Modeling of solar radiation management: a comparison of simulations using reduced solar constant and stratospheric sulphate aerosols, *Clim. Dynam.*, *44*, 2909-2925, doi:10.1007/s00382-014-2240-3.

Kravitz, B., A. Robock, O. Boucher, H. Schmidt, K. E. Taylor, G. Stenchikov, and M. Schulz (2011), The Geoengineering Model Intercomparison Project (GeoMIP), *Atm. Sci. Lett.*, *12,* 162-167, doi:10.1002/asl.316.

Kravitz, B., K. Caldeira, O. Boucher, A. Robock, P. J. Rasch, K. Alterskjær, D. Bou Karam, J. N. S. Cole, C. L. Curry, J. M. Haywood, P. J. Irvine, D. Ji, A. Jones, J. E. Kristjánsson, D. J. Lunt, J. Moore, U. Niemeier, H. Schmidt, M. Schulz, B. Singh, S. Tilmes, S. Watanabe, S. Yang, and J.-H. Yoon (2013a), Climate model response from the Geoengineering Model Intercomparison Project (GeoMIP), *Journal of Geophysical Research*, *118*(15), 8320-8332, doi:10.1002/jgrd.50646.

Kravitz, B., P. J. Rasch, P. M. Forster, T. Andrews, J. N. S. Cole, P. J. Irvine, D. Ji, J. E. Kristjánsson, J. C. Moore, H. Muri, U. Niemeier, A. Robock, B. Singh, S. Tilmes, S. Watanabe, and J.-H. Yoon (2013b), An energetic perspective on hydrological cycle changes in the Geoengineering Model Intercomparison Project (GeoMIP), *Journal of Geophysical Research*, *118*, 13087-13102, doi:10.1002/2013JD020502.

Kravitz, B., P. M. Forster, A. Jones, A. Robock, K. Alterskjær, O. Boucher, A. K. L. Jenkins, H. Korhonen, J. E. Kristjánsson, H. Muri, U. Niemeier, A.-I. Partanen, P. J. Rasch, H. Wang, and S. Watanabe (2013c), Sea spray geoengineering experiments in the Geoengineering Model Intercomparison Project (GeoMIP): Experimental design and preliminary results, *Journal of Geophysical Research*, *118*(19), 11175-11186, doi:10.1002/jgrd.50856.

Kravitz, B., D. G. MacMartin, P. J. Rasch, and A. J. Jarvis (2015), A new method of comparing forcing agents in climate models, *J. Climate, 28*, 8203–8218, doi:10.1175/JCLI-D-14-00663.1.

Kravitz, B., D. G. MacMartin, H. Wang, and P. J. Rasch (2016), Geoengineering as a design problem, *Earth System Dynamics, 7*, 469-497, doi:10.5194/esd-7-469-2016.

Latham, J. (1990), Control of global warming? *Nature*, *347*, 339–340.

MacMartin, D.G., B. Kravitz, D. W. Keith, and A. Jarvis (2014), Dynamics of the coupled human-climate system resulting from closed-loop control of solar geoengineering, *Clim. Dynam., 43*, 243-258, doi:10.1007/s00382-013-1822-9.

Mitchell, D. L. and W. Finnegan (2009), Modification of cirrus clouds to reduce global warming, *Environ. Res. Lett.*, *4*, 045102, doi:10.1088/1748-9326/4/4/045102.

Moore, J. C., A. Rinke, X. Yu, D. Ji, X. Cui, Y. Li, K. Alterskjær, J. E. Kristjánsson, O. Boucher, N. Huneeus, B. Kravitz, A. Robock, U. Niemeier, H. Schmidt, M. Schulz, S. Tilmes, and S. Watanabe (2014), Arctic sea ice and atmospheric circulation under the GeoMIP G1 scenario, *J. Geophys. Res., 119*, 567-583, doi:10.1002/2013JD021060.

NAS (2015a), Climate Intervention: Carbon Dioxide Removal and Reliable Sequestration, National Research Council, The National Academies Press, Washington, DC, 141 pp.

NAS (2015b), Climate Intervention: Reflecting Sunlight to Cool Earth, National Research Council, The National Academies Press, Washington, DC, 235 pp.

Niemeier, U., H. Schmidt, K. Alterskjær, and J. E. Kristjánsson (2013), Solar irradiance reduction via climate engineering--impact of different techniques on the energy balance and the hydrological cycle, *Journal of Geophysical Research*, *118*, 11905-11917, doi:10.1002/2013JD020445.

Oreopoulos, L. and S. Platnick (2008), Radiative susceptibility of cloudy atmospheres to droplet number perturbations: 2. Global analysis from MODIS, *J. Geophys. Res.*, *113*, D14S21, doi:10.1029/2007JD009655.

Pandey, D. K., R. B. Lee III, and J. Paden (1995), Effects of atmospheric emissivity on clear sky temperatures, *Atmos. Environ.*, *29*, 2201-2204, doi:10.1016/1352-2310(94)00243-E.

Phipps, S. J., L. D. Rotstayn, H. B. Gordon, J. L. Roberts, A. C. Hirst, and W. F. Budd (2011), The CSIRO Mk3L climate system model version 1.0 – Part 1: Description and evaluation, *Geosci. Model Dev.*, *4*, 483-509, 10.5194/gmd-4-483-2011.

Robock, A. (2011), Bubble, bubble, toil and trouble. An editorial comment. *Climatic Change*, *105*, 383-385, doi:10.1007/s10584-010-0017-1.

Schmidt, H., K. Alterskjær, D. Bou Karam, O. Boucher, A. Jones, J. E. Kristjánsson, U. Niemeier, M. Schulz, A. Aaheim, F. Benduhn, M. Lawrence, and C. Timmreck (2012), Solar irradiance reduction to counteract radiative forcing from a quadrupling of CO_2: Climate responses simulated by four Earth system models, *Earth System Dynamics, 3*, 63-78, doi:10.5194/esd-3-63-2012.

Schmidt, Gavin A., Max Kelley, Larissa Nazarenko, Reto Ruedy, Gary L. Russell, Igor Aleinov, Mike Bauer, Susanne E. Bauer, Maharaj K. Bhat, Rainer Bleck, Vittorio Canuto, Yong-Hua Chen, Ye Cheng, Thomas L. Clune, Anthony Del Genio, Rosalinda de Fainchtein, Greg Faluvegi, James E. Hansen, Richard J. Healy, Nancy Y. Kiang, Dorothy Koch, Andy A. Lacis, Allegra N. LeGrande, Jean Lerner, Ken K. Lo, Elaine E. Matthews, Surabi Menon, Ron L. Miller, Valdar Oinas, Amidu O. Oloso, Jan P. Perlwitz, Michael J. Puma, William M. Putman, David Rind, Anastasia Romanou, Makiko Sato, Drew T. Shindell, Shan Sun, Rahman A. Syed, Nick Tausnev, Kostas Tsigaridis, Nadine Unger, Apostolos

753 Voulgarakis, Mao-Sung Yao, and Jinlun Zhang (2014), Configuration and
754 assessment of the GISS ModelE2 contributions to the CMIP5 archive, *J. Adv.*
755 *Model. Earth Syst., 6*, 141–184, doi:10.1002/2013MS000265.
756 Seitz, R. (2011), Bright water: hydrosols, water conservation and climate change,
757 *Climatic Change*, *105*, 365-381, doi:10.1007/s10584-010-9965-8.
758 Shepherd, J., K. Caldeira, P. Cox, J. Haigh, K. Keith, B. Launder, G. Mace, G. MacKerron,
759 J. Pyle, S. Rayner, C. Redgwell, and A. Watson (2009), Geoengineering the
760 climate: Science, governance, and uncertainty, Royal Society Policy
761 document 10/09, 82 pp.
762 Sherwood, S. C., S. Bony, O. Boucher, C. Bretherton, P. M. Forster, J. M. Gregory, and B.
763 Stevens (2015), Adjustments in the forcing-feedback framework for
764 understanding climate change, *Bull. Amer. Meteor. Soc., 96*, 217–228,
765 doi:10.1175/BAMS-D-13-00167.1.
766 Stephens, G. L., D. O'Brien, P. J. Webster, P. Pilewski, S. Kato, and J.-L. Li (2015), The
767 albedo of Earth, *Rev. Geophys.*, *53*, 141-163, doi:10.1002/2014RG000449.
768 Stjern, C. W., H. Muri, L. Ahlm, O. Boucher, J. N. S. Cole, D. Ji, A. Jones, J. Haywood, B.
769 Kravitz, A. Lenton, J. C. Moore, U. Niemeier, S. J. Phipps, H. Schmidt, S.
770 Watanabe, and J. E. Kristjánsson (2018), Response to marine cloud
771 brightening in a multi-model ensemble, *Atmos. Chem. Phys.*, *18*, 621-634,
772 doi:10.5194/acp-18-621-2018.
773 Taylor, K. E., R. J. Stouffer, and G. A. Meehl (2012), An overview of CMIP5 and the
774 experiment design, *Bull. Amer. Meteor. Soc.*, *93*, 485-498, doi:10.1175/BAMS-
775 D-11-00094.1.
776 Tilmes, S., J. Fasullo, J.-F. Lamarque, D. R. Marsch, M. Mills, K. Alterskjær, O. Boucher,
777 J. N. S. Cole, C. L. Curry, J. M. Haywood, P. J. Irvine, D. Ji, A. Jones, D. B. Karam,
778 B. Kravitz, J. E. Kristjánsson, J. C. Moore, H. O. Muri, U. Niemeier, P. J. Rasch, A.
779 Robock, H. Schmidt, M. Schulz, B. Singh, S. Watanabe, S. Yang, and J.-H. Yoon
780 (2013), The hydrological impact of geoengineering in the Geoengineering
781 Model Intercomparison Project (GeoMIP), *Journal of Geophysical Research*,
782 *118*(19), 11036-11058, doi:10.1002/jgrd.50868.
783 Watanabe, S., T. Hajima, K. Sudo, T. Nagashima, T. Takemura, H. Okajima, T. Nozawa,
784 H. Kawase, M. Abe, T. Yokohata, T. Ise, H. Sato, E. Kato, K. Takata, S. Emori,
785 and M. Kawamiya (2011), MIROC-ESM 2010: Model description and basic
786 results of CMIP5-20c3m experiments, *Geosci. Mod. Dev.*, *4*, 845-872,
787 doi:10.5194/gmd-4-845-2011.
788

Table 1. Description of the 11 models participating in this study. Column 1 gives the standard model name. Columns 2 and 3 give the default and perturbed surface ocean albedo, defined as upward shortwave divided by downward shortwave radiative flux at the surface, both averaged over ocean regions and over years 11-50 of simulation. Column 4 is the ratio of column 3 to column 2 (calculated prior to rounding the values in Columns 2 and 3). Column 5 gives the factor (δ) by which the model default ocean albedo was multiplied to achieve negligible top-of-atmosphere radiative flux changes under an abrupt4xCO2 simulation (described in greater detail by Kravitz et al., 2015). The differences between Ratio and δ are caused in part by cloud responses. Column 6 gives a relevant reference for each model. All values are rounded to two decimal places.

Model name	**piControl ocean albedo**	**G1OA ocean albedo**	**Ratio**	**δ**	**Reference**
BNU-ESM	0.12	0.17	1.48	2.50	Ji et al. (2014)
CanESM2	0.11	0.19	1.73	2.45	Arora et al. (2011)
CESM-CAM5.1-FV	0.10	0.18	1.79	2.70	Hurrell et al. (2013)
CSIRO-Mk3L-1.2	0.12	0.19	1.61	2.04	Phipps et al. (2011)
EC-Earth	0.10	0.19	1.97	3.17	Hazeleger et al. (2011)
GISS-E2-R	0.08	0.16	1.95	2.53	Schmidt et al. (2014)
HadGEM2-ES	0.10	0.17	1.83	2.44	Collins et al. (2011)
IPSL-CM5A-LR	0.10	0.17	1.78	2.33	Dufresne et al. (2013)
MIROC-ESM	0.10	0.20	2.00	3.10	Watanabe et al. (2011)
MPI-ESM-LR	0.09	0.23	2.40	5.42	Giorgetta et al. (2013)
NorESM1-M	0.09	0.18	1.95	2.77	Alterskjær et al. (2012)

Table 2. Feedback parameters (Section 3.2; units W m^{-2}) for global, land, and ocean averages, calculated via the "Gregory method" (Gregory et al., 2004), where annual mean top-of-atmosphere net radiative flux is regressed against annual mean temperature.

	λ_g	λ_ℓ	λ_o
BNU-ESM	0.9019	0.7181	0.9838
CanESM2	1.1539	1.1898	1.1260
CESM-CAM5.1-FV	1.1435	1.0357	1.1591
CSIRO-Mk3L-1.2	1.0192	0.9300	0.8034
EC-Earth	1.2124	1.1937	1.3155
GISS-E2-R	2.2440	1.9751	2.3560
HadGEM2-ES	0.8411	0.8363	0.8351
IPSL-CM5A-LR	0.8367	1.2891	0.5894
MIROC-ESM	1.0378	0.8736	1.0383
MPI-ESM-LR	1.3701	1.0573	1.3986
NorESM1-M	1.4285	1.8828	1.6063

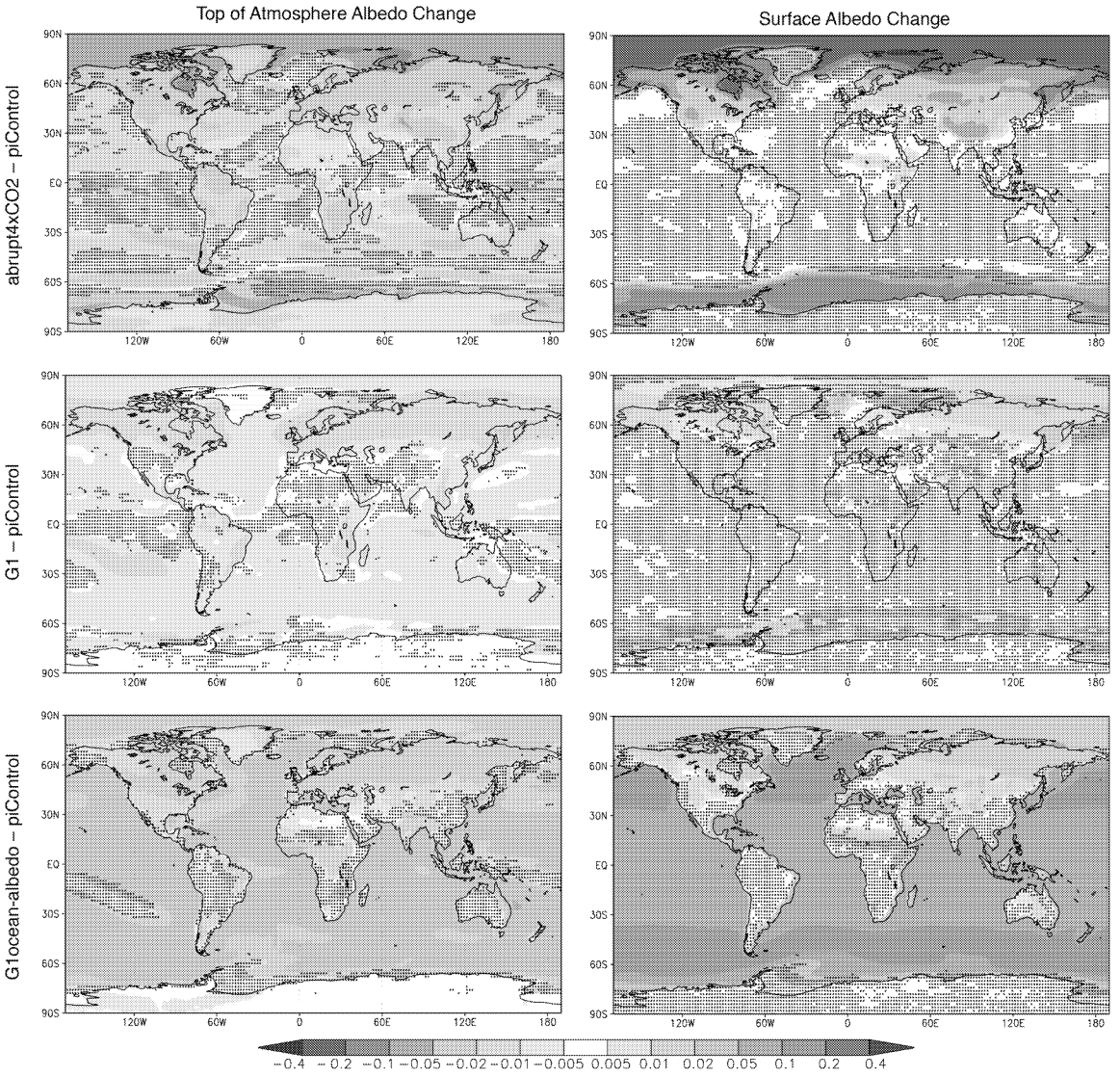

Figure 1. Top-of-atmosphere (TOA) and surface albedo differences (relative to piControl) for the abrupt4xCO2, G1, and G1ocean-albedo experiments. Albedo here is calculated as the ratio of upwelling to downwelling all-sky shortwave radiative flux, either at TOA or at the surface. Values are averages over years 11-50 of simulation. Stippling indicates where fewer than 8 out of 11 models agree on the sign of the response.

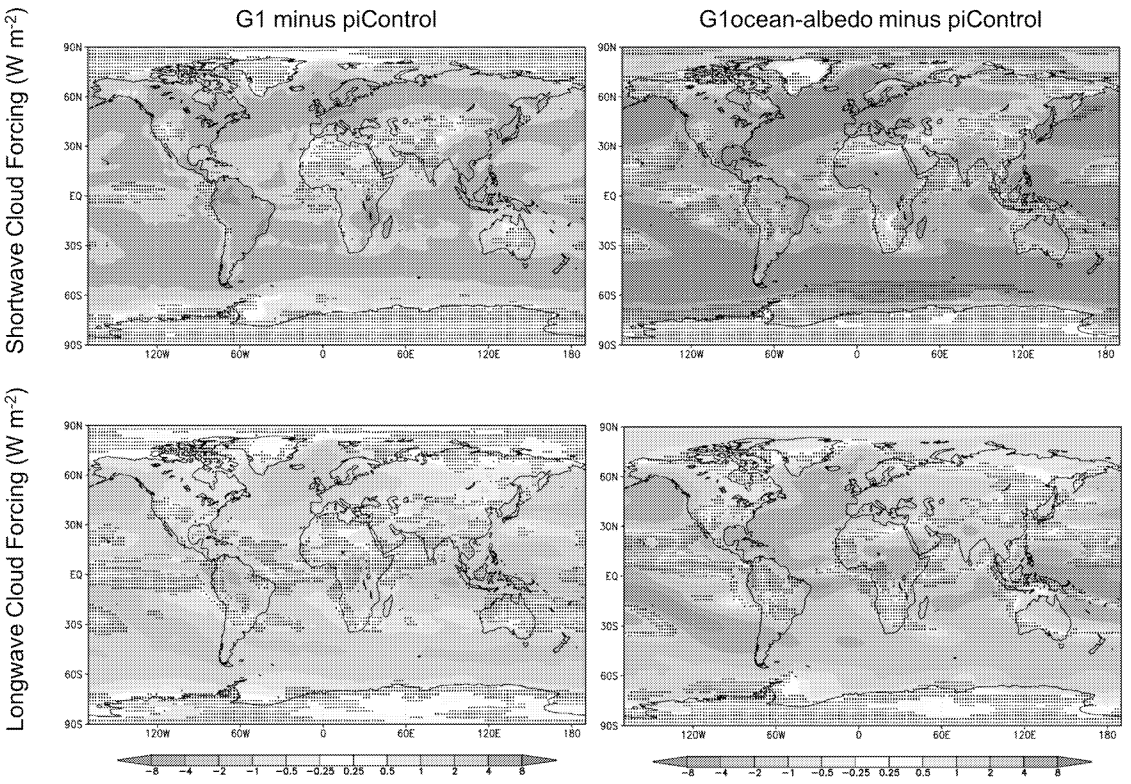

Figure 2. Shortwave (top) and longwave (bottom) cloud forcing changes due to the G1 (left) and G1ocean-albedo perturbations. Cloud forcing is defined as all-sky minus clear-sky radiative flux at the top of the atmosphere.

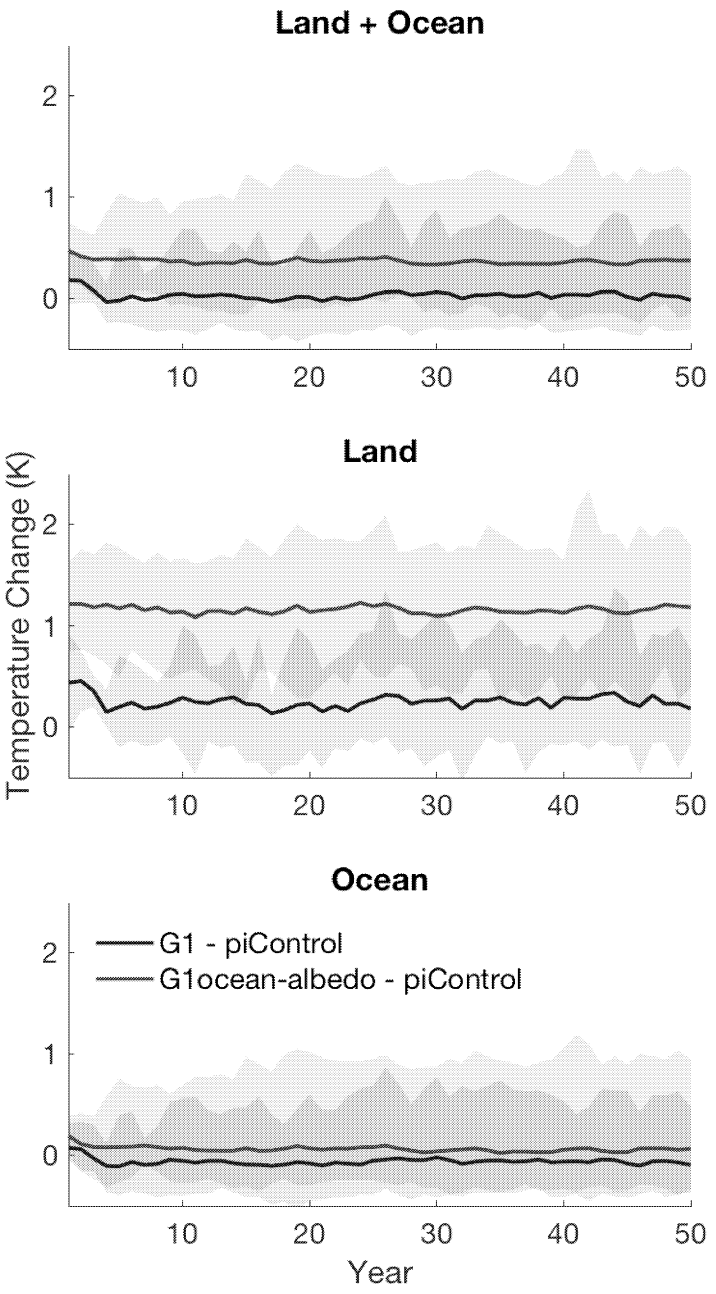

819
820
821 **Figure 3.** Global (top), land (middle), and ocean (bottom) average temperature
822 change for the G1 (blue) and G1ocean-albedo (red) simulations. Lines show the all-
823 model ensemble mean, and shading shows model spread (smallest to largest
824 values).

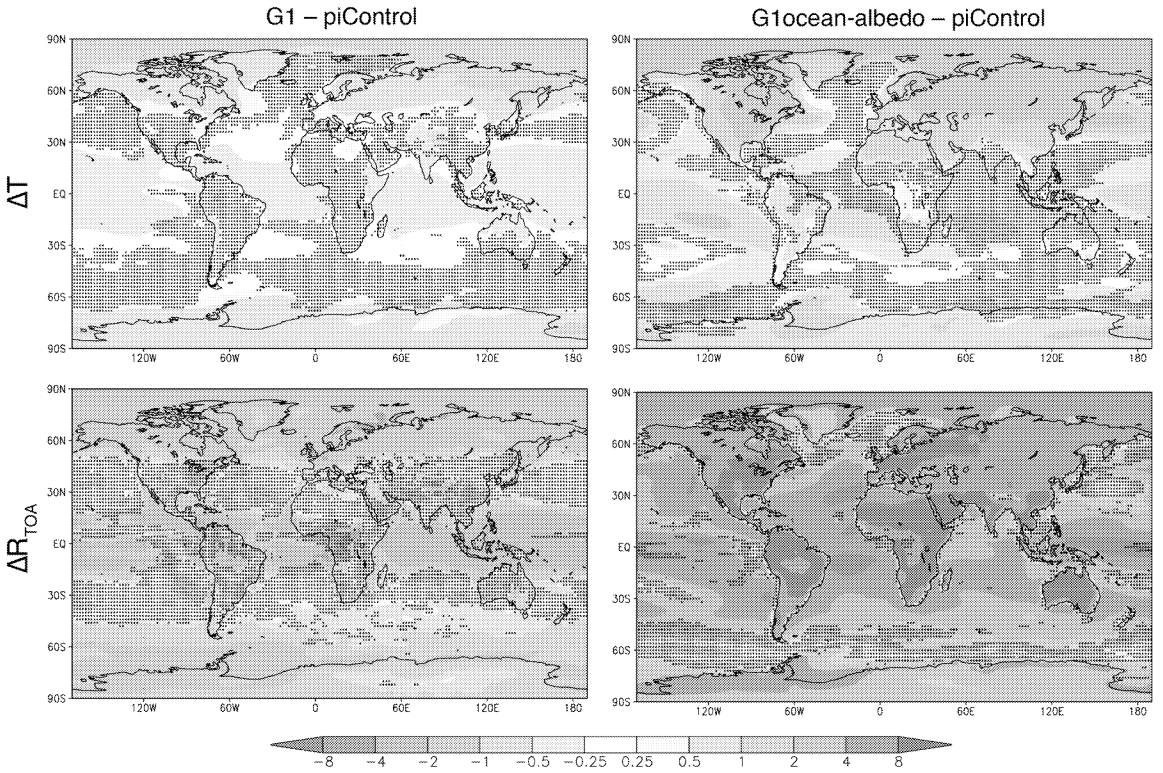

Figure 4. Surface air temperature (top row; K) and TOA net radiative flux (bottom row; W m^{-2}) changes for experiments G1 (left) and G1ocean-albedo (right). Values are averages over years 11-50 of simulation. Stippling indicates where fewer than 8 out of 11 models agree on the sign of the response.

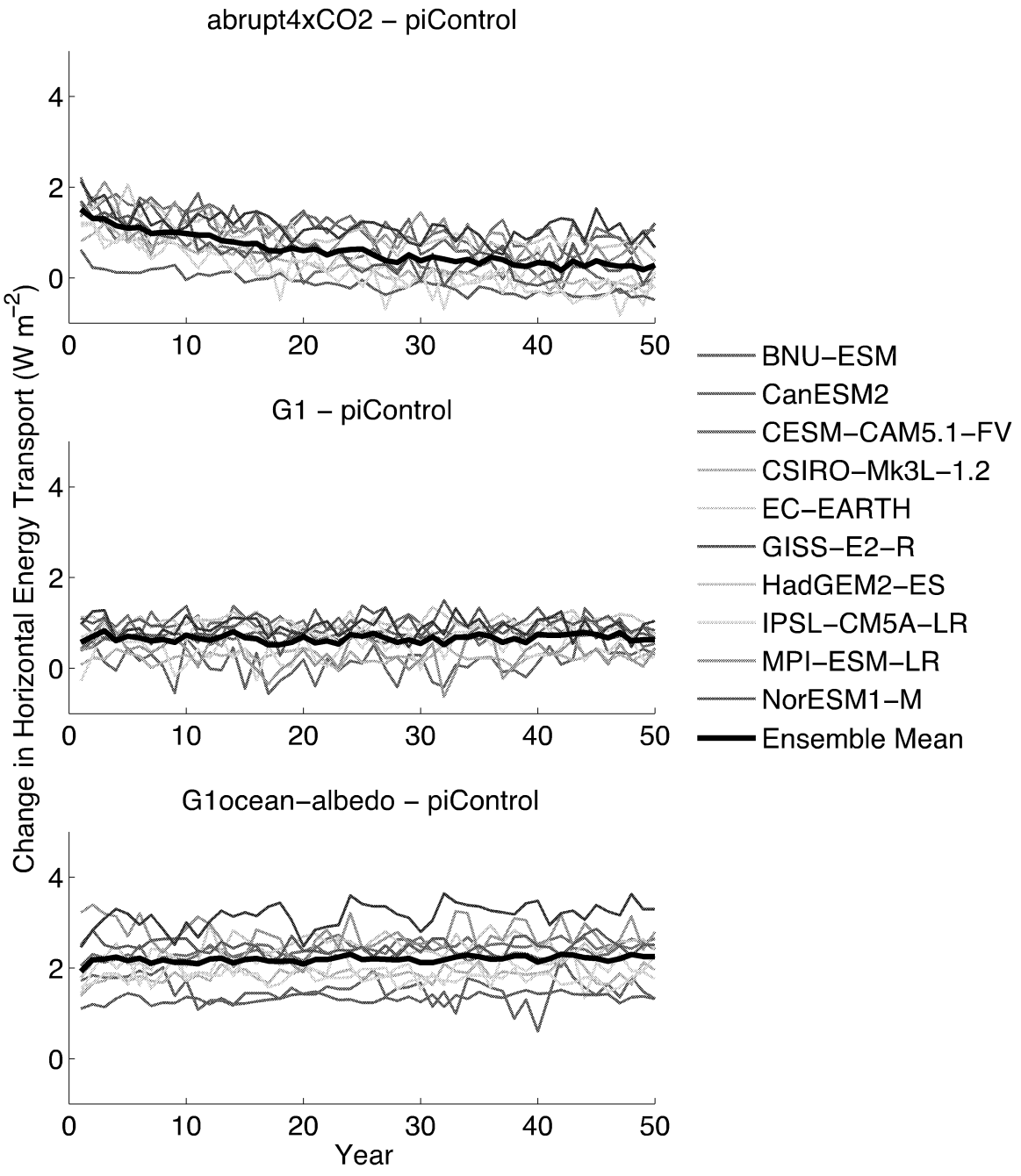

Figure 5. Annual mean change in land-ocean energy transport (Section 3.3; W m^{-2}) from piControl. See Equation 2 for a formal definition.

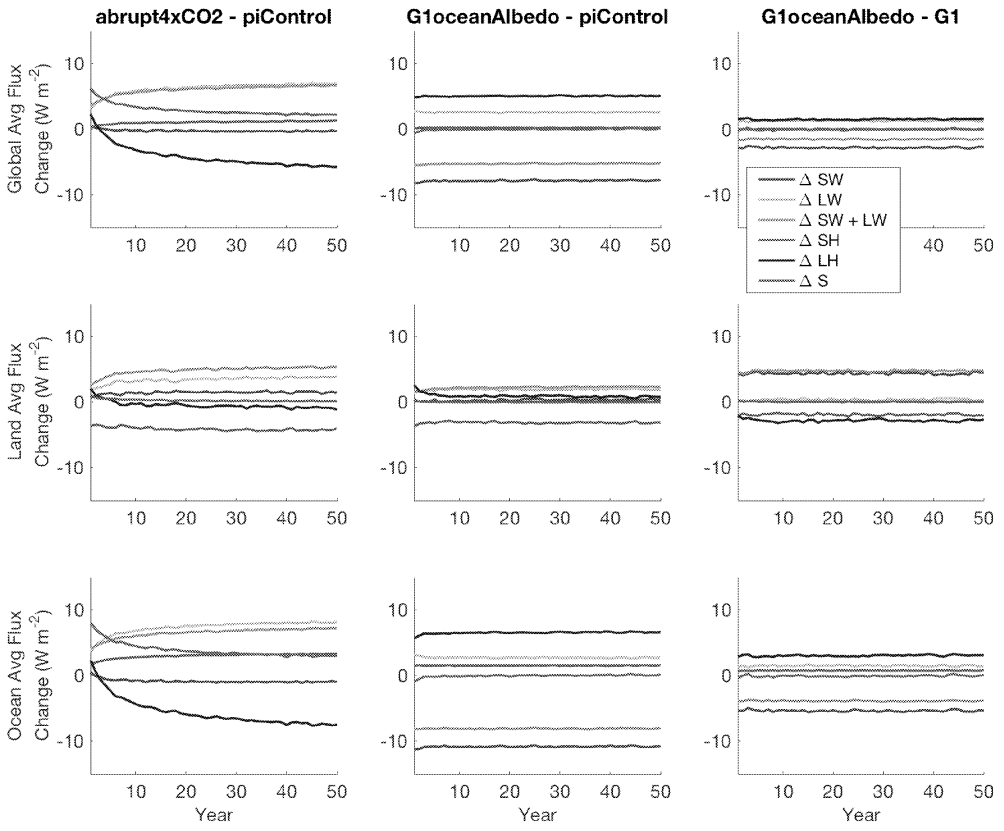

835
836
837 **Figure 6.** Annual mean time series of all-model mean surface fluxes (terms in
838 Equation 3) for global averages (top), land averages (middle), and ocean averages
839 (bottom). All fluxes are positive in the downward direction.

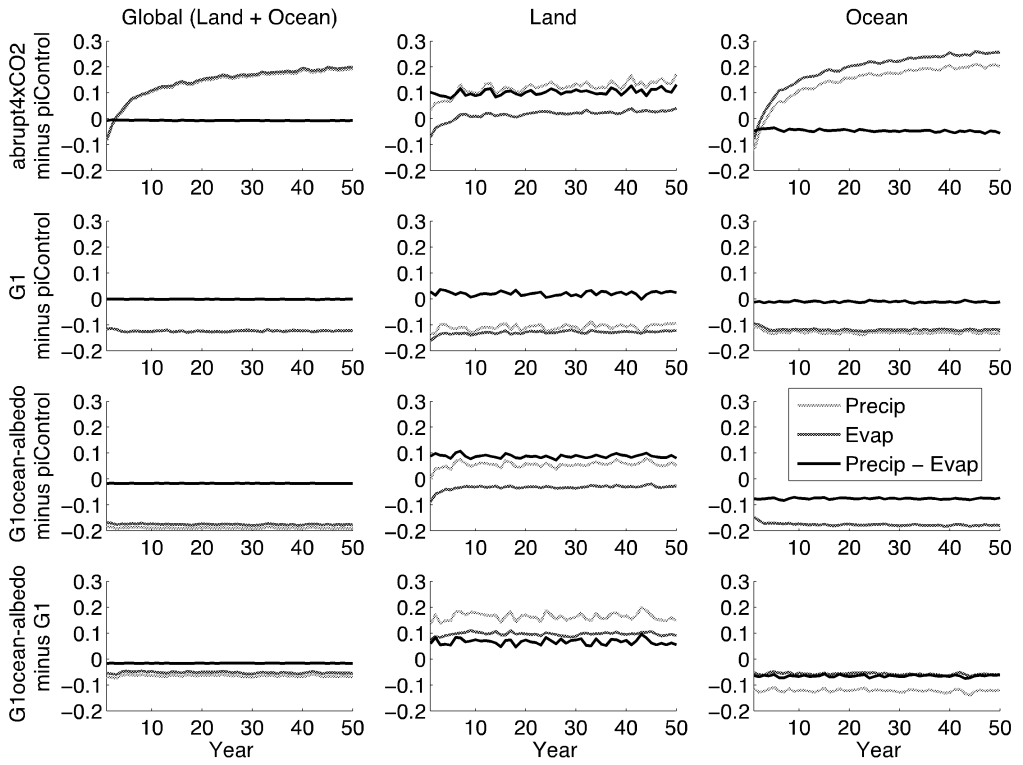

840
841
842 **Figure 7.** Annual mean time series of hydrological cycle changes (all in mm day^{-1}).
843 Green lines show precipitation changes, red lines show evaporation changes, and
844 black lines show precipitation minus evaporation. In the first column, green lines
845 are difficult to see because they are largely overlaid by red lines. In the third row,
846 third column, the green line has values below -0.2 for all years.

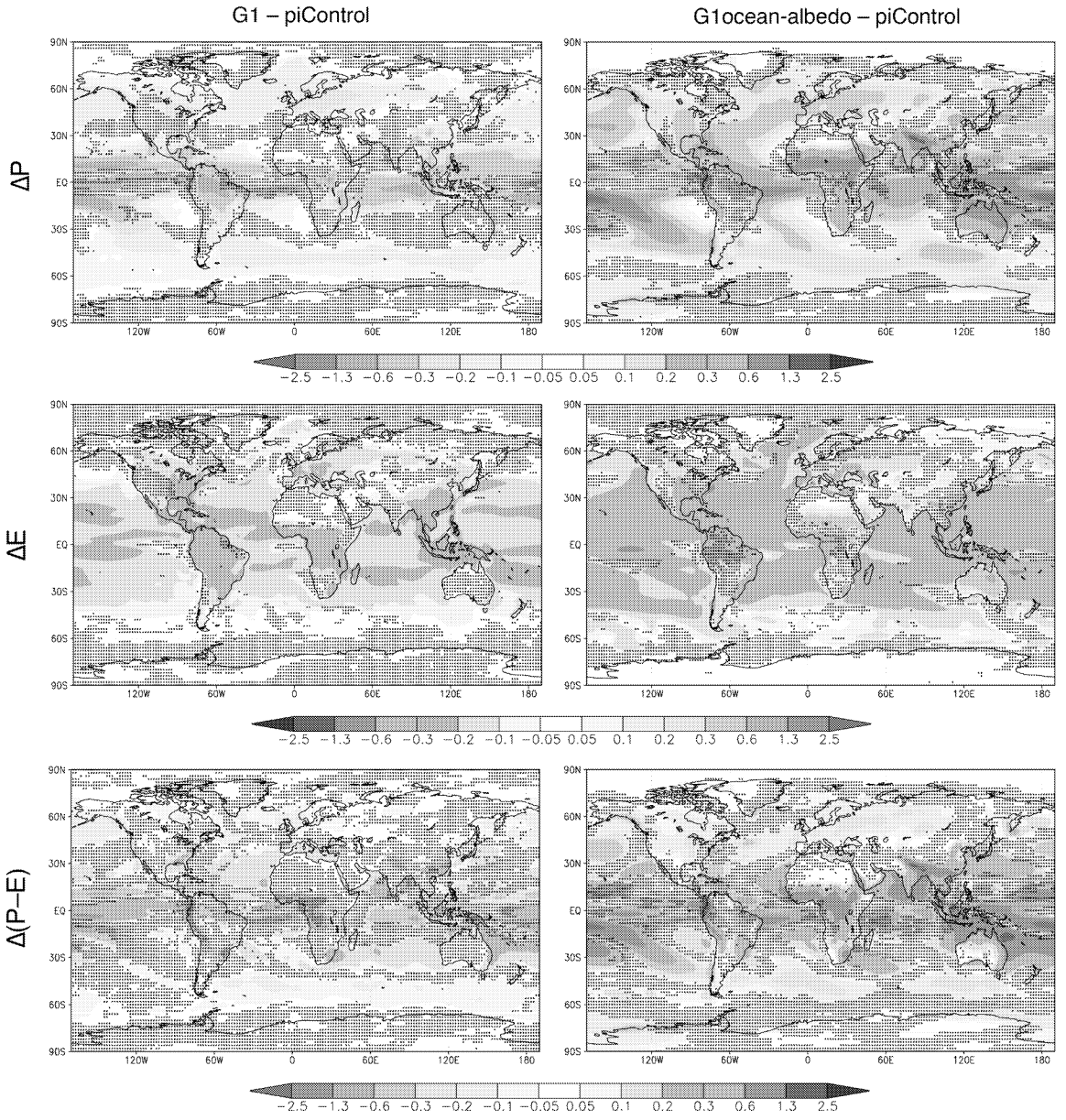

847
848
849 **Figure 8.** Precipitation (top row), evaporation (middle row), and precipitation
850 minus evaporation (bottom row) changes (all panels have units mm day^{-1}) for
851 experiments G1 and G1ocean-albedo. Values are averages over years 11-50 of
852 simulation. Stippling indicates where fewer than 8 out of 11 models agree on the
853 sign of the response.
854

The climate effects of increasing ocean albedo: An idealized representation of solar geoengineering

Ben Kravitz[1], Philip J. Rasch[1], Hailong Wang[1], Alan Robock[2], Corey Gabriel[3], Olivier Boucher[4], Jason N. S. Cole[5], Jim Haywood[6,7], Duoying Ji[8], Andy Jones[6], Andrew Lenton[9], John C. Moore[8], Helene Muri[10,11], Ulrike Niemeier[12], Steven Phipps[13,14], Hauke Schmidt[12], Shingo Watanabe[15], Shuting Yang[16], and Jin-Ho Yoon[17]

[1]Atmospheric Sciences and Global Change Division, Pacific Northwest National Laboratory, Richland, WA, USA
[2]Department of Environmental Sciences, Rutgers University, New Brunswick, NJ, USA
[3]Scripps Institution of Oceanography, La Jolla, CA, USA
[4]Laboratoire de Météorologie Dynamique, CNRS / Sorbonne Université, Paris, France
[5]Environment and Climate Change Canada, Toronto, Canada
[6]Met Office Hadley Centre, Exeter, UK
[7]College of Engineering, Mathematics, and Physical Sciences, University of Exeter, Exeter, UK
[8]State Key Laboratory of Earth Surface Processes and Resource Ecology, College of Global Change and Earth System Science, Beijing Normal University, Beijing, China
[9]CSIRO Oceans and Atmosphere, Hobart, Tasmania, Australia
[10]Department of Geosciences, University of Oslo, Oslo, Norway
[11]Department of Energy and Process Engineering, Norwegian University of Science and Technology, Trondheim, Norway
[12]Max Planck Institute for Meteorology, Hamburg, Germany
[13]Climate Change Research Centre, University of New South Wales, Sydney, Australia
[14]Institute for Marine and Antarctic Studies, University of Tasmania, Hobart, Tasmania, Australia
[15]Japan Agency for Marine-Earth Science and Technology, Yokohama, Japan
[16]Danish Meteorological Institute, Copenhagen, Denmark
[17] School of Earth Sciences and Environmental Engineering, Gwangju Institute of Science and Technology, Gwangju, South Korea

Correspondence: Ben Kravitz, P.O. Box 999, MSIN K9-30, Richland, WA 99352, USA. (ben.kravitz@pnnl.gov)

Abstract. Geoengineering or climate intervention describe methods of deliberately altering the climate system to offset anthropogenic climate change. As an idealized representation of near-surface solar geoengineering over the ocean, this paper discusses experiment G1ocean-albedo of the Geoengineering Model Intercomparison Project (GeoMIP), involving an abrupt quadrupling of the CO_2 concentration and an instantaneous increase in ocean albedo to maintain approximate net top-of-atmosphere radiative flux balance. Eleven Earth System Models are relatively consistent in their temperature, radiative flux, and hydrological cycle responses to this experiment. Due to the imposed forcing, air over the land surface warms by a model average of 1.14 K, while air over most of the ocean cools. Some parts of the near-surface air temperature over ocean warm due to heat transport from land to ocean. These changes generally resolve within a few years, indicating that changes in ocean heat content play at most a small role in the warming over the oceans. The hydrological cycle response is a general slowing down, with high heterogeneity in the response, particularly in the tropics. While idealized, these results have important implications for marine cloud brightening, or other methods of geoengineering involving spatially heterogeneous forcing, or other general

forcings with a strong land/ocean contrast. It also reinforces previous findings that keeping top-of-atmosphere net radiative flux constant is not sufficient for preventing changes in global mean temperature.

1 Introduction

Geoengineering (also called "climate intervention") describes a set of technological approaches to reduce the effects of climate change by deliberately intervening in the climate system (e.g., Shepherd et al., 2009). There are two broad categories of geoengineering that are commonly discussed: solar geoengineering (modifying the amount of shortwave radiation incident at the surface; NAS, 2015b) and carbon dioxide removal (NAS, 2015a). There are also proposals, such as cirrus cloud thinning (Mitchell and Finnegan, 2009) that do not fit neatly into either of these two categories. In all subsequent discussions in this manuscript, we only discuss solar geoengineering methods.

Two of the most commonly proposed methods of global geoengineering are stratospheric sulfate aerosol geoengineering and marine cloud brightening (MCB). Comparison of the different climate effects of these two methods (e.g., Niemeier et al., 2013; Crook et al., 2015) reveals that, among other things, the spatial distribution of the applied forcing strongly affects the climate effects. Many of the effects of sulfate geoengineering can be reasonably well approximated by a uniform reduction in shortwave radiative flux reaching the surface (Kalidindi et al., 2014). Conversely, MCB targets low clouds over oceans (Latham, 1990), which are not ubiquitous. In addition, there are higher-order effects due to the altitude at which the shortwave scattering occurs, including multiple scattering effects, infrared absorption of shortwave and longwave radiative flux by sulfate aerosols or cloud particles, and absorption of shortwave radiative flux by atmospheric CO_2 and water vapor (e.g., Kravitz et al., 2013b).

Idealized simulations of solar geoengineering are useful in the context of multi-model intercomparisons, in that they capture many of the effects of more complicated methods of representing geoengineering, yet can be performed by a wide variety of models. In simulations conducted under the Geoengineering Model Intercomparison Project (GeoMIP; Kravitz et al., 2011), an idealized method of representing stratospheric sulfate aerosol geoengineering is via reductions in total solar irradiance. As an example of this representation, experiment G1 involved offsetting the global radiative flux imbalance from a quadrupling of the CO_2 concentration via solar reduction. Thus far, 15 models have participated in this simulation, providing information about model commonalities and differences in the global climate response, including effects on temperature, the hydrological cycle, cryosphere, terrestrial biosphere, and extreme events (Schmidt et al., 2012; Kravitz et al., 2013a, b; Tilmes et al., 2013; Moore et al., 2014; Glienke et al., 2015; Curry et al., 2014, among numerous other studies). The GeoMIP website (http://climate.envsci.rutgers.edu/GeoMIP/) provides an up-to-date list of publications using GeoMIP model output.

While total solar irradiance reductions are straightforward to simulate in all models, this idealization is not a good approximation of MCB, nor of near-surface solar geoengineering approaches over the ocean in general. The dominant effect of MCB

would be an increase in albedo of marine low clouds through aerosol effects. More generally, changes in the albedo near the marine surface (such as in the G4Foam experiment; Gabriel et al., 2017) can produce different signatures from reductions in energy input at the top of the atmosphere, particularly in terms of spatial distribution. While some forms of albedo modification like stratospheric sulfate aerosol geoengineering operate over broad areas (on a hemispheric or larger scale), albedo changes produced by near-surface marine geoengineering would operate on smaller spatial scales and be concentrated over particular oceanic regions.

In this study, we investigate the climate effects of using ocean albedo increases to offset CO_2 warming and compare those effects with those of total solar irradiance reduction (experiments are described in more detail in the following section). All simulations were conducted under the auspices of GeoMIP, allowing us to characterize a range of model responses to these different idealized methods of representing solar geoengineering.

2 Methodology and Description

Our analyses focus on four simulations: (1) a preindustrial control simulation (piControl), (2) a simulation in which the CO_2 concentration is abruptly quadrupled from its preindustrial value (abrupt4xCO2), (3) a simulation in which the net radiative flux imbalance in abrupt4xCO2 is offset by a reduction in total solar irradiance (G1), and (4) a simulation in which the net top-of-atmosphere radiative flux imbalance in abrupt4xCO2 is offset by an increase in ocean albedo everywhere by a uniform factor (G1ocean-albedo). piControl and abrupt4xCO2 are standard experiments in the Coupled Model Intercomparison Project Phase 5 (CMIP5; Taylor et al., 2012). G1 is described further by Kravitz et al. (2011), and many of the gross features of the results are described by Kravitz et al. (2013a). All models participating in experiment G1 needed to reduce model total solar irradiance by 3.5-5.0% to offset the radiative forcing from a quadrupling of the CO_2 concentration. In G1ocean-albedo, the ocean surface albedo was increased abruptly at the start of the simulation such that net top-of-atmosphere radiative flux perturbation was within ± 0.1 W m^{-2} of the piControl value in an average over years 21-30 of simulation. Based on preliminary simulations described by Kravitz et al. (2013c), it took approximately 20 years for the climate to reach steady state after an abrupt simultaneous change in the CO_2 concentration and the ocean albedo. As will be shown in subsequent sections, once the appropriate value of ocean albedo increase is found and imposed, the climate system adjusts rapidly, requiring at most a few years to reach steady state (as was the case in experiment G1). Table 1 lists the models participating in this study, including relevant references and the required change in albedo to meet the objectives of experiment G1ocean-albedo. A similar table for experiment G1 is given by Kravitz et al. (2013a). One of the advantages of G1ocean-albedo is that, like G1, all models can conduct this simulation fairly easily. Supplemental Table S1 quantifies how well each model achieved radiative balance in the G1 and G1ocean-albedo experiments.

Kravitz et al. (2013c) found that in test simulations, one could only determine whether the objectives of G1ocean-albedo were met after several decades of simulation. However, as our analysis will show, once the proper value of ocean albedo increase is ascertained, the climate response reaches steady state in a few years, as in experiment G1 (Kravitz et al., 2013a). Supplemental Table S2 quantifies temperature trends in each participating model over years 11-50 of simulation. The mean

model trend over this period is approximately zero K decade^{-1} (to four decimal places), and with little exception, the trends in G1 and G1ocean-albedo are an order of magnitude smaller than the trends in the abrupt4xCO2 simulation. As such, for the purpose of analysis, we assume that "slow responses," i.e., responses operating on time scales longer than a few years (e.g., Andrews and Forster, 2010; Sherwood et al., 2015) are negligible in the G1 and G1ocean-albedo simulations. We do not separate results into rapid adjustment and slow response timescales, and with the exception of time series plots, all figures show averages over the years 11-50 of simulation, which we take as a sufficient indication of the dominant climate response after the transient response has resolved.

Except where indicated, all plots show the mean model response. All values in the text are reported as mean (min to max), where mean indicates the all-model mean for that particular quantity, min is the lower bound of the range of model responses, and max is the upper bound of the range of model responses. In all maps, stippling indicates where fewer than 75% of the models agree on the sign of the response. All models in Table 1 were able to provide output for all variables except for cloud radiative forcing. The models included in cloud forcing analyses are BNU-ESM, CanESM2, CESM-CAM5.1-FV, HadGEM2-ES, IPSL-CM5A-LR, and MPI-ESM-LR. Supplemental Tables S1-S15 provide more quantitative information for all of the analyses presented in this study.

3 Results

3.1 Albedo and Temperature

Figure 1 shows the change in albedo at the top-of-atmosphere and at the surface for the abrupt4xCO2, G1, and G1ocean-albedo simulations, where albedo is defined as the ratio of upwelling to downwelling all-sky shortwave radiative flux. Quantitative values are given in Supplemental Tables S3 and S4. Results for abrupt4xCO2 and G1 are consistent with known responses of an increase in absorbed shortwave by increased CO_2, reduced cloud cover, and reduced snow and sea ice cover (e.g., Schmidt et al., 2012; Kravitz et al., 2013b). These result in a broad decrease in albedo at the top of atmosphere and a decrease in surface albedo in many regions with substantial snow and ice cover. G1ocean-albedo retains many of these local high latitude features, but with large albedo increases over ocean, consistent with the experimental design and imposed forcing.

Figures 2 and 3 expand upon this picture by showing changes in shortwave and longwave cloud forcing and clear sky flux in G1 and G1ocean-albedo. In Figure 2, cloud forcing is defined as all-sky minus clear-sky radiative flux measured at the top of the atmosphere. Positive shortwave values and negative longwave values in Figure 2 are indicative of less cloud cover. In Figure 3, values indicate changes in top-of-atmosphere net clear sky flux, where net is defined as downward minus upward. Positive values indicate less upward flux in the perturbed experiment (G1 or G1ocean-albedo), and negative values indicate more upward flux.

Kravitz et al. (2013b) showed that cloud cover in G1 tends to be reduced, which is consistent with what is depicted in Figure 2 over broad swaths of the globe. For G1ocean-albedo, cloud cover is reduced over most ocean regions and large portions of land. Exceptions include negative shortwave and positive longwave values over the Arctic, much of Africa, South Asia, Australia, and the leeward side of the Andes. The results of Figure 3 are consistent with an increase in the CO_2 concentration, with more

absorption of shortwave and more outgoing longwave radiative flux. Exceptions are many of the same regions as in Figure 2, which show negative (or less positive) shortwave values and less negative longwave values. Thus, over most regions of the globe, the results are consistent with a combination of increased CO_2 and less cloud cover. Over the other regions (named previously), Figure 2 would indicate that cloud cover increases, which would result in less shortwave absorption and less outgoing longwave radiative flux, consistent with the results in Figure 3. These changes in cloudiness have implications for the hydrologic cycle, which we revisit in Section 3.5.

Figures 2 and 3 admittedly only report the first-order explanations of the radiative flux changes in G1 and G1ocean-albedo. Second-order effects could include additional shortwave absorption by clouds or feedbacks on water vapor flux due to reduced evaporation. Additional work is needed to better understand the role of individual flux changes and processes on clouds and circulation patterns.

Figure 4 shows changes in global mean, land mean, and ocean mean surface air temperature for the G1 and G1ocean-albedo multi-model ensembles. Quantitative values are provided in Supplemental Table S5. Whereas the G1 simulation largely offsets global temperature changes due to increased CO_2 concentration, G1ocean-albedo is approximately 0.36 K (-0.12 to 1.20) warmer than the control simulation. This is predominantly due to warming over land by 1.14 K (0.41 to 1.83). The temperature results in Figure 4 indicate that the temperature change happens within the first few years, and while some models show a slight trend in temperature over the 50-year G1ocean-albedo simulation (Supplemental Table S2), in general, any such trends are small, especially as compared to the warming in the abrupt4xCO2 simulation. This lack of substantial transient behavior after an initial fast response indicates that G1ocean-albedo has entered a new approximate steady state.

Figure 5 shows spatial patterns of change in temperature and top-of-atmosphere net radiative flux. (Also see Supplemental Tables S5 and S6.) The temperature changes are broadly consistent with the net radiative flux changes in the respective experiments. As was discussed by Kravitz et al. (2013a), G1 results in an "overcooling" of the tropics and an "undercooling" of the poles, consistent with offsetting the ubiquitous longwave forcing from CO_2 with a latitudinally dependent reduction in shortwave. G1ocean-albedo shows warming at high latitudes, over land regions, and in some ocean regions near or downwind of large continents, with the remaining ocean regions generally showing cooling.

While the warming over land is easily explainable from first principles, the temperature response over the ocean is heterogeneous (likely due to clouds – see above), and it is perhaps somewhat counterintuitive that on average temperatures over the global oceans do not decrease. Because net top-of-atmosphere radiative flux is approximately zero in G1ocean-albedo, the global warming cannot be the result of energy being added to or subtracted from the climate system, and instead must be the result of energy redistribution. Three hypotheses for why these temperature change patterns look the way they do (which will be tested in subsequent sections) include

1. Based on energy balance arguments, G1ocean-albedo should experience global average warming.
2. Most warming over oceanic regions is due to transport of heat from land to ocean.
3. Any contributions to temperature or radiative flux changes from changes in ocean heat content are small on the timescales being evaluated here.

3.2 Hypothesis 1: Energy Balance

The Earth system can be considered as a simple surface-atmosphere energy budget model

$$\frac{S(1-A)}{4} = (1-\epsilon/2)\sigma T_s^4 \tag{1}$$

where S is total solar irradiance at the top of the atmosphere (i.e., the solar "constant"), A is albedo of Earth, ϵ is the longwave emissivity of the atmosphere, and T_s is surface temperature. In this model, $T_s = 2^{1/4}T_a$, where T_a is atmospheric temperature.

Taking the total differential yields

$$\frac{dS(1-A)}{4} - \frac{SdA}{4} = \left(1-\frac{\epsilon}{2}\right)4\sigma T_s^3 dT_s - \frac{d\epsilon}{2}\sigma T_s^4 \tag{2}$$

Isolating dT_s yields

$$dT_s = \left[\frac{dS(1-A)}{4} - \frac{SdA}{4} + \frac{d\epsilon}{2}\sigma T_s^4\right] / \left[\left(1-\frac{\epsilon}{2}\right)4\sigma T_s^3\right] \tag{3}$$

Simplifying,

$$dT_s = \frac{dS(1-A)}{16\sigma T_s^3(1-\epsilon/2)} - \frac{SdA}{16\sigma T_s^3(1-\epsilon/2)} + \frac{d\epsilon/2}{1-\epsilon/2}\frac{T_s}{4} \tag{4}$$

From Equation 1 and using $T_s = 286.491$ K (the average piControl value from the Earth System Models), $S = 1366$ W m^{-2}, and $A = 0.3$, it follows that $\epsilon = 0.748$.

Equation 4 can be augmented to consider changes in land and ocean components separately. F_ℓ and F_o are the land and ocean fractions, 0.3 and 0.7 respectively, such that $F_\ell + F_o = 1$. The land and ocean albedos are A_ℓ and A_o, respectively. Greenhouse gases are assumed to be well mixed (i.e., $d\epsilon$ is the same over land and ocean). Then after solving for change in ocean temperature $dT_{s,o}$, Equation 4 becomes

$$dT_{s,o} = \frac{1}{F_o}\left[\frac{(F_\ell dS_\ell + F_o dS_o)(1-A)}{16\sigma T_s^3(1-\epsilon/2)} - \frac{S(F_\ell dA_\ell + F_o dA_o)}{16\sigma T_s^3(1-\epsilon/2)} + \frac{d\epsilon/2}{1-\epsilon/2}\frac{T_s}{4} - F_\ell dT_{s,\ell}\right] \tag{5}$$

Nearly all of the variables on the right sides of Equations 4 and 5 can be solved from values provided in the supplemental material, values provided above, and $dS/S = -0.042$ (Kravitz et al., 2013b). The only variable that is difficult to solve for in this idealized context is $d\epsilon$, representing changes in emissivity. Such changes can occur due to changes in the CO_2 concentration (or other greenhouse gases), changes in water vapor, or changes in cloud cover. Estimating this quantity using the abrupt4xCO2 scenario would correctly capture changes in emissivity due to CO_2 changes under the G1ocean-albedo simulation, but it would likely overestimate contributions due to water vapor because of tropospheric warming. As such, estimates of $d\epsilon$ under G1ocean-albedo will be calculated using G1, which will capture changes in emissivity from the CO_2 changes but without large changes in atmospheric water vapor. Admittedly, water vapor and cloud cover will likely differ between G1 and G1ocean-albedo, rendering this estimate imperfect. However, this process is far more likely to yield an appropriate result than using abrupt4xCO2.

Using Equation 4 and substituting $dT_s = 0$ K, $dS = 1366 \cdot (-0.042)$ W m^{-2}, $A = 0.3$, $T_s = 286.491$ K, $\epsilon = 0.748$, and $dA = -0.007$ (Supplemental Table S3) yields $d\epsilon = 0.0401$. For G1, each of the three terms on the right side of Equation 4 are

then -3.01, 0.72, and 2.29 K, respectively. The first of these terms corresponds to solar changes, the second term is for planetary albedo changes, and the third term is for emissivity (greenhouse gas) changes.

From the Supplemental Tables, for G1ocean-albedo, $dA_o = 0.023$, $dA_\ell = -0.004$, $dS_\ell = dS_o = 0$, and $dT_{s,\ell} = 1.14$ K. Then substituting into Equation 5 yields $dT_{s,o} = 0.61$ K, which is higher than the Earth System Model ensemble average of 0.03 K. For comparison with the values from G1, the term corresponding to changes in solar input is 0 K, the term corresponding to changes in albedo is -1.52 K, and the term for changes in emissivity is 2.29 K. By Equation 4, these values yield a global mean temperature change of 0.77 K, which is higher than the Earth System Model ensemble average of 0.36 K.

This simple energy balance formulation clearly cannot incorporate all of the feedbacks and complex behaviors of the Earth System Models. Nevertheless, based on energy balance constraints, G1ocean-albedo results in both land and ocean warming. However, the values recovered by the energy balance model are not entirely consistent with the results of the Earth System Models for G1ocean-albedo. To account for these differences, we turn to circulation changes, which are described in the following section.

3.3 Hypothesis 2: The role of Land-Ocean Energy Transport (LOET)

Although the air over the ocean warms somewhat in G1ocean-albedo, it does not warm uniformly. Figure 5 shows that much of the warming over the ocean is in areas near land, indicating the potential for some of the heating energy over land to be transported to ocean regions. Indeed, the oceans far from land experience cooling, which is consistent with expectations for a large increase in albedo (Table 1).

Transport of heating energy from land to ocean can be quantified via calculating what Geoffroy et al. (2015) call horizontal energy transport, and which we call land-ocean energy transport (LOET), as it represents an aggregate transport of energy from the atmosphere over the land (averaged over all land regions) to the atmosphere over the ocean (averaged over all ocean regions). Geoffroy et al. (2015) provide a more detailed description, calculation, and validation of this concept using a three-box energy balance model that can be fitted to changes in land/ocean temperature and TOA energy imbalance such that the model captures the relevant energy transport dynamics; we repeat here only the calculations germane to our discussions.

Gregory et al. (2004) describe a method of estimating adjusted radiative forcing and the aggregate strength of global feedbacks via linear regression of the net global, annual mean TOA radiative flux imbalance (ΔR) against the global, annual mean temperature change (ΔT) in response to a forcing. The y-intercept of the regression line gives an estimate of adjusted radiative forcing ($\mathcal{F}$), and the negative of the slope of the regression line gives the feedback parameter (λ). Similarly, one can perform regression just over land-averaged quantities (denoted with the subscript ℓ) or just over ocean quantities (subscript o). Feedback parameter values are provided in Table 2.

In addition, as is derived in detail by Geoffroy et al. (2015), one can regress ΔT_ℓ against ΔT_o to obtain the equation

$$\Delta T_\ell = \frac{\alpha_o / F_\ell}{\lambda_\ell + \alpha_\ell / F_\ell} \delta T_o + \frac{\mathcal{F}}{\lambda_\ell + \alpha_\ell / F_\ell} \tag{6}$$

where α_ℓ is the land heat transport parameter (units of W m^{-2} K^{-1}) and F_ℓ is the land fraction (approximately 0.3). If one solves this equation for α_ℓ and α_o, then one can define

$$\Delta Q = \alpha_\ell \Delta T_\ell - \alpha_o \Delta T_o \tag{7}$$

The quantity ΔQ is the time-dependent LOET (units of W m^{-2}).

Figure 6 provides calculations of LOET for the simulations presented here. See Supplemental Table S7 for more details on individual model values. In the abrupt4xCO2 simulation, changes in LOET are positive (indicating an increase in heat transport from the land to the ocean) and decrease in magnitude steadily over the course of the simulation; these results are discussed in more detail by Geoffroy et al. (2015).

In experiment G1, LOET increases by a model-dependent constant value and remains relatively unchanged over the course of the simulation. Although the air temperature over land in G1 increases slightly, and the air temperature over ocean decreases slightly (Kravitz et al., 2013a), the temperature changes in G1 are more latitude-dependent than representative of a clear land-ocean contrast (Figure 5), so it is perhaps not unexpected that LOET would be small.

Experiment G1ocean-albedo exhibits a strong land-ocean contrast in temperature (Figure 5), and the response is in steady state after a few years. As such, consistent with the behavior of other fluxes, LOET in G1ocean-albedo does not show transient behavior. LOET in G1ocean-albedo is approximately 2.20 (1.35 to 3.21) W m^{-2}, which is larger than in the other experiments examined here.

Based on the calculations in the present section, it seems unlikely that LOET can on average transport enough energy from the land to the ocean to offset the radiative deficit over the ocean due to an ocean albedo increase. However, locally, LOET appears to be able not only to offset these radiative changes, but also result in net warming.

3.4 Hypothesis 3: Atmospheric Column Energetics and Net Energy Flux into the Oceans

An additional potential source of energy to the atmosphere is a reduction in net ocean heat uptake. Calculating changes in ocean heat uptake are challenging and not particularly revealing in this study for three reasons:

1. It is possible that the models used in simulating G1ocean-albedo were not entirely spun up to steady state. As such, any remaining imbalances could manifest as changes in ocean heat content. In principle, one could subtract off the preindustrial control value, which likely has a similar trend in ocean heat content arising from spinup. However, this would not remove the influence of nonlinearities (state dependence), so there is no way to guarantee that the signal is entirely due to the G1ocean-albedo forcing.

2. As is seen in Supplemental Table S1, not all models were able to achieve top-of-atmosphere net radiative flux balance over the course of the simulation. These small changes can lead to large changes in ocean heat content over the course of a 50-year simulation, consistent with CMIP5 models (Hobbs et al., 2016). For example, a 0.1 W m^{-2} imbalance over a 50-year period can lead to an additional 5.5×10^{22} J of energy incident at the ocean surface. As such, we are unable to properly assess the degree to which ocean heat content changes may be due to small imbalances.

3. Ocean heat content can be (and is often) calculated up to a certain depth, meaning calculations of it can be sensitive to redistribution of heat to/from lower depths, obscuring the signal of the forcing.

As an alternative, we calculate net energy exchange across the surface in terms of changes in radiative and turbulent fluxes. Kravitz et al. (2013b) calculated energetics changes in the entire atmospheric column. However, because we are only interested in net surface fluxes, we calculate

$$\Delta B = \Delta R_{\text{surf}} + \Delta SH + \Delta LH \tag{8}$$

where ΔR_{surf} is the change in net surface radiative flux (shortwave and longwave), ΔSH is change in sensible heat flux from the atmosphere to the surface, and ΔLH is change in latent heat flux from the atmosphere to the surface. By convention, all fluxes are positive downward unless specifically noted. Calculations of individual terms in this budget, as well as of ΔB, are provided in Supplemental Tables S8-S12. Because these calculations are performed at the surface, no advection term (e.g., LOET) is needed, and ΔB is well defined as a land or ocean average.

Figure 7 shows the all-model mean for all of the terms in Equation 8. Several clear conclusions emerge. The first is that ΔB is approximately zero globally, over land, and over ocean for nearly the entire 50-year period, after an initial rapid adjustment that resolves within a few years. With the exception of latent heat over land, all fluxes for G1ocean-albedo reach a steady state after a few years (Figure 7), and even latent heat flux over land reaches an approximate steady state within ten years. If ΔB indeed serves as a useful proxy for global net energy flux into or out of the ocean, then these results indicate that there is no sizable contribution to atmospheric energetics by changes in global mean ocean heat content. Moreover, even if ΔB were not zero over ocean, global mean ocean heat content changes would still be an insufficient explanation for global mean temperature changes due to incongruent timescales. The oceanic mixed layer operates on an approximately decadal timescale, but all transient behavior in these simulations is resolved well before ten years. The transient response is much more consistent with a land surface time scale, which is on the order of 1-3 years. As such, it seems plausible that the temperature changes over ocean in G1ocean-albedo are due to land processes and land surface feedbacks rather than ocean heat content changes. This is not to say that the ocean plays no role in the observed temperature changes. Rather, given the discussions in this section and the two previous sections, the role of global mean ocean heat content in causing temperature changes over the ocean in G1ocean-albedo (over the timescales being analyzed here) is likely small. Because forcings and feedbacks are likely to be realized heterogeneously, there may be roles for local changes or for patterns of circulation (e.g., the Atlantic meridional overturning circulation) in altering oceanic heat content. However, such analyses are beyond the scope of the present work.

The remainder of the results in Figure 7 are consistent with the applied forcing. There is a large sensible heat flux increase from the land to the atmosphere of 2.87 (-0.99 to 6.00) W m^{-2}, with a comparatively smaller sensible heat flux decrease from the ocean to the atmosphere of 1.47 (0.34 to 2.20) W m^{-2}. Over the ocean, latent heat flux from the surface to the atmosphere is 6.71 (4.95 to 7.89) W m^{-2} lower in G1ocean-albedo than in the preindustrial control simulation. These results indicate a greater shift of energy away from evaporating water and toward increasing land temperature. Large differences in flux magnitude between G1 and G1ocean-albedo can be found over land for net shortwave flux and latent heat flux, and differences

in sign can be found over land for total radiative flux. These features are consistent with the applied forcing being different over land and ocean.

3.5 Hydrological cycle changes

Introducing a strong land-ocean energy and temperature gradient, as in G1ocean-albedo, will undoubtedly impact the hydrological cycle. Although the G1ocean-albedo simulation is idealized, more realistic representations of MCB have shown important hydrological cycle impacts, including secondary circulation patterns that shift precipitation onto land in the tropics and extratropics (Bala et al., 2010; Alterskjær et al., 2013) and changes in the Walker circulation (Niemeier et al., 2013). Here we evaluate the large-scale hydrological cycle changes in G1ocean-albedo, with possible applicability to other realizations of MCB.

Figure 8 shows global, land, and ocean averaged precipitation, evaporation, and precipitation minus evaporation (P-E) for all of the simulations considered in this manuscript; quantitative descriptions are given in Tables S13-15. The abrupt4xCO2 simulation is the only one with a distinct rapid adjustment and slow response. Over both land and ocean, G1 shows decreases in precipitation and evaporation of approximately equal magnitude, resulting in net changes in P-E of 0.02 (-0.05 to 0.11) mm day^{-1} over land and -0.01 (-0.04 to 0.01) mm day^{-1} over ocean. In G1ocean-albedo, global precipitation and evaporation both decrease by approximately 0.19 (0.11 to 0.26) mm day^{-1} to yield little net change in P-E. However, this net small change is due to differential effects over land and ocean. Over land, precipitation remains relatively unchanged, but evaporation decreases, resulting in a net change in P-E by 0.09 (-0.18 to 0.18) mm day^{-1}. Over the ocean, both precipitation and evaporation decrease, with a net negative P-E of -0.06 (-0.19 to -0.01) mm day^{-1}.

Annual mean land/ocean contrasts in precipitation and evaporation changes tend to be more uniform in sign in experiment G1 (Figure 9), resulting in few large regions of change in P-E with the exception of the tropics (mostly driven by a southward shift in the intertropical convergence zone; Kravitz et al., 2013a). In G1ocean-albedo, precipitation and evaporation over the oceans are reduced in most regions, consistent with the applied forcing. Over land, the signs of precipitation and evaporation changes are regionally heterogeneous, yet the precipitation and evaporation changes are concordant, e.g., land regions with increased precipitation also generally show increased evaporation. The net P-E map is highly heterogeneous, but in general, tropical land areas are projected to have more available moisture (as measured by P-E) under G1ocean-albedo, and midlatitude land areas are projected to have less. There is a general drying (reduced P-E) in the midlatitudes, as well as some reductions in the intertropical convergence zone, with important implications for tropospheric circulation (to be evaluated in future work).The implications of these changes for people and ecosystems are also important to investigate further.

4 Discussion and Conclusions

In Section 3.1, three hypotheses were posed as to why G1ocean-albedo experienced warming over both land and ocean. Based on the analysis presented here, we confirmed that G1ocean-albedo should experience global average warming, based on energy balance arguments. However, energy balance arguments alone cannot explain the magnitude of oceanic warming.

Explaining that warming requires a model that can represent horizontal transport of heat from the land to the ocean. Because these processes reach steady state within a decade or less, it is unlikely that long-term oceanic processes, including changes in global mean ocean heat content, are responsible for the majority of the changes seen in G1ocean-albedo.

The results presented here indicate that even though experiments G1 and G1ocean-albedo both achieve approximate net top-of-atmosphere radiative flux balance, the climate system responses differ dramatically between the two experiments. The idea that global energy balance can still result in local changes is perhaps not surprising, as feedbacks operate locally (Armour et al., 2013). These different climate responses for the same magnitude in global forcing are effectively an illustration of different efficacies (Hansen et al., 2005). Even in the absence of slow responses, forcings with different efficacies can cause different climate system changes (Kravitz et al., 2015). G1ocean-albedo serves as an excellent reminder not to conflate small net top-of-atmosphere radiative flux imbalance with small temperature change; a clear relationship between those two quantities is not guaranteed.

Relatedly, the results obtained for G1ocean-albedo were to some extent by design. The objective of G1ocean-albedo was to achieve net top-of-atmosphere radiative flux balance, which resulted in warming. Conceivably, one could define an objective of no global temperature change, implying a net negative radiative flux at the top-of-atmosphere, or no global land temperature change, requiring adjustments over the oceans to make up the imbalance. It is unclear whether, unlike G1ocean-albedo, such alternate approaches would result in transient behavior that lasts longer than a few years. Such an experiment could be accomplished using feedback methods that have been introduced to geoengineering research in recent years (e.g., MacMartin et al., 2014b; Kravitz et al., 2016).

Related to this discussion, Supplemental Figures S1-S3 show monthly differences (from piControl) of net top-of-atmosphere radiative flux change and temperature change for the abrupt4xCO2, G1, and G1ocean-albedo simulations. These were calculated by naively subtracting each monthly value of the three perturbed experiments from the monthly values of the corresponding piControl simulation, so all differences are subject to noise introduced by chaos. G1 shows an indication of slight transient behavior, starting out with positive temperature anomaly that relaxes to near-zero within a few years. G1ocean-albedo does not show any discernible anomaly, in that it starts out slightly warmer (globally) than piControl and stays slightly warm. The Gregory plot for G1ocean-albedo similarly shows no discernible trend, unlike the abrupt4xCO2 simulation. There are several possibilities of explanations for this behavior. One is that the adjustments are happening on a short enough timescale in G1ocean-albedo that any transient response is difficult to detect with only monthly averages (Cao et al., 2012). Another possibility is that the noise introduced by chaos on the timescales of interest (months to a few years) obscures our ability to detect any transient behavior. An ensemble of shorter simulations (e.g., Wan et al., 2014) might be well equipped to reveal transience in the response on these timescales. A third option is model artifact related to how the climate models treat energy conservation, indicating that experiments like G1ocean-albedo could be useful in testing models beyond their originally conceived application space. While it is beyond the scope of the present manuscript to fully assess all of these possibilities, it becomes clear that G1ocean-albedo and simulations of geoengineering in general are useful for improving understanding about climate modeling and climate science.

The results presented here have several features that were not necessarily expected from the outset. (Kravitz et al., 2013c) found that determining whether the climate system was in balance took up to 30 years of simulation. However, once that balance is achieved, the climate does not change appreciably after the initial rapid adjustment. Potential future work could investigate these results, shedding light on timescales of climate response and potential thresholds, e.g., how large does the energy imbalance need to be to trigger slower adjustments?

Related to this issue of different timescales of adjustment is the traditional separation of climate response into rapid adjustment and slow response components (e.g., Andrews and Forster, 2010; Sherwood et al., 2015). The rapid adjustment is often defined as the climate response unassociated with global mean temperature change, and the slow response describes a transient response due to temperature change, largely as a result of climate system feedbacks. The results from Glocean-albedo, like those of Gl (Kravitz et al., 2013b), show an initial rapid change and no appreciable slower change. However, in Glocean-albedo, there is a sustained temperature increase without appreciable transient behavior. Thus, Glocean-albedo represents an experiment that does not cleanly delineate into the traditional definitions of rapid adjustment and slow response. Additionally, this sustained temperature increase is to some extent decoupled from net energy imbalances in the climate system, as ΔR_{TOA} and ΔS (Equation 8) are both approximately zero. Reconciling all of these features suggests a potentially rich research topic focused on understanding the relationships between radiative flux changes, temperature changes, and the circumstances under which climate feedbacks are excited, particularly for forcings with strong land/ocean contrast (e.g., anthropogenic aerosols).

The results presented here are broadly relevant to more sophisticated representations of MCB, such as increasing cloud droplet number concentration or directly injecting sea salt aerosols into the marine boundary layer (Kravitz et al., 2013c). Stjern et al. (2018) analyzed a multi-model ensemble of simulations of G4cdnc (Kravitz et al., 2013c), involving a 50% increase in cloud droplet number concentration in all marine low clouds, wherever the model forms those clouds. Although smaller in magnitude, they found similar patterns of top-of-atmosphere radiative flux change as in Glocean-albedo. Also similar between the two experiments was an increase in land precipitation and a decrease in ocean precipitation. Perhaps an even more realistic representation is G4sea-salt (Ahlm et al., 2017), involving direct injection of sea salt into the marine boundary layer between 30°S and 30°N to achieve an effective radiative forcing of -2.0 W m^{-2}. In the injection area (the tropics), this experiment also showed similar patterns of net top-of-atmosphere radiative flux perturbation and hydrologic cycle response. As such, while Glocean-albedo is highly idealized and exerts a perhaps unrealistically large forcing, it has relevance for other global representations of MCB or sea spray geoengineering. However, there are important differences in boundary layer stability changes from surface albedo increases versus marine stratocumulus cloud top brightening. Also, it appears impossible for marine cloud brightening to be conducted over all ocean regions and with a sufficient magnitude to offset the radiative forcing from a quadrupling of the CO_2 concentration. The purpose of this manuscript is to describe the broad features of change under a uniform ocean albedo increase, and some of these changes are likely to be present with more realistic scenarios of marine cloud brightening. We anticipate that future research can more deeply explore the applicability of this simulation to marine cloud brightening.

Glocean-albedo may be more apposite to the impact of geoengineering via "ocean microbubbles," whereby surfactants are added to the ocean surface, promoting the formation of microscopic, highly reflective bubbles (Robock, 2011). An area of

investigation we did not undertake, yet one that repeatedly emerges in discussions of microbubbles, is the resulting effects of surface albedo increase on the ocean mixed layer. By reflecting more solar radiation, microbubbles have the potential to inhibit vertical mixing and available light in the euphotic zone, which could have profound effects on marine biota. This implies that another useful future area of investigation for the G1ocean-albedo simulation is an analysis of the marine carbon cycle.

There are numerous potential areas of research prompted by this study. The stark land/ocean contrast in warming has potential implications for ocean dynamics, including the meridional overturning circulation, Western boundary ocean currents, and mixed layer depths, with consequent implications for marine ecosystems and the ocean carbon cycle. This contrast also has implications for the terrestrial biosphere, including ecosystem services and the land and ocean carbon cycles. Although we did not evaluate seasonal changes in this manuscript, such investigations could prove fruitful for more detailed assessments of variability, such as monsoon precipitation, extreme events, and sea ice extent. In addition, the changes in precipitation described earlier indicate important potential changes in large-scale circulation, atmospheric dynamics, and the hydrological cycle, all of which warrant further study.

Data availability. All output involved in the Geoengineering Model Intercomparison Project is publicly available, and much of it is accessible through the Earth System Grid Federation. Please see the GeoMIP website (http://climate.envsci.rutgers.edu/GeoMIP/) or contact the corresponding author for details.

Competing interests. None.

Acknowledgements. We thank Jón Egill Kristjánsson, who tragically passed away, for invaluable comments on an earlier version of this manuscript. We acknowledge the World Climate Research Programme's Working Group on Coupled Modelling, which is responsible for CMIP, and we thank the climate modeling groups for producing and making available their model output. For CMIP the U.S. Department of Energy's Program for Climate Model Diagnosis and Intercomparison provides coordinating support and led development of software infrastructure in partnership with the Global Organization for Earth System Science Portals. We thank all participants of the Geoengineering Model Intercomparison Project and their model development teams, CLIVAR/WCRP Working Group on Coupled Modeling for endorsing GeoMIP, and the scientists managing the Earth System Grid data nodes who have assisted with making GeoMIP output available. The Pacific Northwest National Laboratory is operated for the U.S. Department of Energy by Battelle Memorial Institute under contract DE-AC05-76RL01830. Simulations performed by Ben Kravitz were supported by the NASA High-End Computing (HEC) Program through the NASA Center for Climate Simulation (NCCS) at Goddard Space Flight Center. Alan Robock is supported by NSF grant AGS-1617844. Olivier Boucher acknowledges HPC resources from CCRT under the allocation 2015-t2012012201 made by GENCI (Grand Equipement National de Calcul Intensif). This work is a contribution to the German DFG-funded Priority Program 'Climate Engineering: Risks, Challenges, Opportunities?' (SPP 1689). Helene Muri was supported by the Research Council of Norway (229760/E10), and acknowledges Sigma2 NOTUR resources nn9182k, NS9033K and nn9448k. U. Niemeier and H. Schmidt are supported by the SPP 1689 within the projects

CEIBRAL and CELARIT. This research was supported under the Australian Research Council's Special Research Initiative for the Antarctic Gateway Partnership (project SR140300001). Shingo Watanabe was supported by the Integrated Research Program for Advancing Climate Models, MEXT, Japan. The Earth Simulator was used in his simulations. Jin-Ho Yoon was supported by the National Strategic Project – Find particle of the National Research of Korea (NRF) funded by the Ministry of Science and ICT (MSIT), the Ministry of Environment (ME), and the Ministry of Health and Welfare (MOHW) NRF-2017M3D8A1092022.

References

Ahlm, L., Jones, A., Stjern, C. W., Muri, H., Kravitz, B., and Kristjánsson, J. E.: Marine cloud brightening – as effective without clouds, Atmospheric Chemistry and Physics, 17, 13 071–13 087, https://doi.org/10.5194/acp-17-13071-2017, 2017.

Alterskjær, K., Kristjánsson, J. E., Boucher, O., Muri, H., Niemeier, U., Schmidt, H., Schulz, M., and Timmreck, C.: Sea-salt injections into the low-latitude marine boundary layer: The transient response in three Earth system models, J. Geophys. Res., 118, 12 195–12 206, https://doi.org/10.1002/2013JD020432, 2013.

Andrews, T. and Forster, P. M.: The transient response of global-mean precipitation to increasing carbon dioxide levels, Environ. Res. Lett., 5, 025 212, https://doi.org/10.1088/1748-9326/5/2/025212, 2010.

Armour, K. C., Bitz, C. M., and Roe, G. H.: Time-varying climate sensitivity from regional feedbacks, J. Climate, 26, 4518–4534, https://doi.org/10.1175/JCLI-D-12-00544.1, 2013.

Arora, V. K., Scinocca, J. F., Boer, G. J., Christian, J. R., Denman, K. L., Flato, G. M., Kharin, V. V., Lee, W. G., and Merryfield, W. J.: Carbon emission limits required to satisfy future representative concentration pathways of greenhouse gases, Geophys. Res. Lett., 38, L05 805, https://doi.org/10.1029/2010GL046270, 2011.

Bala, G., Caldeira, K., and Nemani, R.: Fast versus slow response in climate change: Implications for the global hydrological cycle, Clim. Dyn., 35, 423–434, https://doi.org/10.1007/s00382-009-0583-y, 2010.

Bentsen, M., Bethke, I., Debernard, J. B., Iversen, T., Kirkevåg, A., Seland, Ø., Drange, H., Roelandt, C., Seierstad, I. A., Hoose, C., , and Kristjaánsson, J. E.: The Norwegian Earth System Model, NorESM1-M – Part 1: Description and basic evaluation of the physical climate, Geoscientific Model Development, 6, 687–720, 2013.

Cao, L., Bala, G., and Caldeira, K.: Climate response to changes in atmospheric carbon dioxide and solar irradiance on the time scale of days to weeks, Environ. Res. Lett., 7, 034 015, https://doi.org/10.1088/1748-9326/7/3/034015, 2012.

Collins, W. J., Bellouin, N., Doutriaux-Boucher, M., Gedney, N., Halloran, P., Hinton, T., Hughes, J., Jones, C. D., Joshi, M., Liddicoat, S., Martin, G., O'Connor, F., Rae, J., Senior, C., Sitch, S., Totterdell, I., Wiltshire, A., and Woodward, S.: Development and evaluation of an Earth-System model—HadGEM2, Geosci. Model Dev., 4, 1051–1075, https://doi.org/10.5194/gmd-4-1051-2011, 2011.

Crook, J. A., Jackson, L. S., Osprey, S. M., and Forster, P. M.: A comparison of temperature and precipitation responses to different Earth radiation management geoengineering schemes, J. Geophys. Res., 120, 9352–9373, https://doi.org/10.1002/2015JD023269, 2015.

Curry, C. L., Sillmann, J., Bronaugh, D., Alterskjær, K., Cole, J. N. S., Kravitz., B., Kristjánsson, J. E., Muri, H., Niemeier, U., Robock, A., and Tilmes, S.: A multi-model examination of climate extremes in an idealized geoengineering experiment, J. Geophys. Res., 119, 3900–3923, https://doi.org/10.1002/2013JD020648, 2014.

Dufresne, J.-L., Foujols, M.-A., Denvil, S., Caubel, A., Marti, O., Aumont, O., Balkanski, Y., Bekki, S., Bellenger, H., Benshila, R., Bony, S., Bopp, L., Braconnot, P., Brockmann, P., Cadule, P., Cheruy, F., Codron, F., Cozic, A., Cugnet, D., de Noblet, N., Duvel, J.-P., Ethé, C., Fairhead, L., Fichefet, T., Flavoni, S., Friedlingstein, P., Grandpeix, J.-Y., Guez, L., Guilyardi, E., Hauglustaine, D., Hourdin, F., Idelkadi, A., Ghattas, J., Joussaume, S., Kageyama, M., Krinner, G., Labetoulle, S., Lahellec, A., Lefebvre, M.-P., Lefevre, F., Levy, C., Li, Z. X., Lloyd, J., Lott, F., Madec, G., Mancip, M., Marchand, M., Masson, S., Meurdesoif, Y., Mignot, J., Musat, I., Parouty, S., Polcher, J., Rio, C., Schulz, M., Swingedouw, D., Szopa, S., Talandier, C., Terray, P., Viovy, N., and Vuichard, N.: Climate change projections using the IPSL-CM5 Earth System Model: From CMIP3 to CMIP5, Clim. Dynam., 40, 2123–2165, https://doi.org/10.1007/s00382-012-1636-1, 2013.

Gabriel, C. J., Robock, A., Xia, L., Zambri, B., and Kravitz, B.: The G4Foam Experiment: Global climate impacts of regional ocean albedo modification, Atmospheric Chemistry and Physics, 17, 595–613, https://doi.org/10.5194/acp-17-595-2017, 2017.

Geoffroy, O., Saint-Martin, D., and Voldoire, A.: Land-sea warming contrast: the role of the horizontal energy transport, Clim. Dynam., 45, 3493–3511, https://doi.org/10.1007/s00382-015-2552-y, 2015.

Giorgetta, M. A., Jungclaus, J., Reick, C. H., Legutke, S., Bader, J., Böttinger, M., Brovkin, V., Crueger, T., Esch, M., Fieg, K., Glushak, K., Gayler, V., Haak, H., Hollweg, H.-D., Ilyina, T., Kinne, S., Kornblueh, L., Matei, D., Mauritsen, T., Mikolajewicz, U., Mueller, W., Notz, D., Pithan, F., Raddatz, T., Rast, S., Redler, R., Roeckner, E., Schmidt, H., Schnur, R., Segschneider, J., Six, K. D., Stockhause, M., Timmreck, C., Wegner, J., Widmann, H., Wieners, K.-H., Claussen, M., Marotzke, J., and Stevens, B.: Climate and carbon cycle changes from 1850 to 2100 in MPI-ESM simulations for the Coupled Model Intercomparison Project Phase 5, J. Adv. Model. Earth Syst., 5, 572–597, https://doi.org/10.1002/jame.20038, 2013.

Glienke, S., Irvine, P. J., and Lawrence, M. G.: The impact of geoengineering on vegetation in experiment G1 of the GeoMIP, J. Geophys. Res., 120, 10 196–10 213, https://doi.org/10.1002/2015JD024202, 2015.

Gregory, J. M., Ingram, W. J., Palmer, M. A., Jones, G. S., Stott, P. A., Thorpe, R. B., Lowe, J. A., Johns, T. C., and Williams, K. D.: A new method for diagnosing radiative forcing and climate sensitivity, Geophys. Res. Lett., 31, L03 205, https://doi.org/10.1029/2003GL018747, 2004.

Hansen, J., Sato, M., Ruedy, R., Nazarenko, L., Lacis, A., Schmidt, G. A., Russell, G., Aleinov, I., Bauer, M., Bauer, S., Bell, N., Cairns, B., Canuto, V., Chandler, M., Cheng, Y., Del Genio, A., Faluvegi, G., Fleming, E., Friend, A., Hall, T., Jackman, C., Kelley, M., Kiang, N., Koch, D., Lean, J., Lerner, J., Lo, K., Menon, S., Miller, R., Minnis, P., Novakov, T., Oinas, V., Perlwitz, J., Perlwitz, J., Rind, D., Romanou, A., Shindell, D., Stone, P., Sun, S., Tausnev, N., Thresher, D., Wielicki, B., Wong, T., Yaho, M., and Zhang, S.: Efficacy of Climate Forcings, J. Geophys. Res., 110, D18 104, https://doi.org/10.1029/2005JD005776, 2005.

Hazeleger, W., Wang, X., Severijns, C., Ştefănescu, S., Bintanja, R., Sterl, A., Wyser, K., Semmler, T., Yang, S., van den Hurk, B., van Noije, T., van der Linden, E., and van der Wiel, K.: EC-Earth V2.2: Description and validation of a new seamless Earth system prediction model, Clim. Dynam., 39, 2611–2629, https://doi.org/10.1007/s00382-011-1228-5, 2011.

Hobbs, W., Palmer, M. D., and Monselesan, D.: An Energy Conservation Analysis of Ocean Drift in the CMIP5 Global Coupled Models, J. Climate, 29, 1639–1653, https://doi.org/10.1175/JCLI-D-15-0477.1, 2016.

Hurrell, J. W., Holland, M. M., Gent, P. R., Ghan, S., Kay, J. E., Kushner, P. J., Lamarque, J.-F., Large, W. G., Lawrence, D., Lindsay, K., Lipscomb, W. H., Long, M. C., Mahowald, N., Marsh, D. R., Neale, R. B., Rasch, P., Vavrus, S., Vertenstein, M., Bader, D., Collins, W. D., Hack, J. J., Kiehl, J., , and Marshall, S.: The Community Earth System Model: A Framework for Collaborative Research, Bull. Amer. Meteor. Soc., 94, 1339–1360, https://doi.org/10.1175/BAMS-D-12-00121.1, 2013.

Ji, D., Wang, L., Feng, J., Wu, Q., Cheng, H., Zhang, Q., Yang, J., Dong, W., Dai, Y., Gong, D., Zhang, R.-H., Wang, X., Liu, J., Moore, J. C., Chen, D., and Zhou, M.: Description and basic evaluation of Beijing Normal University Earth System Model (BNU-ESM) version 1, Geosci. Model. Dev., 7, 2039–2064, https://doi.org/10.5194/gmd-7-2039-2014, 2014.

Kalidindi, S., Bala, G., Modak, A., and Caldeira, K.: Modeling of solar radiation management: A comparison of simulations using reduced solar constant and stratospheric sulfate aerosols, Clim. Dynam., 44, 2909–2925, https://doi.org/10.1007/s00382-014-2240-3, 2014.

Kravitz, B., Robock, A., Boucher, O., Schmidt, H., Taylor, K. E., Stenchikov, G., and Schulz, M.: The Geoengineering Model Intercomparison Project (GeoMIP), Atmos. Sci. Lett., 12, 162–167, https://doi.org/10.1002/asl.316, 2011.

Kravitz, B., Caldeira, K., Boucher, O., Robock, A., Rasch, P. J., Alterskjær, K., Karam, D. B., Cole, J. N. S., Curry, C. L., Haywood, J. M., Irvine, P. J., Ji, D., Jones, A., Kristjánsson, J. E., Lunt, D. J., Moore, J., Niemeier, U., Schmidt, H., Schulz, M., Singh, B., Tilmes, S.,

Watanabe, S., Yang, S., , and Yoon, J.-H.: Climate model response from the Geoengineering Model Intercomparison Project (GeoMIP), J. Geophys. Res., 118, 8320–8332, https://doi.org/10.1002/jgrd.50646, 2013a.

Kravitz, B., Rasch, P. J., Forster, P. M., Andrews, T., Cole, J. N. S., Irvine, P. J., Ji, D., Kristjánsson, J. E., Moore, J. C., Muri, H., Niemeier, U., Robock, A., Singh, B., Tilmes, S., Watanabe, S., , and Yoon, J.-H.: An energetic perspective on hydrological cycle changes in the Geoengineering Model Intercomparison Project (GeoMIP), J. Geophys. Res., 118, 13 087–13 102, https://doi.org/10.1002/2013JD020502, 2013b.

Kravitz, B., Forster, P. M., Jones, A., Robock, A., Alterskjær, K., Boucher, O., Jenkins, A. K. L., Korhonen, H., Kristjánsson, J. E., Muri, H., Niemeier, U., Partanen, A.-I., Rasch, P. J., Wang, H., , and Watanabe, S.: Sea spray geoengineering experiments in the Geoengineering Model Intercomparison Project (GeoMIP): Experimental design and preliminary results, J. Geophys. Res., 118, 11 175–11 186, https://doi.org/10.1002/jgrd.50856, 2013c.

Kravitz, B., MacMartin, D. G., Rasch, P. J., and Jarvis, A. J.: A new method of comparing forcing agents in climate models, J. Climate, 28, 8203–8218, https://doi.org/10.1175/JCLI-D-14-00663.1, 2015.

Kravitz, B., MacMartin, D. G., Wang, H., and Rasch, P. J.: Geoengineering as a design problem, Earth System Dynamics, 7, 469–497, https://doi.org/10.5194/esd-469-2016, 2016.

Latham, J.: Control of global warming?, Nature, 347, 339–340, 1990.

MacMartin, D. G., Kravitz, B., Keith, D. W., and Jarvis, A.: Dynamics of the coupled human-climate system resulting from closed-loop control of solar geoengineering, Clim. Dynam., 43, 243–258, https://doi.org/10.1007/s00382-013-1822-9, 2014b.

Mitchell, D. L. and Finnegan, W.: Modification of cirrus clouds to reduce global warming, Environ. Res. Lett., 4, 045 102, https://doi.org/10.1088/1748-9326/4/4/045102, 2009.

Moore, J. C., Rinke, A., Yu, X., Ji, D., Cui, X., Li, Y., Alterskjær, K., Kristjánsson, J. E., Boucher, O., Huneeus, N., Kravitz, B., Robock, A., Niemeier, U., Schmidt, H., Schulz, M., Tilmes, S., and Watanabe, S.: Arctic sea ice and atmospheric circulation under the GeoMIP G1 scenario, J. Geophys. Res., 119, 567–583, https://doi.org/10.1002/2013JD021060, 2014.

NAS: Climate Intervention: Carbon Dioxide Removal and Reliable Sequestration, Tech. rep., National Research Council, https://www.nap.edu/catalog/18805/climate-intervention-carbon-dioxide-removal-and-reliable-sequestration, (last access: 7 May 2015), 2015a.

NAS: Climate Intervention: Reflecting Sunlight to Cool Earth, Tech. rep., National Research Council, http://www.nap.edu/catalog/18988/climate-intervention-reflecting-sunlight-to-cool-earth, (last access: 7 May 2015), 2015b.

Niemeier, U., Schmidt, H., Alterskjær, K., and Kristjánsson, J. E.: Solar irradiance reduction via climate engineering: Impact of different techniques on the energy balance and the hydrological cycle, J. Geophys. Res., 118, 11 905–11 917, https://doi.org/10.1002/2013JD020445, 2013.

Phipps, S. J., Rotstayn, L. D., Gordon, H. B., Roberts, J. L., Hirst, A. C., , and Budd, W. F.: The CSIRO Mk3L climate system model version 1.0 – Part 1: Description and evaluation, Geosci. Model Dev., 4, 483–509, https://doi.org/10.5194/gmd-4-483-2011, 2011.

Robock, A.: Bubble, bubble, toil and trouble. An editorial comment., Climatic Change, 105, 383–385, https://doi.org/10.1007/s10584-010-0017-1, 2011.

Schmidt, G. A., Kelley, M., Nazarenko, L., Ruedy, R., Russell, G. L., Aleinov, I., Bauer, M., Bauer, S. E., Bhat, M. K., Bleck, R., Canuto, V., Chen, Y.-H., Cheng, Y., Clune, T. L., Genio, A. D., de Fainchtein, R., Faluvegi, G., Hansen, J. E., Healy, R. J., Kiang, N. Y., Koch, D., Lacis, A. A., LeGrande, A. N., Lerner, J., Lo, K. K., Matthews, E. E., Menon, S., Miller, R. L., Oinas, V., Oloso, A. O., Perlwitz, J. P., Puma, M. J., Putman, W. M., Rind, D., Romanou, A., Sato, M., Shindell, D. T., Sun, S., Syed, R. A., Tausnev, N., Tsigaridis, K., Under,

N., Volugarakis, A., Yao, M.-S., and Zhang, J.: Configuration and assessment of the GISS ModelE2 contributions to the CMIP5 archive, J. Adv. Modell. Earth Syst., 6, 141–184, https://doi.org/10.1002/2013MS000265, 2014.

Schmidt, H., Alterskjær, K., Karam, D. B., Boucher, O., Jones, A., Kristjánsson, J. E., Niemeier, U., Schulz, M., Aaheim, A., Benduhn, F., Lawrence, M., and Timmreck, C.: Solar irradiance reduction to counteract radiative forcing from a quadrupling of CO_2: Climate responses simulated by four Earth system models, Earth System Dynamics, 3, 63–78, https://doi.org/10.5194/esd-3-63-2012, 2012.

Shepherd, J., Caldeira, K., Cox, P., Haigh, J., Keith, K., Launder, B., Mace, G., MacKerron, G., Pyle, J., Rayner, S., Redgwell, C., and Watson, A.: Geoengineering the climate: Science, governance, and uncertainty, Tech. rep., royal Society Policy document 10/09, 82 pp., 2009.

Sherwood, S. C., Bony, S., Boucher, O., Bretherton, C., Forster, P. M., Gregory, J. M., and Stevens, B.: Adjustments in the forcing-feedback framework for understanding climate change, Bull. Amer. Meteor. Soc., 96, 217–228, https://doi.org/10.1175/BAMS-D-13-00167.1, 2015.

Stjern, C. W., Muri, H., Ahlm, L., Boucher, O., Cole, J. N. S., Ji, D., Jones, A., Haywood, J., Kravitz, B., Lenton, A., Moore, J. C., Niemeier, U., Phipps, S. J., Schmidt, H., Watanabe, S., and Kristjánsson, J. E.: Response to marine cloud brightening in a multi-model ensemble, Atmospheric Chemistry and Physics, 18, 621–634, https://doi.org/10.5194/acp-18-621-2018, 2018.

Taylor, K. E., Stouffer, R. J., and Meehl, G. A.: An overview of CMIP5 and the experiment design, Bull. Amer. Meteor. Soc., 93, 485–498, https://doi.org/10.1175/BAMS-D-11-00094.1, 2012.

Tilmes, S., Fasullo, J., Lamarque, J.-F., Marsh, D. R., Mills, M., Alterskjær, K., Muri, H., Kristjánsson, J. E., Boucher, O., Schulz, M., Cole, J. N. S., Curry, C. L., Jones, A., Haywood, J., Irvine, P. J., Ji, D., Moore, J. C., Karam, D. B., Kravitz, B., Rasch, P. J., Singh, B., Yoon, J.-H., Niemeier, U., Schmidt, H., Robock, A., Yang, S., and Watanabe, S.: The hydrological impact of geoengineering in the Geoengineering Model Intercomparison Project (GeoMIP), J. Geophys. Res., 118, 11 036–11 058, https://doi.org/10.1002/jgrd.50868, 2013.

Wan, H., Rasch, P. J., Zhang, K., Qian, Y., Yan, H., , and Zhao, C.: Short ensembles: an efficient method for discerning climate-relevant sensitivities in atmospheric general circulation models, Geosci. Model. Dev., 7, 1961–1977, https://doi.org/10.5194/gmd-7-1961-2014, 2014.

Watanabe, S., Hajima, T., Sudo, K., Nagashima, T., Takemura, T., Okajima, H., Nozawa, T., Kawase, H., Abe, M., Yokohata, T., Ise, T., Sato, H., Kato, E., Takata, K., Emori, S., and Kawamiya, M.: MIROC-ESM 2010: Model description and basic results of CMIP5-20c3m experiments, Geosci. Mod. Dev., 4, 845–872, https://doi.org/10.5194/gmd-4-845-2011, 2011.

Table 1. Description of the 11 models participating in this study. Column 1 gives the standard model name. Columns 2 and 3 give the default and perturbed surface ocean albedo, defined as upward shortwave divided by downward shortwave radiative flux at the surface, both averaged over ocean regions and over years 11-50 of simulation. Column 4 is the ratio of column 3 to column 2 (calculated prior to rounding the values in Columns 2 and 3). Column 5 gives the factor (δ) by which the model default ocean albedo was multiplied to achieve negligible top-of-atmosphere radiative flux changes under an abrupt4xCO2 simulation (described in greater detail by Kravitz et al., 2015). The differences between Ratio and δ are caused in part by cloud responses. Column 6 gives a relevant reference for each model. All values are rounded to two decimal places.

Model name	piControl ocean albedo	G1ocean-albedo ocean albedo	Ratio	δ	Reference
BNU-ESM	0.12	0.17	1.48	2.50	Ji et al. (2014)
CanESM2	0.11	0.19	1.73	2.45	Arora et al. (2011)
CESM-CAM5.1-FV	0.10	0.18	1.79	2.70	Hurrell et al. (2013)
CSIRO-Mk3L-1.2	0.12	0.19	1.61	2.04	Phipps et al. (2011)
EC-Earth	0.10	0.19	1.97	3.17	Hazeleger et al. (2011)
GISS-E2-R	0.08	0.16	1.95	2.53	Schmidt et al. (2014)
HadGEM2-ES	0.10	0.17	1.83	2.44	Collins et al. (2011)
IPSL-CM5A-LR	0.10	0.17	1.78	2.33	Dufresne et al. (2013)
MIROC-ESM	0.10	0.20	2.00	3.10	Watanabe et al. (2011)
MPI-ESM-LR	0.09	0.23	2.40	5.42	Giorgetta et al. (2013)
NorESM1-M	0.09	0.18	1.95	2.77	Bentsen et al. (2013)

Table 2. Feedback parameters (Section 3.3; units W m^{-2} K^{-1}) for global, land, and ocean averages, calculated via the "Gregory method" (Gregory et al., 2004), where annual mean top-of-atmosphere net radiative flux is regressed against annual mean temperature.

	Global feedback parameter (λ_g)	Land feedback parameter λ_ℓ	Ocean feedback parameter λ_o
BNU-ESM	0.9019	0.7181	0.9838
CanESM2	1.1539	1.1898	1.1260
CESM-CAM5.1-FV	1.1435	1.0357	1.1591
CSIRO-Mk3L-1.2	1.0192	0.9300	0.8034
EC-Earth	1.2124	1.1937	1.3155
GISS-E2-R	2.2440	1.9751	2.3560
HadGEM2-ES	0.8411	0.8363	0.8351
IPSL-CM5A-LR	0.8367	1.2891	0.5894
MIROC-ESM	1.0378	0.8736	1.0383
MPI-ESM-LR	1.3701	1.0573	1.3986
NorESM1-M	1.4285	1.8828	1.6063

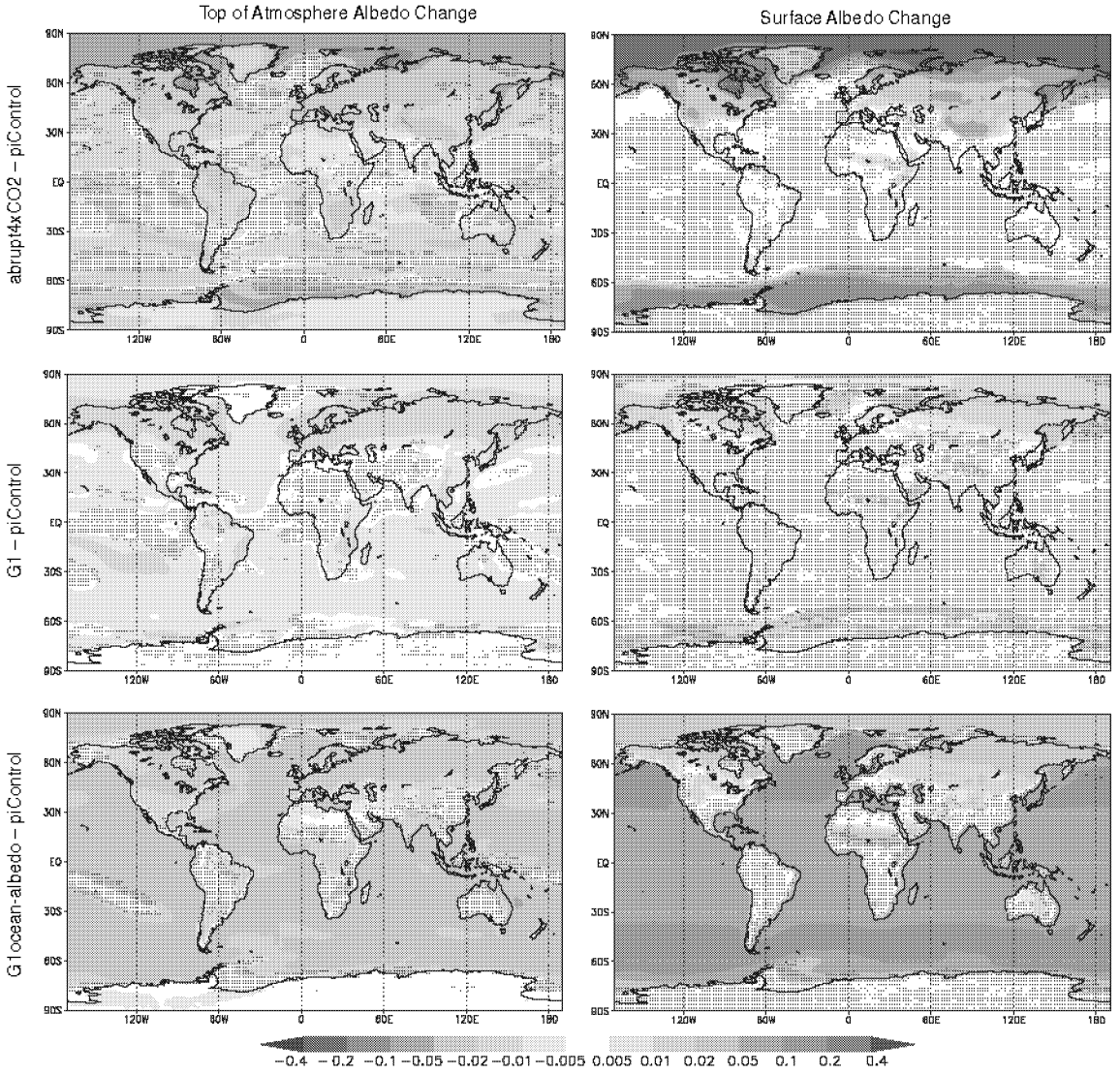

Figure 1. Top-of-atmosphere (TOA) and surface albedo differences (relative to piControl) for the abrupt4xCO2, G1, and G1ocean-albedo experiments. Albedo here is calculated as the ratio of upwelling to downwelling all-sky shortwave radiative flux, either at TOA or at the surface. Values are averages over years 11-50 of simulation. Stippling indicates where fewer than 8 out of 11 models agree on the sign of the response.

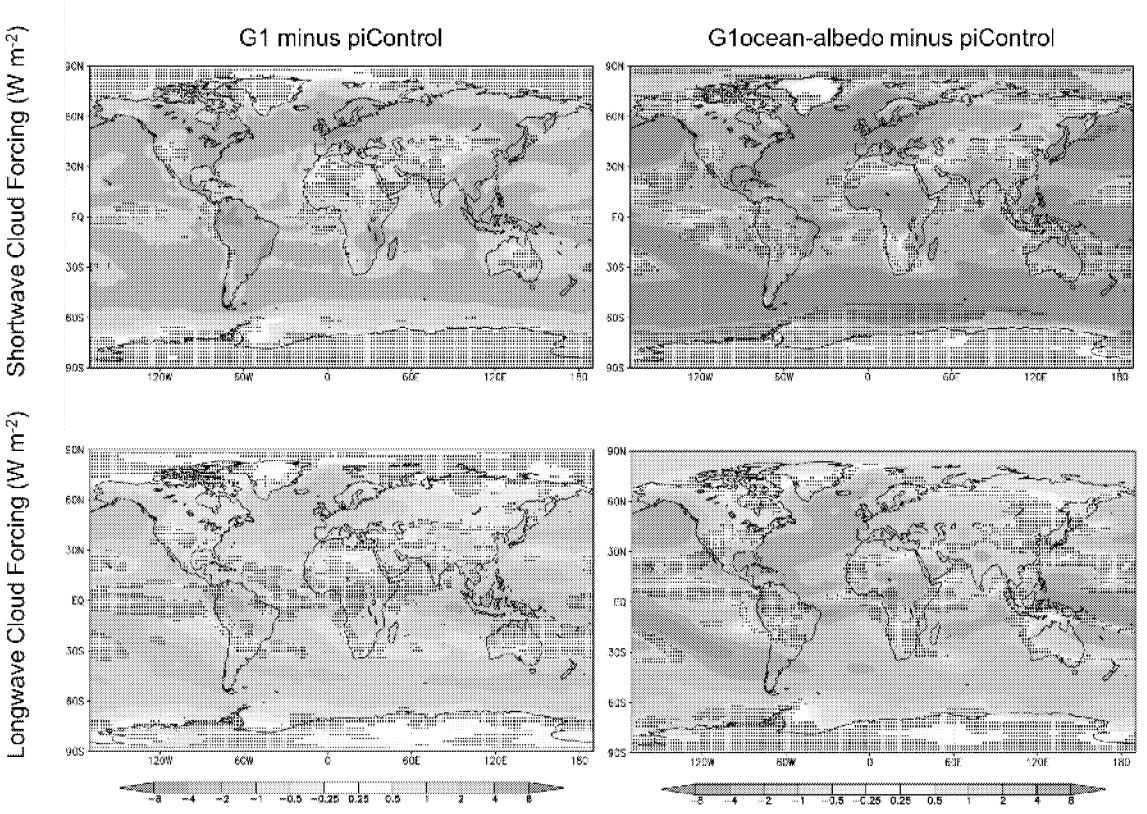

Figure 2. Shortwave (top) and longwave (bottom) cloud forcing changes due to the G1 (left) and G1ocean-albedo perturbations. Cloud forcing is defined as all-sky minus clear-sky radiative flux at the top of the atmosphere, with positive values indicating more net downward flux.

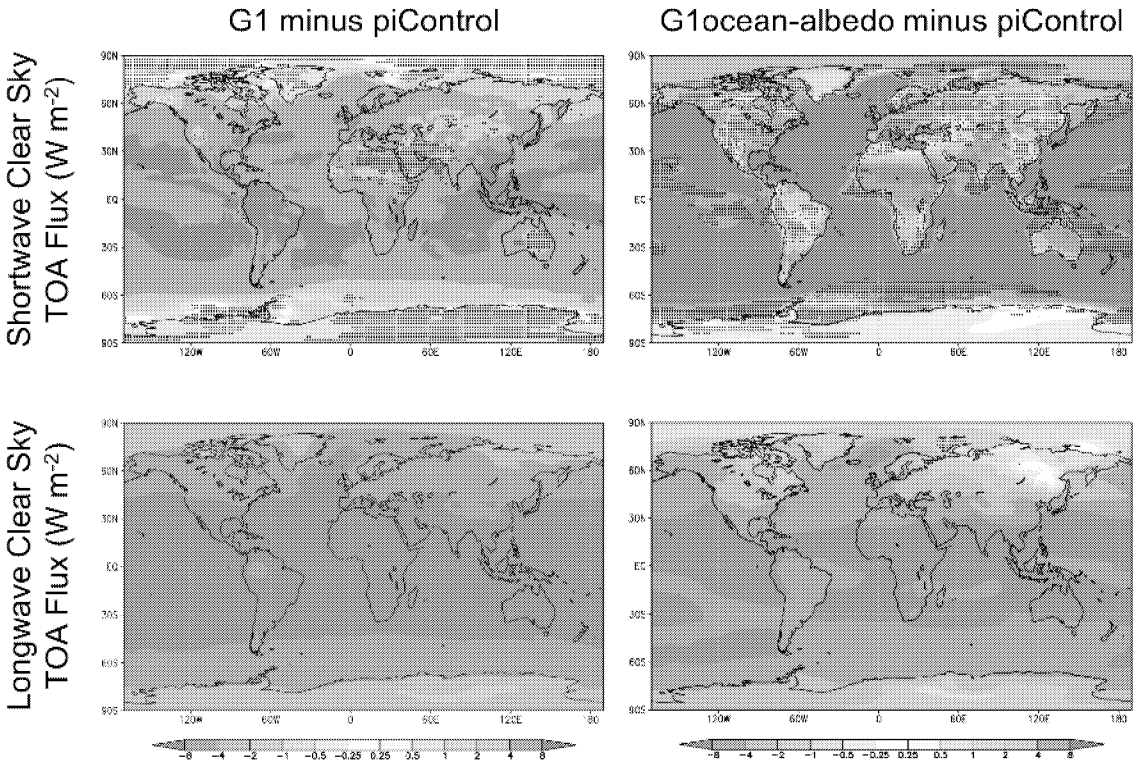

Figure 3. Shortwave (top) and longwave (bottom) net (downward minus upward) clear sky radiative flux changes at the top-of-atmosphere due to the G1 (left) and G1ocean-albedo perturbations, with positive values indicating more net downward flux. Positive values indicate that upward clear sky flux decreased in the perturbed (G1 or G1ocean-albedo) experiments, and negative values indicate that upward clear sky flux increased in the perturbed experiments.

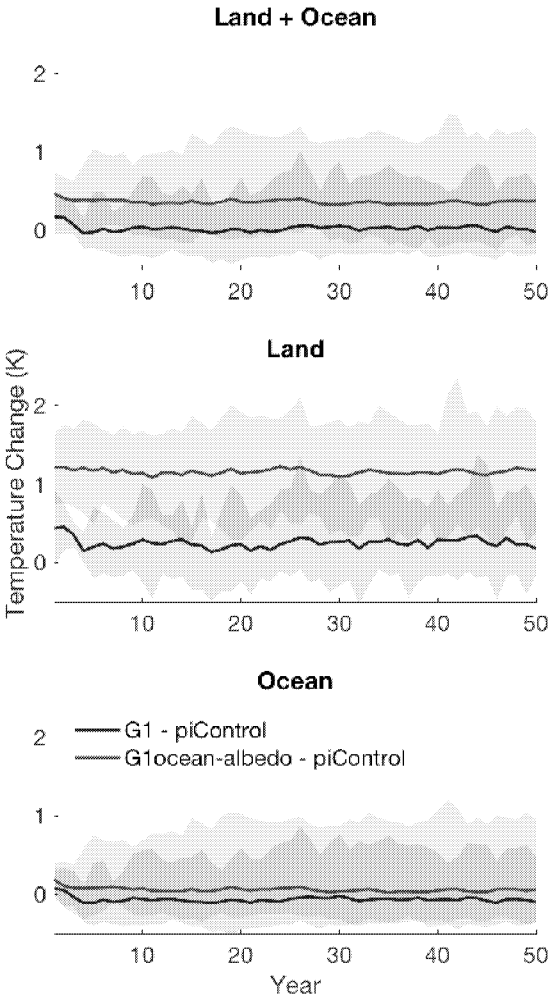

Figure 4. Global (top), land (middle), and ocean (bottom) average temperature change for the G1 (blue) and G1ocean-albedo (red) simulations. Lines show the all-model ensemble mean, and shading shows model spread (smallest to largest values).

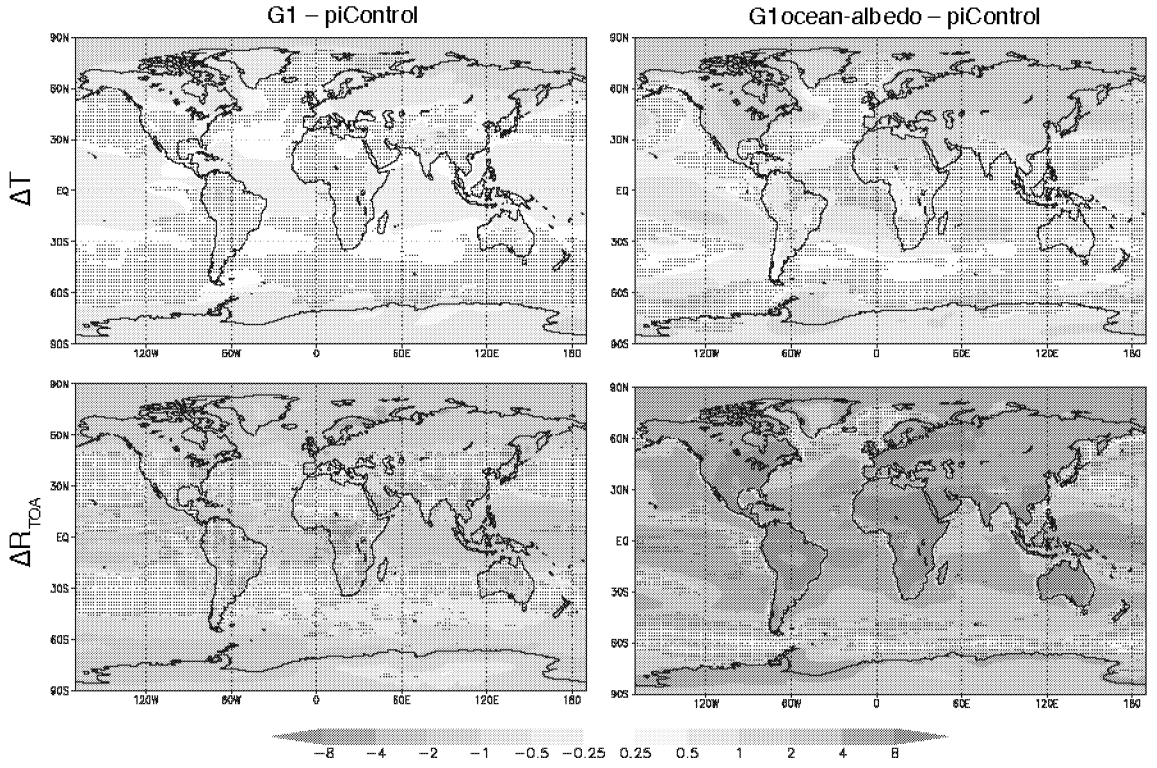

Figure 5. Surface air temperature (top row; K) and TOA net radiative flux (bottom row; W m^{-2}) changes for experiments G1 (left) and G1ocean-albedo (right). Values are averages over years 11-50 of simulation. Stippling indicates where fewer than 8 out of 11 models agree on the sign of the response.

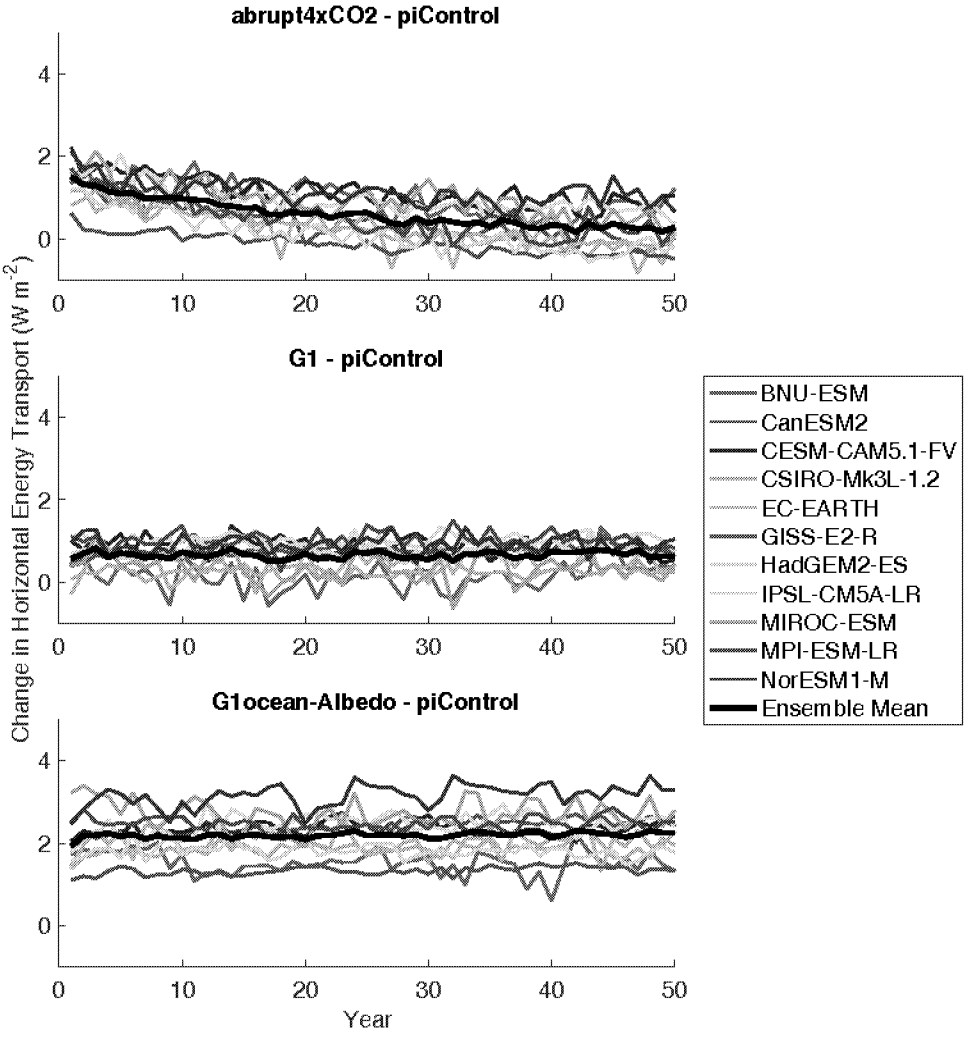

Figure 6. Annual mean change in land-ocean energy transport (Section 3.3; W m^{-2}) from piControl. See Equation 7 for a formal definition.

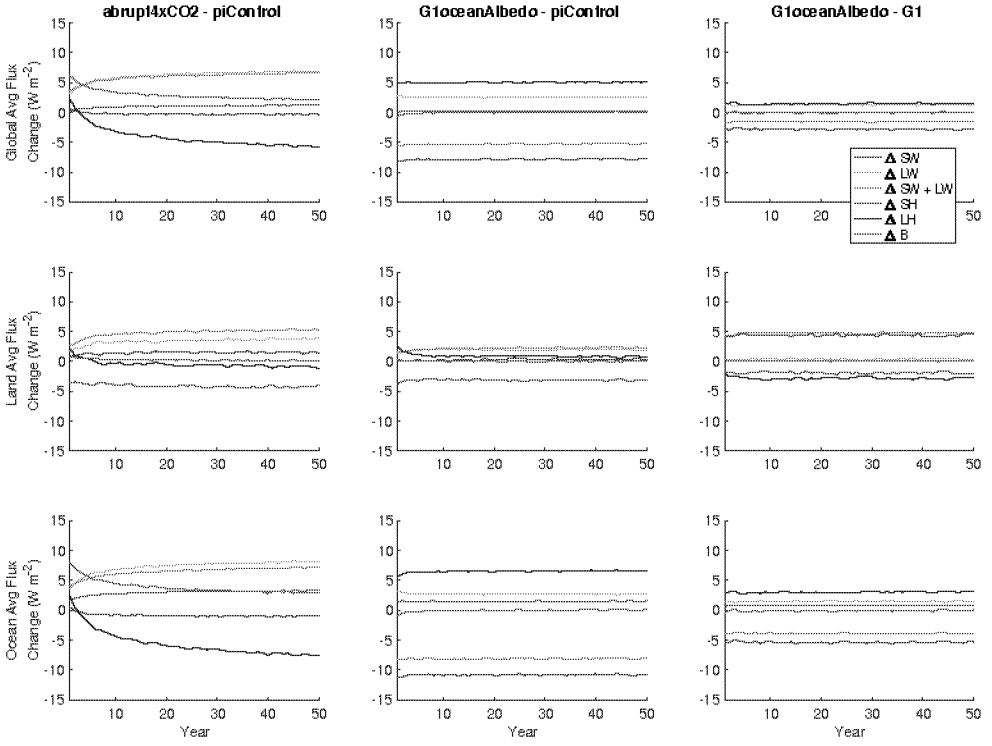

Figure 7. Annual mean time series of all-model mean surface fluxes (terms in Equation 8) for global averages (top), land averages (middle), and ocean averages (bottom). All fluxes are positive in the downward direction.

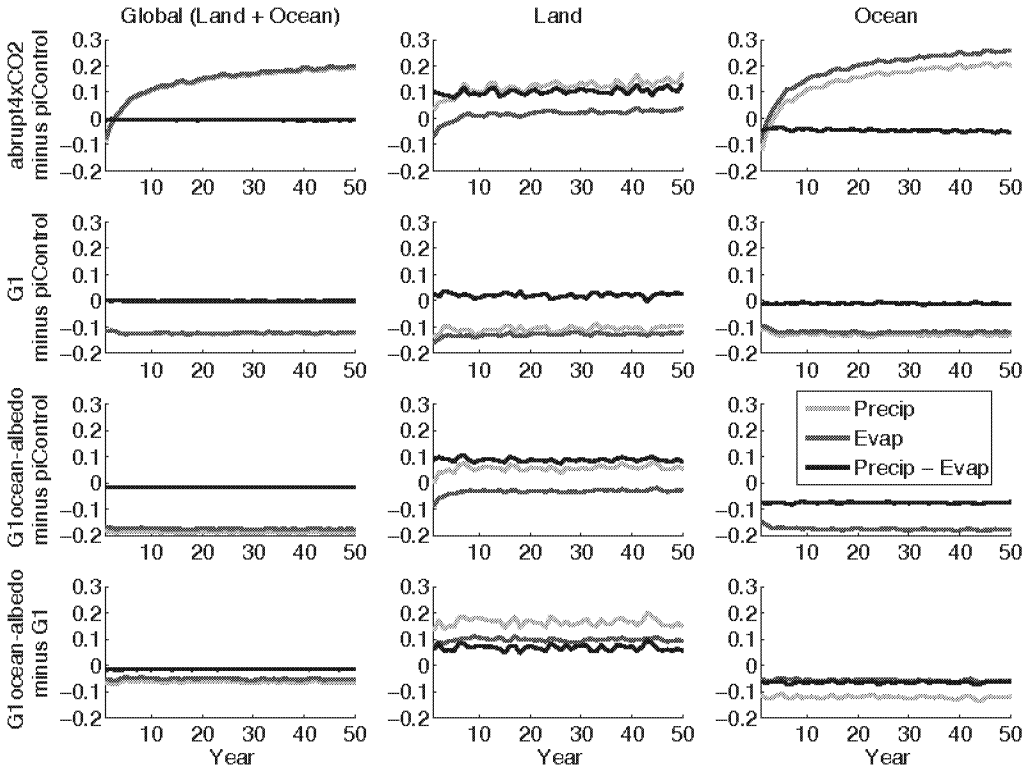

Figure 8. Annual mean time series of hydrological cycle changes (all in mm day^{-1}). Green lines show precipitation changes, red lines show evaporation changes, and black lines show precipitation minus evaporation. In the first column, green lines are difficult to see because they are largely overlaid by red lines. In the third row, third column, the green line has values below -0.2 for all years.

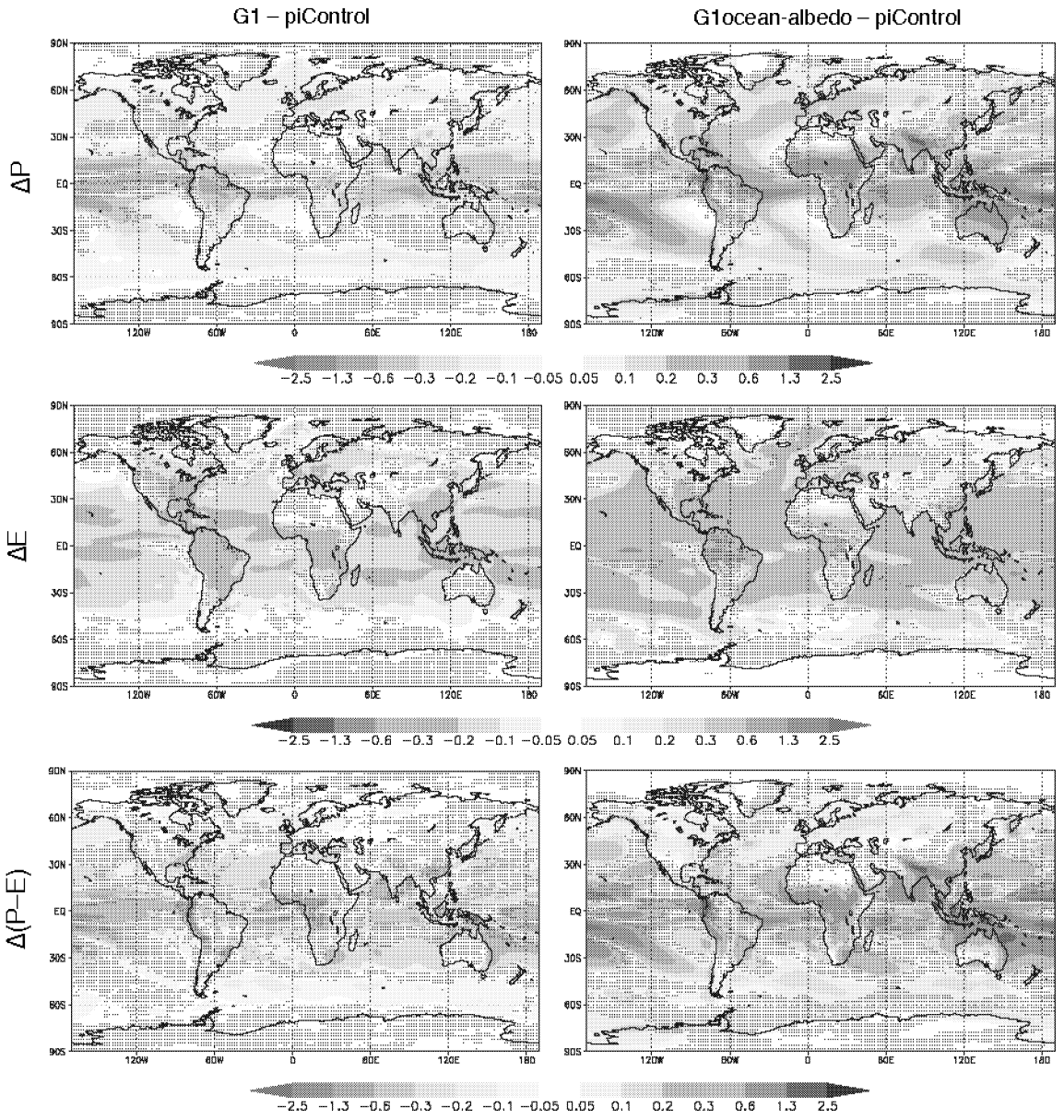

Figure 9. Precipitation (top row), evaporation (middle row), and precipitation minus evaporation (bottom row) changes (all panels have units mm day^{-1}) for experiments G1 and G1ocean-albedo. Values are averages over years 11-50 of simulation. Stippling indicates where fewer than 8 out of 11 models agree on the sign of the response.

DRAFT

Climate Engineering

Background

Climate engineering (sometimes referred to as "geoengineering") refers to the deliberate, large-scale manipulation of the planetary environment to counteract the effects of anthropogenic climate change. Climate engineering generally utilizes one of two methods: solar radiation management (SRM) or carbon dioxide removal (CDR), and is occasionally presented as a third climate policy strategy beyond adaptation and mitigation. This MTP paper provides a high-level outline of climate engineering, while focusing particularly on SRM as a climate engineering method. ***A separate MTP paper is available and provides a more fulsome analysis of Negative Emission Technologies, which covers technologies that fall under CDR.***

Why Climate Engineering?

As there is a significant gap between national pledges under the Paris Agreement and the emissions pathways consistent with holding global temperature to 1.5C above pre-industrial levels, pressure will grow to research and deploy climate-engineering technologies to limit the effects of climate change. At the same time, Canada's previous position in international fora has been that the deployment of climate engineering technologies should not occur without adequate governance structures, or before more research on the issue occurs, to ensure a comprehensive understanding of risks and consequences – both positive and negative.

Drivers: Gaps in Research/Global/National Governance

Consensus on climate engineering governance has been difficult to achieve in international fora, particularly due to the limited understanding of the risks and science of the issue. Certain forms of climate engineering have potential to create adverse, unanticipated, and irreversible environmental, social, and economic impacts. As such, many have expressed ethical objections to its deployment.

Although research on climate engineering has intensified in recent years, mechanisms to govern climate engineering and associated research at the international and domestic levels are limited or non-existent. Although climate engineering has been discussed at international fora, including the United Nations Environmental Assembly (UNEA) and the Conference of the Parties to the Convention on Biological Diversity (COP CBD), formal negotiations on a framework for research governance have stalled, most recently in March 2019 at UNEA in Nairobi.

There is currently no comprehensive legislative framework to govern climate-engineering activities in Canada. Although certain aspects of the *Canadian Environmental Protection Act, 1999* (CEPA), the *Fisheries Act* and the *Migratory Birds Convention Act, 1994* might apply to specific forms of climate engineering, some climate engineering activities could potentially ~~likely~~ be deployed in Canada without regulatory oversight. There is also a threat of unilateral deployment by states or individuals prior to international consensus on climate engineering, particularly given the low costs of some climate engineering methods. As such, the challenges of patchwork governance on these issues are exacerbated. Given these factors, further discussion of climate engineering governance is warranted within ECCC and other government departments, as well as provincial/territorial governments, Indigenous groups, and other relevant partners.

Commenté [F[1]: This is not really correct. Both methods would be more accurately described as aiming to 'reduce climate forcing' or 'reduce the drivers of climate change' or something like that. They are generally discussed in the context of proactive measures that would help avoid some level of climate change, rather than something done reactively to deal with the consequences of change already experience, which is what 'counteract the effects' seems to imply

Commenté [F[2]: Again, wording is not appropriate. The argument is really that there will be a need to augment emission reduction efforts, not to let climate change and then limit the effects of that change. I think this is more than a semantic issue – it goes to the underlying reason for thinking about these engineering approaches.

Commenté [F[3]: I found this sentence rather odd – I'm not aware there has really been an effort to achieve consensus at this point. There has been research, there have been discussions (as noted in the next para), but I don't believe there has been a forum in which governments sat down and tried to reach consensus on this issue.

Commenté [F[4]: While they are all legitimate objections, the list in the previous sentence does not capture the reason for ethical objections. Ethical objections arise primarily because of the transboundary consequences of climate engineering – e.g. a country doing something to avoid warming in their territory causing drought or deprivation elsewhere in the world. Ethical concerns also arise because implementation of climate engineering may impose financial and other burdens on future generations (because stopping would un-mask the forcing that has been masked).

Commenté [F[5]: Should also state that ongoing engagement at the international level is essential – this is more of an international governance issue than it is a domestic issue at this point.

DRAFT

There are ethical challenges associated with climate engineering, particularly the idea that it can give the public a false sense of security that climate change is "solved." This in turn could lead to greater CO2 emissions. As such, the international community has focused much of its climate policy action on adaptation and mitigation, and has often been hesitant to even discuss climate engineering. Despite this, climate engineering has been seen by some as a third pillar of climate policy alongside adaptation and mitigation. Given the length of time needed to conduct proper research on climate engineering (likely years), some have argued that there is an urgency to develop these techniques for deployment, *if or when* they are deemed necessary.

Climate Engineering Methods

Climate engineering technologies fall under two broad categories: carbon dioxide removal (CDR) and solar radiation management (SRM).

Carbon Dioxide Removal

CDR refers to the removal of carbon dioxide from the atmosphere, whether through direct removal or through indirect measures that sequester CO2 (including afforestation). These technologies are also known as Negative Emissions Technologies (NET). NET is a subset of CDR focusing solely on carbon-dioxide removal technology.

There are a number of CDR techniques, including forest management, soil management, biochar, bio-energy with carbon capture and storage, direct air capture of CO2 from ambient air and storage, carbon mineralization, and ocean fertilization (~~Dumping~~ spreading/distributing iron or other micro-nutrients to promote ~~marine algal growth~~enhanced marine primary productivity) and ocean pumping.

Some forms of CDR are currently available at a low cost, including afforestation and ocean fertilization. While afforestation is widely accepted, ocean fertilization represent a potential for widespread, long lasting and severe effects on the marine environment. As such, ocean fertilization is prohibited under London Protocol and London Convention, with the exception of legitimate scientific research, which would require a permit. Other CDR technologies are not yet available at scale, due to the technology being in early development stages or not yet economically viable.

It is important to emphasize that both CDR and SRM technologies could create adverse environmental consequences. Although the risks of large-scale CDR are perhaps less extreme than the termination effects associated with SRM, there remain other potential environmental consequences. Adverse environmental effects associated with some forms of CDR include adverse impacts on ecosystems and natural cycles. Unlike SRM, the IPCC modelled emissions pathways rely on the use of CDR to ~~absorb~~ remove carbon from the atmosphere. In Canada, certain CDR technologies have received public support, including Squamish British Columbia's Carbon Engineering. Formed in 2009, Carbon Engineering piloted direct-air capture technologies to remove carbon dioxide directly from ambient air. This technology, a form of NET, is already largely accepted.

For more information, see MTP on NET

Commenté [F[6]: As noted above, I'm not convinced this is really the core ethical issue. To me, this is more of a communication issue – the need to convey what climate engineering really is and what it is and is not doing. It would be an ethical issue only if it was being (mis)represented as a solution.

Commenté [F[7]: If you are going to talk about CDR, I think you have to talk about ocean fertilization. I concur with organizing this around the three categories listed in Eric's comment above. However, I find it a bit odd that this paper states at the outset that CDR will be covered in another paper, but yet it leads off with CDR here. I would suggest that either it all be combined into one paper (my preference) or you make a clear separation into one paper on CDR and one paper on SRM. As it stands, it is rather confusing.

Commenté [C[8]: Question for the working group:

Should we also include marine geoengineering here?

Or should we separate CDR into three categories. Natural (e.g., soil and forest management); marine geoengineering (e.g., ocean fertilization); and NETs (e.g., carbon capture and storage, direct air capture). Note that the NET paper is now with NRCan.

Commenté [F[9]: These two sentences are internally inconsistent. The middle sentence of this paragraph suggests that NET and CDR are synonyms; the third sentence says they're not (and doesn't make sense as written). Need to establish clear and consistent nomenclature.

Commenté [F[10]: What is meant here? I think there may be some confusion. The ocean 'biological pump' is the mechanism by which ocean fertilization leads to enhanced ocean uptake of carbon. It is not a CDR technique per se.

Commenté [F[11]: I think it should be made clear somewhere in here that enhanced ocean uptake of CO2 leads directly to increased ocean acidification (with related ecosystem implications). It would be good to introduce this here because it arises again in the context of SRM.

Commenté [F[12]: Please re-word. The IPCC does not do any modelling. The IPCC assesses the published climate science literature.

Solar Radiation Management

Solar Radiation Management refers to technologies that reflect solar radiation back into space before it can warm the planet. There are a number of ways to conduct SRM, including surface-based, troposphere-based, stratosphere-based, or space-based. While all of these methods look to achieve a similar goal, certain methods might present greater risks and ethical concerns, particularly stratospheric, tropospheric, and space-based methods. SRM research is currently moving forward globally, despite the lack of governance mechanisms on the issue. There could be significant risks and trade-offs associated with this. Particularly, there are significant risks in allowing uncontrolled SRM experiments led by rogue countries or private actors, particularly because of weak or non-existent governance on this issue.

While similar in purpose, SRM and CDR are fundamentally different in approach. CDR is a potential mitigation mechanism, while SRM is a preventative measure. Although SRM has the potential to slow the rate of global warming, it does not directly add or remove carbon from the atmosphere. While CDR is used to calculate IPCC long-term pathways in recent reports, SRM is excluded from these calculations due to remaining uncertainties.

Different methods of SRM can create adverse environmental impacts including the termination effect, ozone depletion, impacts on the hydrological cycle, and even changes in regional climate.

Types of Solar Radiation Management

1. Surface Albedo Enhancement

SRM through surface albedo enhancement refers to methods that enhance the reflectivity of the earth by whitening surfaces, whether cities, oceans, crops, deserts, or ice sheets. These proposals have involved painting city roofs white, covering deserts in reflective plastics, and creating a layer of reflective microbubbles below the surface of lakes and oceans. Additionally, one other method proposed "ICE 911", a project to spread glass beads in the Arctic to slow ice melt, is very controversial. ECCC has had several conversations with ICE 911 in 2018. Proponents of the project were told that dumping glass beads in Canada would be treated as prohibited dumping under the CEPA, until they can send information to complete an assessment framework showing that the activity would be legitimate scientific research and can be done so as not to cause marine pollution. ICE 911 chose to pursue their first permit under the U.S. ocean dumping scheme in Alaska.

Another method proposed is the planting of deciduous trees in areas where coniferous trees dominate. This is because that during winter, deciduous trees lose their leaves, allowing solar radiation to be reflected back into space by the snow below. This method could be deployed at a large scale with a low associated cost. Different forms of surface albedo enhancement have different risks and benefits.

While painting city roofs white has no associated risks, it is unlikely to have significant impacts. In contrast, surface albedo enhancement in deserts or lakes/oceans can be highly effective, but could create serious adverse environmental impacts on the ecosystems involved.

2. Cloud-Albedo Enhancement (Tropospheric)

Commenté [F[13]: Somewhere in this section, it should be noted that SRM methods only offset temperature increase. They do not offset ocean acidification associated with ongoing CO2 emissions

Commenté [F[14]: This is not correct and should be deleted.

Commenté [F[15]: I would also delete this sentence – the introduction in the previous paragraph already says what SRM does and it is clear that it has nothing to do with adding of removing carbon.

Commenté [F[16]: Please re-word. The IPCC does not produce pathways or do calculations. It assesses scientific literature.

Commenté [F[17]: This is not really true. SRM is excluded from scenario or pathway calculations assessed by the IPCC because the pathways deal with emissions. SRM is completely independent of emission pathway. Has nothing to do with uncertainties.

Commenté [F[18]: This doesn't really say much, does it?

Commenté [F[19]: I think you mean 'at' the surface, not below.

Commenté [F[20]: Why are we singling out individual proposals. There are many proposals that could be listed, but I don't think any should be specifically mentioned here – it gives the impression that this one is somehow more mature or plausible than others (which I don't believe is the case).

Commenté [F[21]: This all seems superflouous for a document that is ostensibly about providing a concise overview of the topic rather than specific interactions/issues.

Commenté [F[22]: I have not heard of this as a SRM scheme and couldn't find anything on this in my quick google search. What is the source?

Commenté [F[23]: It seems to me that if judgment statements like this are to be included, they should be supported by reference to literature. In particular, stating that painting city rooftops white is unlikely to have significant impact may be true at the global or regional scale, but not at the urban scale where it is viewed as a way to offset urban heat island – there are many scientific papers on this.

SRM through cloud albedo enhancement often refers to the practice of marine cloud brightening, which involves spraying sea salt into the lowest clouds above the ocean. In doing so, these salt particles help to brighten clouds and increase their reflectivity. Proposals to conduct this form of SRM include launching a fleet of ships to patrol the ocean while spraying seawater into the troposphere. It is important to note that there is a termination effect for this type of SRM, as these particles dissipate within days. This refers to the reality that for many forms of SRM must be continuous to maintain their effects. If SRM methods are halted abruptly, the termination effect might create extremely rapid warming and potentially disastrous impacts on natural and human systems.

There also remain some uncertainties regarding the effectiveness of cloud-albedo enhancement. It is likely that this form of SRM could also create changes in regional climate. Given the need for a large fleet of ships (or planes) to conduct this form of SRM, the costs of deployment would likely be high. However, other proposals to conduct this form of SRM, including through the use of drone ships, could be deployed at a much lower cost.

Commenté [F[24]: It is not yet a 'practice'.

Commenté [F[25]: It is not the salt particles themselves that brighten clouds. It is their role in changing cloud droplet size and lifetime.

3. Stratospheric Aerosols

Stratospheric aerosol injection is perhaps the most controversial form of SRM, and involves releasing reflective particles (e.g., sulfate aerosols) into the upper atmosphere to scatter sunlight back into space. Similar to cloud albedo enhancement, this form of SRM also faces a termination effect, as particles slowly fall back to earth unless continuously replenished. Despite this, this technique would very likely be effective, particularly as it looks to mimic the natural cooling the Earth experiences after major volcanic eruptions.

The technology needed to conduct SRM using stratospheric aerosols largely exists, and could be available for a relatively low cost. Proposals have included spraying sulfate aerosols from high-altitude aircraft. However, these current technologies would also create a range of adverse environmental side-effects, including chronic health issues linked to increased fine particulate matter, depletion of the ozone layer, increasing acid deposition leading to acid rain, and changes to the hydrological cycle. The World Health Organization currently attributes 4.2 million deaths every year to ambient air pollution. Aerosol injection has the potential to increase the death toll from air pollution, and would have a disproportionate impact on the most vulnerable members of society.

Climate modeling will be needed to fully assess the impacts on the hydrological and climate cycles. We could expect more rain in certain areas and less in others. However, researchers are looking at way to minimize the environmental and human health impacts through research on different aerosol types (e.g., calcium carbonate). The hope is that these alternatives would reduce solar radiation, while neutralizing acids associated with anthropogenic emissions that contribute to ozone loss.

Commenté [F[26]: What is the basis for this statement?

Commenté [F[27]: While perhaps factually correct, I think this is potentially very misleading – at least one published paper that I was able to find (in 1 minute of searching) suggests geoengineering would cause 26,000 premature deaths, which is 0.6% of the WHO total deaths related to air quality. See https://keith.seas.harvard.edu/files/tkg/files/eastham_et_al._-_2018_-_quantifying_the_impact_of_sulfate_geoengineering_o.pdf

4. Space-Based

Space-based SRM involves preventing solar energy from reaching the atmosphere in the first place. This method could include the deployment of space-based sunshades or reflectors to obstruct solar radiation with mirrors or dust. Although theorized, the technologies to conduct space-based SRM do not yet exist

at the necessary scale. Additionally, the costs to develop and deploy space-based SRM technologies would likely be very high.

International Context

The United Nations Convention on Biological Diversity has called for a moratorium on climate engineering activities that might affect biodiversity until there is adequate scientific basis and appropriate consideration of the social, economic, and environmental risks associated with the deployment of these climate-engineering technologies. However, the convention allows for small-scale scientific research.

At the Thirtieth Meeting of the Parties to the Montreal Protocol on Substances that Deplete the Ozone Layer in November 2018, parties discussed the role that climate engineering methods might play in impacting the ozone layer. Particularly, SRM climate engineering through stratospheric aerosols has been identified as one potential future threat to the ozone layer. Some parties expressed their concern that climate engineering technologies are not fully understood and might have risks that outweigh any benefits. At the 41st Open Ended Working Group of the Parties to the Montreal Protocol, held in July 2019, Parties considered a report by the Protocol's Scientific Assessment Panel on the potential impact on the ozone layer of various SRM approaches that have been considered. Several parties, including Canada, agreed that the panel should provide updates on this issue in the context of its quadrennial scientific assessment reports, noting that the Panel should remain focused on relationships between SRM and the ozone layer, given the broader work on SRM being undertaken by the IPCC.

Climate Engineering was also discussed at the UNEA in Nairobi in March 2019. The Swiss delegation tabled a proposal calling for an expert review of climate engineering technologies, processes, and risks. Although this became the highest-level discussion of climate engineering governance in an international fora, opposition from the United States, Saudi Arabia, and Brazil stalled the proposal and led to its eventual withdrawal. These states expressed a preference that the IPCC address climate engineering, as they are set to discuss the issue in AR6, expected in 2021.

Ongoing Research

Although international dialogue surrounding climate engineering and SRM is limited, research in the field is intensifying. While researchers previously focused almost exclusively on theoretical and climate modelling of SRM technologies, researchers are conducting a growing number of real-world experiments. In 2011, British academics planned an outdoor SRM experiment, but cancelled the project after public backlash. Also in 2011, cloud physics researchers conducted an experiment off the coast of California that closely resembled a marine cloud brightening experiment. There are four major SRM pilot projects currently proposed that have gained recent attention: the Marine Cloud Brightening Project, Ice 911 (surface albedo enhancement), Sky River (major cloud seeding proposal in China), and the Stratospheric Controlled Pertubation Experiment (SCoPEx) (small-scale stratospheric aerosol tests led by Harvard University Researchers). It is important to note that none of these field research projects are led by government, and all involve academic researchers or other 3rd party organizations.

Canadian Context

While there is no comprehensive legislative framework in Canada that governs climate engineering, specific provisions of existing Canadian law might be applicable to some aspects of SRM. It is unclear whether any legislation at the provincial/territorial level might be applicable to climate engineering. However, it is important to note that the Canadian territories will likely be ~~much~~ affected much more than other Canadian jurisdictions, given the region's climate.

Commenté [F[28]: What is the basis for this assertion?

For example, the deposit or release of harmful substances into fish-bearing waters or areas where there are migratory birds is prohibited under subsection 36(3) of the *Fisheries Act,* and section 5.1 of the *Migratory Birds Convention Act, 1994*. This could include the release of albedo-enhancing particles deemed harmful.

In 2013, the London Protocol adopted an amendment on ocean fertilization to provide a permit system and a means to distinguish between marine geoengineering techniques that should be prohibited and regulated, allowed in cases of legitimate scientific research, or permitted more generally. Until this amendment is in force for Canada (an amendment to CEPA is required), Canada prohibits all disposal of substances at sea under CEPA and can ask for an assessment of the activity and waste. Once assessed, ECCC can rule that a project is exempted or prohibited. Although there is no permitting mechanism established, a permit is defined by CEPA as the only method to grant an exemption. Despite this, ICE 911, an initiative looking to conduct surface albedo enhancement in the Arctic has developed what they claim is "100% safe" glass microsphere technology to conduct SRM. This proposed approach, which releases a substance on sea ice, is considered to be disposal at sea. This means that ICE 911 proposal requires assessment before it can be authorized under a permit, or be exempted from needing a permit.

Commenté [M[29]: Seeking clarification on this

Commenté [F[30]: Again, not sure why this specific issue is being raised again in this document. How about an appendix or something in which some specific examples like this are listed, rather than including in the main text

In addition, the *Weather Modification Information Act* requires proponents to notify the department if they intend to take actions to modify precipitation. Although this Act would likely not apply to small-scale climate engineering research, it might apply to large-scale deployment of SRM methods, particularly stratospheric aerosol methods that might affect the hydrological cycle.

Commenté [M[31]: Seeking clarification

As stratospheric aerosol injections involve the use of sulfur dioxide, the CEPA could regulate SRM activities that specifically involve the release of toxic substances. Additionally, it could be possible to require an impact assessment for SRM activities in specific circumstances.

Ethical Considerations

Given the range of social, economic, and environmental risks associated with climate engineering, the somewhat limited scientific understanding of the processes involved, the presence of a termination effect, and the lack of research, national, or international governance mechanisms, SRM has generally been regarded as the more controversial climate engineering approach (when compared to CDR). It is important to acknowledge that while SRM can limit the effects of global warming, it is not a "silver bullet" solution to the challenges of climate change and should not be considered one.

Commenté [F[32]: This needs to be re-worded. It does not limit the effects of warming, it is aimed at avoiding/reducing warming

There are also ethical considerations behind the decision of whether to pursue further research or eventually deploy climate engineering technologies in the first place. Many of the risks of these technologies have been acknowledged. However, if these technologies can present an effective solution

to climate-related ecological disasters, are governments obligated to continue to research and prepare these technologies for potential deployment? Questions of this nature warrant careful consideration in discussions on climate engineering.

Considerations

- Even with lower-risk forms of climate engineering, it is important to note that climate engineering *should not* be considered a substitute for mitigation and adaptation.
- Further research is needed to determine the merits and risks of SRM climate engineering. Despite this, academic and private organizations have already begun to field-test some of these SRM techniques at small scales.
- The merits and risks associated with CDR technologies have been studied in greater detailed than those associated with SRM. The Government of Canada has previously supported some CDR technologies, including Squamish BC's Carbon Engineering and their direct air capture technologies. However, it should be noted that the environmental impacts of CDR technology deployment at a large scale remain largely unknown.
- Although climate engineering relates primarily to long-term decarbonization, research on climate engineering has already begun to move from theoretical modelling to real-world demonstration projects. Regardless of the Government's own position on the merits/risks of climate engineering, it may be necessary to develop a framework to govern academic and 3rd-party research on climate engineering in Canada, particularly as this research is likely to continue regardless, and could entail substantial risks.

Commenté [F[33]: This sentence doesn't make sense

Recommendations

Commenté [F[34]: Shouldn't there also be a recommendation that ECCC undertakes dedicated research on climate engineering in order to inform future policy and regulatory considerations?

- ECCC needs to develop and agree on the key principles that should guide the development of domestic policy and how to operationalize them in Canada.
- Given the increased attention to climate engineering in international fora, it is recommended that Canada begin engage in international discussion on climate engineering research and policy.
- ECCC needs consider the development of a domestic research governance system in order to allow small-scale field research to proceed legitimately as per international agreements to which Canada is a party.
- As research on climate engineering will continue to intensify in the coming years, it is recommended that Canada explore means of implementing a moratorium on large-scale experiments or deployment of atmospheric climate engineering methodologies.

Solar Radiation Management: A Brief Introduction

G.M. Flato – 24 July 2019

Climate Research Division, ECCC

Solar radiation management (SRM) is one category of activities or interventions that fall under the umbrella of Geoengineering or Climate Engineering, that is, deliberate large-scale intervention in the Earth's climate system, in order to moderate global warming[1]. SRM involves interventions that increase reflection of solar radiation (sunlight), thereby reducing incoming energy and hence providing a cooling effect that would offset greenhouse gas warming. Techniques that have been proposed include: injection of reflective (sulphate) aerosols into the stratosphere (in some ways mimicking the cooling effect that arises from explosive volcanic eruptions); launching of space-based mirrors or other reflective material; injecting salt-water spray into the lower atmosphere over the ocean to alter the reflectivity or lifetime of marine clouds; modifying the surface by planting more reflective crops; and painting or coating building rooftops or other surfaces with more reflective material. It should be noted that SRM does not address the causes of global warming (namely greenhouse gas emissions), but rather seeks to offset the warming that would otherwise occur.

SRM has gained attention as a climate change intervention because it has the potential to act very quickly and could be implemented at relatively low cost (as compared to many carbon dioxide removal, CDR, approaches). For example, sulphate aerosols injected into the stratosphere have an essentially instantaneous cooling effect, although large amounts would have to be transported to offset a substantial part of anthropogenic warming[2]. Such aerosols also have a relatively short lifetime in the atmosphere (a couple years) and so on-going effort is required, and if terminated, would almost immediately unmask the warming that had been avoided.

There is a fairly large and growing body of scientific literature on SRM, including global climate model simulations that illustrate the potential effectiveness and unintended consequences (like changing rainfall patterns) of stratospheric aerosol injection or space-based technologies. These unintended consequences give rise to a range of ethical and international governance/liability issues, and the termination effects constitute an ongoing commitment to SRM technology and an ongoing exposure to the risks associated with interruption. The Climate Research Division has been involved in SRM simulations using its global Earth System Model, and is participating in current international model intercomparison projects on this topic[3], but at this point there is not a dedicated SRM (or geoengineering) research program in the Department at the scale that would be needed to fully inform domestic and international policy and regulatory development.

---

[1] https://royalsociety.org/~/media/Royal_Society_Content/policy/publications/2009/8693.pdf

[2] https://iopscience.iop.org/article/10.1088/1748-9326/aae98d

[3] http://climate.envsci.rutgers.edu/GeoMIP/

Geoengineering
Impacts of stratospheric sulfur injections on radiation and climate

Context

The ultimate goal of this project is to use the CCCma full Earth System Model, including ocean, carbon, and sea ice feedbacks to determine impacts of sulfur injection on stratospheric ozone and tropospheric chemistry and do the comparison with results from other modelling systems and observations.

Short term

First stratospherically extended version of CCCma aerosol microphysics model to simulate stratospheric sulfur injections

The current version of the atmospheric global climate model (CanAM5) will be modified to simulate possible future solar radiation management (SRM) techniques based on stratospheric sulfur injection. This will require two developments for CanAM5. First, the vertical model domain in CanAM5 will be extended into the stratosphere to create a dynamical middle atmosphere version of CanAM5. Simulations of stratospheric dynamical processes will be conducted and evaluated. Second, the tropospheric aerosol microphysics model (PAM) in CanAM5 will be modified to allow simulations of stratospheric aerosol processes. Specifically, particulate sulfuric acid and a stratospheric source of SO_2 will be added. Concentrations of stratospheric sulfur oxidants will be included in the model based on simulations with CMAM.

Medium term

A unified model for stratospheric and tropospheric aerosol to account for different techniques for stratospheric sulfur injection and comparing modeling results with observations for Pinatubo eruption

To evaluate the model it will be validated by simulating the eruption of Mount Pinatubo in 1991 and comparing with available observations. Since SRM applications can be a very different regime from a volcanic eruption additional validation of the model will be performed by comparison with model data from existing SRM applications. Model experiments will be performed to identify the sensitivity of aerosol concentrations to key SRM processes. Results from these simulations will be used to determine and compare the efficiency of different SRM deployment strategies.

Further model improvements will be made based on results of the model evaluation. For instance, different techniques for stratospheric sulfur injection and the formation of new aerosol particles near the injection source will be investigated. Parameterizations of aerosol optical properties and the treatment of radiative transfer in the upper atmosphere will be evaluated and improved, as necessary. For example, improvement of non thermal equilibrium processes in the current radiative transfer calculations in CanAM5 may need to be addressed.

Furthermore, an interactive representation of gas-phase chemical processes for stratospheric ozone and the exchange of aerosols and gases between the stratosphere and troposphere may need to be included in the model. Natural sources of stratospheric aerosols and gases may also be added to the model, if necessary. Overall, model improvements for sulfur injection, radiation, and chemistry will lead to a fully coupled Earth System Model which includes ocean, sea ice, carbon and ozone feedbacks.

Ongoing

A full Earth System Model determining the impacts of sulfur injection

The Earth System & SRM Model will be used to determine impacts of sulfur injections on climate and air quality. In particular, the impacts of SRM techniques on regional temperatures in Canada and the Arctic will be investigated. Furthermore, earlier studies showed that SRM may lead to complex and perhaps undesirable changes in hydrological and carbon cycles. Therefore, impacts of SRM techniques on precipitation rates, soil moisture, and carbon sinks will be investigated, too.

Results of the CCCma Earth System Model will be compared to results from other modelling systems and climate scenarios. Model results will be made available to the international research community through participation in geoengineering model intercomparison project. Furthermore, the impacts of SRM techniques and potential future volcanic eruptions will be considered for the development of the seasonal and decadal prediction model system (CanSISE).

Resource Requirement in Short-term

- 1 x SE-RES
  - Develop and evaluate a stratospherically extended dynamical version of CanAM5
  - Develop and evaluate aerosol microphysical parameterizations for stratospheric sulfur
- 1 x PC
  - Configure and test a stratospherically extended version of CanAM5
  - Develop, implement, and test data sets for stratospheric sulfur emissions and oxidant concentrations
  - Develop diagnostic tools for stratospheric processes
  - Maintain and manage model data sets and a single column model version for stratospheric aerosol processes in support of collaborations with external experts

Additional Resources Requirement (medium-term and ongoing) term

- 1 x SE-RES
  - Plan and analyze:
    - Simulations of the Eruption of Mt Pinatubo
    - Model sensitivity experiments to identify key processes and uncertainties for SRM
    - Earth System model simulations to investigate impacts of SRM on carbon cyle and chemistry
    - Contribute to development of seasonal prediction modelling system to account for volcanic eruptions
  - Participate in model intercomparison projects
  - Develop and evaluate new parameterizations of aerosol microphysical, chemical, and radiative processes in the stratosphere
  - Collaborate with other experts to facilitate the development of new parameterizations
- 1 x PC-02
  - Configure and test CanAM and CanESM for simulations of stratospheric volcanic eruptions and SRM
  - Conduct simulations in support of SRM model intercomparison projects and research

- Develop, implement, and test data sets for emissions and stratospheric model boundary conditions
- Develop improved model diagnostic tools
- Investigate and improve code efficiency and coupling of different model components

Platform alignment

Response to the reviewers

We thank the reviewers for their critical assessment of our work. In the following we address their concerns point by point.

Reviewer 1

General comments

Reviewer Point P 1.1 — Moseid et al. compare surface downwelling shortwave radiation from CMIP6 models and from ground stations. They show the discrepancy between modeled and observed SDSR is partly caused by erroneous aerosol and aerosol precursor emission inventories, thus providing important information for the evaluation of ESM. While the research topic is essential, the methodology can be improved to clarify the impacts of clouds and cloud-aerosol interaction. Instead of using all-sky SDSR, I would suggest the authors compare the sunny-day SDSR from CMIP6 and from ground stations throughout the whole text.

Reply: We thank the reviewer for their comment and agree that the manuscript should include a more detailed description of the impact of clouds and cloud-aerosol interactions. This has been added both in the introduction section and in the discussion section.
Unfortunately neither GEBA nor CMIP6 models provide sunny day SDSR. Previous studies such as Allen et al. (2013) have used the GEBA data set to create a clear sky proxy for a selection of stations to compare with the clear sky flux variable of CMIP models. However, this is beyond the scope of our study.

Reviewer Point P 1.2 — To be more accurate, I would also suggest the authors compare the SDSR conditions on the atmospheric relative humidity, which is associated with the scattering from water vapor.
Note that the clear-sky SDSR from climate models is usually used for calculating cloud radiative forcing and is not the same as sunny-day SDSR.

Reply: We are looking at long time fluctuations in SDSR. Water vapor has not changed in a sufficient magnitude in recent decades to have an effect on decadal fluctuations in SDSR (Wang and Yang (2014), Hoyt and Schatten (1993),Ramanathan and Vogelmann (1997),Solomon et al. (2010)). We therefore assume in this study that the SDSR effects of water vapor scattering is negligible. We do ,however, improve the manuscript in the explanation of the effect of clouds on SDSR. A paragraph on Clouds and SDSR has been added in the introduction, and the section connected to the current Figure 3 has been improved for clarity.

Minor comments

Reviewer Point P 1.3 — The title: I would not use the "1961-2014" in the title. It provides little information.

Reply: Fixed.

Reviewer Point P 1.4 — The title: compare to -> compare with.

Reply: Fixed.

Reviewer Point P 1.5 — The title: maybe the authors should include "aerosol", which is the theme of the paper

Reply: Fixed.

Reviewer Point P 1.6 — Figure 3: Please double check the cloud fraction and the calculation of anomaly. If the trend is reversed, it explains everything.

Reply: This is double checked and the presented Figure is correct. In the future version of this manuscript this figure will be made into a table for clarity.

Reviewer 2

General comments

Reviewer Point P 2.1 — It would improve the paper if more background information in the introduction section was provided on the key drivers of SDSR i.e. clouds and greenhouse gases can also influence SDSR in addition to aerosol effects.

Reply: We added a more detailed description in the introduction section of what can influence SDSR, especially in regards to clouds, but also greenhouse gases and solar irradiance.

Reviewer Point P 2.2 — Throughout the paper there are numerous mentions to the fact that aerosols play a key role in the dimming signal of SDSR observed and simulated across all regions. However, the same cannot be said for the observed brightening signal in more recent years. A key question seems to be why are aerosols a key driver in the dimming but not brightening?
If the emission inventories and aerosols were in error throughout the whole period of study then surely the models would not be able to simulate the temporal evolution of both phenomenon across all regions?

Reply: We answer this point in two parts - first the role of aerosols in brightening:
We would like to point the reviewer to the following studies Allen et al. (2013), Chiacchio et al. (2015) and Wild (2011), which show that indeed aerosols are a key driver to the observed brightening in recent years. The reduction of antropogenic aerosol emission leads to brightening. We would also like to thank the reviewer for mentioning this point that we did not explicitly say in the original manuscript, but has now been added in the second paragraph of the introduction.
Then the final question on emission inventories: Correct, this is why we are proposing errors in emission inventories as a possible reason for discrepancies in the regions where the models are not able to simulate the temporal evolution of dimming (and brightening).

Reviewer Point P 2.3 — The paper states that the CMIP6 models are able to represent the observed SDSR signal over Europe relatively well. However, I think there are a few interesting discrepancies which should be discussed further. Prior to 1980 the observations do not show much of a dimming signal (in fact the observed anomaly is slightly positive at times) but the CMIP6 models do show a consistent dimming signal. Is there a specific reason for the absence of a dimming in the observations, when we know there were large concentrations of aerosols over Europe at this time? Contrary to what was mentioned in point 2 above Europe is the only region where there is a simulated brightening signal in both the model and observations, implying that models are able to reproduce brightening signal over certain regions. It would be good to know if there a reason for this over Europe and does it occur over other regions like for example North America.

Reply: The referee is right that Figure 1b does show some interesting discrepancies in the beginning of the time period in the study that was not mentioned in the original manuscript. The observational data set used in this study starts in 1961, and the anomaly shown in the figure is made as a difference from the the mean value of SDSR from 1961-1966. Since the European dimming started before 1960 (Wild, 2011) the "true" European SDSR anomaly might not be achieved using this data set, as is also seen by the weak European dimming in Storelvmo et al. (2018) using the same data set.
The reason for the discrepancy between model SDSR and observed SDSR Europe in the mid 1970s is unknown at this time, but has been added as a comment in the manuscript in Section 3.1 first paragraph.
The observed and simulated brightening in Europe duplicate each other well and thereby we propose that the emission inventories of aerosols in Europe are estimated well.
North America has not been shown in Figure 1, but is included here in the reply as supplementary Figure S1. See Leibensperger et al. (2012b) and Leibensperger et al. (2012a) for a closer look at the climatic effects in North America to anthropogenic aerosol emissions. We chose Europe and Asia as areas of focus to give the readers a clean impression of one example region where the models perform well and one example region where they do not perform well. The comparison of results for North America in our study together with previous findings in North America climatic effects is complicated, and is beyond the scope of this study.

Reviewer Point P 2.4 — For the analysis over China the paper suggests that the error between the models and observations of SDSR are due to the errors in emission inventories that translate into errors in the calculation of atmospheric burden of aerosols. (1)Are we certain that the errors in the emission inventories are that large to account for the discrepancy in model and observed SDSR? Is there an estimate of the uncertainty for the CMIP6 emission inventory and how does CMIP6 compare to other global and regional emission inventories? (2) Can these differences explain some of the inconsistencies of models with observations? I am not convinced that the observed trend reversal in SDSR over China in 1990 can be explained by errors in the emission inventories alone. (3) Are we anticipating a slowing down of SO2 emissions in China from the 1990s onwards? As far as I understand, anthropogenic emissions of aerosols and their precursors (particularly SO2) have largely been increasing over China up until 2010 when air pollutant control measures were then implemented to reduce emissions. Therefore, if aerosols were driving the temporal change in SDSR over China a dimming signal should have been observed up until this point, but it isn't. This is present in the observed and simulated change in SDSR over India but not China. (4) How do this discrepancy match with the conclusions of the paper and what else could be driving the SDSR trend over China throughout this period? I think this needs to be explored further in the paper as the assumed underlying trend in emissions (and therefore aerosols) and SDSR do not seem

to match over China and from what I can tell it cannot be reconciled by errors in the emission inventories alone.

Reply: To make it easier for the reader we have marked up numbers to the questions in the reviewer point. (1) We are not certain that the errors in the emission inventories are large enough to account for the discrepancy in model and observed SDSR alone, but we propose that this error plays an important part. Unfortunately there is no estimate of uncertainty in the CMIP6 emission inventories, but this is planned to be included in the next generation of CMIP emission inventories (see Hoesly et al. (2018)). Because there is no estimation of uncertainty we do not have evidence to say that errors in emission inventories are small to cause a discrepancy between model and observation.
(2) The CMIP6 emission inventory is made using CEDS that makes datasets based on EDGAR, as in written in more detail in Hoesly et al. (2018). There is probably some differences between the CMIP6 data set and other regional emission data sets, but this study does not look further into finding such differences. We propose at least some of the discrepancy between model and observed SDSR is caused by errors in emission inventories, but we do not have enough evidence to propose all discrepancy is emission sourced. We recognize that the manuscript have given the wrong impression to the reader that errors in emission inventories *alone* cause all discrepancy, and this has been made clearer throughout the text.
(3) During the review process we found more information regarding the observed trend reversal in the GEBA data in China. According to the CMIP6 data set of sulfate emission we do not expect a slow down of emitted SO_2 from 1990, but rather from around 2005. The observed trend reversal in SDSR does therefor not fit with CMIP6 emitted sulfate. However, previous studies have found the trend reversal in SDSR is to a considerable extent caused by the fact that the Chinese radiation network was replaced with new measurement devices between 1991 and 1993, which caused a spurious upward jump in the records (Wang and Wild (2016), Wang and Yang (2014), Yang et al. (2019)). With this new information we have added a section under discussion where the trend reversal in China is in focus, where we do not disregard the trend reversal completely. The trend reversal begins in 1989 - before the instrument were replaced, and we see a distinct signal of a trend reversal in Japan which is downwind form China, with this in mind we try to disentangle the observed SDSR in China in our new section under discussion.
(4) The conclusions of the paper proposes that errors in anthropogenic aerosol emission inventories plays a part in the discrepancy seen between model and observed SDSR. Even if the trend reversal in the observed SDSR in China was to be an artifact the models would largely underestimate the magnitude of dimming. In regards to the trend reversal, the assumed underlying trend of increasing sulfate emission until 2010 as proposed by the reviewer (and CMIP6) is being questioned in this manuscript. We thank the reviewer for this comment and we have updated our discussion section to include possible causes of the mismatch, and we are performing a station-test to see where the stations with the strongest trend reversal is found that will be added in the supplementary of the manuscript.

Reviewer Point P 2.5 — Only limited discussion within the paper is provided on clouds and aerosol-cloud interactions, which needs to be improved throughout the paper. Within section 3.3 a link is made between cloud cover change and SDSR but how much of an influence do clouds have on all-sky SDSR? How reliable are the observed and simulated cloud cover changes and can some uncertainty bounds be placed on them? Is a regional cloud cover change of 1-2% significant in terms of SDSR? In figure 3 the temporal change in observed cloud cover is similar to that in observed SDSR so even if clouds can't explain the magnitude and all of the observed change then surely they must be exerting some influence on SDSR? Is it possible to compare a clear-sky derived

observed SDSR to that from model simulations to eliminate any influence of clouds on the signal?

Reply: We thank the reviewer for this comment, and we have included more information on aerosol-cloud interaction in the introduction, results and discussion. Previous studies have found that the link between cloud cover and SDSR trends depends on what region you are looking into. For Europe cloud cover has most of an effect on SDSR on the shorter time scales, and the dimming and following brightening observed in Europe is dominantly caused by changes in anthropogenic aerosol emission and thereby the aerosol absorption and scattering (Norris and Wild, 2007). For China cloud cover made a negligible contribution to all sky SDSR trend in GEBA until 1989. After 1980 the heavily discussed trend reversal is observed in China, and Norris and Wild (2009) suggests half of the observed brightening between 1990 and 2002 is caused by a reduction in cloud cover. Please note that this paper was published before the proposal of the trend reversal being an artifact of a change in instrumentation (Wang and Wild, 2016). Which complicates the story. In North America cloud cover is found to have played an important role in the observed brightening (?). The observed cloud cover in Figure 3 shows a reduction in cloud cover in the dimming period, and an increase in the brightening period, which is the opposite of what is expected in cloud cover played an important part in dimming and brightening in China. We have decided to replace Figure 3 with a table and make the manuscript more clear on what role cloud cover plays in all-sky SDSR. Other studies have made clear-sky derived observed SDSR (Norris and Wild (2007),Norris and Wild (2009)) when assessing the cloud signal for Europe and China (mentioned above in this reply), but this goes beyong the scope of our study.

Reviewer Point P 2.6 — The previous comparison of CMIP5 models to observed SDSR by Storelvom et al., (2018) is mentioned throughout this study, with similar results presented here for CMIP6 models. A key question is therefore why has there been no improvement in simulating observed SDSR between CMIP5 and CMIP6 models? This is despite some changes to individual aerosol schemes within models and also different historical aerosol precursor emission datasets being used. Some discussion is needed on what is continually missing from the models and what are the model developments to focus on to improve the future simulation of SDSR.

Reply: To answer this question we must first find out whether the source of the error is within the model's codes or within the emission inventories, or a combination. Storelvmo et al. (2018) argues that the discrepancy between observed and modelled SDSR may be attained to errors in the treatment of processes that translate aerosol emissions into clear-sky and all-sky radiative forcings. Here, we show that simulated SDSR develops similarly in time, but opposite in sign, to simulated atmospheric burden of SO2. By doing this we narrow down the potential source of error by suggesting that the atmospheric burden in the models are at fault, and that the processes translating burden into clear-sky and all-sky radiative forcings are behaving as expected. The final answer of what is at fault is still not found, but we suggest to have found a piece of the puzzle in the emission inventories.
Future studies include doing model experiments with changes in emission to see what it takes for the models to recreate the magnitude of dimming that is observed. We thank the reviewer for this comment and we have added a section in the bottom of the conclusion that explains what our next step is.

Reviewer Point P 2.7 — Further details are required, either in Table 1 or a new table, on each of the CMIP6 models used in this study. In particular, it would be useful to know horizontal resolution and some information on the individual chemistry and aerosol schemes in each model. This could provide useful information to the reader of the potential causes of discrepancies between

models. In addition, it would be good to have a record somewhere of the actual output used from the ESGF (e.g. temporal period, variant ID, CMIP table ID etc). Furthermore, if there is data now available for additional CMIP6 models then it would be useful to include it, as long as it further informs the current study.

Reply: We thank the reviewer for this comment and we have added information on the resolution of the models in Table 1, in addition to a supplementary section on where to find the data used in this paper, including the model schemes. More data has been published since the first submission of this paper, and we have therefore decided to include more models in this study. In addition, some of the models already in the paper has now released more data in some of the experiments that they didn't have in the original manuscript, and this data has now been included in this study.

Reviewer Point P 2.8 — The methods section (2.3) appears to lack important details of what model data is being used (see point 7) and how the gridded model data has actually been compared to the observations which are at point locations. In calculating the regional means at observation locations, do the number of sites used change over time period and does this have any impact on the results? Furthermore, in the results section the clear-sky SDSR is discussed but is not mentioned in the methods section. I also think that it is important to use multiple ensemble for meaning purposes when using coupled experiments members from models so that the internal variability in each model can be shown (this would give a range of variability important to show on some of the Figures for certain variables).

Reply: We thank the reviewer for this comment and agree that the methods section was indeed lacking both clarity and details. This has been fixed in the new version of the manuscript. We have added three ensemble members per model for the historical simulation, which will be presented in the new version of Figure 1. This figure will then present the internal variability per model in addition to the comparison to observations.

Reviewer Point P 2.9 — A General comment on the figures is that they could be improved to make them easier to read by using better colours (I found the light green very bright), tick marks on the axis and line types that are easier to distinguish between different model experiments. Also, if it is possible to include a measure of observational and model uncertainty on any of the figures then this would improve the comparisons. When values from figures are continually referred to in the text it would help the reader if there is reference table containing some of the key numbers included (like the supplementary table).

Reply: We thank the reviewer and have chosen a different a color chart for the figures, more tick marks, and different line types to better differ the graphs. Uncertainty estimates have been included in Figure 1. A reference table with key numbers is an excellent idea, and has been added to the manuscript.

Minor comments

Reviewer Point P 2.10 — Page 1, line 9 – Reword this sentence as mentioning SO2 emissions, which are not aerosols, and then other aerosols relevant to SDSR. Be more precise in this statement.

Reply: Clarified and fixed.

Reviewer Point P 2.11 — Page 1, line 13 – Can you say how much error is associated with aerosols and emission inventories that might contribute to error in SDSR?

Reply: Unfortunately the emission inventory data set for CMIP6 does not have estimates of uncertainty, which is why we use the word "partly" in line 13 as we have no evidence telling us how much of the discrepancy can be attributed to emission estimates.

Reviewer Point P 2.12 — Page 2, Line 30 – Is this statement true across all regions? What about for Europe?

Reply: This statement is only true globally based on previous studies. Added the word "global" to clarify.

Reviewer Point P 2.13 — Page 2, line 35 – For the introduction it would be good to include a bit more detail on what the GEBA observations on their own show before introducing any comparisons to models.

Reply: We thank the reviewer for pointing this out, as the introduction to global dimming mentioned several citations that all used GEBA to identify dimming (and regional brightening), which was not exclusively mentioned. This has now been clarified in the text.

Reviewer Point P 2.14 — Page 2, line 46 – here the study says that two observational datasets are used but only one has been mentioned in the previous paragraph. Please include details of what is the second dataset used in this study.

Reply: The second observational data set has been added to the previous paragraph. "We also use observational cloud cover data to briefly assess the role of cloud cover in the historical development of SDSR".

Reviewer Point P 2.15 — Page 2, line 47 – please reword sentence "An explanation of the methods used to obtain and analyse the data complete Section 2."

Reply: Fixed.

Reviewer Point P 2.16 — Page 3, line 57 – it would be good to include the error in the observations on all figures to show the uncertainty in the observations.

Reply: Unfortunately sources of error in observation differs from station to station and we only have a general estimation of error from the instruments used. We have chosen to include a light grey line with the "raw" observational data in the background of the smoothed black observational line in time series graphs to show the variability of observations. A section discussing the observations in China has also been added in the discussion section on the manuscript.

Reviewer Point P 2.17 — Page 3, line 60 – Please clarify if this temporal gap filling technique allows for all 1487 stations to have a complete record of observations over the entire 1961-2014 and how this technique impacts the observations. If the number of stations used changes over the entire time period then it could be important for the analysis.

Reply: Fixed.

Reviewer Point P 2.18 — Page 3, line 74 – insert 'is' between "these the"

Reply: Fixed.

Reviewer Point P 2.19 — Page 4, line 93 – replace 'stales' with "stalls"

Reply: Fixed.

Reviewer Point P 2.20 — Page 4, line 94-95 – "So these experiments will show to what extent the removal of cloud cover change from global warming has an effect on SDSR." – I am sure that this is the case as there will be still be variability in the cloud fields simulated by climate models in these experiments. In addition, as the aerosol fields are changing in these experiments, they will also impact the simulated clouds in the models. Therefore, to make this statement further evidence would be required from each model that the cloud fields are being properly constrained to isolate their impacts on SDSR.

Reply: We are not stating that all cloud cover change is removed, only the cloud cover change that is induced by global warming - as global warming essentially is removed in these experiments. Cloud cover will change due to aerosol emissions and thereby impact SDSR - but not due to global warming. Changed the wording from "cloud cover change from global warming" to "cloud cover change caused by global warming" to clarify.

Reviewer Point P 2.21 — Page 4, line 107 – It would be good to show on a figure the spatial distribution of the GEBA observations within each defined region.

Reply: Storelvmo et al. (2018)s Figure 1 is an excellent figure showing the spacial distribution of the stations used in both this and her study in addition to the trends of the stations in colours. I have added a reference to that figure in the text.

Reviewer Point P 2.22 — Page 4, line 110-112 – Please clarify exactly how anomalies have been calculated. Are anomalies calculated for each individual observation site within a region first before then calculating a regional mean value?

Reply: Clarified.

Reviewer Point P 2.23 — Page 4, line 112 - Supplementary table number is not shown

Reply: Fixed.

Reviewer Point P 2.24 — Page 4, line 113 – Provide more information on exactly what model data has been obtained from the ESGF (perhaps in a separate table) e.g. CMIP table ID, variant label etc. (see general comment 8)

Reply: Added a table in supplementary.

Reviewer Point P 2.25 — Page 4, line 115 – I think it would be more prudent to use more ensemble members for coupled experiments and with this an idea of the internal variability for each model could be obtained for variables such as cloud cover and SDSR.

Reply: Three ensemble member are now being used in the historical experiment, and the manuscript has been updated to explain this.

Reviewer Point P 2.26 — Page 4, line 116 – It is not clear if the 10-year running mean is used for the model data, observation data or both?

Reply: Fixed and clarified in the methods section.

Reviewer Point P 2.27 — Page 5, line 121 – it is hard to see from Figure 1 a) as to whether the global SDSR representation in the models is similar to the observations at all. There is clearly a difference in magnitude but there does not appear to be a strong dimming signal in many of the models. Is this just the scale on the figure or is there not much change in the model at all? Can the Figure be improved in any way to make this easier to see?

Reply: There is no strong dimming or brightening signal in the models when they have been interpolated to all the GEBA stations. But there is a very weak downward trend followed by a weak positive trend in most of the models, although the trend reversal seems to happen at different times. This figure will be improved by adding ensemble members and change from a timeseries-graph to a semi-decadal mean box plot. The models generally does not represent the *global* change in SDSR as observed and this point is made clearer in the text.

Reviewer Point P 2.28 — Page 5, line 122 – Change "these discrepancy originate" to "this discrepancy originates"

Reply: Fixed.

Reviewer Point P 2.29 — Page 5, line 125 – More discussion on European model observational differences (see general comments point 3)

Reply: Added.

Reviewer Point P 2.30 — Page 5, line 135 – I think that this is only true for certain models as others seem to have opposite temporal changes compared to observations e.g. NorESM2.

Reply: We agree and have clarified the text.

Reviewer Point P 2.31 — Page 5, line 138 – It is hard to say without tick marks on the figures as to whether the end points in models are similar to the observations. For example, is a -10 Wm-2 anomaly in 2014 from GEBA considered to be similar to a -6 Wm-2 from NorESM2?

Reply: The new figures have more clear tick marks, and the text has been changed to more accurately describe the behaviour of the models. The end points in observations are not comparable to NorESM2 and CNRM-ESM2-1 and this has been cleared out in the text.

Reviewer Point P 2.32 — Page 5, line 140 – please explain what "temporal forcing evolution" means in this context.

Reply: This line has been removed due to the added discussion of the trend reversal in China in observations.

Reviewer Point P 2.33 — Page 6, line 156-157 – does this imply that the greenhouse gases impact on SDSR over China throughout this period?

Reply: Yes, and this has been added to the text. However we also note that MIROC6 tells the opposite story and we cannot draw conclusions on what effect greenhouse gases without their SST-warming have on SDSR from these results.

Reviewer Point P 2.34 — Page 6, line 157-158 – I am not sure this is true for all models. The temporal evolution of SDSR from CanESM5 seems quite different in the historical and piClim-histall but perhaps not so much in MIROC6.

Reply: The reviewer is right and we have changes the text to highlight the difference between piClim experiments and historical for CanESM5.

Reviewer Point P 2.35 — Page 6, line 167 – Aerosols have a key role in dimming but not it appears brightening – why not? (see general comment 2)

Reply: The reduction of aerosol emission have a key role in brightening, as is seen in Europe where brightening occurs at the same time as anthropogenic aerosol and aerosol precursor gases was reduced. This is further explained in the reply for general comment 2.

Reviewer Point P 2.36 — Page 6, lines 168-169 – similar to point above in that there are differences between these simulations which don't appear to be the temporal driver of SDSR but perhaps can influence it? It would be good to show the actual differences between models in these simulations and what influence other factors (like clouds and greenhouse gases) can have on SDSR.

Reply: Clouds and greenhouse gases can influence SDSR, but is as mentioned in the introduction not a dominant driver of SDSR changes. It is therefore expected to see small differences in between these simulations. The overall picture of models showing dimming with anthropogenic aerosol emissions, and no dimming without it remains whether or not you include greenhouse gases or SST changes. This has been made clearer in the text.

Reviewer Point P 2.37 — Page 6, line 173 – how has all-sky SDSR been decomposed into clear-sky?

Reply: This is diagnostics that is outputted from the models. The general idea is that clear-sky SDSR from models represents the amount of sunlight reaching the surface if all shortwave effects from clouds were removed. Clear-sky SDSR is not to be confused with sunny day SDSR which is from actual cloud free days.

Reviewer Point P 2.38 — Page 6, line 179-180 – Can the clear-sky and all-sky changes be shown on the same figure to compare differences?

Reply: This figure has been replaced by a table and the table will include all-sky changes as well to more easily compare the two (three including cloud cover).

Reviewer Point P 2.39 — Page 6, line 182-189 –How have the changes in model cloud cover been calculated? This needs to be in the methods section. Also line 183-184 states that cloud cover changes mask the clear-sky SDSR signal. This implies that the clear-sky decrease would have been even larger without changes to clouds indicating that clouds do have an important influence on SDSR in models. I think this needs to be explained more - see general comment section 5 for more details.

Reply: a paragraph on how cloud affect SDSR has been added in the introduction which will be referred to in this current section. Cloud cover is a standard output from climate models and has not been calculated by the author, and the source of the data has been added in the supplementary explaining how we obtained the data. The new table will present both clear sky and all sky SDSR which will show that most models do have a stronger dimming when cloud effects have been removed, meaning that clouds historically in China have had a "masking" effect on SDSR in the model simulations. This has now been clarified in the text.

Reviewer Point P 2.40 — Page 7, line 193 – "session" should be "section"

Reply: Fixed.

Reviewer Point P 2.41 — Page 7, line 194 – "In this session we found the clear-sky SDSR to be stronger than all-sky SDSR, indicating the simulated dimming is primarily caused by aerosol-radiation interactions." But also that clouds have an influence on SDSR too.

Reply: Cloud have an influence on SDSR - but aerosols are the primary cause of dimming.

Reviewer Point P 2.42 — Page 7, line 205 – "SO2 burden" is mentioned but should this not be SO4 burden.

Reply: Fixed.

Reviewer Point P 2.43 — Page 7, line 205-206 – Given that all models have the same SO2 emissions, do we know why the changes in SO4 burden are so different between NorESM2 and CESM2? Could this indicate some of the potential problems in translating emissions into atmospheric burden or aerosols, which lead to errors in SDSR?

Reply: Burdens are a result of emission and deposition. The emissions in both models are the same but the deposition is dependent on many different processes within each model. The atmospheric circulation in CESM2 and NoreSM2 differs, among other things, so for example a sulfate particle may be brought higher up in the atmosphere in NorESM2 - giving sulfate a longer lifetime and thereby making NorESM2 have a higher sulfate burden.

Reviewer Point P 2.44 — Page 7, line 210 – can a more scientific term be used than "real story".

Reply: Definitely. Fixed.

Reviewer Point P 2.45 — Page 7, line 210-211 – This sentence makes the assumption that aerosols are the sole driving force in SDSR and that it is only the emissions and removal processes that could be in error. Other potential causes could be mentioned like the model translation of emissions to burden which leads to the larger differences in simulated SO4 burdens between models. Also see major comments above.

Reply: The model burden is translated from emission and removal processes. If there is an error in burden than the error is sourced in either emissions or removal professes. The difference in burden magnitude between the models is not seen as problematic as their effect on SDSR is comparable to each other. The burdens are calculated using the grid boxes with GEBA stations and with their difference in circulation one would not assume the exact same burden per gridbox anyway. TODO bad answer

Reviewer Point P 2.46 — Page 7, line 212 – "the precursor of SO2", should this not be SO4?

Reply: Fixed.

Reviewer Point P 2.47 — Page 7, line 215-218 – Should we be expecting a trend reversal in SO2 emissions over China between 1980 and 1990? At this point in time emissions would have been increasing over China and emissions have only begun to reduce recently (since 2010). See general comment point 4

Reply: This is up for debate and is further investigated in the new section under Discussion.

Reviewer Point P 2.48 — Page 8, line 235 – Is it possible to include the clear-sky proxy from GEBA here and compare to that from models on Figure 3 to show how well models simulate the aerosol radiation interactions?

Reply: Unfortunately that is not easily done and is beyond the scope of this study. There is currently a project working on creating clear sky proxies at ETH Zurich under Dr Martin Wild.

Reviewer Point P 2.49 — Page 8, line 238 – change "shown in Figure displayed" to "(Fig. 2) show"

Reply: Fixed.

Reviewer Point P 2.50 — Page 8, line 242 – But the magnitude of the dimming was not sufficient to reproduce that observed (same as Allen?) and implies emissions are not high enough historically?

Reply: Correct.

Reviewer Point P 2.51 — Page 8, line 247 - change "burden of SO2" to "burden of SO4".

Reply: Fixed.

Reviewer Point P 2.52 — Page 8, Lines 246-249 - The study only shows change in SDSR is opposite to SO4 burden over Europe and not the case over China so can we really say that the

process of translating burden to forcings are ok? What about over other regions? Might not just be due to errors in atmospheric burdens, but other factors combining?

Reply: Model translation from burden to forcing is not region dependent, but burden is. Therefore if the translation is ok in one region we assume the translation works as expected. But the burden is based on emissions which is highly region dependent, and we propose that errors in emission plays a part in the discrepancy of radiation between observations and model simulations, but keep the possibility open for other factors we do not yet know about to also play a role.

Reviewer Point P 2.53 — Page 8, Line 250 – "The models of this study ..." changed to "The models used in this study ..."

Reply: Fixed.

Reviewer Point P 2.54 — Page 9, line 254-255 – Should we expect a reversal of emissions across China over this period?

Reply: This is debated in the section added under discussion on the observed trend reversal in China.

Reviewer Point P 2.55 — Page 9, line 256 – Is this referring to Figure 3 in Hoesly et al., (2018)? Make clearer.

Reply: Fixed.

Reviewer Point P 2.56 — Page 9, line 258 – should we expect BC and OC to influences SDSR much? Need to mention these aerosol components earlier in the manuscript if going to mention now as no introduction to them at all. All discussion previously has been made about SO4 so why suddenly bring them in now?

Reply: The mentioning of these aerosols and their effect on SDSR have been added in the introduction.

Reviewer Point P 2.57 — Page 9, line 259-261 – Do these studies give an uncertainty in emission inventories and can this be used to see if it can account for the differences between model and observed SDSR.

Reply: Unfortunately none of these studies presents number for uncertainty in emission inventories, but Aas et al. (2019) show annual average trend in sulfate in aerosols from 2000-2015 and found that the standard deviation was larger than the actual trend for East Asia, and none of the locations used in that study was located in China Aas et al. (2019)[Tab. 1].

Reviewer Point P 2.58 — Page 9, line 270 – change "CMIP6 experiment models" to "experiments, CMIP6 models"

Reply: Fixed.

Reviewer Point P 2.59 — Page 9, line 273 – mention that the dimming is underestimated by the models.

Reply: Fixed.

Reviewer Point P 2.60 — Page 9, line 276-279 – Would we not have anticipated the SO4 burden to have increased across China over this period as SO2 emissions are anticipated to have also increased? Are the errors in SO4 burden and SO2 emissions really that large to account for the observed discrepancy in SDSR? More work to back up this statement and other factors should be included in conclusions. Uncertainty in emission inventories probably do contribute to this but the trend changes in SDSR and anticipated emission changes don't match for China, so this cannot be the sole reason and needs to be expanded on. see general comment point 4.

Reply: As we do not know the estimation uncertainty for emission we do not have evidence to rule out that the emission inventories can have large errors. The observed trend reversal in China have a new discussion section which expands the understanding of the anticipated emission inventories of China and the observed SDSR changes.

Reviewer Point P 2.61 — Page 10, line 285-287 – how would these future investigations improve our understanding of SDSR temporal evolution?

Reply: Clarified.

Reviewer Point P 2.62 — Fig. 2b – why is CanESMS so different in Hist-Nat and does show that other drivers influence the SDSR trend?

Reply: We do not know why CanESM5 differs from the others in it's hist-nat experiment, but this single experiment is unfortunately not enough evidence to say that other drivers influence the SDSR trend - except for in CanESM5 only.

Reviewer Point P 2.63 — Fig. 3b – Can the uncertainty in cloud cover from observations and models be shown?

Reply: We will make this figure into a table and there show the standard deviations from three ensemble members in addition to mentioning the uncertainty of the CRU data in the methods section of the manuscript.

Reviewer Point P 2.64 — Fig. 4 – CESM2 seems to show a small change, can you confirm that this model has interact aerosols included? If not then why such a small change compared to others?

Reply: Aerosols interact with the climate in CESM2.

References

Aas, Wenche, Augustin Mortier, Van Bowersox, Ribu Cherian, Greg Faluvegi, Hilde Fagerli, Jenny Hand, Zbigniew Klimont, Corinne Galy-Lacaux, Christopher M. B. Lehmann, Cathrine Lund Myhre, Gunnar Myhre, Dirk Olivié, Keiichi Sato, Johannes Quaas, P. S. P. Rao, Michael Schulz, Drew Shindell, Ragnhild B. Skeie, Ariel Stein, Toshihiko Takemura, Svetlana Tsyro, Robert Vet, and Xiaobin Xu (2019), "Global and regional trends of atmospheric sulfur." *Scientific Reports*, 9, 953, URL https://www.nature.com/articles/s41598-018-37304-0.

Allen, R. J., J. R. Norris, and M. Wild (2013), "Evaluation of multidecadal variability in CMIP5 surface solar radiation and inferred underestimation of aerosol direct effects over Europe, China, Japan, and India." *Journal of Geophysical Research: Atmospheres*, 118, 6311–6336, URL https://agupubs.onlinelibrary.wiley.com/doi/abs/10.1002/jgrd.50426.

Chiacchio, Marc, Fabien Solmon, Filippo Giorgi, Paul Stackhouse, and Martin Wild (2015), "Evaluation of the radiation budget with a regional climate model over Europe and inspection of dimming and brightening." *Journal of Geophysical Research: Atmospheres*, 120, 1951–1971, URL https://agupubs.onlinelibrary.wiley.com/doi/full/10.1002/2014JD022497.

Hoesly, Rachel M., Steven J. Smith, Leyang Feng, Zbigniew Klimont, Greet Janssens-Maenhout, Tyler Pitkanen, Jonathan J. Seibert, Linh Vu, Robert J. Andres, Ryan M. Bolt, Tami C. Bond, Laura Dawidowski, Nazar Kholod, June-ichi Kurokawa, Meng Li, Liang Liu, Zifeng Lu, Maria Cecilia P. Moura, Patrick R. O'Rourke, and Qiang Zhang (2018), "Historical (1750–2014) anthropogenic emissions of reactive gases and aerosols from the Community Emissions Data System (CEDS)." *Geoscientific Model Development*, 11, 369–408, URL https://www.geosci-model-dev.net/11/369/2018/.

Hoyt, Douglas V. and Kenneth H. Schatten (1993), "A discussion of plausible solar irradiance variations, 1700-1992." *Journal of Geophysical Research: Space Physics*, 98, 18895–18906, URL https://agupubs.onlinelibrary.wiley.com/doi/abs/10.1029/93JA01944. _eprint: https://agupubs.onlinelibrary.wiley.com/doi/pdf/10.1029/93JA01944.

Leibensperger, E. M., L. J. Mickley, D. J. Jacob, W.-T. Chen, J. H. Seinfeld, A. Nenes, P. J. Adams, D. G. Streets, N. Kumar, and D. Rind (2012a), "Climatic effects of 1950–2050 changes in US anthropogenic aerosols – Part 1: Aerosol trends and radiative forcing." *Atmospheric Chemistry and Physics*, 12, 3333–3348, URL https://www.atmos-chem-phys.net/12/3333/2012/. Publisher: Copernicus GmbH.

Leibensperger, E. M., L. J. Mickley, D. J. Jacob, W.-T. Chen, J. H. Seinfeld, A. Nenes, P. J. Adams, D. G. Streets, N. Kumar, and D. Rind (2012b), "Climatic effects of 1950–2050 changes in US anthropogenic aerosols – Part 2: Climate response." *Atmospheric Chemistry and Physics*, 12, 3349–3362, URL https://www.atmos-chem-phys.net/12/3349/2012/acp-12-3349-2012.html. Publisher: Copernicus GmbH.

Norris, Joel R. and Martin Wild (2007), "Trends in aerosol radiative effects over Europe inferred from observed cloud cover, solar "dimming," and solar "brightening"." *Journal of Geophysical Research: Atmospheres*, 112, URL https://agupubs.onlinelibrary.wiley.com/doi/abs/10.1029/2006JD007794. _eprint: https://agupubs.onlinelibrary.wiley.com/doi/pdf/10.1029/2006JD007794.

Norris, Joel R. and Martin Wild (2009), "Trends in aerosol radiative effects over China and Japan inferred from observed cloud cover, solar "dimming," and solar "brightening"." *Journal of Geophysical Research: Atmospheres*, 114, URL https://agupubs.onlinelibrary.wiley.com/doi/abs/10.1029/2008JD011378. _eprint: https://agupubs.onlinelibrary.wiley.com/doi/pdf/10.1029/2008JD011378.

Ramanathan, V. and Andrew M. Vogelmann (1997), "Greenhouse Effect, Atmospheric Solar Absorption and the Earth's Radiation Budget: From the Arrhenius-Langley Era to the 1990s." *Ambio*, 26, 38–46, URL https://www.jstor.org/stable/4314548. Publisher: [Springer, Royal Swedish Academy of Sciences].

Solomon, Susan, Karen H. Rosenlof, Robert W. Portmann, John S. Daniel, Sean M. Davis, Todd J. Sanford, and Gian-Kasper Plattner (2010), "Contributions of Stratospheric Water Vapor to Decadal Changes in the Rate of Global Warming." *Science*, 327, 1219–1223, URL https://science.sciencemag.org/content/327/5970/1219. Publisher: American Association for the Advancement of Science Section: Research Article.

Storelvmo, Trude, Ulla K. Heede, Thomas Leirvik, Peter C. B. Phillips, Philipp Arndt, and Martin Wild (2018), "Lethargic Response to Aerosol Emissions in Current Climate Models." *Geophysical Research Letters*, 0, URL https://agupubs.onlinelibrary.wiley.com/doi/abs/10.1029/2018GL078298.

Wang, Y. W. and Y. H. Yang (2014), "China's dimming and brightening: evidence, causes and hydrological implications." *Annales Geophysicae*, 32, 41–55, URL https://www.ann-geophys.net/32/41/2014/.

Wang, Yawen and Martin Wild (2016), "A new look at solar dimming and brightening in China: CHINA DIMMING AND BRIGHTENING REVISITED." *Geophysical Research Letters*, 43, 11,777–11,785, URL http://doi.wiley.com/10.1002/2016GL071009.

Wild, Martin (2011), "Enlightening Global Dimming and Brightening." *Bulletin of the American Meteorological Society*, 93, 27–37, URL https://journals.ametsoc.org/doi/abs/10.1175/BAMS-D-11-00074.1.

Yang, Su, Xiaolan L. Wang, and Martin Wild (2019), "Causes of Dimming and Brightening in China Inferred from Homogenized Daily Clear-Sky and All-Sky in situ Surface Solar Radiation Records (1958–2016)." *Journal of Climate*, 32, 5901–5913, URL http://journals.ametsoc.org/doi/10.1175/JCLI-D-18-0666.1.

1 Supplementary Material

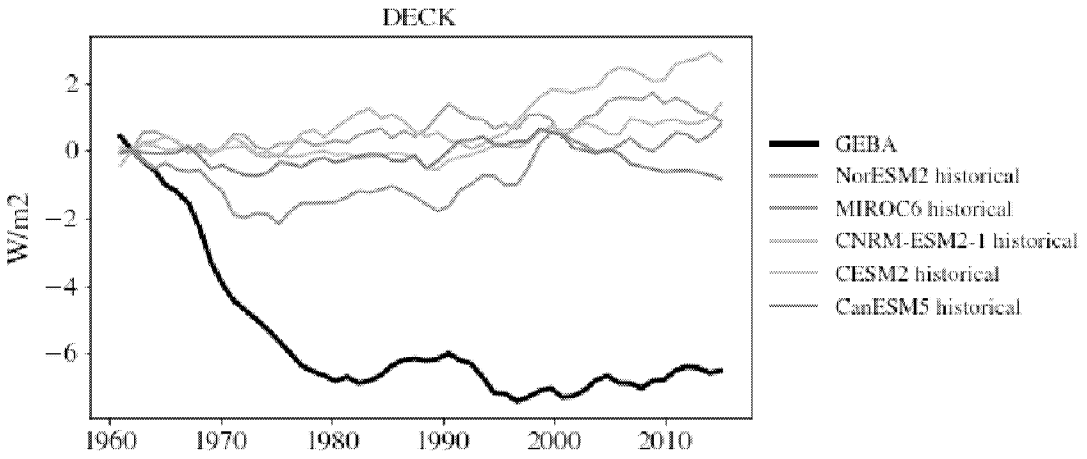

Figure S1: SDSR anomaly north america